

C-H BORYLATION MEDIATED BY GROUP 9 PINNACOLATE COMPLEXES AND
SYNTHESIS OF IRIIDIUM TRIFLATES AND TRIARYLMETHYL SPECIES

A Dissertation

by

CHUN-I LEE

Submitted to the Office of Graduate and Professional Studies of
Texas A&M University
in partial fulfillment of the requirements for the degree of

DOCTOR OF PHILOSOPHY

Chair of Committee,	Oleg V. Ozerov
Committee Members,	Donald J. Darensbourg
	François P. Gabbaï
	Mustafa Akbulut
Head of Department,	François P. Gabbaï

May 2015

Major Subject: Chemistry

Copyright 2015 Chun-I Lee

ABSTRACT

The importance of organoboron compounds in chemical synthesis is apparent from the Nobel Prizes awarded to Herbert C. Brown (1979) and Akira Suzuki (2010) for their contribution to the development of new synthetic methodologies involving C-B bonds. Recently, dehydrogenative C-H borylation has emerged as an attractive approach to organoboron compounds. Multiple examples of catalytic conversion of unactivated C-H bonds in alkanes, benzylic and allylic C(sp³)-H bonds, as well as C(sp²)-H bonds in alkenes have been reported. Notably, the dehydrogenative C(sp)-H borylation of terminal alkynes (abbreviated as DHBTA) is missing in the list above.

Here we describe the first example of DHBTA catalyzed by a new SiNN iridium pincer complex. The reaction is strictly chemoselective and can be performed under very mild conditions with terminal alkynes in high yield. We then explore Rh analogs of these SiNN iridium complexes. Although the new Rh compounds turned out to be inactive as DHBTA catalysts, they brought to light the unusual dual non-innocence behavior of the SiNN ligand. The (SiNN)Rh system also turned out to be a modest benzene borylation catalyst.

Later, impressive TONs of 6500 for DHBTA were achieved by a new unsymmetric PNP iridium complex from ligand screening. The synthesis and characterization of the possible intermediates in DHBTA are also discussed. We also present the discovery of a new selective dehydrogenative diboration of the DHBTA products, alkynylboronates.

The independent synthesis and characterization of the possible catalytic intermediates in the diboration are also described.

Electrophilic iridium complexes have shown their great ability to activate strong bonds or serve as strong Lewis acids to catalyze reactions. We describe synthetic approaches to a highly electrophilic iridium triflate complex supported by a PNP pincer ligand and its equilibrium with ether solvents.

The value of making new triarylmethyl cations is relevant to both hydrodefluorination of C(sp³)-F bonds and organometallic chemistry. We illustrate the synthesis of selected triarylmethanol and triarylmethyl chloride bearing electron withdrawing groups. Preliminary attempts to generate highly electrophilic triarylmethyl cations are also shown.

ACKNOWLEDGEMENTS

I would like to thank my research advisor, Prof. Oleg Ozerov, for his guidance over the past five years. I appreciate his time, effort, and wisdom to make me a mature chemist. Most importantly, he kindly gave me all the freedom and support to let me have fun with the chemistry I discovered. I would also like to thank my committee members Prof. Donald Darensbourg, Prof. François Gabbaï, and Prof. Mustafa Akbulut.

Thanks also to the Ozerov research group members. I would particularly like to acknowledge Jessica DeMott. Her knowledge, humbleness, and dedication to chemistry provided a great model that I admire most in my generation. I would also like to thank Dr. Sam Timpa and Dr. Jillian Davidson. I cannot imagine what my graduate life would be like without them and all of the memories we have together. I would like to thank my coworkers, Dr. Jia Zhou and Nathanael Hirscher. The story of the borylation chemistry would not be this beautiful without any of them. In addition I would like to thank Dr. Morgan MacInnis, Dr. Yanjun Zhu, Dr. Rafael Huacuja, Wei-Chun Shih, and Chris Pell for being wonderful colleagues to discuss chemistry and share experiences.

I would like to thank my Taiwanese friends, better known as the “Taiwanese Mafia” in the Department of Chemistry. Because of them, the loneliness brought by studying abroad was removed from my graduate experience. Finally, I would like to thank my parents and my sister. If I have any tiny achievement today, it is all because of their unconditional love and encouragement.

NOMENCLATURE

L	ligand
THF	tetrahydrofuran
DBU	1,8-diazabicycloundec-7-ene
HBpin	pinacolborane
HBcat	catecholborane
B ₂ pin ₂	bis(pinacolato)diboron
B ₂ cat ₂	bis(catecholato)diboron
COD	1,5-cyclooctadiene
COE	<i>cis</i> -cyclooctene
ind	indenyl
dba	dibenzylideneacetone
BINAP	2,2'-bis(diphenylphosphino)-1,1'-binaphthyl
DPPF	1,1'-bis(diphenylphosphino)ferrocene
dtbpy	4,4'-di- <i>tert</i> -butyl-2,2'-dipyridyl
py	pyridine
OTf	triflate
OAc	acetate
Mes	mesityl
Ts	tosyl
PTFE	polytetrafluoroethylene

HDF	hydrodefluorination
DHBTA	dehydrogenative borylation of terminal alkynes
RT	room temperature
TON	turnover number
TOF	turnover frequency
DFT	density functional theory

TABLE OF CONTENTS

	Page
ABSTRACT	ii
ACKNOWLEDGEMENTS.....	iv
NOMENCLATURE	v
TABLE OF CONTENTS	vii
LIST OF SCHEMES	x
LIST OF FIGURES	xiii
LIST OF TABLES	xvii
CHAPTER I INTRODUCTION AND LITERATURE REVIEW	1
1.1 General introduction for pincer ligands	1
1.2 Group 9 pincer complexes in C-H bond activation	3
1.2.1 C(sp ³)-H bond activation: Catalytic alkane dehydrogenation	3
1.2.2 C(sp ²)-H bond activation: C-H vs C-X (X = halide or O) activation	5
1.2.3 C(sp)-H bond activation: Alkyne dimerization	7
1.3 Hydroboration and C-H borylations (dehydrogenative borylation)	10
1.3.1 Overview	10
1.3.2 Arene borylation by Ir bipyridine & bisphosphine complexes	11
1.3.3 Application of pincer complexes in borylation	14
1.3.3.1 Dehydrogenative borylation of arenes	14
1.3.3.2 Hydroboration of alkenes	16
1.3.3.3 Dehydrogenative borylation of alkenes	18
1.3.3.4 Hydroboration of terminal alkynes	21
1.3.3.5 Borylation of other substrates	23
CHAPTER II CATALYTIC DEHYDROGENATIVE BORYLATION OF TERMINAL ALKYNES BY A SINN PINCER COMPLEX OF IRIDIUM	25
2.1 Introduction	25
2.2 Results and discussion	28
2.2.1 Synthesis of the SiNN ligand	28
2.2.2 Synthesis of the SiNN complexes of Ir	30

2.2.3 XRD and DFT studies of the SiNN complexes of Ir	30
2.2.4 Catalytic DHBTA studies	33
2.3 Mechanistic considerations	39
2.4 Conclusion	41
2.5 Experimental	42
CHAPTER III DUAL-SITE NON-INNOCENCE OF THE SINN PINCER LIGAND IN COMPLEXES OF RHODIUM	66
3.1 Introduction	66
3.2 Results and discussion	67
3.3 Conclusion	73
3.4 Experimental	73
CHAPTER IV DEHYDROGENATIVE BORYLATION OF TERMINAL ALKYNES BY PNP PINCER COMPLEXES OF IRIDIUM	90
4.1 Introduction	90
4.2 Results and discussion	91
4.2.1 Synthesis and screening of ligands for DHBTA	91
4.2.2 Testing of (PNP)Ir complexes with various phosphine substituents	95
4.2.3 Synthesis of proposed intermediates in DHBTA	99
4.2.4 X-ray diffraction and density functional theory studies of 408-Ir-HBpin, 408-Ir-Bpin ₂ , 408-Ir-v-tol, and 408-Ir-p-Ftol	107
4.2.5 Stoichiometric reactions of (^{Me} PNP ⁱ Pr)Ir complexes	110
4.2.6 Catalytic results for DHBTA using various (^{Me} PNP ⁱ Pr)Ir complexes	113
4.3 Conclusion	114
4.4 Experimental	115
CHAPTER V DEHYDROGENATIVE DIBORATION OF ALKYNYLBORONATES CATALYZED BY SINN IRIDIUM COMPLEXES	147
5.1 Introduction	147
5.2 Results and discussion	149
5.2.1 Discovery and optimization of dehydrogenative diboration of alkynylboronates	149
5.2.2 Substrate scope of one-pot dehydrogenative diboration of alkynylboronates.....	151
5.2.3 Independent synthesis of (SiNN)Ir(CO) and its equilibrium with (SiNN)Ir(CO) ₂	153
5.2.4 Examination of isolated 501 and other CO complex in the borylation	155
5.2.5 Observation of irreproducible borylation in the blank reaction	158
5.3 Mechanistic considerations	159
5.4 Conclusion	160

5.5 Experimental	160
CHAPTER VI SYNTHESIS OF PNP IRIDIUM TRIFLATE COMPLEXES	176
6.1 Introduction	176
6.2 Results and discussion	176
6.2.1 Synthesis of (PN(H)P)Ir(H)(OTf) ₂	176
6.2.2 Synthesis and characterization of (PNP)Ir(H)(OTf)	178
6.2.3 Synthesis and characterization of [(PNP)Ir(H)(L ₂)](OTf)	182
6.3 Conclusion	183
6.4 Experimental	183
CHAPTER VII DESIGN AND SYNTHESIS OF HIGHLY ELECTROPHILIC TRIARYLMETHYL CATION PRECURSORS	190
7.1 Introduction	190
7.2 Results and discussion	192
7.2.1 Design and synthesis of triarylmethanols	192
7.2.2 Synthesis of triarylmethyl chlorides	197
7.2.3 Attempt to synthesize triarylmethyl carboranes and triarylmethyl triflates	199
7.3 Conclusion	200
7.4 Experimental	200
CHAPTER VIII SUMMARY	209
REFERENCES	211

LIST OF SCHEMES

	Page
Scheme 1-1. General scheme for pincer metal complexes.	1
Scheme 1-2. Metal complexes bearing representative examples of pincer ligands.	2
Scheme 1-3. Alkane dehydrogenation with PCP Ir complex by Jensen.	4
Scheme 1-4. POCOP iridium complexes as the alkane dehydrogenation catalysts (top) and proposed mechanism of transfer hydrogenation catalyzed by 102 (bottom).	5
Scheme 1-5. C-H vs C-Cl oxidative addition on Ir pincer complexes by Milstein (top) and Ozerov (bottom).	6
Scheme 1-6. Reaction of PNP Rh fragment with various esters.	7
Scheme 1-7. Stoichiometric dimerization of phenylacetylene.	7
Scheme 1-8. Catalytic alkyne dimerization by (PNP)Rh complexes.	8
Scheme 1-9. Possible mechanisms for alkyne dimerization catalyzed by (PNP)Rh complexes.	9
Scheme 1-10. Oxidative addition of terminal alkyne with a PNP cobalt complex.	9
Scheme 1-11. Hydroboration of alkenes or alkynes with dialkoxyboranes.	10
Scheme 1-12. Traditional methods for making arylboronates and dehydrogenative borylation of arenes.	11
Scheme 1-13. Initial reports of arene borylation by Smith (top) and Ishiyama, Miyaura and Hartwig (bottom).	12
Scheme 1-14. Proposed mechanism for the iridium-catalyzed borylation of arenes.	13
Scheme 1-15. <i>ortho</i> -Directed arene borylation and proposed mechanism.	14
Scheme 1-16. Cobalt-catalyzed arene borylation (top) and proposed mechanism for borylation of methylfuran by 146 (bottom).	16
Scheme 1-17. Iron pincer complex catalyzed alkene hydroboration by Huang.	17

Scheme 1-18. Iron dinitrogen complexes as alkene hydroboration catalysts by Chirik.	17
Scheme 1-19. Cobalt complexes as alkene hydroboration catalysts by Chirik and Huang.	18
Scheme 1-20. Dehydrogenative borylation of alkenes by a NCN pincer palladium 162 (top) and proposed mechanism (bottom).	19
Scheme 1-21. Dehydrogenative borylation of alkenes by a PSiP pincer palladium (top) and proposed mechanism (bottom).	20
Scheme 1-22. Z-selective hydroboration of terminal alkynes and proposed mechanism.	22
Scheme 1-23. Borylation of vinyl cyclopropanes, vinyl aziridines and allyl acetates 101 (top), and borylation of allyl alcohols 103 (bottom).	23
Scheme 1-24. Proposed mechanism of borylation of allyl alcohols.	24
Scheme 3-1. Synthesis of SiNN complexes of Ir and Rh, and DHBTA catalysis by Ir complexes.	67
Scheme 4-1. Synthesis of ligands used in screening DHBTA.	92
Scheme 4-2. DHBTA catalyzed by 206 generating <i>in situ</i> from 205.	93
Scheme 4-3. Synthesis of (PNP)Ir(COE) complexes.	96
Scheme 4-4. The synthesis of 408-Ir-HBpin and its equilibrium with 408-Ir-H ₃ Bpin (top). The synthesis of 408-Ir-Bpin ₂ (bottom).	101
Scheme 4-5. Unsuccessful attempts of making terminal alkyne related complexes. ...	103
Scheme 4-6. Synthesis of vinylidene complexes 408-Ir-v-tol and 408-Ir-v-TMS.	105
Scheme 4-7. Synthesis of 408-Ir-p-tol.	106
Scheme 4-8. Synthesis of 408-Ir-p-Ftol.	107
Scheme 4-9. Boryl transfer from 408-Ir-HBpin to terminal alkynes (top) and reactivities of 408-Ir-Bpin ₂	111
Scheme 4-10. Reactivities of 408-Ir-v-tol (top) and 408-Ir-p-Ftol (bottom).	112

Scheme 5-1. Attempts at further borylation of alkynylboronates.	150
Scheme 5-2. The synthesis of 501 and its equilibrium with 502.	153
Scheme 5-3. Borylation of 209P with HBpin catalyzed by 501.	156
Scheme 5-4. Borylation of 5A-Bpin ₂ with HBpin catalyzed by 501.	156
Scheme 5-5. Borylation of terminal alkynes with HBpin catalyzed by 501.	157
Scheme 5-6. Control experiments.	158
Scheme 6-1. Previous attempts to 601 and proposed alternative synthesis.	177
Scheme 6-2. Synthesis of 604 and observation of 605.	178
Scheme 6-3. Synthesis of 601 from 604.	180
Scheme 6-4. Synthesis of 606-608.	183
Scheme 7-1. Silylium mediated C-F bond activations.	191
Scheme 7-2. Representative values of fluoride (FA) and hydride (HA) affinities, all values were calculated in chlorobenzene.	191
Scheme 7-3. Objective triarylmethanol (top) and strategy of making triarylmethyl carboranes (bottom).	193
Scheme 7-4. Synthesis of 701-OH to 704-OH.	194
Scheme 7-5. Polar and SET pathways for the reaction between Grignard reagents and ketone compounds.	195
Scheme 7-6. Synthesis 701-Cl to 704-Cl.	198
Scheme 7-7. Attempt of synthesis of triarylmethyl carboranes.	199

LIST OF FIGURES

	Page
Figure 1-1. Various pincer catalysts for arene borylation.	15
Figure 2-1. Representative examples of dehydrogenative borylation (a) alkane borylation by Hartwig (b) arene borylation by Ishiyama, Miyaura, Hartwig and Smith (c) benzylic borylation by Ishiyama and Miyaura (d) alkene borylation by Brown (e) allylic borylation by Szabó.	26
Figure 2-2. Synthesis of the SiNN ligand and its iridium complexes.	29
Figure 2-3. ORTEP drawings (50% probability ellipsoids) of 206 (top left) and 207 (top right) showing selected atom labeling, and drawings of the DFT-calculated structures of 206 (bottom left) and 207 (bottom right). Hydrogen atoms are omitted for clarity, except for the hydride on the Ir atom. Selected bond distances (Å) and angles (deg) for 206, with DFT-derived metrics in square brackets: Ir1-Si1, 2.3573(15) [2.391]; Ir1-H, [1.596]; Si1-H, [2.007]; C1-C2, 1.423(9) [1.413]; Si1-Ir1-H, [56.3]. For 207: Ir1-Si1, 2.4130(14) [2.452]; Ir1-H, [1.609]; Si1-H, [1.889]; Ir1-B1, 2.069(5) [2.064]; Ir1-B2, 2.062(6) [2.055]; Si1-Ir1-H, [50.4]; B1-Ir1-B2, 66.5(2), [64.4].	31
Figure 2-4. Drawings showing the immediate coordination environment about Ir in 206 (left) and 207 (right) based on the DFT-calculated structures.	32
Figure 2-5. Catalytic DHBTA reaction (details in Tables 2-1, 2-2 and 2-3).	33
Figure 2-6. Original proposed DHBTA mechanism.	39
Figure 2-7. Energy profile for for Ph-C≡C-Bpin elimination reaction (top) and H ₂ production reaction (bottom). Relative free energies (in kcal/mol) in solvent at various levels of theory are shown.	40
Figure 2-8. From left to right: Skraup reaction mixture before work-up; side product, acrolein polymer; 8-bromo-6-methylquinoline after distillation; solidified 8-bromo-6-methylquinoline.	45
Figure 2-9. Left: Setup of a sublimation apparatus. Right: Alkynylboronate collection after sublimation.	62
Figure 2-10. From left to right: Before distillation; After distillation, before removal of coolant; After removal of coolant.	62

Figure 3-1. ORTEP drawings of 301 (left, 80% probability ellipsoids) and 302-x (right, 50% probability ellipsoids) showing selected atom labeling. Hydrogen atoms are omitted for clarity. Select bond distances (Å) and angles (deg) for 301: Rh-Si, 2.3787(13); C1-C2, 1.388(8); Si-Rh-N2, 140.87(11). For 302-x: Rh-Si, 2.2223(9); Rh-B2, 2.007(3); N1-B1, 1.459(4); Si-Rh-N2, 106.51(7); N1-Rh-B2, 175.33(11).	69
Figure 3-2. Drawings of the DFT calculated structures of 301 (left), 302-x (middle) and 302 (right). N2 is the quinoline N.	69
Figure 3-3. Metric parameters in the M/Si/H triangles (M = Rh or Ir) in compounds 206/207(-x)/301/302(-x). DFT calculated distances (Å) in blue, Si-M-H angles (°) in red, XRD-determined M-Si distances in black.	71
Figure 3-4. Intermediate proposed by Hartwig et al. (143) and 302-x.	73
Figure 3-5. ORTEP drawings (50% probability ellipsoids) of 206 (left) and 301 (right) showing select atom labeling.	77
Figure 3-6. Left: Removal of all volatiles before filtration. Right: Filtration through a fritted funnel.	79
Figure 3-7. ¹ H NMR spectra of 302-x in C ₆ D ₆ after RT 10 min (top) and RT 6 h (bottom).	83
Figure 3-8. ¹¹ B{ ¹ H} NMR (top) and ¹¹ B NMR (bottom) spectra of 302-x in C ₆ D ₆ after RT 6 h.	84
Figure 3-9. ¹ H NMR spectra of 302-x in C ₆ D ₁₂ after RT 10 min (top) and RT 6 h (bottom).	85
Figure 3-10. ¹¹ B{ ¹ H} NMR (top) and ¹¹ B NMR (bottom) spectra of 302-x in C ₆ D ₁₂ after RT 6 h. The signals of 302-x were not observable due to its low solubility in C ₆ D ₁₂	85
Figure 4-1. DHBTA catalyzed by 206.	90
Figure 4-2. General strategy of ligand screening for DHBTA.	91
Figure 4-3. Partial ¹ H NMR spectra of DHBTA reaction mixtures catalyzed by a) 1 mol% 413-Ir-COE (entry 3 in Table 4-3) and b) 1 mol% 206 (entry 1 in Table 4-3).	98
Figure 4-4. Strategy of examining possible intermediates in DHBTA.	100

Figure 4-5. The upfield region of ^1H and $^1\text{H}\{^{11}\text{B}\}$ NMR spectrum (400 MHz, C_6D_6) of 408-Ir-HBpin (left) and 408-Ir- H_3Bpin (right).	102
Figure 4-6. Partial (upfield region) ^1H NMR spectrum (500 MHz, toluene- d_8) of 408-Ir- H_3Bpin as a function of temperature. Small amount of unidentified impurity (marked with asterisks) was shown near -9.2 ppm.	102
Figure 4-7. DFT calculation of three possible isomers of $(^{\text{Me}}\text{PNP}^{i\text{Pr}})\text{Ir} + 209\text{P}$	104
Figure 4-8. ORTEP drawing (50% probability ellipsoids) of 408-Ir-HBpin (top left) showing selected atom labeling and depiction of 410-Ir-HBpin (top right). Hydrogen atoms are omitted for clarity in the ORTEP drawing, except for the hydride on the Ir atom. The selected bond distances (\AA) and angles (deg) for 408-Ir-HBpin and 410-Ir-HBpin are summarized in the table at bottom.	108
Figure 4-9. ORTEP drawing (50% probability ellipsoids) of 408-Ir-Bpin $_2$ (top left) showing selected atom labeling and depiction of 207 (top right). Hydrogen atoms are omitted for clarity in the ORTEP drawing. The selected bond distances (\AA) and angles (deg) for 408-Ir-Bpin $_2$ and 207 are summarized in the table at bottom.	109
Figure 4-10. ORTEP drawings (50% probability ellipsoids) of 408-Ir-v-tol (left) and 408-Ir-p-Ftol (right) showing selected atom labeling and hydrogen atoms are omitted for clarity. For 10-Ir-v-tol, one of two molecules in the asymmetric unit is shown, and a non-coordinated fluorobenzene molecule is omitted for 408-Ir-p-Ftol. Selected bond distances (\AA) and angles (deg) for 408-Ir-v-tol: Ir-C1, 1.807(4); C1-C2, 1.334(5); P2-Ir1-P1, 164.84(3); C2-C1-Ir, 178.2(3); C1-C2-C3, 120.1(3); C1-C2-B 113.1(3); C3-C2-B, 126.8(3). Selected bond distances (\AA) and angles (deg) for 408-Ir-p-Ftol: Ir-C1, 2.165(11); Ir-C2, 2.101(12); C1-C2, 1.301(15); C1-C2-C3, 147.5(11); B-C1-C2, 161.9(11).	110
Figure 4-11. Left: Fiber-like 408-Ir-HBpin; Right: 408-Ir-HBpin after recrystallization from hexamethyldisiloxane.	130
Figure 4-12. From top to bottom: 408-Ir- H_3Bpin , 408-Ir-Bpin $_2$, 408-Ir-HBpin in C_6D_6	132
Figure 5-1. Syntheses of 1,1-diborylalkenes (top), 1,2- <i>cis</i> -diborylalkenes (middle) and triborylalkenes (bottom).	147
Figure 5-2. DHBTA catalyzed by (SiNN)Ir complexes.	148

Figure 5-3. Original idea of one-pot synthesis of diborylalkenes.	149
Figure 5-4. ORTEP drawing (50% probability ellipsoids) of 501 (top) showing selected atom labeling, and drawing of the DFT-calculated structures of 501 (bottom). Hydrogen atoms are omitted for clarity, except for the hydride on the Ir atom. Selected bond distances (Å) and angles (deg) for 501, with DFT-derived metrics in square brackets: Ir1-Si1, 2.3366(15) [2.376]; Si1-H, [2.183]; Ir1-H1, [1.592]; Ir2-H1, [3.117]; Ir1-Ir2, 2.9074(8) [3.046]; Si1-Ir1-N2, 124.89(11) [127.51]; Si1-Ir1-H1, [63.17]; Ir1-C1-O1, 176.1(5) [177.75].	154
Figure 5-5. Proposed mechanism for diboration.	160
Figure 6-1. H-D exchange rate measurement of 601.	181
Figure 6-2. Catalytic H-D exchange reaction and proposed mechanism by Grubbs. ...	182
Figure 7-1. Synthesis of 705-OH.	197
Figure 7-2. Synthesis of 705-OAc.	198

LIST OF TABLES

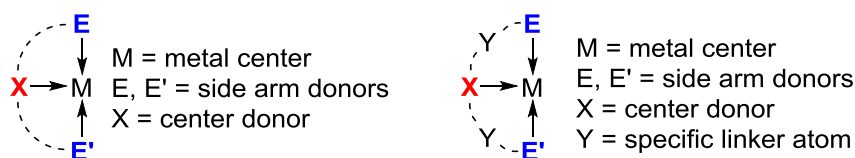
	Page
Table 2-1. Optimization of DHBTA (reaction in Figure 2-5).	34
Table 2-2. DHBTA of various alkynes catalyzed by 206.	36
Table 2-3. DHBTA of various enynes catalyzed by 206.	38
Table 2-4. DHBTA in different solvents.	54
Table 2-5. Pinacolborane/alkyne ratio optimization for DHBTA.	55
Table 2-6. Optimization of the method of addition of alkyne.	55
Table 3-1. Catalytic borylation of neat C ₆ D ₆ (80 °C, 48 h) using 301 and 302-x.	72
Table 3-2. Calculated energies of compounds under study (gas phase, 298 K).	75
Table 4-1. Ligand screening in DHBTA.	94
Table 4-2. DHBTA catalyzed by 111.	95
Table 4-3. Catalytic results for DHBTA using various PNP Ir complexes.	97
Table 4-4. DHBTA of representative terminal alkynes catalyzed by 415-Ir-COE.	99
Table 4-5. Catalytic results for DHBTA using various (^{Me} PNP ^{iPr})Ir complexes.	114
Table 5-1. Summary of the optimization of alkynylboronates diboration.	151
Table 5-2. Substrate scope of one-pot diboration of alkynylboronates.	152
Table 5-3. Borylation of 209 in different solvents.	172
Table 6-1. Equilibrium between 601 and 601-THF.	179
Table 7-1. Solvent effect in making of 704-OH.	196

CHAPTER I

INTRODUCTION AND LITERATURE REVIEW

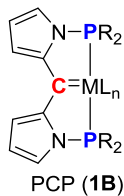
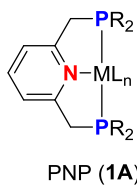
1.1 General introduction for pincer ligands

The beauty of organometallic chemistry is that the properties of metal centers can be controlled by the surrounding ligands. Pincer ligands are tridentate ligands that commonly bind to metal in the meridional fashion which provide their transition metal complexes with great stability and often impose unusual reactivity.¹ Since the first example of pincer ligands was reported by Shaw in the mid-1970s,² metal complexes with pincer ligands have attracted lots of attention especially in strong bond (e.g. C-H,³ C-N,^{4,5} C-O⁶ bonds) and small molecule (e.g. NH₃,⁷ CO₂,^{8,9} CH₄¹⁰) activation. Pincer ligands are usually abbreviated by their donor atoms, EXE' (E and E': side arm donors; X: center donor) (Scheme 1-1, left). Occasionally, the abbreviation EYXYE' would be used instead, where Y denotes the specific linker atom (Scheme 1-1, right).

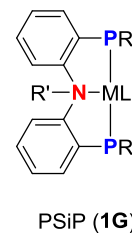
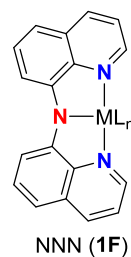
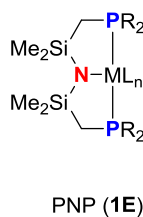
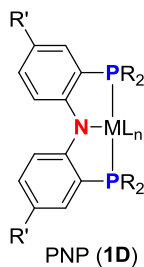
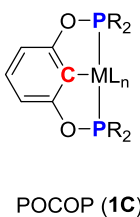


Scheme 1-1. General scheme for pincer metal complexes.

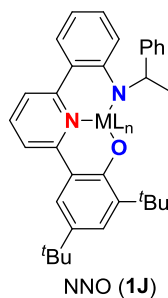
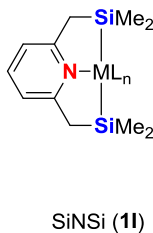
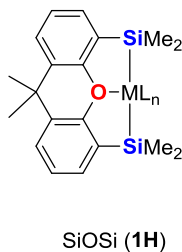
Metal complexes with neutral pincer ligands



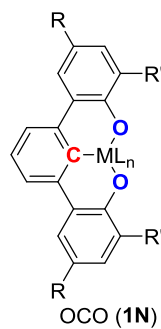
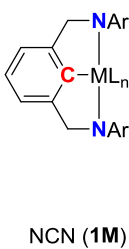
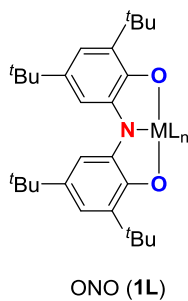
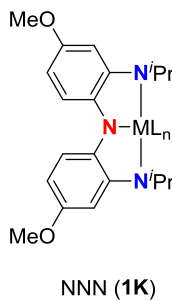
Metal complexes with monoanionic pincer ligands



Metal complexes with dianionic pincer ligands



Metal complexes with trianionic pincer ligands



Scheme 1-2. Metal complexes bearing representative examples of pincer ligands.

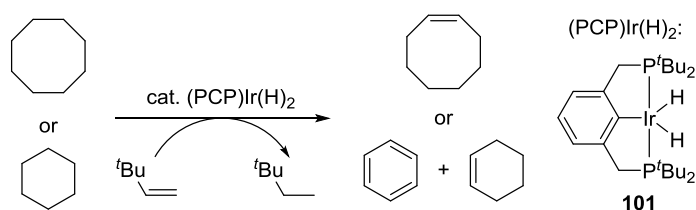
Representative examples of pincer ligands are shown in Scheme 1-2. The pincer ligand arrays are generally divided into four main categories. The first one is the neutral array in which all three donors are neutral. Most of neutral pincers ligands contain carbene (**1A**)¹¹ or pyridine (**1B**)¹² as the central donors. The second pincer motif is the monoanionic array, including widely used POCOP ligands that are based on resorcinols (**1C**),^{13,14} diarylamino PNP ligands (**1D**) developed by Liang¹⁵ and Ozerov,¹⁶ Fryzuk's PNP ligands (**1E**),¹⁷ Peters' NNN ligand (**1F**),¹⁸ and PSiP ligands (**1G**).¹⁹ Dianionic pincer ligands are relatively rare. The few examples to date include the SiOSi (**1H**)^{20,21} and SiNSi ligands (**1I**)²² reported by Tobita and Bercaw's unsymmetrical NNO ligand (**1J**).²³ The final pincer motif is the trianionic array. Representative examples include the NNN (**1K**)²⁴ and ONO ligands (**1L**)²⁵ by Heyduk, Veige's NCN ligand (**1M**),²⁶ and the OCO ligand (**1N**) reported by Bercaw.²⁷

1.2 Group 9 pincer complexes in C-H bond activation

1.2.1 $C(sp^3)$ -H bond activation: Catalytic alkane dehydrogenation

The first stoichiometric alkane dehydrogenation mediated by a homogeneous metal complex was reported by Crabtree in 1979.²⁸ Catalytic transfer dehydrogenation and acceptorless dehydrogenation of alkanes was then developed by Felkin²⁹⁻³¹ and Crabtree.³²⁻³⁴ The TONs in these systems were limited by the instability of the metal catalysts at the high temperatures required for reaction. Goldman also reported a thermochemical transfer-dehydrogenation of different alkanes and hydrogen acceptors catalyzed by $(PMe_3)_2Rh(CO)Cl$.^{35,36} The rhodium catalyst was very durable, however, the requirement of a H_2 atmosphere restricted the applicability of this system. The

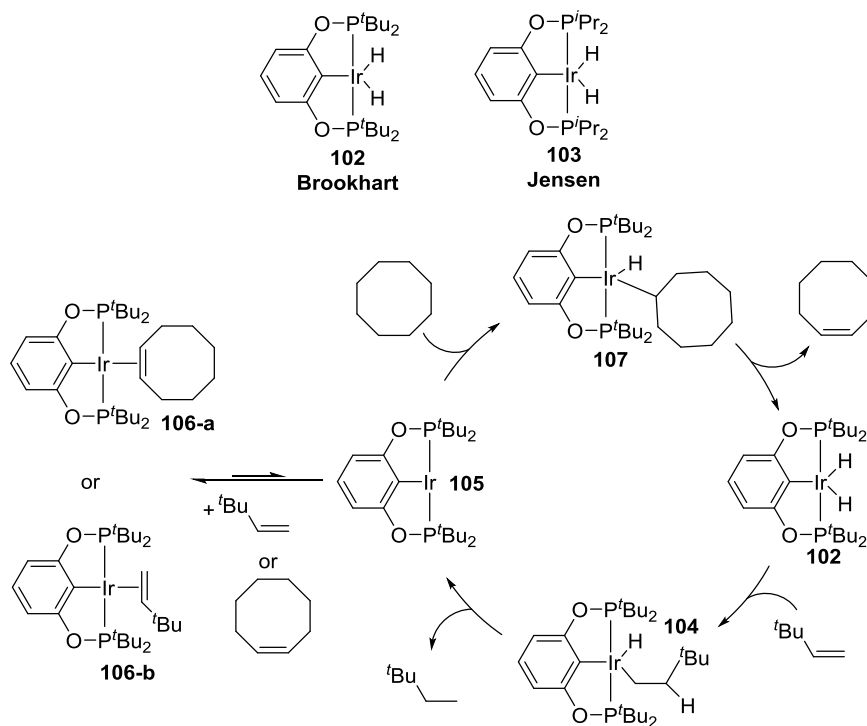
application of pincer complexes to alkane dehydrogenation was first reported by Jensen (Scheme 1-3) in 1996.³⁷ PCP iridium complex **101** displayed high activity for transfer hydrogenation between cyclooctane and *tert*-butylethylene with exceptional thermal stability. The (PCP)Ir motif can be seemed as a chelating mimic of Goldman's [(PMe₃)₂RhCl] system. No observable decomposition was observed after heating at 200 °C for one week. The robustness of **101** induced by the PCP pincer ligand apparently is the key to the extended lifetime of catalysis.



Scheme 1-3. Alkane dehydrogenation with PCP Ir complex by Jensen.

The various modified PCP iridium complexes are active in alkane dehydrogenation.³ Independently developed by Brookhart^{38,39} and Jensen,⁴⁰ one noteworthy modification was the application of bisphosphinite POCOP iridium complexes as catalysts (Scheme 1-4, top). Both **102** and **103** showed significantly higher reactivity than the benchmark catalyst **101** in the transfer hydrogenation between cyclooctane and *tert*-butylethylene. The success of catalytic alkane dehydrogenation by PCP and POCOP iridium complexes did not only limit in dehydrogenation of cycloalkanes but also led to other applications, such as alkane metathesis, dehydroaromatization of *n*-alkanes, dehydrogenation of saturated polyolefins.³ The mechanism proposed for transfer hydrogenation by **102** and **103** is similar to **101**

(Scheme 1-4, bottom). *tert*-Butylethylene inserts into an Ir-H bond of **102** and reductively eliminates to yield (PCP)Ir 3-coordinated species **105** that is in equilibrium with its alkene adducts **106**. Cyclooctane oxidatively adds on the iridium center and undergoes β -H elimination to yield cyclooctene and produces **102** to complete the catalytic cycle.



Scheme 1-4. POCOP iridium complexes as the alkane dehydrogenation catalysts (top) and proposed mechanism of transfer hydrogenation catalyzed by **102** (bottom).

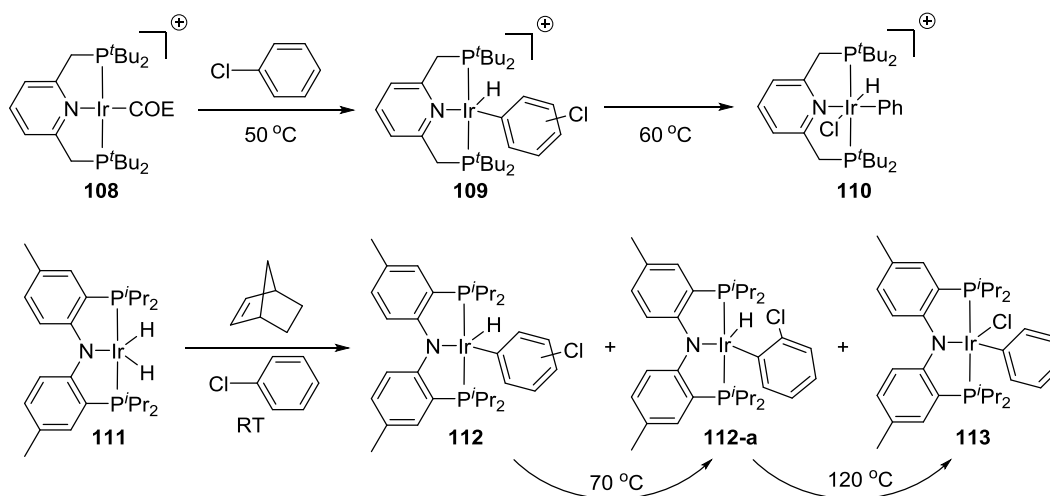
1.2.2 $C(sp^2)$ -H bond activation: C-H vs C-X (X = halide or O) activation

Utilization of aryl halides or aryl esters (ArO_2CR , O_2CR = carboxylate, carbamate, carbonate) in C-C coupling reactions with a Pd(0) or Ni(0) catalyst has been explored intensely and has become one of the most useful synthetic methods.⁴¹⁻⁴³ Recently Rh complexes have also demonstrated their catalytic reactivity in the coupling reactions

where the oxidative addition of C-X (X = halide or O) appears to be the crucial step.⁴⁴⁻⁴⁹

In these substrates, the metal has a choice between multiple C-H bonds or a C-X bond; hence the selectivity is an important question.

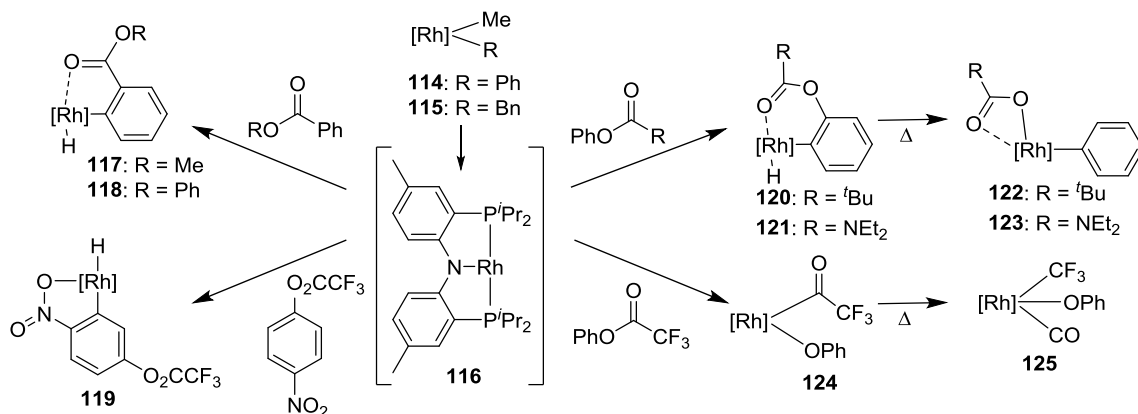
Milstein showed only C-H activation of halobenzenes occurs when using the cationic pyridine based PNP Ir complex **108** (Scheme 1-5, top) and yields aryl halide hydride product **110** after mild heating.⁵⁰ In Ozerov's research,⁵¹ the reaction of diarylamido PNP Ir complex **111** and norbornene in chlorobenzene yields a mixture of C-H oxidative addition products **112** (Scheme 1-5, bottom). Heating the mixtures at 70 °C showed isomerization of other isomers of **112** into **112-a**. Further heating at even higher temperature led to >80% C-Cl oxidative addition product **113**.



Scheme 1-5. C-H vs C-Cl oxidative addition on Ir pincer complexes by Milstein (top) and Ozerov (bottom).

Studies of C-H oxidative addition of aryl halides⁵² and aryl carboxylates⁵³ (with various functional groups) to the (PNP)Rh fragment have also been reported. For aryl carboxylates (Scheme 1-6), only C-H oxidative addition onto the rhodium center was

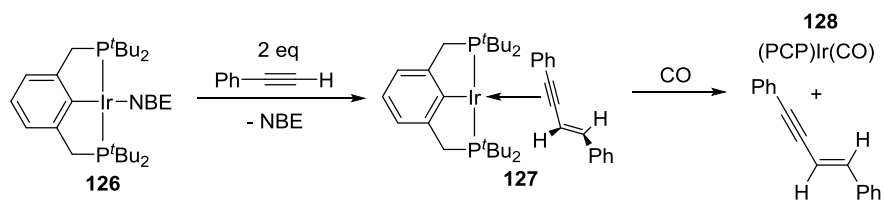
observed when PhO₂CPh and MeO₂CPh were used as substrates. Direct acyl-O oxidative addition was observed for PhO₂CCF₃. For PhO₂C^tBu and PhO₂CNEt₂, activation of the *ortho*-C-H bond occurred first and thermolysis led to phenyl-O oxidative addition products.



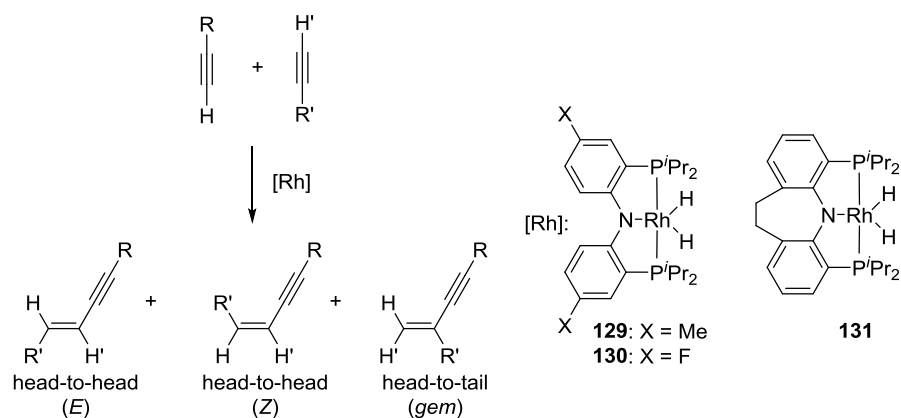
Scheme 1-6. Reaction of PNP Rh fragment with various esters.

1.2.3 C(sp)-H bond activation: Alkyne dimerization

Alkyne dimerization is a 100% atom-economical method of synthesizing 1,3-conjugated enynes. The stoichiometric dimerization of terminal alkynes by a PCP iridium pincer complex **126** was first reported by Krogh-Jespersen and Goldman⁵⁴ (Scheme 1-7). Following the thorough mechanistic studies, the authors concluded the dimerization does not proceed catalytically due to the steric crowding which inhibits C-C reductive elimination.



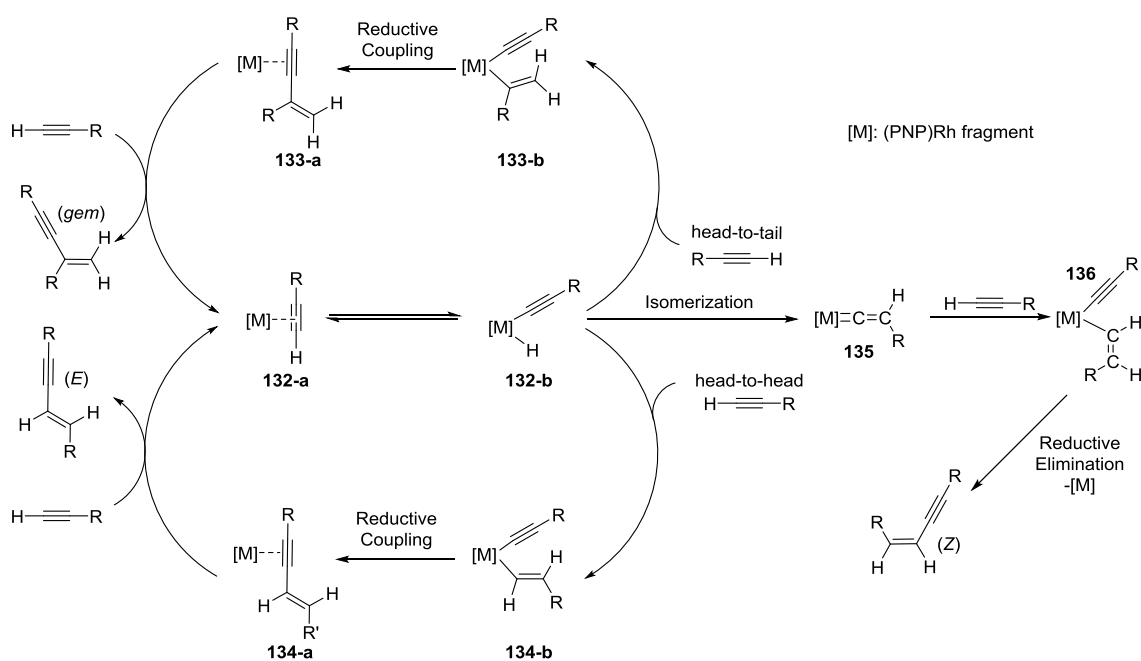
Scheme 1-7. Stoichiometric dimerization of phenylacetylene.



Scheme 1-8. Catalytic alkyne dimerization by (PNP)Rh complexes.

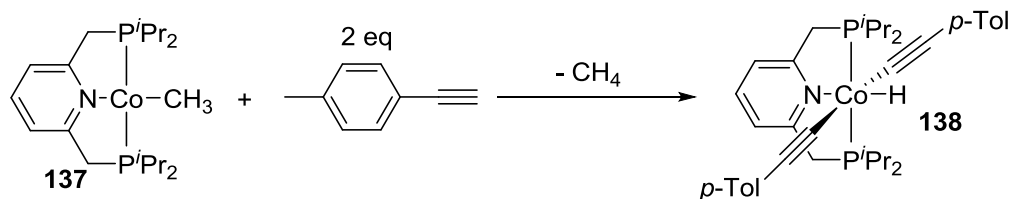
In 2006, Ozerov group reported three PNP rhodium complexes which are capable of catalyzing alkyne dimerization (Scheme 1-8).⁵⁵ The proposed mechanism of the catalytic reaction is shown at Scheme 1-9. The alkyne complex **132-a** is generated from the dihydride precatalyst with two equivalents of alkyne. Oxidative addition of C(sp)-H bond gives the Rh(III) hydride alkynyl complex **132-b**. Insertion of another equivalent of alkyne followed by reductive coupling and ligand displacement leads to the 1,3-enyne products. The selectivity between *gem*- and *E*- isomers is determined by the difference in the reaction barrier of 1,2- or 2,1-insertion. The *Z*-isomer is generally not observed.

The rhodium complex **131** supported by a “tied” PNP ligand appeared as a highly regioselective catalyst that led to >90% *E*-selectivity with both aliphatic and aromatic substrates. Originally the selectivity difference between **131** and **129/130** was believed to be due to the greater steric pressure induced at the rhodium center by the tied ligand compared to the untied ligands. However, after careful examination of a series of related PNP, PCP, and POCOP ligands, no clear trends were observed.⁵⁶



Scheme 1-9. Possible mechanisms for alkyne dimerization catalyzed by (PNP)Rh complexes.

It is also relevant to mention that Chirik's recent report discussing the reaction of Co(I) methyl complex **137** with two equivalents of terminal alkynes immediately to yield **138** with the loss of CH₄ (Scheme 1-10).⁵⁷ **138** has been characterized by X-ray crystallography and confirmed as an octahedral Co(III) complex with *trans*-acetylide ligands. **138** is stable both in the solid state and in benzene-*d*₆ at room temperature. The catalytic reactivity of **138** towards to alkynes is still under investigation.

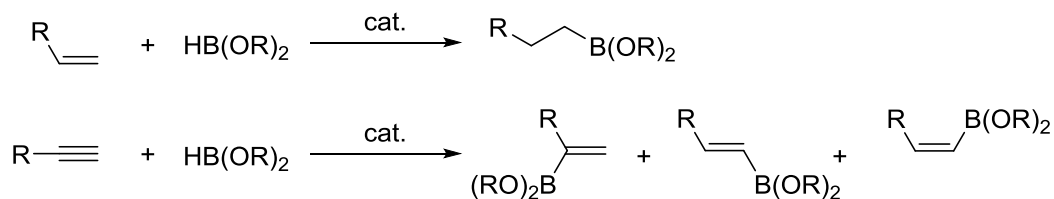


Scheme 1-10. Oxidative addition of terminal alkyne with a PNP cobalt complex.

1.3 Hydroboration and C-H borylations (dehydrogenative borylation)

1.3.1 Overview

The importance of organoboron compounds in organic chemistry is evident from the Nobel Prize awarded to Herbert C. Brown⁵⁸ (1979) and Akira Suzuki⁵⁹ (2010) for their contribution to the development of new synthetic methodologies involving C-B bonds. Numerous methods have been employed to synthesize organoboron compounds,⁶⁰ and one of the oldest and most important methods is hydroboration. Hydroboration refers to the addition of H-B bonds onto C-Y (Y = C, N, O) double bonds or C-C triple bonds. Dialkylboranes can react with alkenes or alkynes without catalysts in a *syn*-addition and *anti*-Markovnikov fashion to yield alkylboranes or alkenylboranes.⁶¹ The reactions between dialkoxyboranes (e.g. pinacolborane or catecholborane) with alkenes or alkynes are usually sluggish and require catalysts (Scheme 1-11).^{62,63} The use of catalysts is not merely to accelerate hydroboration but is also required for regioselectivity or chemoselectivity.

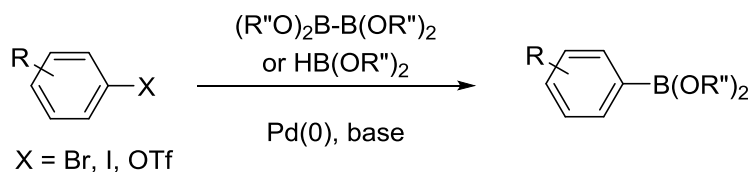
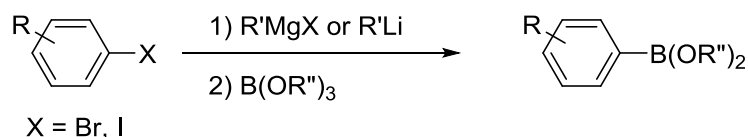


Scheme 1-11. Hydroboration of alkenes or alkynes with dialkoxyboranes.

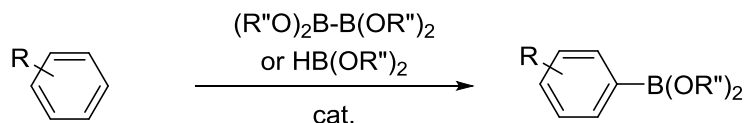
In the last two decades, dehydrogenative C-H borylation has become another attractive approach to organoboron compounds,^{64,65} especially in making arylboronates. Arylboronates are traditionally synthesized in two ways. First, making aryl lithium or

Grignard reagents from aryl halides then reacting with boric ester.⁶⁰ Second, reacting aryl halides with diboron reagents or boranes under palladium catalysis to yield arylboronates (Scheme 1-12, top).⁶⁶ Both protocols would generate stoichiometric salts as the by-products. Synthesis of arylboronates through direct C-H borylation is more atom-economic and environmentally friendly (Scheme 1-12, bottom).^{67,68} Besides arenes, dehydrogenative borylation of C(sp³)-H bonds in alkanes,⁶⁹⁻⁷¹ C(sp²)-H bonds in alkenes^{72,73} as well as benzylic⁷⁴ and allylic⁷⁵ borylation have also been reported.

Traditional syntheses of arylboronates:



Dehydrogenative borylation of arenes:

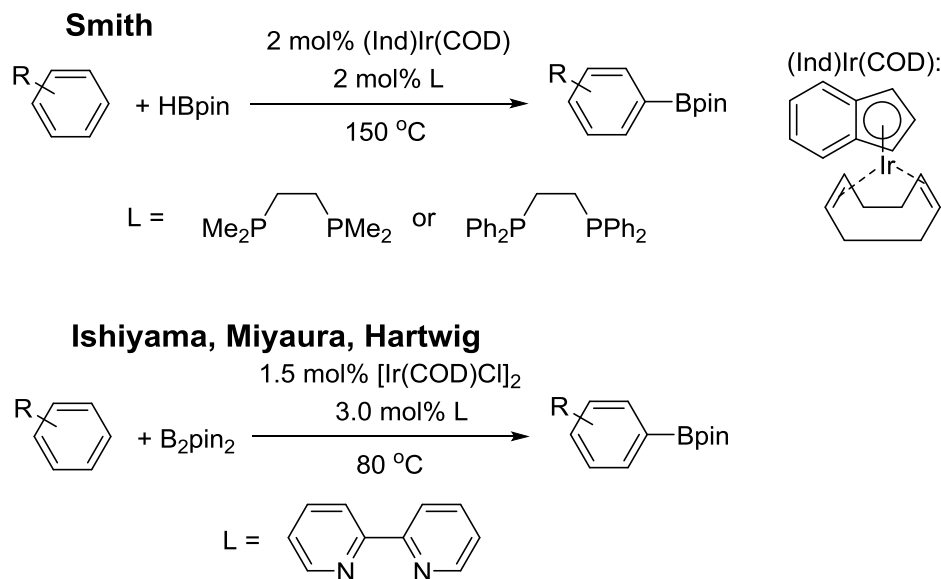


Scheme 1-12. Traditional methods for making arylboronates and dehydrogenative borylation of arenes.

1.3.2 Arene borylation by Ir bipyridine & bisphosphine complexes

In 2002, Smith⁶⁷ and Hartwig⁶⁸ et al. independently reported dehydrogenative arene borylation catalyzed by iridium complexes (Scheme 1-13). Bisphosphine ligands were employed in Smith's system and the catalysis generally required heating to 100 – 150 °C.

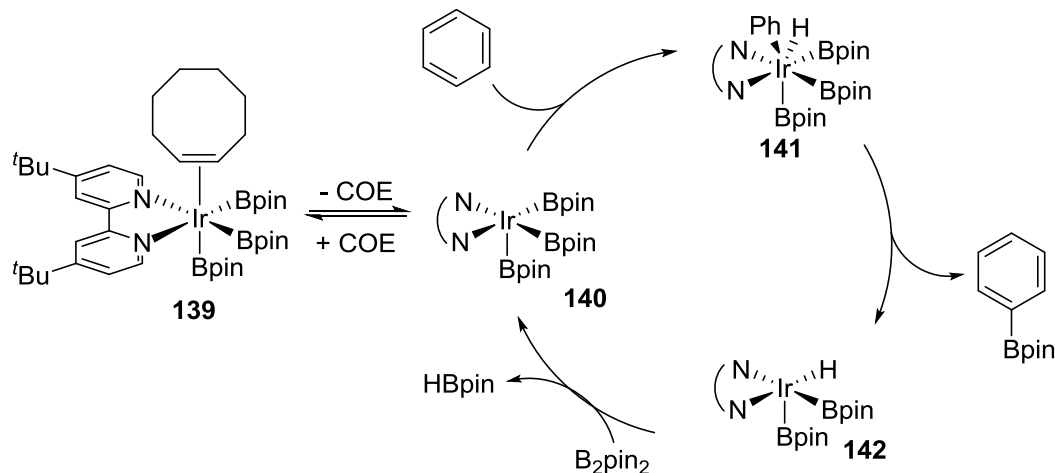
In contrast, the reactions catalyzed by the Hartwig's iridium bipyridine complexes would function at a lower temperature range, between room temperature and 80 °C. The iridium bipyridine systems have been optimized with TON exceeding 24,000 recorded in the most favorable case.⁷⁶



Scheme 1-13. Initial reports of arene borylation by Smith (top) and Ishiyama, Miyaura and Hartwig (bottom).

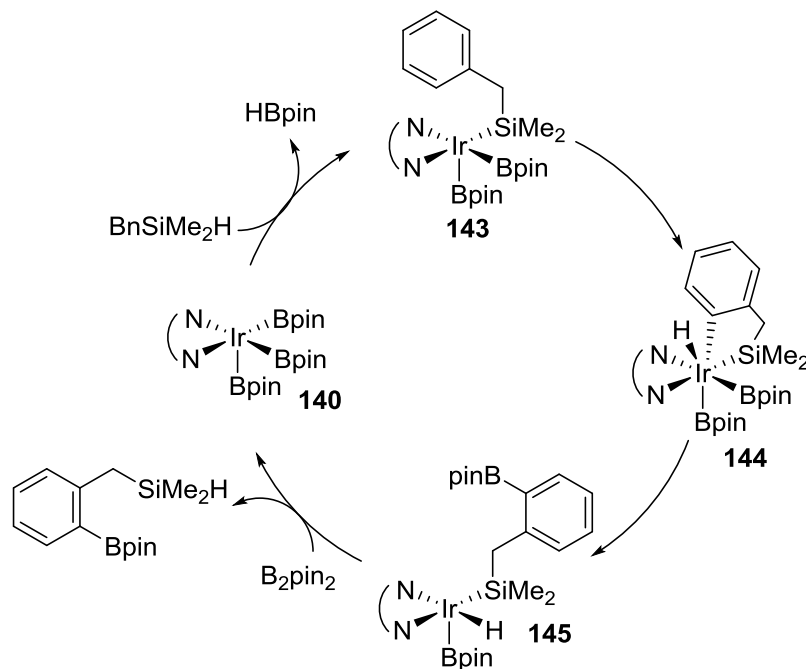
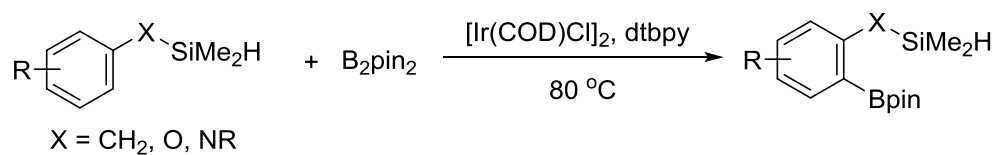
Arene borylation by Ir bipyridine and bisphosphine complexes are both favor mechanisms involving Ir(III)/Ir(V) cycles based on experimental and DFT studies.^{67,76-78} A representative proposed mechanism of arene borylation catalyzed by the iridium bipyridine system is depicted in Scheme 1-14.⁷⁶ Triboryl cyclooctene complex **139** has been independently synthesized and its boryl transferring ability has been demonstrated.^{68,76} The labile cyclooctene ligand dissociates from **139** to generate an empty coordination site for incoming arenes. C(sp²)-H activation then occurs on the

electron-rich Ir(III) center of **140** to form an Ir(V) intermediate **141**. C-B bond formation yields Ar-Bpin through reductive elimination and reacts with B₂pin₂ to regenerate **140**.



Scheme 1-14. Proposed mechanism for the iridium-catalyzed borylation of arenes.

Tremendous subsequent research has made iridium catalyzed arene borylation as one of the most powerful methods for the synthesis of arylboronates, and these methodologies have also been applied to polymer functionalization and natural products total syntheses.⁶⁴ The regioselectivity in borylation of monosubstituted arenes is predominately controlled by the steric factors, resulting in a mixture of *m*- and *p*-disubstituted products. In 2008, Hartwig described the selective directed *ortho*-borylation of arenes by using dialkyl hydrosilyl groups as the directing groups (Scheme 1-15).⁷⁹ The origin of *ortho*-selectivity is proposed to be from initial activation of the silane moiety yielding a bisboryl silyl species **143**. C-H bond cleavage of this intermediate would then be directed at the *ortho* position through the chelation effect.



Scheme 1-15. *ortho*-Directed arene borylation and proposed mechanism.

1.3.3 Application of pincer complexes in borylation

1.3.3.1 Dehydrogenative borylation of arenes

Numerous examples of arene borylation catalyzed by pincer complexes have been reported (Figure 1-1).⁸⁰⁻⁸⁷ In general, the performances of these pincer complexes did not reach the height of Hartwig's and Smith's systems that was described in the last section. Relatively high catalyst loading (5 mol%) are usually required to achieve reasonable yields.

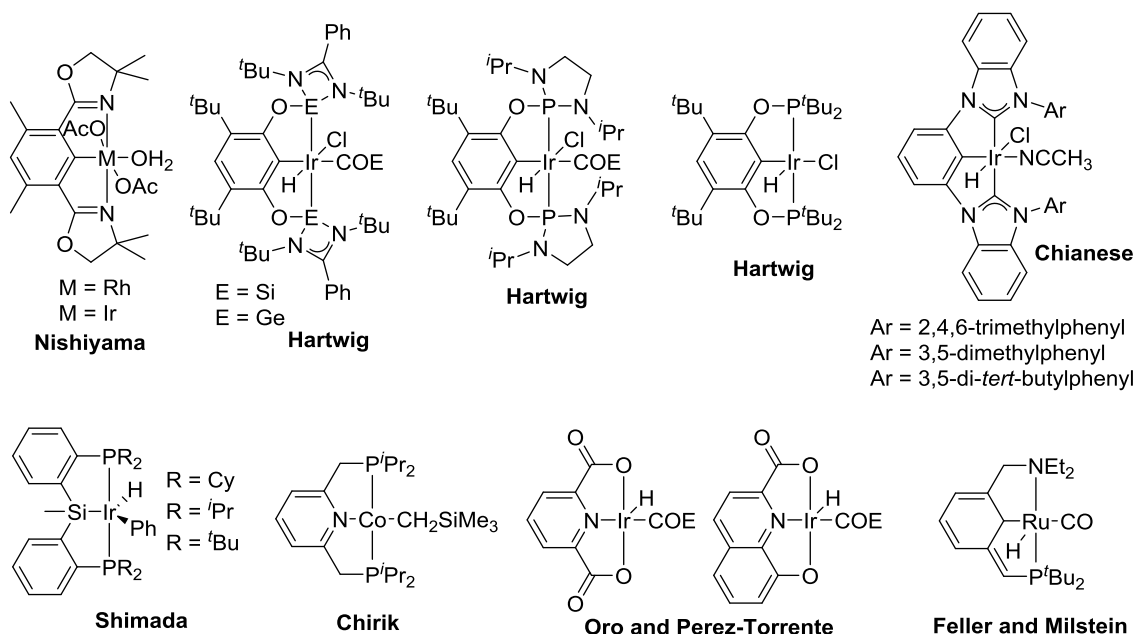
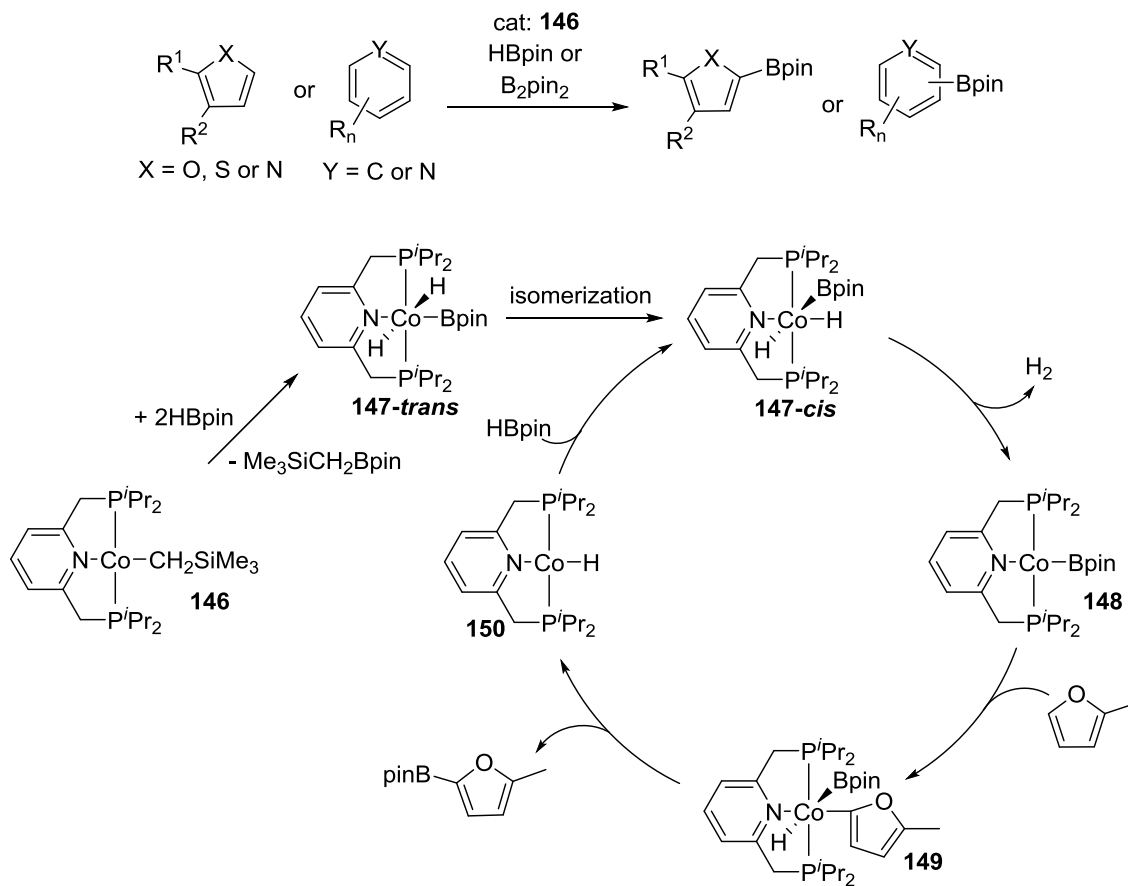


Figure 1-1. Various pincer catalysts for arene borylation.

Nevertheless, it is worthy to mention a rare example of cobalt-catalyzed arene borylation by Chirik (Scheme 1-16, top).⁸³ Several PNP and NNN cobalt pincer complexes have shown their ability to catalyze borylation of methylfuran and **146** is the most active catalyst. Using 0.02 mol% of **146**, a TON close to 5000 was recorded for the borylation of methyl furan-2-carboxylate at room temperature. **146** also showed impressive borylation performance on other heteroarenes and arenes. A plausible mechanism for **146** catalyzed borylation of furan is depicted in the bottom of Scheme 1-16. The cobalt precatalyst **146** first reacts with two equivalents of HBpin to yield **147-trans** which was observed in-situ by NMR spectroscopies. **147-trans** then isomerizes to **147-cis** and eliminates dihydrogen to give boryl complex **148**. C-H activation of furan

occurs on the cobalt center then undergoes reductive elimination to furnish the product.

Finally HBpin oxidatively adds onto **150**, regenerating **147-cis**.

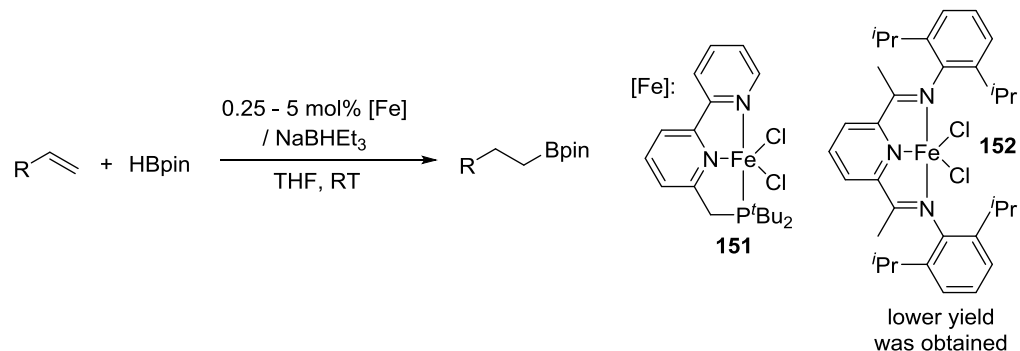


Scheme 1-16. Cobalt-catalyzed arene borylation (top) and proposed mechanism for borylation of methylfuran by **146** (bottom).

1.3.3.2 Hydroboration of alkenes

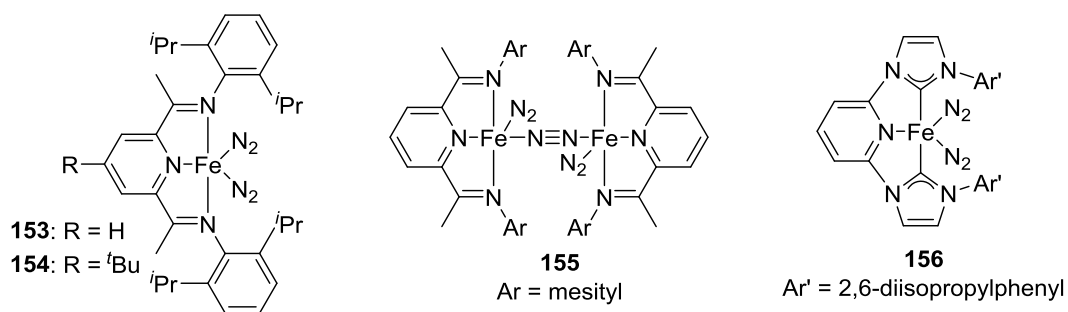
Comparing to other C(sp³) organometallic nucleophiles, the high stability of alkylboronates makes them valuable building blocks in organic synthesis.^{60,88} Hydroboration of alkenes by Rh and Ir complexes, especially Wilkinson's catalyst, has been used extensively for alkylboronates production.^{89,90} However, side reactions and relatively high catalyst loadings using expensive metals were still problematic in many

cases. The first example of Fe-catalyzed alkene hydroborations was reported by Huang (Scheme 1-17).⁹¹



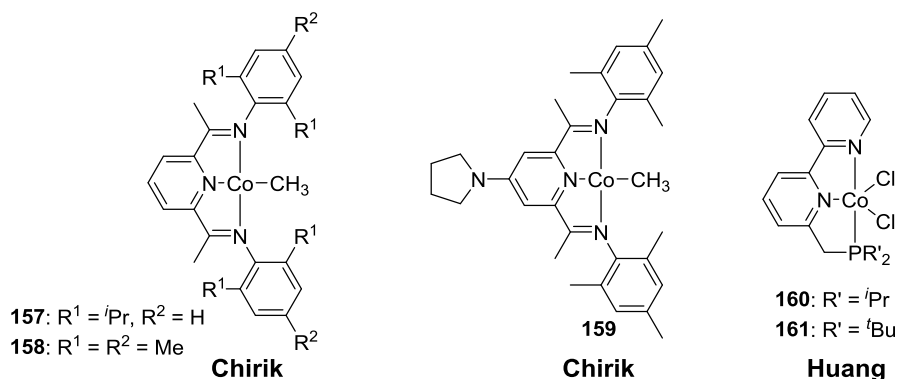
Scheme 1-17. Iron pincer complex catalyzed alkene hydroboration by Huang.⁹²

Using the iron dichloride complex **151** supported by the Milstein PNN ligand⁹² as the precatalyst, excellent yields were obtained with aliphatic alkenes upon addition of NaHBET₃. In the presence of CH₃CN, reactions of vinylarenes with HBpin exclusively formed alkylboronates. Unlike what is usually observed when Rh and Ir complexes are used as the catalysts, no hydrogenation and dehydroborylation was detected. Soon after Huang's report, Chirik also demonstrated several iron dinitrogen pincer complexes are capable of catalyzing alkene hydroboration (Scheme 1-18),⁹³ including **153** which is analogous to **152** that Huang was using in the catalyst screening.



Scheme 1-18. Iron dinitrogen complexes as alkene hydroboration catalysts by Chirik.

After the success in iron catalysis, alkene hydroboration catalyzed by cobalt pincer compounds was also reported by Chirik⁸³ and Huang⁹⁴ (Scheme 1-19). Compared to iron catalysis, exclusive hydroboration of vinylarenes was observed by cobalt catalysts without the need for any additives. Notably, an unprecedented TON (19,800) and TOF (40,000 h⁻¹) was recorded when using **160** as the catalyst.⁹⁴

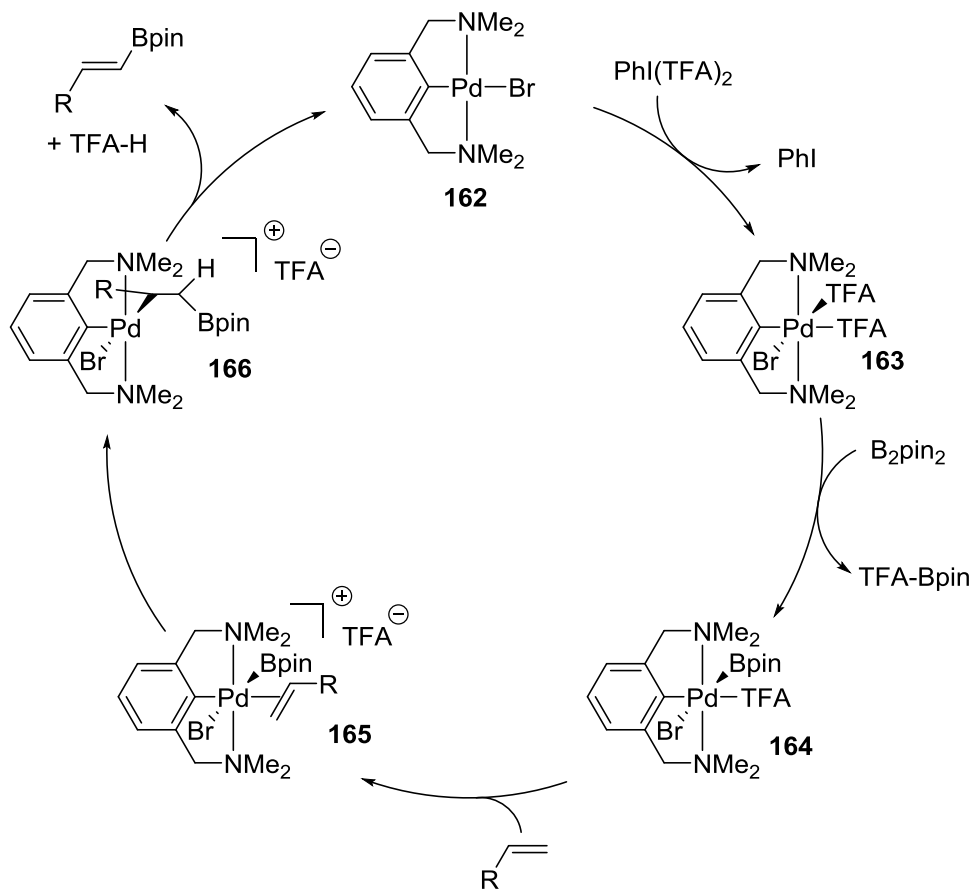


Scheme 1-19. Cobalt complexes as alkene hydroboration catalysts by Chirik and Huang.

1.3.3.3 Dehydrogenative borylation of alkenes

Dehydrogenative borylation of alkenes was originally reported as the side reaction of the hydroboration. Instead of avoiding this “deleterious” pathway, several fine-tuned catalyst systems have been reported to yield alkenylboronates selectively.⁹⁵ Szabó discovered a highly vinylic selective C-H borylation that was catalyzed by a palladium NCN pincer complex **162** (Scheme 1-20, top).⁹⁶ The substrate scope was limited to cyclic alkenes or functionalized terminal alkenes, and the reaction was carried out under oxidative conditions with hypervalent iodine reagent PhI(TFA)₂ as the stoichiometric oxidant. A proposed mechanism incorporating a Pd(II)/Pd(IV) cycle is shown in Scheme 1-20 (bottom). **162** is first oxidized by PhI(TFA)₂ to Pd(IV) complex **163** followed by

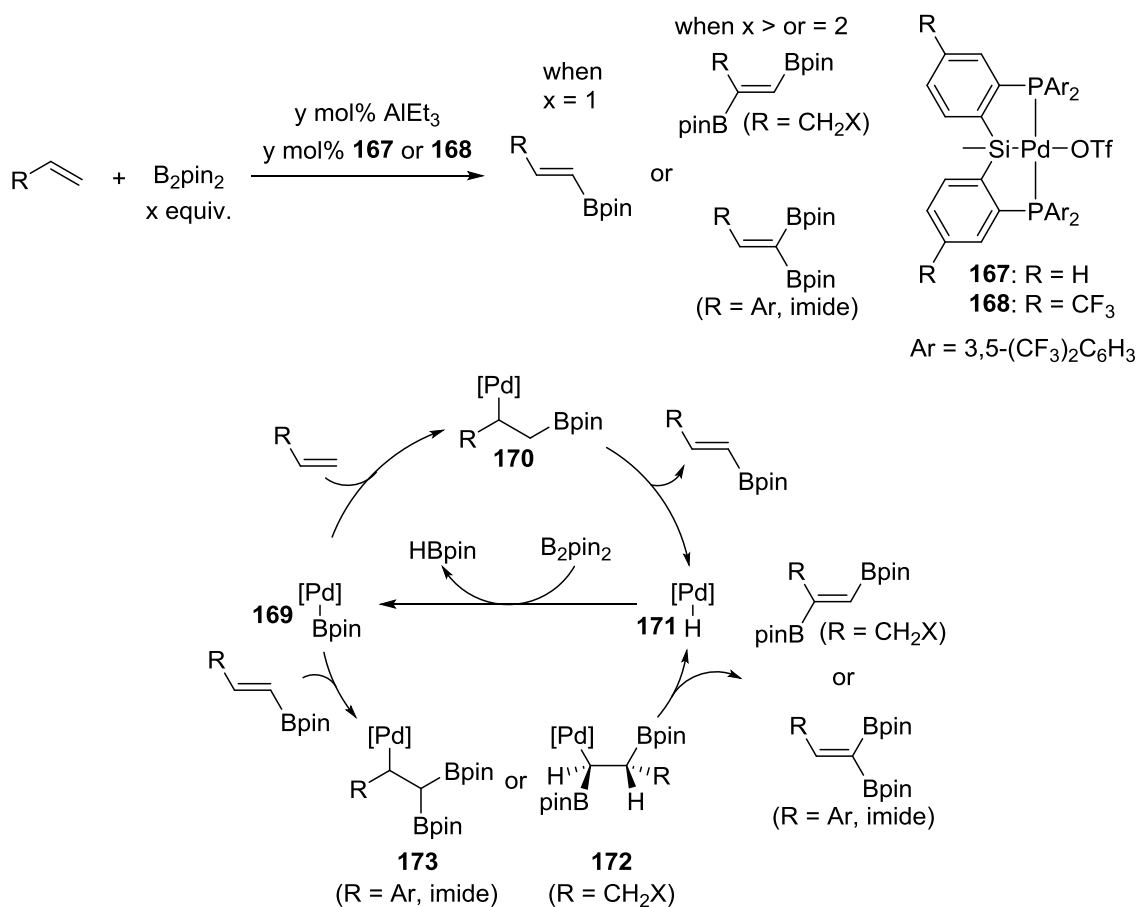
transmetallation with B_2pin_2 . An alkene then inserts to the Pd-B bond and eliminates an alkenylboronate to regenerate **162**.



Scheme 1-20. Dehydrogenative borylation of alkenes by a NCN pincer palladium **162** (top) and proposed mechanism (bottom).

Iwasawa later presented dehydrogenative borylation of alkenes catalyzed by PSiP Pd complexes with a wider substrate scope (Scheme 1-21, top).^{97,98} More impressively, diborylalkenes can be obtained simply by controlling the number of equivalents of B_2pin_2 . In the stoichiometric reaction study, the corresponding palladium boryl complex has been synthesized independently from **167** and shown to react with styrene to form the corresponding alkenylboronate. In contrast to Szabó's system, a Pd(0)/Pd(II)

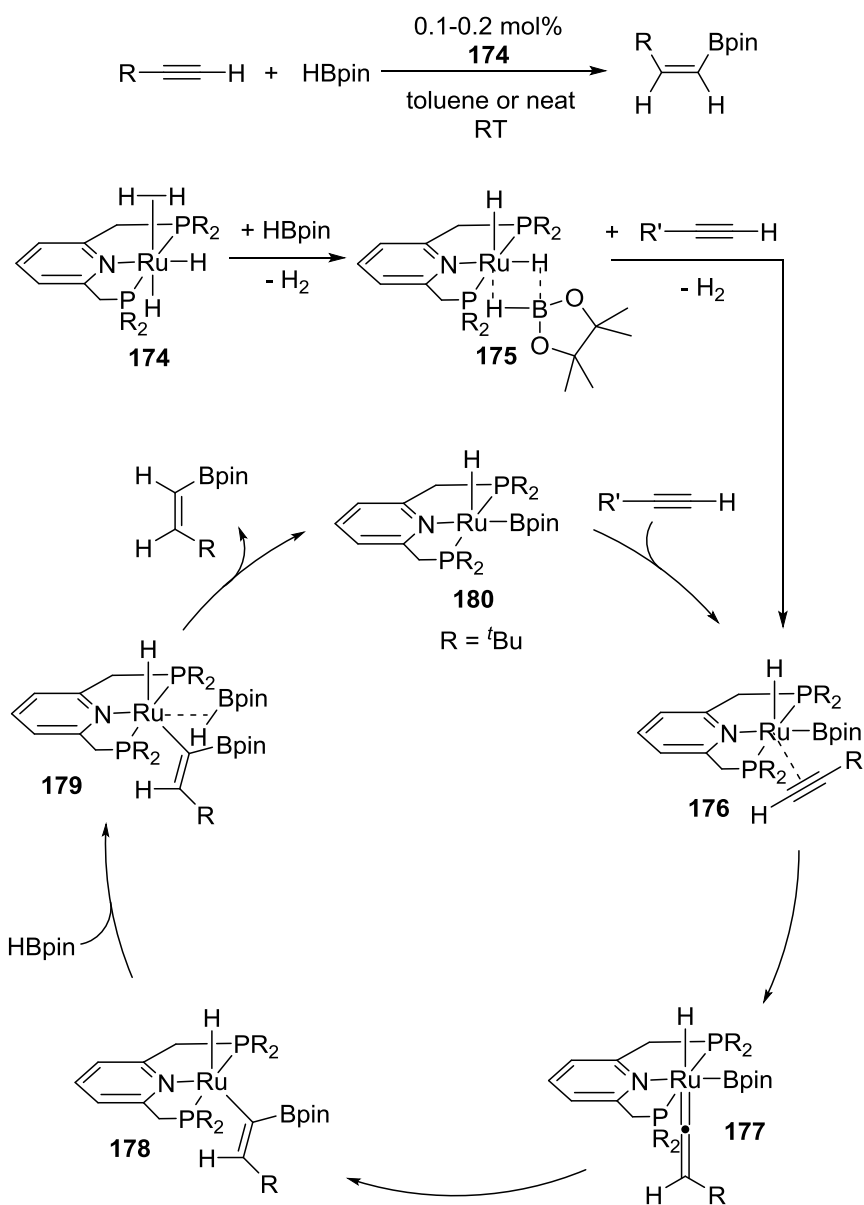
catalytic cycle is proposed for the PSiP Pd system (Scheme 1-21, bottom). The catalytic cycle starts from insertion of an alkene to the Pd-B bond of **169** and performs β -H elimination to yield an alkenylboronate. The forming palladium hydride complex **171** can react with B_2pin_2 to regenerate **169**. An alkenylboronate can undergo a second borylation in the presence of an excess of B_2pin_2 through a similar insertion/ β -H elimination sequence. The regioselectivity of the second borylation is dictated by the R-group on the alkenes.



Scheme 1-21. Dehydrogenative borylation of alkenes by a PSiP pincer palladium (top) and proposed mechanism (bottom).

1.3.3.4 Hydroboration of terminal alkynes

Hydroboration of terminal alkynes with dialkylboranes typically undergoes *anti*-Markovnikov and *syn*-addition resulting in *E*-vinylboronates as products.⁶¹ Catalytic reactions of terminal alkynes with less active dialkoxyboranes have also been reported with different levels of regioselectivity (mainly *E*-selective).^{62,63} In 2012, Leitner reported an unusual *Z*-selective hydroboration of terminal alkynes catalyzed by a PNP ruthenium pincer hydride complex **174** (Scheme 1-22, top).⁹⁹ Good to excellent yields were obtained for various terminal alkyl and aryl alkynes with >90% *Z*-selectivity with remarkably low catalyst loading. **174** reacts with HBpin to yield the boryl complex **175** with evolution of H₂. Analysis by X-ray crystallography shows three hydride ligands are located on the same plane. One is a terminal hydride and the other two hydrides are bridging to the boron on the Bpin. Analogous yield and selectivity were observed when using isolated **175** as the catalyst, and examination of the reaction mixtures after catalysis with ³¹P NMR spectroscopy showed **175** as the only P-containing species. These findings suggest **175** as the entry point into the catalytic cycle. Combining with the deuterium-labeled experiment, the mechanism for the *Z*-selective hydroboration was proposed (Scheme 1-22, bottom).



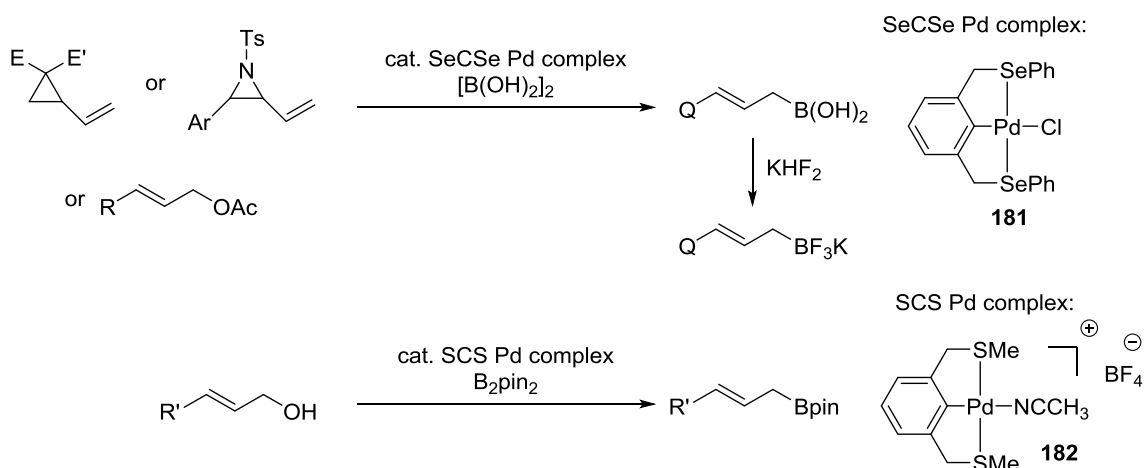
Scheme 1-22. Z-selective hydroboration of terminal alkynes and proposed mechanism.

175 is first obtained from **174** and HBpin, and reacts with a terminal alkyne to yield **176** with release of H₂. The terminal alkyne in **176** undergoes 1,2-hydrogen migration to the vinylidene intermediate **177**. Pinacolborate then couples to the α-carbon on vinylidene to form the C-B bond in **178**. Coordination of HBpin and liberation of

alkenylboronate yields **179**. Finally, terminal alkyne binds to ruthenium to close the catalytic cycle. The unique *Z*-selectivity presumably comes from the steric repulsions in the formation of vinylidene intermediate **177**. The mechanism has been further supported and examined in details with DFT calculation by Chen.¹⁰⁰

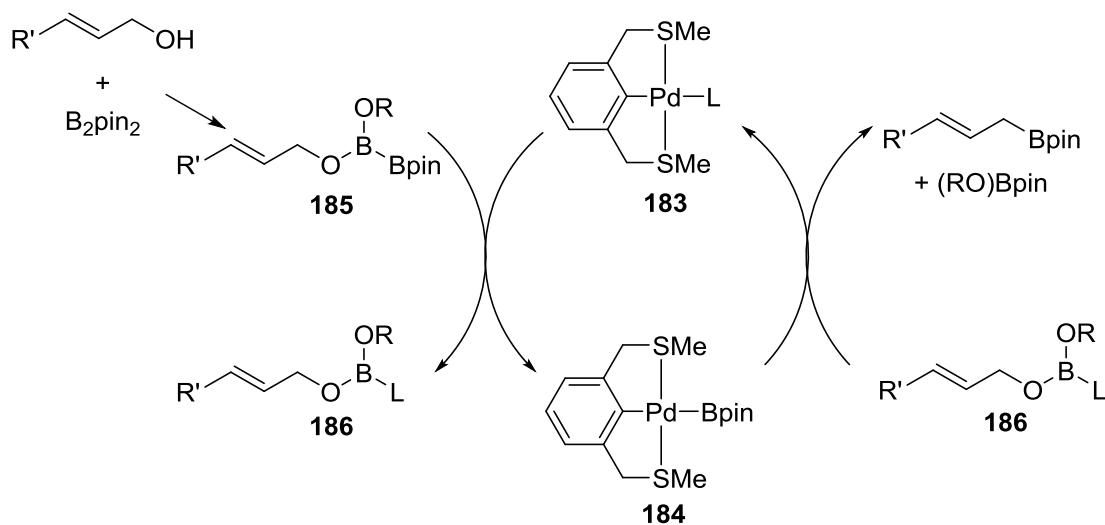
1.3.3.5 Borylation of other substrates

Szabó demonstrated that SeCSe Pd pincer complex **181** could catalyze boryl transfer reaction of vinyl cyclopropanes, vinyl aziridines and allyl acetates with tetrahydroxydiboron to yield allylboronic acids (Scheme 1-23, top).¹⁰¹ The unstable allylboronic acids were further treated with KHF_2 to obtain the stable potassium trifluoro(allyl)borates. The substrate scope was later extended to allyl alcohols¹⁰² and B_2pin_2 could be used as a cheaper boron source when using **182** as the catalyst to directly yield allylboronates (Scheme 1-23, bottom).¹⁰³



Scheme 1-23. Borylation of vinyl cyclopropanes, vinyl aziridines and allyl acetates (top), and borylation of allyl alcohols (bottom).

A plausible mechanism of borylation of allyl alcohol was proposed in Scheme 1-24. The first step is transesterification of B_2pin_2 with allyl alcohol to obtain **185** that may be catalyzed by **183**. The Bpin moiety then transfers from **185** to palladium to give boryl complex **184**. **184** finally reacts with activated allyl alcohol substrate **186** to result in allylboronate and alkoxy-Bpin.¹⁰³



Scheme 1-24. Proposed mechanism of borylation of allyl alcohols.

CHAPTER II

CATALYTIC DEHYDROGENATIVE BORYLATION OF TERMINAL ALKYNES

BY A SiNN Pincer Complex of Iridium¹

2.1 Introduction

Conversion of hydrocarbon carbon-hydrogen bonds into carbon-boron bonds has progressed over the last two decades from initial reports^{104,105} to a prominent and widely used synthetic method.^{64,65,106} Dehydrogenative borylation of aromatic C-H bonds has been brought to particularly impressive heights with the advent of highly active iridium catalysts of Hartwig et al.⁶⁸ and Smith et al.⁶⁷ with supporting bipyridine and bidentate phosphine ligands. Multiple examples of catalytic conversion of unactivated C-H bonds in alkanes,⁶⁹⁻⁷¹ benzylic⁷⁴ and allylic C(sp³)-H bonds,⁷⁵ as well as C(sp²)-H bonds in alkenes^{72,73} have been reported (See Figure 2-1). Conspicuously absent from this list are the C(sp)-H bonds of terminal alkynes. C(sp)-H bonds are quite strong thermodynamically, but possess substantially higher acidity than C(sp²)-H and C(sp³)-H bonds in hydrocarbons without strongly electron-withdrawing groups. Thus, activation of C(sp)-H bonds is often not viewed as a challenge because they can be fairly reliably “activated” by deprotonation. In spite of this, catalytic dehydrogenative C(sp)-H borylation of terminal alkynes (referred to as DHBTA from here on) has not yet been reported.

¹ Reprinted in part with permission from “Catalytic Dehydrogenative Borylation of Terminal Alkynes by a SiNN Pincer Complex of Iridium” by Lee, C.-I.; Zhou, J.; Ozerov, O. V. *J. Am. Chem. Soc.* **2013**, *135*, 3560, Copyright [2013] by American Chemical Society. In this chapter, all DFT calculations are done by Dr. Jia Zhou.

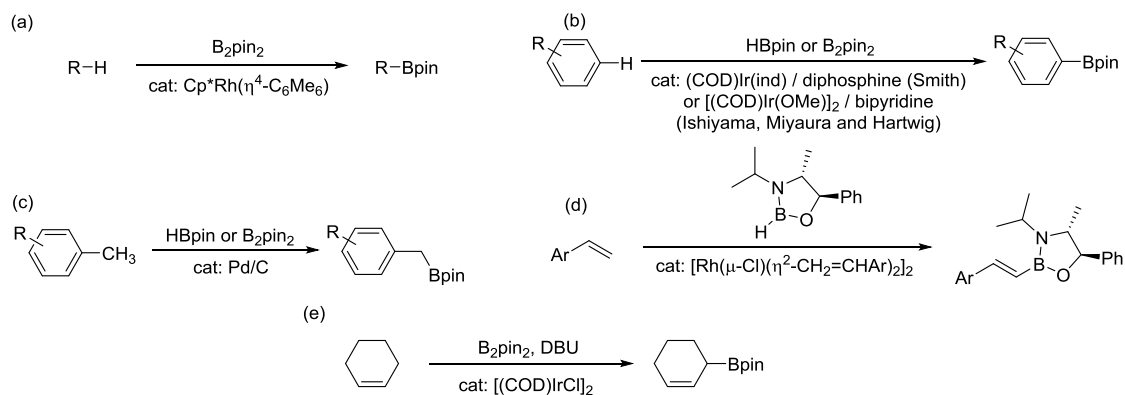


Figure 2-1. Representative examples of dehydrogenative borylation (a) alkane borylation by Hartwig (b) arene borylation by Ishiyama, Miyaura, Hartwig and Smith (c) benzylic borylation by Ishiyama and Miyaura (d) alkene borylation by Brown (e) allylic borylation by Szabó.

The products of DHBTA, alkynylboronic esters (alkynylboronates), are valuable building blocks in organic synthesis. A very recent review summarized the use of alkynylboron compounds (alkynylboronates, dialkylalkynylboranes, and others) in organic synthesis.¹⁰⁷ Alkynylboronates can be viewed as potentially convenient coupling partners in the alkynyl version of the Suzuki coupling, similar to the most common use of aryl- and alkenyl-boronic esters, but their convenience is severely diminished by sensitivity to moisture.^{108,109} Even more attractive are their reactions that utilize the boryl-substituted $C\equiv C$ functionality “simply” as a substituted alkyne: cyclotrimerization,¹¹⁰ [3+2] cycloaddition,¹¹¹ cyclopentenone synthesis,¹¹² hydrozirconation,¹¹³ enyne metathesis,¹¹⁴ and others.¹¹⁵⁻¹¹⁸ These reactions produce new organic structures containing C-B bonds that would be difficult or impossible to introduce by late-stage C-H or C-X borylation and that themselves could be used for C-C bond forming Suzuki-type coupling or C-B oxidation reactions. Currently, the

attractiveness of alkynylboronic esters is limited by the three-step conventional synthesis that involves treatment of the deprotonated alkyne with a boric ester, followed by carefully controlled protonation with dry Brønsted acids.¹¹⁹ Dehydrogenative C-H borylation would clearly be a much more attractive route that would help unleash the full synthetic promise of alkynylboronic esters. It seems to us that the challenge in discovering a method for catalytic DHBTA to alkynylboronates lies not “merely” in the finding of a catalyst that would convert a C-H bond of the terminal alkyne to a C-B bond, but rather in the finding of such a catalyst that does not more rapidly catalyze addition of a B-H bond across the triple bond. Traditionally, terminal alkynes react with dialkylboranes to yield alkenylboranes.⁶¹ Catalysis of hydroboration of alkynes with the less reactive dialkoxyboranes (e.g., pinacolborane and catecholborane) has also been reported with various levels of regioselectivity.^{62,63}

The C-H activation step of the state-of-the-art iridium catalysts for aromatic C-H borylation apparently involves a concerted hydrogen transfer from a coordinated arene to a boryl ligand on trivalent iridium. This hydrogen transfer has significant proton transfer character and the basic character of the Ir-boryl bond is boosted by two other, strongly donating spectator boryl ligands attached to Ir.⁷⁸ Our group’s interest in transition metal complexes of pincer ligands (typically defined as tridentate, meridionally or T-shaped binding ligands)^{1,120} led us to wonder whether this step is adaptable to a pincer-derived framework. Without pursuing a precise structural analogy to the Hartwig/Smith Ir catalysts, we envisioned that a tridentate, dianionic pincer ligand carrying a strong donor comparable to a boryl might provide an operationally related environment.

Incorporating boryl donors into pincer ligands remains somewhat of a challenge, and we focused on silyl as another ligand of strong σ -donating ability. We conceived of a ligand combining a central amido site for ease of attachment to a metal, a side silyl donor, and another neutral side donor opposite the silyl. We now report our success in synthesizing such a ligand, characterizing its iridium complexes that contain unusual structural features, and their successful use in catalysis. Although our original expectations of broad-scope C-H borylation catalysis have not come to pass, the catalytic system we arrived at is very active and selective in C-H borylation of terminal alkynes.

2.2 Results and discussion

2.2.1 Synthesis of the SiNN ligand

The synthesis of the proto-pincer ligand **204** is depicted in Figure 2-2. 4-Toluidine served as the precursor for both “halves” of the ligand. Selective bromination of 4-toluidine with NBS gave 2-bromo-4-toluidine in excellent yield. We then employed a variation of the Skraup reaction¹²¹ to synthesize 8-bromo-6-methylquinoline. This reaction produced a mixture of 8-bromo-6-methylquinoline and 6-methylquinoline, but optimization of the conditions enabled us to obtain a 96:4 mixture with **202** as the major component, in 80% isolated yield on >10 g scale. The mixture was successfully used directly in the subsequent syntheses of **203Br** and **203H**. 8-Bromoquinoline has been used in ligand synthesis before,^{18,122-124} but is relatively expensive or needs to be made from the 8-aminoquinoline via diazotization.¹²⁵ Our simple and scalable synthesis of **202** can be quite useful for constructing other polydentate ligands with a quinoline unit. We originally envisioned Buchwald-Hartwig coupling of **202** with 4-toluidine to give

203H, followed by bromination to obtain **203Br**. Unfortunately, bromination of **203H** led to a different isomer **203Br-x**.¹²⁶ We were thus forced to use 2-bromo-4-toluidine in the coupling with **202**. This was not ideal because both substrates possessed an aryl bromide functionality, but we were nonetheless able to isolate **203Br** in 44% yield.

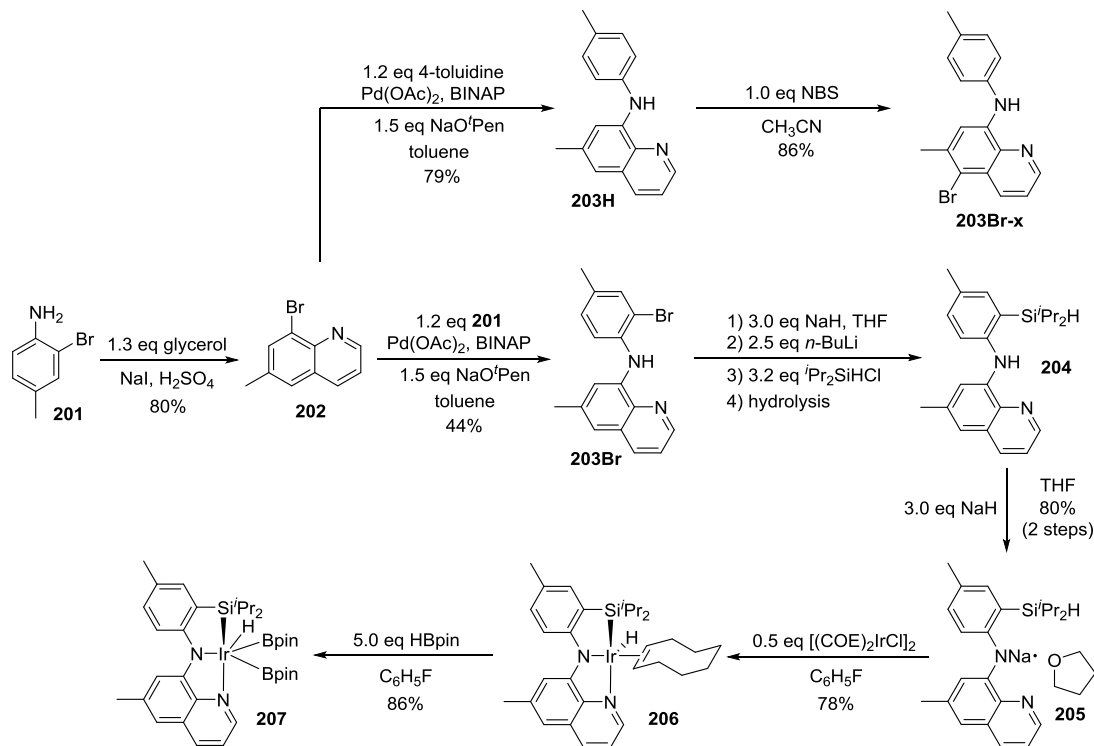


Figure 2-2. Synthesis of the SiNN ligand and its iridium complexes.

Installation of the silyl group was accomplished by deprotonation of the NH in **203Br** with NaH, followed by addition of *n*-BuLi,¹²⁷ quenching with 3.2 equivalents of ^tPr₂SiHCl, and hydrolysis. The material obtained from this reaction was an oil that contained ca. 90% of **204** and proved very difficult to purify. However, the Na derivative **205** could be isolated in a pure form in 80% yield (based on **203Br**) by recrystallization. Pure samples of **204** could then be obtained via hydrolysis of **205**. The

NMR spectroscopic features of **204** and **205** were unsurprising, including the $^1J_{\text{Si-H}} = 183$ Hz for **204**, a typical value for triorganosilanes.¹²⁸

2.2.2 Synthesis of the SiNN complexes of Ir

Compound **205** reacted smoothly with $[(\text{COE})_2\text{IrCl}]_2$ (Figure 2-2, COE = cyclooctene) to produce complex **206** in 78% yield after workup and recrystallization. One of the COE ligands was retained in the Ir coordination sphere in **206**. Crucially, the iridium center inserted into the Si-H bond of the resulting in a silyl/hydride functionality. Complex **206** displayed a hydridic resonance at -21.1 ppm in the ^1H NMR spectrum with a small $J_{\text{Si-H}}$ (8 Hz), and a resonance at 28.4 ppm in the ^{29}Si NMR spectrum.

Reaction of **206** with HBpin (Figure 2-2, HBpin = pinacolborane) resulted in the clean formation of the new product **207**, concurrent with the liberation of cyclooctane which displayed a singlet at 1.5 ppm in the ^1H NMR spectrum. The hydridic resonance of complex **207** was at -14.7 ppm in the ^1H NMR spectrum with a larger $J_{\text{Si-H}}$ (32 Hz) than that in **206** and a ^{29}Si resonance at 35.2 ppm in the ^{29}Si NMR spectrum. In the ^{11}B NMR spectrum, the Bpin resonances were accidentally degenerate with a signal at 28.9 ppm.

2.2.3 XRD and DFT studies of the SiNN complexes of Ir

X-ray diffraction studies on the single crystals of **206** and **207** allowed the determination of their structures in the solid state (Figure 2-3, top). In order to augment the X-ray studies, particularly with respect to the location of the Ir-bound hydrogen in each complex, we also carried out DFT calculations on the molecules of **206** and **207** in the gas phase using the M06 functional (Figure 2-3, bottom). The calculated structures

closely reproduced the positions of the non-hydrogen atoms from the experimental XRD determination. The longer calculated Si-H distance in **206** (2.007 Å) vs **207** (1.889 Å) is consistent with the observed $J_{\text{Si-H}}$ values of 8 and 32 Hz, respectively.

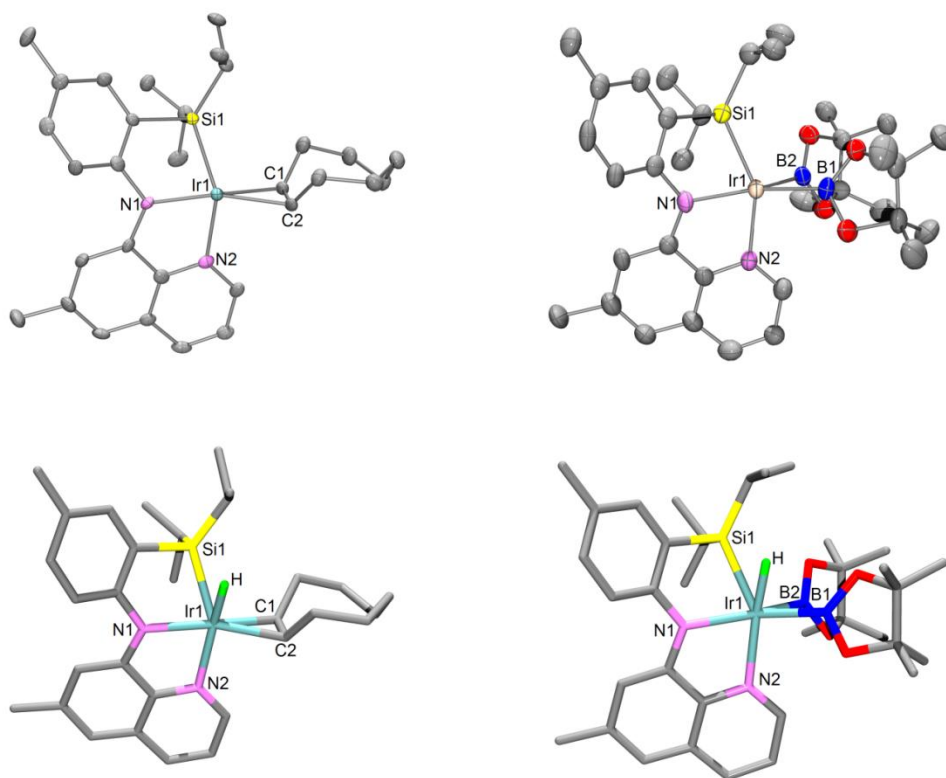


Figure 2-3. ORTEP drawings¹²⁹ (50% probability ellipsoids) of **206** (top left) and **207** (top right) showing selected atom labeling, and drawings of the DFT-calculated structures of **206** (bottom left) and **207** (bottom right). Hydrogen atoms are omitted for clarity, except for the hydride on the Ir atom. Selected bond distances (Å) and angles (deg) for **206**, with DFT-derived metrics in square brackets: Ir1-Si1, 2.3573(15) [2.391]; Ir1-H, [1.596]; Si1-H, [2.007]; C1-C2, 1.423(9) [1.413]; Si1-Ir1-H, [56.3]. For **207**: Ir1-Si1, 2.4130(14) [2.452]; Ir1-H, [1.609]; Si1-H, [1.889]; Ir1-B1, 2.069(5) [2.064]; Ir1-B2, 2.062(6) [2.055]; Si1-Ir1-H, [50.4]; B1-Ir1-B2, 66.5(2), [64.4].

The Ir-Si distance in **207** is ca. 0.05 Å longer than in **206** and ca. 0.08 Å longer than Tilley's Ir(V) complexes with SiPh_3 ligands.¹³⁰ Non-classical Si-H interactions in metal

complexes have received a significant amount of attention.^{128,131,132} The values for **207** are borderline for the presence of an Si-H bonding interaction, but the values for **206** are rather outside of that range. Thus, **206** should be viewed as containing trivalent iridium with classical silyl and hydride ligands, whereas **207** could be considered an Ir^V silyl/hydride or an Ir^{III} Si-H complex depending on the rather arbitrary divide based on the Si-H metrics.

The B-H interactions in **207** can be conclusively ruled out. The two Ir-boryl fragments feature essentially the same metrics, there is no apparent B-H coupling, and the calculated B-H distances are far outside of the B-H bonding range. The Ir-B distances in **207** are similar to the analogous Ir-Bpin and Ir-Bcat* distances reported in the literature (1.97-2.08 Å).^{68,133}

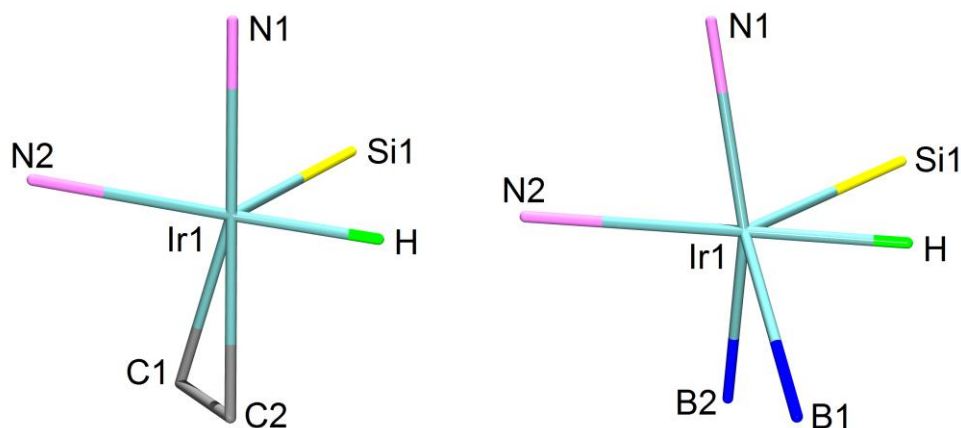


Figure 2-4. Drawings showing the immediate coordination environment about Ir in **206** (left) and **207** (right) based on the DFT-calculated structures.

The structure of **207** can be described as Y-shaped five-coordinate, with N_{quinoline}, Si, and H forming the “Y” about the Ir atom (Figure 2-4). Y-shaped structures are common for five-coordinate d⁶ complexes, but the stem of the Y is almost invariably a π-donor

ligand.¹³⁴ The fact that the stem of the Y in **207** is occupied by N_{quinoline} (not a π -donor) is unusual. The coordination environment about Ir in **207** can be viewed as two Y's in different planes with a common Ir node (Figure 2-4). One of the Y's in **207** is the same as in **206**; the other is defined by N_{amido} (π -donor at the stem) and the two boryl ligands. The B-Ir-B angle in **207** is quite acute at 66.5°, but this is a common feature of the Y-type geometry, particularly when it involves boryl ligands.¹³⁵ The B...B distance of ca. 2.26 Å is too long to contemplate boron-boron bonding.

2.2.4 Catalytic DHBTA studies.

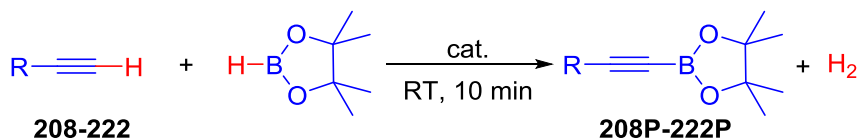


Figure 2-5. Catalytic DHBTA reaction (details in Tables 2-1, 2-2 and 2-3).

The summary of optimization of the DHBTA reactions (Figure 2-5) is given in Table 2-1. Addition of HBpin to 1 mol% **206** in C₆D₆ followed by addition of equimolar (vs HBpin) amount of PhCCH all at once led to vigorous H₂ gas evolution. Analysis of the mixture by NMR spectroscopy after ca. 10 min revealed formation of ca. 50% of the alkynylboronate product, along with ca. 50% of unreacted HBpin and PhCCH (Table 2-1, entry 5). This composition remained virtually unchanged when monitored further at RT. These observations are consistent with the presence of an active and selective, but short-lived catalyst. Performing analogous experiments with a higher loading of **206** allowed us to achieve higher conversion and yield (entry 6), but that did not seem to be an ideal solution. Performing experiments with 1% catalyst loading, but using different molar

ratios of HBpin to PhCCH (entries 9, 10) pointed to the apparent detrimental effect of the higher alkyne concentration or the higher alkyne/HBpin ratio. We surmised that rationed addition of the alkyne to the HBpin reagent solution containing the catalyst should give improve results and that indeed turned out to be the case (entries 11, 12). Even simply spreading the addition of the alkyne over 30 s (1 mmol scale) allowed yields and conversion in excess of 90%.

Table 2-1. Optimization of DHBTA (reaction in Figure 2-5).

Entry ^a	R-	Alkyne: HBpin	Solvent	Catalyst	Yield ^b
1 ^c	Phenyl- (208)	1:1	C ₆ D ₆	no catalyst	0% ^d
2 ^e	Phenyl- (208)	1:1	C ₆ D ₆	2.5 mol% [(COE) ₂ IrCl] ₂	0% ^f
3 ^e	Phenyl- (208)	1:1	C ₆ D ₆	20 mol% PCy ₃ + 5 mol% [(COE) ₂ IrCl] ₂	0% ^f
4 ^e	Phenyl- (208)	1:1	C ₆ D ₆	20 mol% PPh ₃ + 5 mol% [(COE) ₂ IrCl] ₂	0% ^f
5	Phenyl- (208)	1:1	C ₆ D ₆	1 mol% 206	46%
6	Phenyl- (208)	1:1	C ₆ D ₆	5 mol% 206	>95%
7	Phenyl- (208)	1:1	C ₆ H ₅ F	1 mol% 206	57%
8	Phenyl- (208)	1:1	THF	1 mol% 206	48%
9	Phenyl- (208)	5:1	C ₆ D ₆	1 mol% 206	15% ^g
10	Phenyl- (208)	1:5	C ₆ D ₆	1 mol% 206	>95%

Table 2-1 Continued. Optimization of DHBTA (reaction in Figure 2-5).

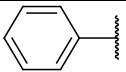
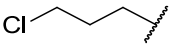
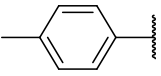
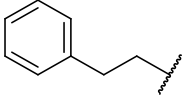
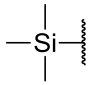
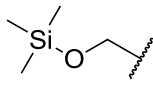
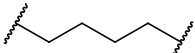
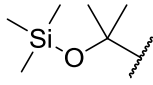
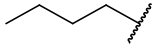
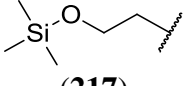
Entry ^a	R-	Alkyne:	Solvent	Catalyst	Yield ^b
		HBpin			
11	Phenyl- (208)	1:2	C ₆ D ₆	1 mol% 206	76%
12	Phenyl- (208)	1:2	C ₆ D ₆	1 mol% 206	>95%
13	4-Me-C ₆ H ₄ - (209)	1:2	C ₆ D ₆	1 mol% 207	99%
14	4-Me-C ₆ H ₄ - (209)	1:2	C ₆ D ₆	1 mol% 205 + 0.5 mol% [(COE) ₂ IrCl] ₂	99%

^a The catalyst and HBpin were dissolved in specific solvent in a J. Young tube. Alkyne was then added in once (entries 1-11) or added in 4 portions with 1 min intervals (entries 12-14) and the mixture was allowed to stand at ambient temperature for 10 min, see experimental for details. ^b NMR yield. ^c 70 °C, 24 h. ^d Only unreacted HBpin and phenylacetylene were present. ^e RT, 30 min. ^f Multiple products, including alkenylboronates, were observed but not alkynylboronate (**208P**). ^g Based on HBpin.

Table 2-2 detail the substrate scope of our investigations and shows that this methodology is readily applicable to aryl-, alkyl-, and silyl-substituted alkynes. By NMR spectroscopy the reaction resulted in nearly quantitative yields of the alkynylboronic esters. The crude products appear to be >95% pure, but are significantly darkened by the highly colored Ir complexes (catalyst residue and decomposition products). The alkynylboronate products that are solids at RT (Table 2-2, entries 1-4 and 9) were isolated in the pure, colorless form in 88-95% yield by sublimation from the crude reaction mixture after the removal of solvent and excess HBpin *in vacuo*. Even liquid alkynylboronate product (Table 2-2, entry 10) could be isolated in 85% yield by using a modified sublimation apparatus. Trimethylsilyl propargyl ether (Table 2-2, entry 8) gave only a very poor yield of the product. Given that DHBTA can be run in THF as

solvent, there is no reason to think that coordination of an ether via oxygen to Ir is a problem. It seems more likely that propargylic C-O cleavage is possible and leads to catalyst deactivation. This notion is supported by that the homopropargyl ether (Table 2-2, entry 10) undergoes DHBTA in high yield and that the bulkier propargylic substrate $\text{Me}_3\text{SiOCMe}_2\text{CCH}$ (Table 2-2, entry 9) also works fine in this reaction.

Table 2-2. DHBTA of various alkynes catalyzed by **206**.

Entry ^a	R-	Yield ^{b,c}	Entry ^a	R-	Yield ^{b,c}
1	 (208)	96% (90%)	6	 (213)	99%
2	 (209)	99% (95%)	7	 (214)	99%
3	 (210)	99% (88%)	8	 (215)	9% ^e
4	 (211)	98% ^d (90% ^d)	9	 (216)	99% (92%)
5	 (212)	99%	10	 (217)	98% (85%)

^a The catalyst **206** (0.0010 mmol) and HBpin (0.20 mmol) were dissolved in C_6D_6 in a J. Young tube. Alkyne (0.10 mmol for monoynes [0.050 mmol for 1,7-octadiyne]) was then added in 4 portions with 1 min intervals and the mixture was allowed to stand at ambient temperature for 10 min, see experimental for details. ^b NMR yield. ^c Yields in parenthesis are isolated yields in preparative-scale reactions which used toluene as solvent instead of C_6D_6 . ^d Yield of diborylated product. ^e The remaining is unreacted alkyne and pinacolborane.

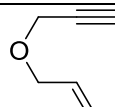
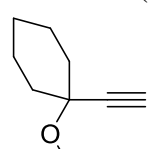
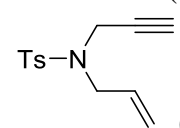
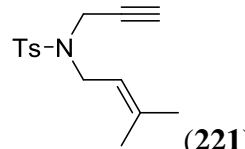
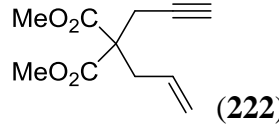
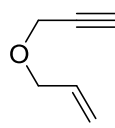
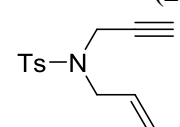
When **206** was treated with excess HBpin, purple **207** is rapidly formed prior to the addition of alkyne and this color turns blue gradually during the addition of the alkyne in successful reactions. Not surprisingly, analogous catalytic turnover was observed when isolated **207** was used in place of **206** (Table 2-1, entry 13). In addition, the active catalyst could also be generated in situ from **205** and [(COE)₂IrCl]₂ with the same reaction outcome (Table 2-1, entry 14). On the other hand, HBpin reacted with 1-hexene, styrene, or 3,4-dihydro-2*H*-pyran only slowly in the presence of 1 mol% **206**, with <40% conversion (to hydroboration products) at RT for 24 h. No reaction was detected between HBpin and furan or thiophene (arguably the most reactive substrates in aromatic C-H borylation)^{64,65,106} in the presence of 1 mol% **206** at 70 °C for 24 h.

No reaction was observed between HBpin and phenylacetylene in C₆D₆ at 70 °C for 24 h (Table 2-1, entry 1). Interestingly, this is in contrast to the previous report uncatalyzed hydroboration of alkynes with in-situ prepared HBpin in CH₂Cl₂.¹³⁶ Using [(COE)₂IrCl]₂ or [(COE)₂IrCl]₂/R₃P as catalysts led to the formation of multiple products at RT (primarily hydroboration) but no alkynylboronate (Table 2-1, entries 2-4).

Intrigued by the facts that HBpin reacted with alkenes much slower than alkynes in the presence of **206**, we thought **206** could be used for selective borylation of C(sp)-H bonds in enynes and the alkene portion remain intact. The results of DHBTA of various enynes catalyzed by **206** are shown in Table 2-3. Low yields were generally obtained for enynes with propargylic heteroatoms (entry 1, 3 and 4) except **219** (entry 2) which has bulky substituents. The low yields could be improved by using higher catalyst loading,

more HBpin, and slower addition of enyne (entry 6 and 7). Fair yield was obtained for using malonic ester-derived enyne (entry 5).

Table 2-3. DHBTA of various enynes catalyzed by **206**.

Entry	Enyne	Alkyne: HBpin	Catalyst loading	Yield ^b
1 ^a	 (218)	1:2	1 mol%	<5%
2 ^a	 (219)	1:2	1 mol%	>95%
3 ^a	 (220)	1:2	1 mol%	<5%
4 ^a	 (221)	1:2	1 mol%	<5%
5 ^a	 (222)	1:2	1 mol%	55%
6 ^b	 (218)	1:10	10 mol%	>95%
7 ^b	 (220)	1:10	10 mol%	>95%

^a The catalyst **206** (0.0010 mmol) and HBpin (0.20 mmol) were dissolved in C₆D₆ in a J. Young tube. Enyne (0.10 mmol) was then added in 4 portions with 1 min intervals and the mixture was allowed to stand at ambient temperature for 10 min. ^b The catalyst **206** (0.0050 mmol) and HBpin (0.50 mmol) were dissolved in C₆D₆ in a Schlenk flask. Enyne (0.050 mmol) was then added in dropwise in a 20 min interval. See experimental for details. ^c NMR yield.

2.3 Mechanistic considerations

Figure 2-6 shows the mechanism of DHBTA that was proposed in our original report.¹³⁷ We have established the formation of the diboryl complex **207**. So we had envisioned that it can likely react with a terminal alkyne to give intermediate **2A** presumably followed by C-B reductive elimination and boryl hydride addition to give complex **2B**. Finally, **2B** would possibly react with pinacolborane to release H₂ and regenerate **207**. However, DFT calculations later performed by Dr. Zhou¹³⁸ indicated the reaction barrier from **207** to **2A** is too high to proceed at ambient temperature. Inspired by the chemistry of SiNN Rh complexes,¹³⁹ an alternative possible mechanism with phenylacetylene as the model substrate depicted in Figure 2-7; it seems more feasible.¹³⁸

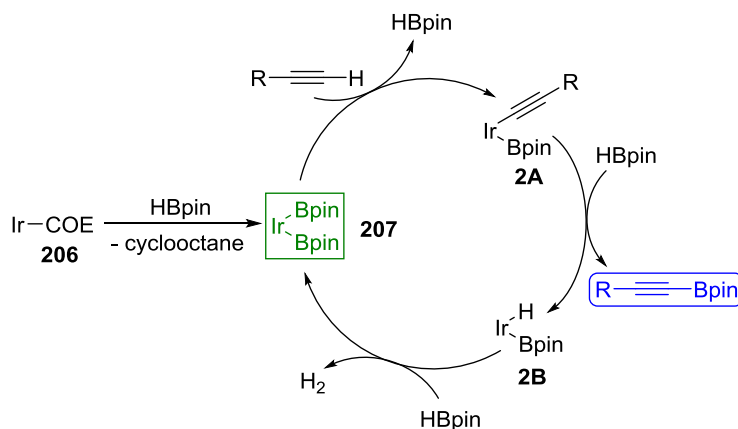


Figure 2-6. Original proposed DHBTA mechanism.

At the beginning, diboryl complex **207** is proposed to undergo isomerization to form a “borotautomer” **207-x**. This process involves the Bpin migration from Ir atom to N(amido) atom. The barrier of this process is reasonably low, only 14.1 kcal/mol at the B2PLYP-D3 level of theory. Structure **207-x** is 2.9 kcal/mol higher in energy than

structure **207**, which is consistent with the experiments in which only structure **207** is observed. The Bpin migration provides more space surrounding Ir atom for an incoming alkyne binding and also makes the formal oxidation state of Ir changing from +3 to +1. Ph-C≡C-H could oxidatively add to **207-x** resulting in complex **223**. In addition, Ph-C≡C-H can form a π complex **230** with structure **207-x**, which is 11.6 kcal/mol lower in energy than when they are separate.

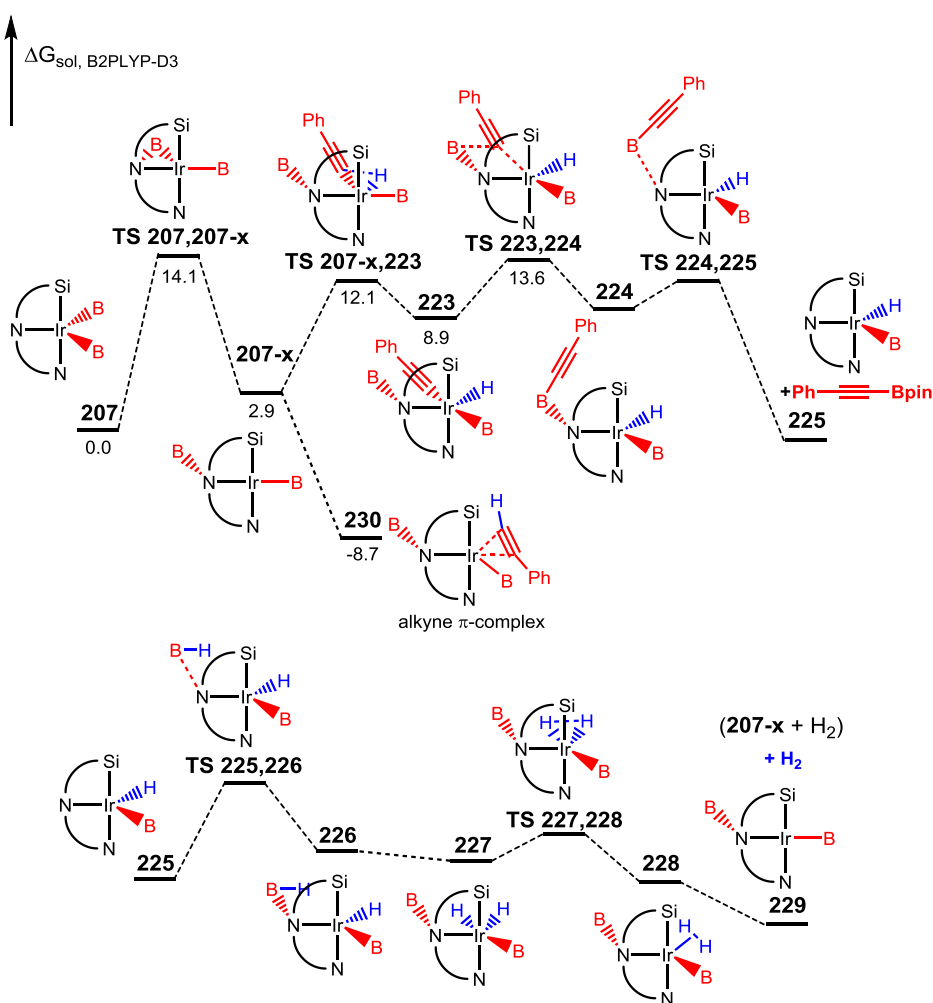


Figure 2-7. Energy profile for Ph-C≡C-Bpin elimination reaction (top) and H₂ production reaction (bottom). Relative free energies (in kcal/mol) in solvent at various levels of theory are shown.

Complex **223** only needs extra 4.7 kcal/mol energy to overcome **TS223,224** to form complex **224**. Afterwards, **225** is generated with B-N bond breaking in complex **224** with elimination of Ph-C≡C-Bpin. Addition of HBpin to **225** results **226** and follows by H migration (**226** to **227**), H₂ formation (**227** to **228**) and H₂ dissociation (**228** to **229**) to form **207-x** to finish the catalytic cycle. These steps are all with small barriers, or even barrierless.

2.4 Conclusion

In this work we are reporting iridium complexes featuring a new silyl-amido-quinoline tridentate SiNN pincer ligand. The silyl moiety of this ligand results from the insertion of the iridium center into the Si-H bond of the parent proto-ligand. The geometry and presumably the electronic interactions in the Ir/Si/H triangle appear to be able to adapt in response to the changes in the metal coordination sphere. This mechanism of electronic adaptability is rather unexplored for a spectator donor site in a polydentate ancillary ligand.

The new iridium SiNN complexes are active catalysts for selective conversion of terminal alkynes into alkynylboronic esters via dehydrogenative C-H borylation (DHBTA) with pinacolborane. This is a new and significantly advantageous method of synthesis of alkynylboronates. Optimization of the reactions conditions allowed us to achieve ca. 100 turnovers at ambient temperature in <10 min with aryl-, alkyl-, and silyl-substituted terminal alkynes. The catalyst is remarkably chemoselective, performing DHBTA, but no other catalytic alkyne transformation under the same conditions. Moreover, the catalyst showed low or no activity towards heteroarenes and alkenes. The

reactivity of the catalyst is limited by a decomposition pathway that apparently stems from a side reaction with the alkyne substrate.

The origins of the high reactivity selectively towards terminal alkynes and the origins of the decomposition reaction are not yet clear. In particular, it is not obvious whether all elements of the rather specific ligand design executed here are critical for the success of alkyne C-H borylation. The great variety of accessible pincer ligands promises exciting directions for exploring this new reaction further.

2.5 Experimental

General Considerations. Unless specified otherwise, all manipulations were performed under an Ar atmosphere using standard Schlenk line or glovebox techniques. Toluene, fluorobenzene, THF, diethyl ether, pentane, C₆D₆ were dried over NaK/Ph₂CO/18-crown-6, distilled or vacuum transferred and stored over molecular sieves in an Ar-filled glovebox. CH₂Cl₂, CD₂Cl₂ and CDCl₃ were dried with and then distilled from CaH₂ and stored over molecular sieves in an Ar-filled glove box. [(COE)₂IrCl]₂,¹⁴⁰ **218**,¹⁴¹ **219**,¹⁴² **220**,¹⁴² **221**,¹⁴² **222**¹⁴³ were prepared according to published procedures. Alkynes were deoxygenated by three freeze-pump-thaw cycles prior to use. All other chemicals were used as received from commercial vendors. NMR spectra were recorded on a Varian Inova 300, Mercury 300 (¹H NMR, 299.952 MHz; ¹³C NMR, 75.421 MHz), Varian Inova 400 (¹H NMR, 399.535 MHz; ¹¹B NMR, 128.185 MHz; ²⁹Si NMR, 79.366 MHz) and NMRS 500 (¹H NMR, 499.703 MHz; ¹³C NMR, 125.697 MHz) spectrometer. ¹H-²⁹Si double quantum filter (DQF)¹⁴⁴ experiments on compounds **206** and **207** were performed on Varian Inova 400. Chemical shifts are

reported in δ (ppm). For ^1H and ^{13}C NMR spectra, the residual solvent peak was used as an internal reference (^1H NMR: δ 7.15 for C_6D_6 , 5.32 for CD_2Cl_2 , 7.24 for CDCl_3 ; ^{13}C NMR: δ 128.06 for C_6D_6 , 53.84 for CD_2Cl_2 , 77.16 for CDCl_3). For ^{29}Si NMR, spectra were referenced externally to $\delta = 0$ ppm by using Me_4Si . For ^{11}B NMR, spectra were referenced externally to $\delta = 0$ ppm by using $\text{BF}_3 \cdot \text{Et}_2\text{O}$. Melting points were measured in the rate of $0.1\text{ }^\circ\text{C}/\text{min}$ by SRS MPA100 Automated Melting Point Apparatus. Elemental analyses were performed by CALI Labs, Inc. (Parsippany, NJ).

Note: In ^{13}C NMR spectra of alkynylboronates, quaternary carbon atoms attached to boron were usually not observed due to low intensity.

Computational details. All computations were carried out with the Gaussian09 program.¹⁴⁵ All of the geometries were fully optimized at the M06¹⁴⁶ level of theory. The Stuttgart basis set and the associated effective core potential (ECP) was used for Ir atom, and an all-electron 6-311G(d,p) basis set was used for the other atoms. The harmonic vibrational frequency calculations were performed to ensure that a minimum was obtained.

2-bromo-4-toluidine (201). Six hundred milliliters of CH_3CN in a 2 L round bottom flask was cooled down to $0\text{ }^\circ\text{C}$ by ice bath and 4-toluidine (30.1 g, 281 mmol) was added to it. N-bromosuccinimide (51.0 g, 287 mmol) was then added in portions during 1.5 h to this stirring solution. After stirring further at ambient temperature for 2 h, the volatiles were removed *in vacuo* and the residue was redissolved in 100 mL CH_2Cl_2 . The CH_2Cl_2 solution was filtered through Celite and washed with 3×50 mL H_2O and then 50 mL of saturated $\text{NaCl}_{(\text{aq})}$ to remove the succinimide by-product. The volatiles

were then removed *in vacuo* to yield a brown liquid. Its ^1H NMR spectroscopic analysis revealed the purity of the liquid is over 98%, and the liquid was used directly in subsequent synthetic steps. Yield: 49.2 g (94%). ^1H NMR (500 MHz, C_6D_6): δ 7.11 (d, $J = 2.0$ Hz, 1H), 6.65 (dd, $J = 8.0, 2.0$ Hz, 1H), 6.20 (d, $J = 8.0$ Hz, 1H), 3.33 (br s, 2H, - NH_2), 1.91 (s, 3H, Ar- CH_3). $^{13}\text{C}\{^1\text{H}\}$ NMR (126 MHz, C_6D_6): δ 142.3, 133.0, 129.2, 128.6, 115.8, 109.3, 20.0.

8-bromo-6-methylquinoline (202). 2-bromo-4-toluidine (**201**) (15.0 g, 80.7 mmol), NaI (18.2 g, 121 mmol) and glycerol (9.96 g, 108 mmol) were transferred to a 250 mL Schlenk flask and cooled to 0 °C by means of an ice bath. (The use of smaller amounts of NaI increased the fraction of the undesired 6-methylquinoline.) Then, 45 mL of 98% H_2SO_4 was added to the stirring mixture over 3 min. Purple vapors were generated during the process which indicated formation of I_2 . The mixture was heated to 140 °C for 1 h and then allowed to cool down to ambient temperature. 200 mL of H_2O and 200 mL of CH_2Cl_2 were added to the flask to assist in transferring mixture to a 1 L Erlenmeyer flask. The Erlenmeyer flask was then placed into an ice bath at 0 °C and 1 M $\text{NaOH}_{(\text{aq})}$ was added slowly to neutralize H_2SO_4 until the litmus paper test indicated an alkaline solution. Na_2SO_3 was then added to mixture to quench excess I_2 . The mixture was then filtered through a fritted funnel (The side product, acrolein polymer, clogged the funnel easily. Stirring the mixture in the funnel was needed to keep a reasonable filtration rate). The filtrate was transferred to a 1 L separation funnel and extracted with 3×200 mL of CH_2Cl_2 . The combined organic phase was dried with anhydrous Na_2SO_4 and filtered into a 2 L three-necked flask. The volatiles were removed *in vacuo* and then

10 mL of CH_2Cl_2 was added to assist in transferring the black oily residue to a 100 mL Schlenk flask. After removing the volatiles *in vacuo*, the residue was subjected to vacuum distillation. Pale yellow oil was collected at 90-100 °C. The oil solidified on standing and was used directly in later synthesis of **203H** and **203Br**. Yield: 14.3 g (80%). ^1H NMR spectroscopic analysis revealed ca. 96:4 ratio of 8-bromo-6-methylquinoline to 6-methylquinoline. 6-methylquinoline could be removed if needed via recrystallization from ethanol to get white crystals of **202**. M.p. (after recrystallization): 51.0-51.3 °C. ^1H NMR (300 MHz, CDCl_3): δ 8.93 (dd, $J = 4.2, 1.8$ Hz, 1H), 8.02 (dd, $J = 8.1, 1.8$ Hz, 1H), 7.87 (d, $J = 1.8$ Hz, 1H), 7.49 (s, 1H), 7.37 (dd, $J = 8.1, 4.2$ Hz, 1H), 2.47 (s, 3H, Ar- CH_3). $^{13}\text{C}\{^1\text{H}\}$ NMR (75 MHz, CDCl_3): δ 149.8, 143.2, 136.7, 135.5, 134.6, 128.9, 126.3, 123.7, 121.4, 20.8. Selected NMR data for 6-methylquinoline. ^1H NMR (300 MHz, CDCl_3): δ 8.79 (dd, $J = 4.2, 1.8$ Hz, 1H), 7.29 (dd, $J = 8.1, 4.2$ Hz, 1H), 2.49 (s, 3H, Ar- CH_3).



Figure 2-8. From left to right: Skraup reaction mixture before work-up; side product, acrolein polymer; 8-bromo-6-methylquinoline after distillation; solidified 8-bromo-6-methylquinoline.

Compound 203H. In an Ar-filled glove box, 8-bromo-6-methylquinoline (**202**) (3.02 g, 13.6 mmol), 4-toluidine (1.79 g, 16.7 mmol) and BINAP (134 mg, 0.215 mmol)

were transferred to a 100 mL PTFE-valved gas-tight flask and dissolved in 15 mL toluene. After stirring for 1 min, Pd(OAc)₂ (30.1 mg, 0.134 mmol Pd) and 5 mL toluene were added and stirred for 3 min. Sodium *tert*-pentoxide (2.25 g, 20.4 mmol) was then added to the solution with 10 mL toluene to assist in transfer. The flask was taken outside the glovebox and heated at 120 °C for 1 d. After allowing the mixture to cool to ambient temperature, 1 mL of H₂O was added to quench the reaction and then the volatiles were removed *in vacuo*. The residue was dissolved in CH₂Cl₂ then passed through a short column of Celite and silica gel. After removing volatiles *in vacuo* and redissolving in CH₃CN, the solution was passed through Celite to get rid of orange precipitate. The volatiles were removed to yield brown liquid; its ¹H NMR spectroscopic analysis revealed indicated >98% purity. Yield: 2.66 g (79%). ¹H NMR (500 MHz, CDCl₃): δ 8.71 (dd, J = 4.5, 1.5 Hz, 1H), 8.09 (br s, 1H, N-H), 7.99 (dd, J = 8.0, 1.5 Hz, 1H), 7.36 (dd, J = 8.0, 4.5 Hz, 1H), 7.31(d, J = 8.0 Hz, 2H), 7.25 (s, 1H), 7.20 (d, J = 8.0 Hz, 2H), 6.96 (s, 1H), 2.45 (s, 3H, Ar-CH₃), 2.37 (s, 3H, Ar-CH₃). ¹³C{¹H} NMR (126 MHz, CDCl₃): δ 146.5, 140.7, 139.3, 137.5, 137.4, 135.5, 132.0, 130.0, 129.1, 121.7, 121.1, 115.4, 109.2, 22.5, 21.0.

Compound 203Br-x. **203H** (2.57g, 10.3 mmol) was dissolved in 50 mL CH₃CN in a 250 mL round bottom flask. The flask was cooled down to 0 °C by means of an ice bath and N-bromosuccinimide (1.84 g, 10.3 mmol) was then added in portions during 40 min to this stirring solution. After stirring further at ambient temperature for 30 min, the solution was poured into a 1 L Erlenmeyer flask which contained 200 mL H₂O. Precipitate was collected by filtration of the solution and the precipitate was dried *in*

vacuo to yield yellow solid. Its ^1H NMR spectroscopic analysis indicated >98% purity. Yield: 2.91 g (86%). ^1H NMR (500 MHz, CDCl_3): δ 8.69 (dd, $J = 4.0, 1.5$ Hz, 1H), 8.50 (dd, $J = 8.5, 1.5$ Hz, 1H), 8.07 (br s, 1H, N-H), 7.46 (dd, $J = 8.5, 4.0$ Hz, 1H), 7.26 (m, 3H), 7.19 (d, $J = 8.5$ Hz, 2H), 2.52 (s, 3H, Ar- CH_3), 2.36 (s, 3H, Ar- CH_3). $^{13}\text{C}\{^1\text{H}\}$ NMR (126 MHz, CDCl_3): δ 146.7, 140.4, 138.8, 138.1, 137.5, 135.5, 132.6, 130.1, 128.2, 122.7, 121.4, 109.8, 109.2, 24.5, 21.0.

Compound 203Br. In an Ar-filled glove box, $\text{Pd}(\text{OAc})_2$ (129 mg, 0.575 mmol Pd) and BINAP (581 mg, 0.933 mmol) were transferred to a 100 mL PTFE-valved gas-tight flask and dissolved in 30 mL toluene. After stirring 3 min, 10 mL of a toluene solution which contained 8-bromo-6-methylquinoline (**202**) (5.10 g, 23.0 mmol) and 2-bromo-4-toluidine (**201**) (6.05 g, 32.5 mmol) was added to the mixture and stirred for 3 min. Sodium *tert*-pentoxide (4.09 g, 37.2 mmol) was then added to the solution with 10 mL toluene to assist in transfer. The flask was taken outside the glovebox and heated at 115 $^\circ\text{C}$ for 2 d. At that point, ^1H NMR spectroscopic analysis of an aliquot revealed 35% conversion based on 8-bromo-6-methylquinoline. After 4 d, ^1H NMR analysis revealed 65% conversion, which did not increase upon further heating. After allowing the mixture to cool to ambient temperature, 1 mL of H_2O was added to quench the reaction and then the volatiles were removed *in vacuo*. The residue was purified via column chromatography (1:10 ethyl acetate/hexane on silica; Rf of (**203Br**): 0.64; Rf of 2-bromo-4-toluidine (**201**): 0.38; Rf of 8-bromo-6-methylquinoline (**202**): 0.18). The volatiles of the eluate were removed *in vacuo* to get yellow needle crystals. Its ^1H NMR spectroscopic analysis indicated >98% purity. Yield: 3.29 g (44%). M.p.: 94.5-95.4 $^\circ\text{C}$.

^1H NMR (300 MHz, CDCl_3): δ 8.75 (dd, $J = 4.2, 1.8$ Hz, 1H), 8.33 (br s, 1H, N-H), 7.99 (dd, $J = 8.4, 1.8$ Hz, 1H), 7.57 (d, $J = 8.4$ Hz, 1H), 7.47 (d, $J = 1.8$ Hz, 1H), 7.37 (dd, $J = 8.4, 4.2$ Hz, 1H), 7.21 (d, $J = 1.8$ Hz, 1H), 7.12 (dd, $J = 8.4, 1.8$ Hz, 1H), 7.01 (s, 1H), 2.44 (s, 3H, Ar- CH_3), 2.33 (s, 3H, Ar- CH_3). $^{13}\text{C}\{^1\text{H}\}$ NMR (75 MHz, CDCl_3): δ 147.0, 139.6, 137.7, 137.4, 137.2, 135.5, 133.7, 133.1, 129.0, 128.8, 121.8, 120.3, 116.4, 116.3, 110.1, 22.5, 20.6.

Compound NaSiNN·THF (205) via 204. In an Ar-filled glovebox, (**203Br**) (2.19 g, 6.68 mmol) and NaH (482 mg, 20.1 mmol) were added to a 250 mL Schlenk flask and dissolved in 30 mL of THF. The solution color changed from yellow to dark red gradually, and the mixture was left to stir at ambient temperature overnight. The flask was taken outside the glovebox, connected to a Schlenk line while maintain an Ar atmosphere, and placed in a -78 °C dry ice/acetone cooling bath. *n*-BuLi (6.68 mL of 2.5 M solution in hexanes, 16.7 mmol) was slowly added to the solution over the course of 1 min via syringe. The mixture was left to stir at -78 °C. After 3 h, diisopropylchlorosilane (3.23 g, 21.5 mmol) was added to the solution slowly over the course of 1 min via syringe. The cooling bath was removed and the mixture was allowed to reach ambient temperature and was stirred for 15 h. 10 mL of 1 M $\text{HCl}_{(\text{aq})}$ was then added to the solution to quench reaction and it was allowed to stir at ambient temperature for 4 h, causing the color to change from dark red to yellow-brown. NaHCO_3 was added to the solution to neutralize until litmus paper test indicated an alkaline solution. The solution was transferred to a separation funnel and extracted with 3×30 mL of CH_2Cl_2 . The combined organic phase was dried with anhydrous MgSO_4 and filtered through Celite.

The volatiles were removed *in vacuo* and the residue was redissolved in pentane. The solution was filtered through Celite to remove pentane-insoluble materials and then the volatiles were removed *in vacuo* to yield a yellow oil. ^1H NMR spectroscopic analysis revealed that the oil contained over 90% **204**. Compound **204** is difficult to purify through column chromatography, so the oil was directly taken in subsequent synthetic steps to make its sodium derivative **205**. (Pure **204** could be obtained through hydrolysis of **205**; this process would be described later.) The Schlenk flask containing the yellow oil was taken into the glovebox. NaH (481 mg, 20.0 mmol) was added along with 30 mL of THF. The solution color changed from yellow to dark red gradually, and the mixture was left to stir at ambient temperature overnight. The mixture was then filtered through Celite and the volatiles were removed *in vacuo* from the filtrate. The residue was recrystallized in THF/pentane and the solids were washed with pentane and then dried *in vacuo* to get red crystals. The recrystallization process was repeated one more time. Combined yield: 2.43 g (80%). ^1H NMR (500 MHz, C_6D_6): δ 7.61 (dd, $J = 8.0, 1.5$ Hz, 1H), 7.48 (m, 2H), 7.35 (d, $J = 8.0$ Hz, 1H), 7.20 (d, $J = 8.0$ Hz, 1H), 6.87 (s, 1H), 6.73 (dd, $J = 8.0, 4.0$ Hz, 1H), 6.37 (s, 1H), 3.80 (s, 1H, Si-*H*), 3.17 (m, 4H, $\text{CH}_2(2,5)$ of THF), 2.39 (s, 3H, Ar- CH_3), 2.26 (s, 3H, Ar- CH_3), 1.24 (m, 2H, CHMe_2), 1.18 (m, 4H, $\text{CH}_2(3,4)$ of THF), 1.07 (d, $J = 7.0$ Hz, 6H, CHMe_2), 0.99 (d, $J = 7.0$ Hz, 6H, CHMe_2). $^{13}\text{C}\{^1\text{H}\}$ NMR (126 MHz, C_6D_6): 163.7, 157.3, 144.5, 142.3, 139.1, 137.9, 136.2, 132.4, 131.9, 128.1, 127.4, 124.2, 120.5, 110.0, 106.4, 67.8, 25.4, 22.6, 21.3, 19.8, 19.3, 11.4. $^{29}\text{Si}\{^1\text{H}\}$ NMR (79 MHz, C_6D_6): -4.62 (s).

Synthesis of 204 by hydrolysis of pure NaSiNN·THF (205). In a Ar-filled glovebox, NaSiNN·THF (**205**) (30 mg, 0.066 mmol) was dissolved in 0.5 mL of C₆D₆ in a 10 mL Schlenk flask. The flask was taken outside the glovebox and H₂O (100 μL, 5.6 mmol) was added to the solution. The solution color changed from red to yellow immediately. After 1 min, the volatiles were removed *in vacuo* and the residue was redissolved in pentane. The solution was filtered through Celite and then the volatiles were removed from the filtrate *in vacuo* to yield a yellow oil. The oil was taken up in C₆D₆ for NMR analysis. ¹H NMR (500 MHz, C₆D₆): δ 8.68 (br s, 1H, N-H), 8.55 (dd, J = 4.0, 1.5 Hz, 1H), 7.58 (d, J = 8.0 Hz, 1H), 7.56 (dd, J = 8.0, 2.0 Hz, 1H), 7.53 (d, J = 2.0 Hz, 1H), 7.27 (d, J = 1.5 Hz, 1H), 7.05 (dd, J = 8.0, 2.0 Hz, 1H), 6.82 (dd, J = 8.0, 4.0 Hz, 1H), 6.74 (s, 1H), 4.47 (t, J = 3.8 Hz, 1H, Si-H), 2.19 (s, 3H, Ar-CH₃), 2.18 (s, 3H, Ar-CH₃), 1.40 (m, 2H, CHMe₂), 1.13 (d, J = 7.0 Hz, 6H, CHMe₂), 1.10 (d, J = 7.0 Hz, 6H, CHMe₂). ¹³C {¹H} NMR (126 MHz, C₆D₆): δ 146.7, 145.2, 142.2, 138.7, 138.0, 137.6, 135.3, 132.6, 131.7, 129.5, 129.1, 122.7, 121.8, 115.4, 109.3, 22.3 (Ar-CH₃), 21.0 (Ar-CH₃), 19.4 (CHMe₂), 19.3 (CHMe₂), 11.5 (CHMe₂). ²⁹Si NMR (79 MHz, C₆D₆): δ 4.63 (d, J_{Si-H} = 183 Hz).

Synthesis of (SiNN)Ir(COE) (206). In a Ar-filled glove box, **205** (500 mg, 1.10 mmol) and [(COE)₂IrCl]₂ (490 mg, 0.546 mmol) were allowed to dissolve in 10 mL of fluorobenzene in a 50 mL Schlenk flask. The solution turned black immediately, and then changed to deep blue over the next 10 min. After 1 h, 10 mL CH₂Cl₂ were added to the flask to assist in filtering the solution through Celite and then the volatiles were removed *in vacuo* from the filtrate. (Note: CH₂Cl₂ could not be used directly as a

reaction solvent since it reacted with **205**.) The residue was redissolved in a CH₂Cl₂/pentane mixture, and the flask was then placed in a -35 °C freezer for overnight. The next day the gray solid was collected, washed with cold pentane, and dried under vacuum. The decanted solution was combined with the washings, and the volatiles were removed *in vacuo*. The residue was then redissolved in CH₂Cl₂/pentane, placed in the freezer and collected in the same manner to yield the second fraction. The recrystallization process was repeated once more to yield the third fraction. Combined yield: 566 mg (78%). ¹H NMR (500 MHz, CD₂Cl₂): δ 8.44 (d, J = 5.0 Hz, 1H), 8.27 (d, J = 8.0 Hz, 1H), 7.59 (s, 1H), 7.55 (dd, J = 8.0, 5.0 Hz, 1H), 7.39 (d, J = 8.0 Hz, 1H), 7.25 (s, 1H), 7.03 (d, J = 8.0 Hz, 1H), 6.77 (s, 1H), 3.94 (m, 2H), 2.42 (s, 3H, Ar-CH₃), 2.37 (m, 2H), 2.34 (s, 3H, Ar-CH₃), 1.66 (m, 6H), 1.45 (m, 6H), 0.94 (m, 12H, CHMe₂), -21.14 (s, 1H, Ir-H). Selected ¹H-²⁹Si DQF (400 MHz, CD₂Cl₂) data for Ir-H: -21.14 (d, J_{Si-H} = 8.0 Hz). ¹³C{¹H} NMR (126 MHz, CD₂Cl₂): δ 159.9, 153.7, 146.3, 142.7, 141.8, 140.6, 139.5, 134.5, 131.2, 130.9, 128.5, 120.9, 119.3, 113.3, 111.3, 55.0, 33.1 (br), 32.7, 27.0, 22.4, 21.0, 19.9, 19.8, 16.0 (br). ²⁹Si NMR (79 MHz, CD₂Cl₂): δ 28.4 (br). Anal. Calcd for C₃₁H₄₃IrN₂Si: C, 56.07; H, 6.53. Found: C, 55.96; H, 6.59.

Synthesis of (SiNN)Ir(Bpin)₂ (207). In a Ar-filled glove box, **206** (100 mg, 0.151 mmol) was dissolved in 3 mL of fluorobenzene in a 25 mL Schlenk flask. After 1 min, pinacolborane (110 μL, 0.758 mmol) was added to the flask and the solution turned purple immediately. After 30 min, the volatiles were removed *in vacuo*. The residue was redissolved in a CH₂Cl₂/pentane mixture, and the flask was then placed in a -35 °C freezer for overnight. The next day the purple precipitate was collected, washed with

cold pentane and dried under vacuum. The decanted solution was combined with the washings, and the volatiles were removed *in vacuo*. The residue was then redissolved in CH₂Cl₂/pentane, placed in the freezer and collected in the same manner to yield the second fraction. Combined yield: 105 mg (86%). ¹H NMR (500 MHz, CD₂Cl₂): δ 10.03 (d, J = 5.5 Hz, 1H), 8.30 (d, J = 8.0 Hz, 1H), 7.67 (s, 1H), 7.55 (dd, J = 8.0, 5.5 Hz, 1H), 7.49 (d, J = 8.0 Hz, 1H), 7.16 (s, 1H), 7.06 (d, J = 8.0 Hz, 1H), 6.85 (s, 1H), 2.45 (s, 3H, Ar-CH₃), 2.35 (s, 3H, Ar-CH₃), 1.90 (m, 2H, CHMe₂), 1.24 (s, 12H, -CH₃ on Bpin), 1.14 (s, 12H, -CH₃ on Bpin), 1.11 (d, J = 6.5 Hz, 6H, CHMe₂), 0.96 (d, J = 6.5 Hz, 6H, CHMe₂), -14.72 (s, 1H, Ir-H). Selected ¹H-²⁹Si DQF (400 MHz, CD₂Cl₂) data for Ir-H: -14.72 (d, J_{Si-H} = 32 Hz). ¹³C{¹H} NMR (126 MHz, CD₂Cl₂): δ 159.2, 155.2, 153.0, 146.2, 139.6, 139.1, 136.8, 135.6, 130.7, 130.1, 129.3, 121.2, 117.9, 113.7, 112.9, 82.5, 25.3, 25.2, 22.3, 20.9, 19.6, 19.3, 15.2. ¹¹B NMR (128 MHz, CD₂Cl₂): δ 28.9. ²⁹Si NMR (79 MHz, CD₂Cl₂): δ 35.2 (br). Anal. Calcd for C₃₅H₅₃B₂IrN₂O₄Si: C, 52.04; H, 6.61. Found: C, 52.03; H, 6.63.

Reaction of pinacolborane with phenylacetylene without any added catalyst.

Pinacolborane (15 μL, 0.10 mmol) and phenylacetylene (11 μL, 0.10 mmol) were dissolved in 0.5 mL C₆D₆ in a J. Young tube. After 1 d at 70 °C, analysis by ¹H NMR spectroscopy revealed that only unreacted pinacolborane and phenylacetylene were present.

Reaction of pinacolborane with phenylacetylene catalyzed by [(COE)₂IrCl]₂.

[(COE)₂IrCl]₂ (5.0 mg, 0.0056 mmol) was dissolved in 0.5 mL C₆D₆ in a J. Young tube. Pinacolborane (32 μL, 0.22 mmol) was added to the solution and followed by

phenylacetylene (26 μL , 0.22 mmol). After 30 min, analysis by ^1H NMR revealed phenylacetylene was all consumed. Multiple products including alkenylboronates were observed but not alkynylboronate (**208P**).

Reaction of pinacolborane with phenylacetylene catalyzed by $[(\text{COE})_2\text{IrCl}]_2/\text{PCy}_3$. $[(\text{COE})_2\text{IrCl}]_2$ (8.3 mg, 0.0093 mmol) and PCy_3 (10.3 mg, 0.037 mmol) were dissolved in 0.5 mL C_6D_6 in a J. Young tube. After 30 min at ambient temperature, pinacolborane (27 μL , 0.19 mmol) was added to the solution and followed by phenylacetylene (21 μL , 0.19 mmol). After 30 min, analysis by ^1H NMR revealed phenylacetylene was all consumed. Multiple products including alkenylboronates were observed but not alkynylboronate (**208P**).

Reaction of pinacolborane with phenylacetylene catalyzed by $[(\text{COE})_2\text{IrCl}]_2/\text{PPh}_3$. $[(\text{COE})_2\text{IrCl}]_2$ (8.5 mg, 0.0095 mmol) and PPh_3 (9.9 mg, 0.038 mmol) were dissolved in 0.5 mL C_6D_6 in a J. Young tube. After 30 min at ambient temperature, pinacolborane (27 μL , 0.19 mmol) was added to the solution and followed by phenylacetylene (21 μL , 0.19 mmol). After 30 min, analysis by ^1H NMR revealed phenylacetylene was all consumed. Multiple products including alkenylboronates were observed but not the alkynylboronate (**208P**).

Dehydrogenative borylation of alkynes in different solvents. Stock solution of **206** (22 μL of 0.045 M stock solution in C_6D_6 , 0.0010 mmol) and pinacolborane (15 μL , 0.10 mmol) were dissolved in 0.5 mL of the specified solvent in a J. Young tube. Phenylacetylene (11 μL , 0.10 mmol) was then added at once and mixed in. After 10 min, a drop of solution was transferred to another J. Young tube followed by 0.5 mL C_6D_6 .

The reaction yield was determined on ^1H NMR by the ratio of integration of methyls on Bpin. The results are summarized in Table 2-4.

Table 2-4. DHBTA in different solvents.

Solvent	Yield of 208P ^a
C_6D_6	46% ^b
$\text{C}_6\text{H}_5\text{F}$	57% ^b
THF	48% ^b

^a based on pinacolborane ^b The remaining percentage is unreacted phenylacetylene and pinacolborane.

Reaction of pinacolborane with phenylacetylene catalyzed by 5 mol% **206.**

Stock solution of **206** (110 μL of 0.045 M stock solution in C_6D_6 , 0.0050 mmol) and pinacolborane (15 μL , 0.10 mmol) were dissolved in 0.5 mL of C_6D_6 in a J. Young tube. Phenylacetylene (11 μL , 0.10 mmol) was then added at once and mixed in. **208P** was obtained in >95% yield which was determined by ^1H NMR spectroscopy.

Pinacolborane/alkyne ratio optimization for dehydrogenative borylation of alkynes. Stock solution of **206** (40 μL of 0.025 M stock solution in C_6D_6 , 0.0010 mmol) and pinacolborane were dissolved in 0.5 mL C_6D_6 in a J. Young tube. Phenylacetylene was then added at once and mixed in. After 10 min, the reaction yield was determined by ^1H NMR analysis via the ratio of integration of the methyl groups on Bpin or of aryl-H signals on phenyls. The results are summarized in Table 2-5.

Table 2-5. Pinacolborane/alkyne ratio optimization for DHBTA.

Pinacolborane	Phenylacetylene	Yield of 208P
0.10 mmol	0.10 mmol	46% ^{a, c}
0.10 mmol	0.50 mmol	15% ^{a, c}
0.50 mmol	0.10 mmol	> 95% ^{b, c}

^a based on pinacolborane ^b based on phenylacetylene ^c The remaining is unreacted phenylacetylene and pinacolborane.

Optimization of the method of addition of alkyne. A: Addition of alkyne all at once. Stock solution of **206** (40 μ L of 0.025 M stock solution in C₆D₆, 0.0010 mmol) and pinacolborane (29 μ L, 0.20 mmol) were dissolved in 0.5 mL C₆D₆ in a J. Young tube. Phenylacetylene (11 μ L, 0.10 mmol) was then added at once and mixed in. After 10 min, the reaction yield was determined on ¹H NMR by the ratio of integration of aryl-H signals of the phenyl groups. **B: Addition of alkyne in 4 portions.** Stock solution of **206** (40 μ L of 0.025 M stock solution in C₆D₆, 0.0010 mmol) and pinacolborane (29 μ L, 0.20 mmol) were dissolved in 0.2 mL C₆D₆ in a J. Young tube. Phenylacetylene (11 μ L, 0.10 mmol) in 0.2 mL C₆D₆ was then added in 4 portions with 1 min intervals. After 10 min, the reaction yield was determined on ¹H NMR by the ratio of integration of aryl-H signals of the phenyl groups. The results are summarized in Table 2-6.

Table 2-6. Optimization of the method of addition of alkyne.

Pinacolborane/phenylacetylene	Alkyne addition method	Yield of 208P ^a
2:1	Add in once	76% ^b
2:1	Add in 4 portions	> 95% ^b

^a based on phenylacetylene ^b The remaining is unreacted phenylacetylene and pinacolborane.

Reaction of pinacolborane with 4-methylphenylacetylene catalyzed by *in-situ* generating **206.** [(COE)₂IrCl]₂ (40 μL of 0.0125 M stock solution in C₆D₆, 0.00050 mmol) and **205** (40 μL of 0.025 M stock solution in C₆D₆, 0.0010 mmol) were mixed in a J. Young tube. After 30 min, pinacolborane (200 μL of 1.0 M stock solution in C₆D₆, 0.20 mmol) was added, and 4-methylphenylacetylene/1,4-dioxane (200 μL of 0.50 M 4-methylphenylacetylene/ 0.35 M 1,4-dioxane stock solution in C₆D₆, 0.10 mmol for 4-methylphenylacetylene and 0.070 mmol for 1,4-dioxane) was then added in 4 portions with 1 min intervals. **209P** was obtained in 99% yield which was determined by ¹H NMR spectroscopy using 1,4-dioxane as an internal standard.

Reaction of pinacolborane with 4-methylphenylacetylene catalyzed by **207.** Stock solution of **207** (80 μL of 0.0125 M stock solution in C₆D₆, 0.0010 mmol) and pinacolborane stock solution (200 μL of 1.0 M pinacolborane stock solution in C₆D₆, 0.20 mmol) were mixed in a J. Young tube. 4-methylphenylacetylene/1,4-dioxane (200 μL of 0.50 M 4-methylphenylacetylene/ 0.35 M 1,4-dioxane stock solution in C₆D₆, 0.10 mmol for 4-methylphenylacetylene and 0.070 mmol for 1,4-dioxane) was then added in 4 portions with 1 min intervals. **209P** was obtained in 99% yield which was determined by ¹H NMR spectroscopy using 1,4-dioxane as an internal standard.

Reaction of pinacolborane with olefins in the presence of **206.** Stock solution of **206** (40 μL of 0.0125 M stock solution in C₆D₆, 0.00050 mmol) and pinacolborane (15 μL, 0.10 mmol) were dissolved in 0.2 mL C₆D₆ in a J. Young tube. Olefin (0.050 mmol of 1-hexene, styrene or 3,4-dihydro-2*H*-pyran) in 0.2 mL C₆D₆ was then added in 4 portions with 1 min intervals. After 1 d at ambient temperature, analysis by ¹H NMR

revealed that ca. 30% conversion for 1-hexene, ca. 20% conversion for styrene based on alkenyl-*H* integration. The major product was alkylboronate, and trace amounts of *trans*-alkenylboronate and *cis*-alkenylboronate were also observed. No reaction was observed with 3,4-dihydro-2*H*-pyran.

Reaction of pinacolborane with heteroarenes in the presence of 206. Stock solution of **206** (40 μL of 0.025 M stock solution in C_6D_6 , 0.0010 mmol) and pinacolborane (29 μL , 0.20 mmol) were dissolved in 0.2 mL C_6D_6 in a J. Young tube. Heteroarenes (0.10 mmol of furan or thiophene) in 0.2 mL C_6D_6 was then added in 4 portions with 1 min intervals. After 1 d at 70 $^\circ\text{C}$, analysis by ^1H NMR revealed that only unreacted pinacolborane and heteroarenes were present.

General procedure for the NMR-scale dehydrogenative borylation of alkynes. In an Ar-filled glove box, stock solution of **206** (80 μL of 0.0125 M stock solution in C_6D_6 , 0.0010 mmol) and pinacolborane stock solution (200 μL of 1.0 M pinacolborane stock solution in C_6D_6 , 0.20 mmol) were mixed in a J. Young tube. Alkyne/1,4-dioxane (200 μL of 0.50 M alkyne [0.25 M for 1,7-octadiyne] / 0.35 M 1,4-dioxane stock solution in C_6D_6 , 0.10 mmol for monoynes [0.050 mmol for 1,7-octadiyne] and 0.070 mmol for 1,4-dioxane) was then added in 4 portions with 1 min intervals. The J. Young tube was taken outside the glovebox, after 10 min, reaction yield was determined on ^1H NMR measurement by using 1,4-dioxane as internal standard. The reagent ratio was calibrated through the integration ratio from a ^1H NMR spectrum of a sample obtained by mixing 100 μL of the pinacolborane stock solution and 100 μL alkyne/1,4-dioxane stock solution in 0.3 mL C_6D_6 in another J. Young tube without adding **206**.

Ph-C≡C-Bpin (208P). ^1H NMR (500 MHz, C_6D_6): δ 7.38 (m, 2H, Ar-*H*), 6.85 (m, 3H, Ar-*H*), 1.02 (s, 12H, - CH_3 on Bpin). $^{13}\text{C}\{^1\text{H}\}$ NMR (126 MHz, C_6D_6): δ 132.7, 129.3, 128.5, 122.7, 101.9 (br, $\underline{\text{C}}\equiv\text{C-B}$), 84.1, 24.7. ^{11}B NMR (128 MHz, C_6D_6): δ 24.7. The ^1H and ^{13}C NMR spectral data were in agreement with those reported in the literature.¹¹⁰

4-Me-C₆H₄-C≡C-Bpin (209P). ^1H NMR (500 MHz, CDCl_3): δ 7.39 (d, $J = 7.5$ Hz, 2H), 7.08 (d, $J = 7.5$ Hz, 2H), 2.31 (s, 3H, Ar- CH_3), 1.29 (s, 12H, - CH_3 on Bpin). $^{13}\text{C}\{^1\text{H}\}$ NMR (126 MHz, CDCl_3): δ 139.8, 132.6, 129.2, 118.9, 102.2 (br, $\underline{\text{C}}\equiv\text{C-B}$), 84.4, 24.8, 21.7. ^{11}B NMR (128 MHz, CDCl_3): δ 23.8. The ^1H and ^{13}C NMR spectral data were in agreement with those reported in the literature.¹⁴⁷

Me₃Si-C≡C-Bpin (210P). ^1H NMR (500 MHz, C_6D_6): δ 0.94 (s, 12H, - CH_3 on Bpin), 0.07 (s, 9H, - CH_3 of SiMe_3). $^{13}\text{C}\{^1\text{H}\}$ NMR (126 MHz, C_6D_6): δ 110.8 (br, $\underline{\text{C}}\equiv\text{C-B}$), 84.1, 24.6, -0.5. ^{11}B NMR (128 MHz, C_6D_6): δ 23.6. The ^1H and ^{13}C NMR spectral data were in agreement with those reported in the literature.¹¹⁰

pinB-C≡C-(CH₂)₄-C≡C-Bpin (211P). ^1H NMR (500 MHz, C_6D_6): δ 1.78 (m, 4H), 1.25 (m, 4H), 0.99 (s, 24H, - CH_3 on Bpin). $^{13}\text{C}\{^1\text{H}\}$ NMR (126 MHz, C_6D_6): δ 103.9 (br, $\underline{\text{C}}\equiv\text{C-B}$), 83.6, 27.3, 24.7, 19.1. ^{11}B NMR (128 MHz, C_6D_6): δ 23.8. The ^1H and ^{13}C NMR spectral data were in agreement with those reported in the literature.¹¹⁰

***n*Bu-C≡C-Bpin (212P).** ^1H NMR (500 MHz, CDCl_3): δ 2.23 (t, $J = 7.0$ Hz, 2H), 1.49 (m, 2H), 1.39 (m, 2H), 1.24 (s, 12H, - CH_3 on Bpin), 0.87 (t, $J = 7.5$ Hz, 3H). $^{13}\text{C}\{^1\text{H}\}$ NMR (126 MHz, CDCl_3): δ 105.3 (br, $\underline{\text{C}}\equiv\text{C-B}$), 84.2, 30.3, 24.8, 22.1, 19.4,

13.7. ^{11}B NMR (128 MHz, CDCl_3): δ 23.4. The ^1H , ^{13}C and ^{11}B NMR spectral data were in agreement with those reported in the literature.^{118,148}

$\text{ClCH}_2\text{-(CH}_2\text{)}_2\text{-C}\equiv\text{C-Bpin (213P)}$. ^1H NMR (500 MHz, CDCl_3): δ 3.61 (t, $J = 6.5$ Hz, 2H), 2.43 (t, $J = 6.5$ Hz, 2H), 1.95 (pentet, $J = 6.5$ Hz, 2H), 1.24 (s, 12H, $-\text{CH}_3$ on Bpin). $^{13}\text{C}\{^1\text{H}\}$ NMR (126 MHz, CDCl_3): δ 102.8 (br, $\underline{\text{C}}\equiv\text{C-B}$), 84.3, 43.6, 31.0, 24.8, 17.1. ^{11}B NMR (128 MHz, CDCl_3): δ 23.3. The ^1H , ^{13}C and ^{11}B NMR spectral data were in agreement with those reported in the literature.¹⁴⁹

$\text{Ph-(CH}_2\text{)}_2\text{-C}\equiv\text{C-Bpin (214P)}$. ^1H NMR (500 MHz, C_6D_6): δ 7.02 (m, 3H), 6.90 (m, 2H), 2.55 (t, $J = 7.5$ Hz, 2H), 2.20 (t, $J = 7.5$ Hz, 2H), 0.99 (s, 12H, $-\text{CH}_3$ on Bpin). $^{13}\text{C}\{^1\text{H}\}$ NMR (126 MHz, C_6D_6): δ 140.6, 128.62, 128.61, 126.5, 103.7 (br, $\underline{\text{C}}\equiv\text{C-B}$), 83.7, 34.8, 24.7, 21.9. ^{11}B NMR (128 MHz, C_6D_6): δ 24.1.

$\text{Me}_3\text{SiO-CH}_2\text{-C}\equiv\text{C-Bpin (215P)}$. Selected NMR data for **215P**: ^1H NMR (500 MHz, C_6D_6): δ 4.08 (s, 2H, $\text{O-CH}_2\text{-C}\equiv\text{C}$); Selected NMR data for **215**: ^1H NMR (500 MHz, C_6D_6): δ 4.05 (d, $J = 2.5$ Hz, 2H, $\text{O-CH}_2\text{-C}\equiv\text{C}$).

$\text{Me}_3\text{SiO-C(Me)}_2\text{-C}\equiv\text{C-Bpin (216P)}$. ^1H NMR (500 MHz, C_6D_6): δ 1.44 (s, 6H), 0.96 (s, 12H, $-\text{CH}_3$ on Bpin), 0.31 (s, 9H, $-\text{CH}_3$ on TMS). $^{13}\text{C}\{^1\text{H}\}$ NMR (126 MHz, C_6D_6): δ 107.9 (br, $\underline{\text{C}}\equiv\text{C-B}$), 84.0, 66.9, 32.8, 24.7, 2.2. ^{11}B NMR (128 MHz, C_6D_6): δ 23.9.

$\text{Me}_3\text{SiO-(CH}_2\text{)}_2\text{-C}\equiv\text{C-Bpin (217P)}$. ^1H NMR (500 MHz, C_6D_6): δ 3.50 (t, 2H, $J = 7.0$ Hz), 2.28 (t, 2H, $J = 7.0$ Hz), 0.98 (s, 12H, $-\text{CH}_3$ on Bpin), 0.01 (s, 9H, $-\text{CH}_3$ on

TMS). $^{13}\text{C}\{^1\text{H}\}$ NMR (126 MHz, C_6D_6): δ 101.4 (br, $\underline{\text{C}}\equiv\text{C-B}$), 83.7, 61.1, 24.7, 24.2, -0.4. ^{11}B NMR (128 MHz, C_6D_6): δ 23.7.

218P. ^1H NMR (500 MHz, C_6D_6): δ 5.66 (m, 1H, alkenyl-*H*), 5.12 (m, 1H, alkenyl-*H*), 4.94 (m, 1H, alkenyl-*H*), 3.87 (s, 2H, O- $\text{CH}_2\text{-C}\equiv\text{C}$), 3.84 (d, $J = 5.2$ Hz, O- $\text{CH}_2\text{-C(H)=C}$), 0.97 (s, 12H, - CH_3 on Bpin).

219P. ^1H NMR (500 MHz, C_6D_6): δ 5.90 (m, 1H, alkenyl-*H*), 5.24 (m, 1H, alkenyl-*H*), 4.98 (m, 1H, alkenyl-*H*), 4.16 (dt, $J = 5.2, 1.6$ Hz, 2H, O- $\text{CH}_2\text{-C(H)=C}$), 1.88 (m, 2H), 1.63 (m, 2H), 1.49(m, 4H), 1.22 (m, 1H), 1.08 (m, 1H), 0.97 (s, 12H, - CH_3 on Bpin).

220P. ^1H NMR (500 MHz, C_6D_6): δ 7.70 (d, $J = 8.1$ Hz, 2H, Ar-*H*), 6.86 (d, $J = 8.1$ Hz, 2H, Ar-*H*), 5.45 (m, 1H, alkenyl-*H*), 4.98 (m, 1H, alkenyl-*H*), 4.83 (m, 1H, alkenyl-*H*), 3.96 (s, 2H, N- $\text{CH}_2\text{-C}\equiv\text{C}$), 3.72 (d, $J = 6.4$ Hz, 2H, N- $\text{CH}_2\text{-C(H)=C}$), 1.97 (s, 3H, Ar- CH_3), 0.91 (s, 12H, - CH_3 on Bpin).

221P. Selected NMR data for **221P**: ^1H NMR (500 MHz, C_6D_6): δ 3.99 (s, 2H, N- $\text{CH}_2\text{-C}\equiv\text{C}$); Selected NMR data for **221**: ^1H NMR (500 MHz, C_6D_6): δ 3.96 (d, $J = 2.5$ Hz, 2H, N- $\text{CH}_2\text{-C}\equiv\text{C}$).

222P. Selected NMR data for **222P**: ^1H NMR (500 MHz, C_6D_6): δ 3.03 (s, 2H, $\text{CH}_2\text{-C}\equiv\text{C}$); Selected NMR data for **222**: ^1H NMR (500 MHz, C_6D_6): δ 2.94 (d, $J = 2.5$ Hz, 2H, $\text{CH}_2\text{-C}\equiv\text{C}$).

NMR-scale dehydrogenative borylation of enynes with higher 206 loading. In an Ar-filled glove box, **206** (3.3 mg, 0.0050 mmol) and pinacolborane (73 μL , 0.50 mmol) were dissolved in 0.5 mL C_6D_6 in a 10 mL Schlenk flask. After stirring 1 min at

ambient temperature, enyne (0.050 mmol of **218** or **220**) in 0.5 mL C₆D₆ was then added dropwise in 20 min. After all enyne was added, 0.5 mL of solution was transferred to a J. Young tube and reaction yield was determined on ¹H NMR measurement.

General procedure for the preparative-scale dehydrogenative borylation of alkynes. In an Ar-filled glove box, **206** (6.8 mg, 0.010 mmol) and pinacolborane (290 μL, 2.00 mmol) were dissolved in 1.5 mL toluene in a 25 mL Schlenk flask. After stirring 3 min at ambient temperature, alkyne (1.00 mmol for monoynes; 0.500 mmol for 1,7-octadiyne) in 0.5 mL toluene was then added dropwise in 30 s. Bubbles evolved immediately which indicated H₂ generation. After all alkyne was added, the mixture was stirred for 5 min and then the volatiles were removed *in vacuo*. The purity of the crude product was >95% by ¹H NMR analysis. **Purification of solid alkynylboronates (208P-211P and 216P, for setup see Figure 2-9):** The crude product was transferred to a sublimation apparatus assisted by Et₂O and then removed Et₂O *in vacuo*. The apparatus was taken outside the glovebox and heated in oil bath. After sublimation was finished, the coolants (dry ice/acetone) were removed carefully and the apparatus was taken into the glovebox. The product condensed on the cold finger was carefully washed to a beaker by Et₂O, and the Et₂O solution was then transferred to a Schlenk flask. The purified product was obtained after removing Et₂O *in vacuo*. **Purification of liquid alkynylboronate (217P, for setup see Figure 2-10):** Two 8 mL and one 20 mL aluminum weigh boats were placed in a sublimation apparatus. The crude product was transferred to 8 mL aluminum weigh boats by toluene and then removed toluene *in vacuo*. The apparatus was taken outside the glovebox and heated in oil bath. After

sublimation was finished, coolants (dry ice/acetone) were removed carefully. The condensed alkynylboronate melted slowly during removal of coolants, and the apparatus was leant slightly to let melted alkynylboronate drop into the 20 mL aluminum weigh boat. After all the alkynylboronate melted, the apparatus was taken into the glovebox. The product collected in the 20 mL weigh boat and residue on the cold finger were carefully washed to a beaker by Et₂O, and the Et₂O solution was then transferred to a Schlenk flask. The zapurified product was obtained after removing Et₂O *in vacuo*.

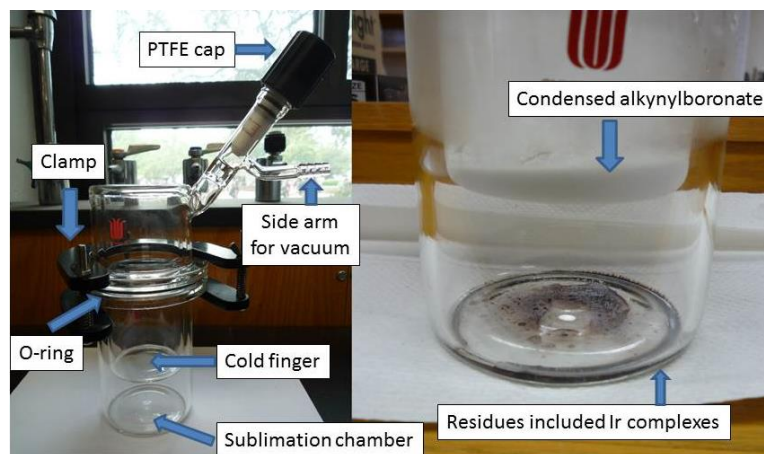


Figure 2-9. Left: Setup of a sublimation apparatus. Right: Alkynylboronate collection after sublimation.

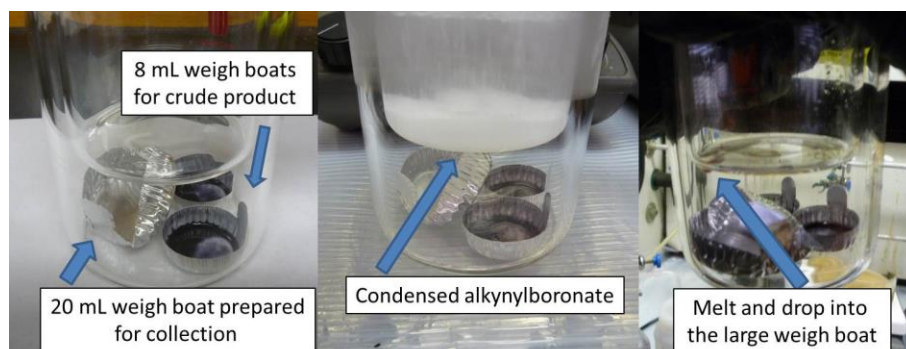


Figure 2-10. From left to right: Before distillation; After distillation, before removal of coolant; After removal of coolant.

Ph-C≡C-Bpin (208P). White solid, yield: 205 mg (90%).

4-Me-C₆H₄-C≡C-Bpin (209P). White solid, yield: 231 mg (95%).

Me₃Si-C≡C-Bpin (210P). White solid, yield: 197 mg (88%).

pinB-C≡C-(CH₂)₄-C≡C-Bpin (211P). White solid, yield: 161 mg (90%).

Me₃SiO-C(Me)₂-C≡C-Bpin (216P). White solid, yield: 259 mg (92%).

Me₃SiO-(CH₂)₂-C≡C-Bpin (217P). Pale yellow oil, yield: 227 mg (85%).

X-Ray data collection, solution, and refinement for 206. A Leica MZ 75 microscope was used to identify a suitable deep-blue multifaceted crystal with dimensions (max, intermediate, and min; in mm) 0.25 × 0.17 × 0.12 from a representative sample of crystals of the same habit. The crystal mounted on a nylon loop was then placed in a cold nitrogen stream (Oxford) maintained at 110 K. A BRUKER GADDS X-ray (three-circle) diffractometer was employed for crystal screening, unit cell determination, and data collection. The goniometer was controlled using the FRAMBO software.¹⁵⁰ The sample was optically centered with the aid of a video camera such that no translations were observed as the crystal was rotated through all positions. The detector was set at 5.0 cm from the crystal sample. The X-ray radiation employed was generated from a Cu sealed X-ray tube ($\lambda = 1.5418 \text{ \AA}$ with a potential of 40 kV and a current of 40 mA) fitted with a graphite monochromator in the parallel mode (175 mm collimator with 0.5 mm pinholes). A total of 180 data frames were taken at widths of 0.5° with an exposure time of 15 s. These reflections were used to determine the unit cell using Cell_Now.¹⁵⁰ A suitable cell was found and refined by nonlinear least-squares and

Bravais lattice procedures. Integrated intensity information for each reflection was obtained by reduction of the data frames with SAINTplus.¹⁵⁰ The integration method employed a three-dimensional profiling algorithm and all data were corrected for Lorentz and polarization factors, as well as for crystal decay effects. Finally the data was merged and scaled to produce a suitable data set. SADABS¹⁵⁰ was employed to correct the data for absorption effects. The structure was solved in the monoclinic P21/n space group using XS¹⁵¹ (incorporated in SHELXTL). All non-hydrogen atoms were refined with anisotropic thermal parameters. The hydrogen atoms were placed in idealized positions and refined using riding model. The structure was refined (weighted least-squares refinement on F^2) to convergence. Although the Ir-*H* ligand couldn't be located in the crystal structure confidently, its presence is indicated both by ¹H and ¹H-²⁹Si DQF NMR spectroscopic data.

X-Ray data collection, solution, and refinement for 207. A Leica MZ 75 microscope was used to identify a suitable purple multifaceted crystal with dimensions (max, intermediate, and min; in mm) $0.18 \times 0.15 \times 0.06$ from a representative sample of crystals of the same habit. The crystal mounted on a nylon loop was then placed in a cold nitrogen stream (Oxford) maintained at 110 K. A BRUKER GADDS X-ray (three-circle) diffractometer was employed for crystal screening, unit cell determination, and data collection. The goniometer was controlled using the FRAMBO software.¹⁵⁰ The sample was optically centered with the aid of a video camera such that no translations were observed as the crystal was rotated through all positions. The detector was set at 5.0 cm from the crystal sample. The X-ray radiation employed was generated from a Cu

sealed X-ray tube ($K\alpha = 1.5418 \text{ \AA}$ with a potential of 40 kV and a current of 40 mA) fitted with a graphite monochromator in the parallel mode (175 mm collimator with 0.5 mm pinholes). A total of 180 data frames were taken at widths of 0.5° with an exposure time of 15 s. These reflections were used to determine the unit cell using Cell_Now.¹⁵⁰ A suitable cell was found and refined by nonlinear least-squares and Bravais lattice procedures. Integrated intensity information for each reflection was obtained by reduction of the data frames with SAINTplus.¹⁵⁰ The integration method employed a three-dimensional profiling algorithm and all data were corrected for Lorentz and polarization factors, as well as for crystal decay effects. Finally the data was merged and scaled to produce a suitable data set. SADABS¹⁵⁰ was employed to correct the data for absorption effects. The structure was solved in the monoclinic $C2/c$ space group using XS¹⁵¹ (incorporated in SHELXTL). All non-hydrogen atoms were refined with anisotropic thermal parameters. The hydrogen atoms were placed in idealized positions and refined using riding model. The structure was refined (weighted least-squares refinement on F^2) to convergence. Although the Ir-*H* ligand couldn't be located in the crystal structure confidently, its presence is indicated both by ^1H and ^1H - ^{29}Si DQF NMR spectroscopic data. The SQUEEZE protocol included in PLATON¹⁵⁰ was used to account for disordered solvent molecules found in the crystal lattice that could not be satisfactorily modeled.

CHAPTER III

DUAL-SITE NON-INNOCENCE OF THE SiNN PINCER LIGAND IN COMPLEXES OF RHODIUM²

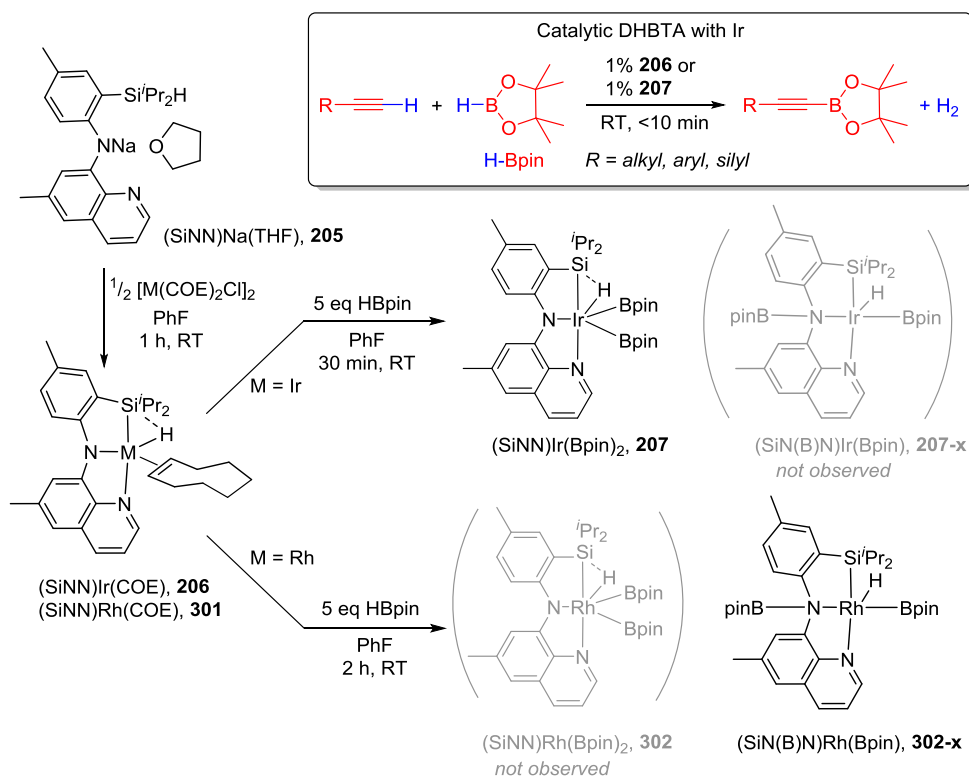
3.1 Introduction

Transition metal-catalyzed borylation of C-H bonds has become an important synthetic tool over the last two decades.^{64,65,106} The products of C-H borylation, organoboronate esters, are versatile building blocks in organic synthesis, enabling facile formation of new carbon-carbon and carbon-heteroatom bonds. In particular, much attention has been dedicated to and considerable success achieved in Ir-catalyzed borylation of aromatic C-H bonds.^{67,68,152} Our group recently reported a complementary Ir catalyst capable of dehydrogenative C-H borylation of terminal alkynes (DHBTA, Scheme 1).¹³⁷ Our Ir system was based on a novel SiNN supporting pincer ligand that combines nitrogenous amido and quinoline-type donors with the Si-H functionality. We showed that **206** can be rapidly converted to **207** in the presence of HBpin and that either **206** or **207** can be used as a pre-catalyst. In the present work, we explore Rh analogs of these Ir SiNN complexes. Although the new Rh compounds turned out to be inactive as DHBTA catalysts, they brought to light an unusual dual non-innocence^{153,154} behavior of the SiNN ligand. The (SiNN)Rh system also turned out to be a modest benzene borylation catalyst.

² In this chapter, all DFT calculations are done by Dr. Jia Zhou. The experimental work was performed by Nathanael A. Hirscher and Chun-I Lee. Nathanael A. Hirscher was a visiting undergraduate research student who worked during the summer of 2013 with Chun-I Lee as his mentor.

3.2 Results and discussion

By analogy with the synthesis of **206**, **205** smoothly reacted with one-half equiv. of $[(\text{COE})_2\text{RhCl}]_2$ in fluorobenzene at ambient temperature to produce a blue solution of **301** (Scheme 3-1). Workup of the reaction by filtration and recrystallization allowed isolation of **301** in 66% yield as an analytically pure blue solid. ^1H and $^{13}\text{C}\{^1\text{H}\}$ NMR spectra of **301** displayed the expected features similar to **206**, with the resonances corresponding to the organic framework of SiNN and of COE readily identifiable. An upfield ^1H NMR resonance was observed at -16.9 ppm corresponding to the SiH hydrogen bound to Rh (cf. δ -21.1 ppm in **206**). This resonance displayed coupling to ^{103}Rh ($J_{\text{Rh-H}} = 31$ Hz) and possessed satellites from coupling to ^{29}Si ($J_{\text{Si-H}} = 51$ Hz).



Scheme 3-1. Synthesis of SiNN complexes of Ir and Rh, and DHBTA catalysis by Ir complexes.

A single-crystal X-ray diffraction study (Figure 3-1) established that **301** is isomorphous with **206**, crystallizing in the same space group ($P2_1/n$) with unit cell volumes within 0.5% of each other. On the molecular level, **301** and **206** are nearly superimposable,¹⁵⁰ with only small differences in the metrics associated with the coordination sphere of the metals. Treatment of **301** with 5 equiv. of HBpin by analogy with the synthesis of **302-x** resulted in the predominant formation of a new product that could be isolated as a yellow solid in 59% yield. It contained ^1H NMR resonances expected for all the constituent groups in “(SiNN)Rh(Bpin)₂”, however several features distinguishing it from **207** were immediately apparent. First of all, the yellow color of **302-x** was suspect, as **207** is purple whereas both **206** and **301** are blue. Instead of a single resonance for the Bpin methyl groups (as is the case for **207**), **302-x** exhibited several.¹⁵⁰ In the ^{11}B NMR spectrum, **302-x** presented two resonances at 41.3 and 23.8 ppm vs. a single one at 28.9 ppm for **207**. Finally, we were not able to measure the $J_{\text{Si-H}}$ value for **302-x** (assumed <1 Hz). That was inconsistent with the exact structural analog of **207** ($J_{\text{Si-H}} = 32$ Hz) because the change from Ir to Rh dramatically increased the $J_{\text{Si-H}}$ value in **301** (51 Hz) vs **206** (8 Hz). These observations led us to envision a different, isomeric structure for **302-x**, which was confirmed by a single-crystal X-ray diffraction study (Figure 3-1). **302-x** can be viewed as a “borotautomer” of **302**, differing by migration of one of the boryl groups onto the central N of the SiNN ligand. The hydride in **302-x** was not located by XRD methods, but its presence is apparent from the doublet ($J_{\text{Rh-H}} = 30$ Hz) at -15.0 ppm in the ^1H NMR spectrum.

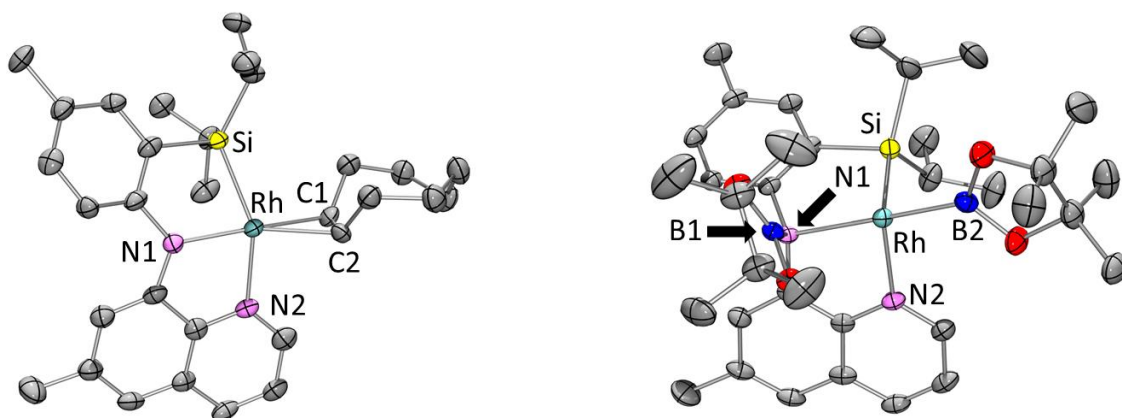


Figure 3-1. ORTEP drawings¹²⁹ of **301** (left, 80% probability ellipsoids) and **302-x** (right, 50% probability ellipsoids) showing selected atom labeling. Hydrogen atoms are omitted for clarity. Select bond distances (Å) and angles (deg) for **301**: Rh-Si, 2.3787(13); C1-C2, 1.388(8); Si-Rh-N2, 140.87(11). For **302-x**: Rh-Si, 2.2223(9); Rh-B2, 2.007(3); N1-B1, 1.459(4); Si-Rh-N2, 106.51(7); N1-Rh-B2, 175.33(11).

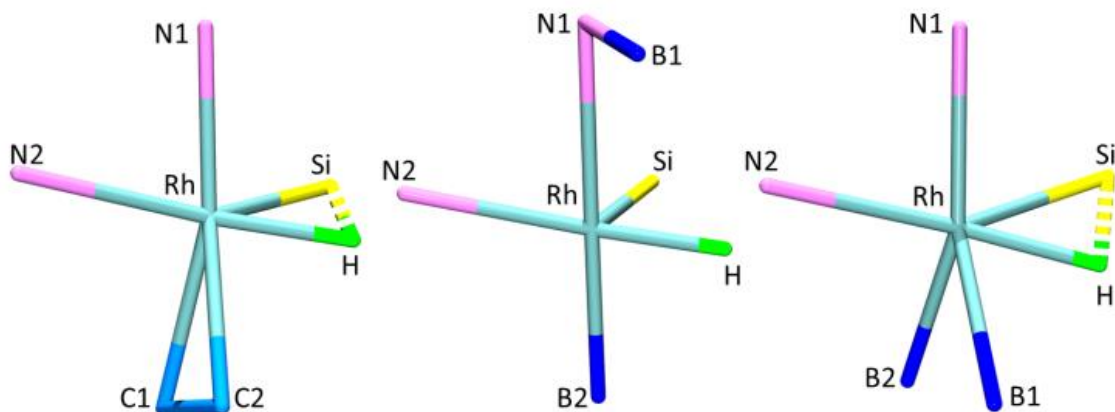


Figure 3-2. Drawings¹²⁹ of the DFT calculated structures of **301** (left), **302-x** (middle) and **302** (right). N2 is the quinoline N.

We used density functional theory (at the M06/SDD/6-311G** level)¹⁴⁶ to calculate structures of **301**, **302**, and **302-x**. Figure 3-2 shows the immediate coordination environment in the three calculated Rh structures. The non-H atom positions reproduce those in the available XRD-determined ones well. The calculated structures of **206** and

207 were reported by us previously,¹³⁷ using the same DFT methods. The three distinct X-type ligands (boryl, silyl, hydride) in **302-x** and are of very strong *trans*-influence and adopt a facial arrangement. The approximately square-pyramidal coordination sphere about Rh is completed by two neutral nitrogenous donors (quinoline and borylated diarylamine); the silyl ligand is *trans* to the empty site.^{155,156} DFT-calculated free energies of the 3a-M/3b-M isomers are consistent with the experimental facts: for Ir, **207** is preferred by 1.8 kcal/mol; while for Rh, **302-x** is favored by 5.2 kcal/mol. The free energy barrier for the direct migration of the boryl from M in **207** or **302** to N was calculated to be 16.9 kcal/mol for M = Ir and 12.0 kcal/mol for M = Rh; both are consistent with rapid migration at ambient temperature.

Figure 3-3 depicts the geometries in the M/Si/H triangles in compounds **206/207(-x)/301/302(-x)**. The variation of the geometric parameters within these structures can be viewed as reflective of the continuum between Si-H σ -complexes and silyl/hydride oxidative addition.^{128,131,132} **301** and **302** clearly belong to the former, while **207-x** and **302-x** to the latter. As discussed previously,¹³⁷ **206** is probably best viewed as a silyl/hydride complex while **207** is a borderline structure. The geometrical changes in **206/207(-x)/301/302(-x)** are not limited only to the Si-H distances. There is a monotonous correlation between the increase in the Si-H distance and increase in the Si-M-H angle on the one hand, and decrease in the M-Si and M-H distances on the other. This is consistent with the notion of strengthening M-Si and M-H interactions upon diminishment of the Si-H interactions. The complexity of interactions of Si-H bonds

with transition metals has been thoroughly studied and analyzed,^{128,131,132} but Si-H as an adaptable spectator donor site in a chelating ligand has not been widely used.¹⁵⁷⁻¹⁵⁹

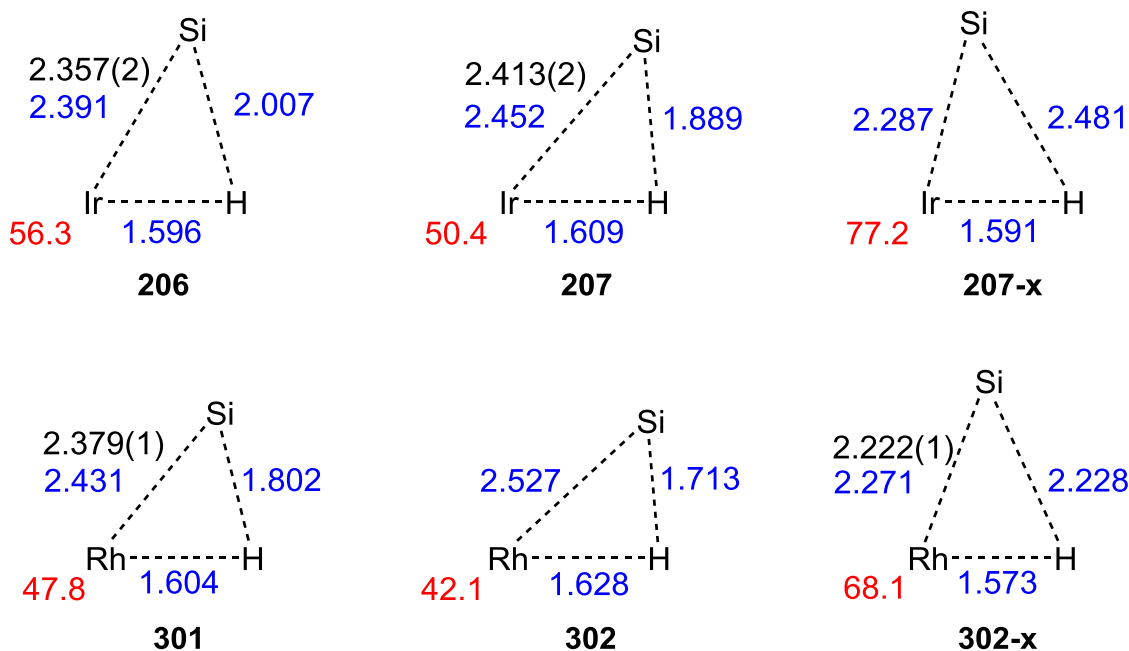


Figure 3-3. Metric parameters in the M/Si/H triangles (M = Rh or Ir) in compounds **206/207(-x)/301/302(-x)**. DFT calculated distances (Å) in blue, Si-M-H angles (°) in red, XRD-determined M-Si distances in black.

In contrast to its iridium analog, **301** showed no DHBTA activity. Treatment of **301** with HBpin in C₆D₆, followed by 4-MeC₆H₄CCH, gave rise to no alkynylboronate after 3 d at RT. Instead, incomplete and unselective hydroboration of 4-MeC₆H₄CCH to various alkenylboronates took place. On the other hand, we noted that **302-x** underwent degradation in benzene solutions over time, with PhBpin signals detectable in the mixture. Thermolysis of **301** or **302-x** in C₆D₆ in the presence of excess HBpin demonstrated that either can function as a modest benzene borylation catalyst, resulting in ca. 30 turnovers after 48 h at 80 °C (Table 3-1). Using B₂pin₂ in place of HBpin

resulted in a smaller number of turnovers of C₆D₆ under the same conditions. The degradation of **302-x** in solution in the absence of HBpin is not simply due to stoichiometric borylation of benzene as it also decomposed in cyclohexane-*d*₁₂ solution with significant HBpin release. Although there are examples of Rh C-H borylation catalysts in the literature,^{70,80,160-164} they have not so far risen to the impressive efficiency of Ir catalysis.^{67,68,152} The catalytic reactivity of the (SiNN)Rh system is in contrast with the lack of arene borylation we previously observed with (SiNN)Ir.

Table 3-1. Catalytic borylation of neat C₆D₆ (80 °C, 48 h) using **301** and **302-x**.

Rh Catalyst ^a	Boron Source	C ₆ D ₅ Bpin Yield ^b
301	HBpin	27%
302-x	HBpin	33%
301	B ₂ pin ₂	7%
302-x	B ₂ pin ₂	5%

^a Rh:Bpin ratio of 1:100. ^b Yield based on Bpin equivalents, determined by ¹H NMR vs C₆Me₆ internal integration standard.

Interestingly, recent work on the “traditional” iridium aromatic C-H borylation catalysts supported by bipyridine-type ligands highlighted the usefulness of an Si-H moiety as a directing group in the substrate.^{79,165} The intermediate **143** proposed⁷⁹ by Hartwig et al. (Figure 3-4) bears a structural resemblance to **302-x** in that the coordination sphere of the metal in **143** also contains three facially-disposed strong *trans*-influence X-type ligands (silyl, boryl, boryl) and two neutral nitrogenous donors.

The use of supporting bidentate and tridentate ligands containing spectating silyl ligands in Ir-catalyzed aromatic borylation has also been reported recently.^{87,166}

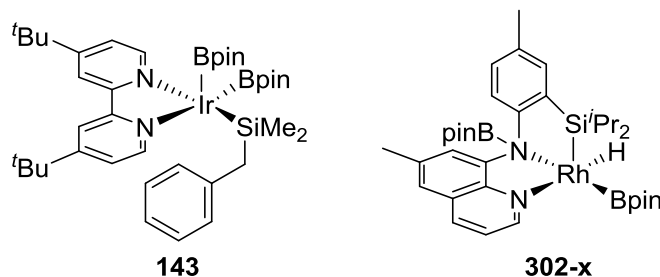


Figure 3-4. Intermediate proposed by Hartwig et al. (**143**) and **302-x**.

3.3 Conclusion

In summary, the new Rh complexes of the SiNN ligand uncovered its potential for unusual double non-innocence. In addition to the previously noted capacity of the Si-H moiety of SiNN to adapt to the changes in the environment about the metal center, we now report that it can be complemented by the non-innocence of the amido site. The amido nitrogen can reversibly accept a boryl group from the metal. Taken together, these two phenomena characterize a ligand with an exceptional ability to reversibly adapt to events at the metal center. While the integrity of the Si-H moiety would likely be challenged in reactions involving polar reagents, we believe the unusual adaptability of SiNN may be advantageous in catalysis with non-polar substrates. Here, we demonstrate modest activity of the SiNN Rh complexes in benzene borylation.

3.4 Experimental

General Considerations. Unless specified otherwise, all manipulations were performed under an Ar atmosphere using standard Schlenk line or glovebox techniques.

Toluene, fluorobenzene, diethyl ether, pentane, benzene, C₆D₆ were dried over NaK/Ph₂CO/18-crown-6, distilled or vacuum transferred and stored over molecular sieves in an Ar-filled glovebox. CH₂Cl₂, CD₂Cl₂, CDCl₃ were dried with and then distilled from CaH₂ and stored over molecular sieves in an Ar-filled glove box. C₆D₁₂ was deoxygenated by three freeze-pump-thaw cycles and stored over molecular sieves in an Ar-filled glovebox. Compound **205** was prepared according to the published procedure.¹³⁷ Alkynes were deoxygenated by three freeze-pump-thaw cycles prior to use. All other chemicals were used as received from commercial vendors. NMR spectra were recorded on a Varian Inova 300, Mercury 300 (¹H NMR, 299.952 MHz; ¹³C NMR, 75.421 MHz), Varian Inova 400 (¹H NMR, 399.535 MHz; ¹¹B NMR, 128.185 MHz; ¹³C NMR, 100.465 MHz; ²⁹Si NMR, 79.366 MHz) and NMRS 500 (¹H NMR, 499.703 MHz; ¹³C NMR, 125.697 MHz) spectrometer. ¹H-²⁹Si double quantum filter (DQF)¹⁴⁴ experiments on compounds **301** and **302-x** were performed on Varian Inova 400. Chemical shifts are reported in δ (ppm). For ¹H and ¹³C NMR spectra, the residual solvent peak was used as an internal reference (¹H NMR: δ 7.15 for C₆D₆, 7.26 for CDCl₃, 5.32 for CD₂Cl₂, 1.38 for cyclohexane-*d*₁₂; ¹³C NMR: δ 128.06 for C₆D₆, 77.16 for CDCl₃, 53.84 for CD₂Cl₂). For ²⁹Si NMR, spectra were referenced externally to δ = 0 ppm by using Me₄Si. For ¹¹B NMR, spectra were referenced externally to δ = 0 ppm by using BF₃·Et₂O. Elemental analyses were performed by CALI Labs, Inc. (Parsippany, NJ).

Computational details. All computations were carried out with the Gaussian09 program.¹⁴⁵ All of the geometries were fully optimized by the M06¹⁴⁶ functional. The

Stuttgart basis set and the associated effective core potential (ECP) was used for Rh and Ir atoms, and an all-electron 6-311G(d,p) basis set was used for the other atoms. The harmonic vibrational frequency calculations were performed to ensure that either a minimum or first-order saddle point was obtained. The energies reported here are Gibbs free energies in the gas phase at 298.15 K and 1 atm unless noted otherwise.

Table 3-2. Calculated energies of compounds under study (gas phase, 298 K).

Compound	Enthalpy in au.	Gibbs Free Energy in au.	Relative Enthalpy in kcal/mol	Relative Gibbs Free Energy in kcal/mol
Rh				
302	-2224.407884	-2224.536999	4.12	5.17
302TS	-2224.390886	-2224.517925	14.79	17.14
302-x	-2224.414451	-2224.545245	0.0	0.0
Ir				
207	-2218.238137	-2218.367228	0.0	0.0
207TS	-2218.211080	-2218.340331	16.98	16.88
207-x	-2218.232884	-2218.364371	3.30	1.79

[Rh(COE)₂Cl]₂. [Rh(COE)₂Cl]₂ was synthesized using a modified literature procedure.¹⁶⁷ In a 100 mL Schlenk flask containing a stir bar, RhCl₃·3H₂O (0.99 g, 3.8 mmol) was dissolved in 6 mL of H₂O and 12 mL of *i*PrOH. To this solution, *cis*-

cyclooctene (COE) (2.0 mL, 15 mmol) was added. The resultant mixture was purged of air by three freeze-pump-thaw cycles on the Schlenk line, after which the system was closed under partial vacuum. The reddish-brown reaction mixture was heated to 45°C in an oil bath and stirred overnight. The flask was allowed to cool to ambient temperature, and the resultant yellow precipitate was separated from the red/brown solution using a glass fritted filter, which was rinsed with cold methanol. A fine mustard-yellow powder was obtained and dried under vacuum (1.18 g, 88% yield).

(SiNN)Rh(COE) (301). In an Ar-filled glovebox, **205** (103 mg, 0.225 mmol) was added along with $[\text{Rh}(\text{COE})_2\text{Cl}]_2$ (79 mg, 0.11 mmol) to a 25 mL Schlenk flask containing a stir bar. This was dissolved in 3 mL of fluorobenzene, and the resultant blue solution was stirred in the glovebox at RT for 50 min. The dark blue solution and precipitate were filtered through Celite, with CH_2Cl_2 used to rinse the flask and Celite. The filtrate was reduced to dryness under vacuum, and reconstituted in 1 mL CH_2Cl_2 . This was layered with 5 mL pentane, and stored in at a -35 °C freezer overnight. Afterward, the dark blue solid was recovered by decanting the dark blue solution off; the solid was rinsed with 1 mL cold pentane and dried under vacuum. A second crop was obtained from the decanted solution in similar fashion, and combined with the first crop (84 mg, 66% yield). ^1H NMR (500 MHz, C_6D_6): δ 7.83 (s, 1H, Ar-*H*), 7.73 (d, $J_{\text{H-H}} = 8.2$ Hz, 1H, Ar-*H*), 7.54 (d, $J_{\text{H-H}} = 4.8$ Hz, 1H, Ar-*H*), 7.45 (d, $J_{\text{H-H}} = 8.2$ Hz, 1 H, Ar-*H*), 7.42 (s, 1H, Ar-*H*), 7.01 (d, $J_{\text{H-H}} = 8.2$ Hz, 1H, Ar-*H*), 6.54 (dd, $J_{\text{H-H}} = 8.2, 4.8$ Hz, 1H, Ar-*H*), 6.39 (s, 1H, Ar-*H*), 4.16 (m, 2H, alkenyl-*H*), 2.48 (m, 2H), 2.32 (s, 3H, Ar- CH_3), 2.16 (s, 3H, Ar- CH_3), 1.82 (m, 2H), 1.75 (m, 2H), 1.62 (m, 4H), 1.38 (m, 10H, includes

Si(CHMe₂)₂), 1.29 (d, J_{H-H} = 7.2 Hz, 6H, Si(CHMe₂)₂), -16.89 (d, J_{Rh-H} = 31 Hz, 1H, Rh-*H*). Selected ¹H-²⁹Si DQF (400 MHz, C₆D₆) data for Rh-*H*: -16.89 (dd, J_{Rh-H} = 301 Hz, J_{Si-H} = 51 Hz). ¹³C{¹H} NMR (126 MHz, CD₂Cl₂): δ 159.7 (d, J = 2.5 Hz, 2-position at the quinoline fragment), 153.0 (br s), 145.1, 142.1, 140.1, 138.5, 136.0, 134.9, 131.2, 129.5, 128.9, 120.8, 118.1, 111.5 (br s), 109.9 (br s) (15 Ar-C), 71.8 (d, J = 10 Hz, alkenyl-C on COE), 32.9, 32.0 (br s), 26.9, 22.4, 21.0, 20.4, 19.9, 17.2 (8 aliphatic C, 2 Ar-CH₃ + 3 on COE + 3 for ^{*i*}Pr). ²⁹Si{¹H} NMR (79 MHz, C₆D₆): δ 42.8 (br). Anal. Calcd for C₃₁H₄₃N₂RhSi: C, 64.79; H, 7.54. Found: C, 64.53; H, 7.49.

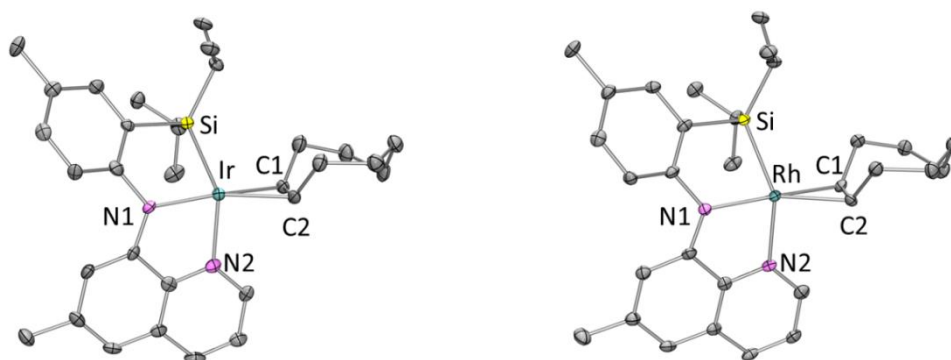


Figure 3-5. ORTEP drawings (50% probability ellipsoids) of **206** (left)¹³⁷ and **301** (right) showing select atom labeling.

(SiN(B)N)Rh(Bpin) (302-x). In an Ar-filled glovebox, **301** (70 mg, 0.12 mmol) was dissolved in 2 mL fluorobenzene in a 25 mL Schlenk flask, and HBpin (90 μL, 0.62 mmol) was then added to the flask. The reaction mixture was allowed to stir for 2 h at RT; the dark blue solution became dark brown over this time. The volatiles were then removed under vacuum. The residues were redissolved in 2 mL pentane, and dried under vacuum. The pentane/vacuum process was repeated two more times. Another 2 mL

pentane was added and the mixture was vigorously stirred for 10 min. The suspension was filtered through a fritted funnel, and the yellow solid was washed with 1 mL pentane twice and dried *in vacuo*. (52 mg, 59% yield). ^1H NMR (400 MHz, C_6D_6): δ 9.95 (d, $J_{\text{H-H}} = 4.8$ Hz, 1H, Ar-*H*), 7.85 (d, $J_{\text{H-H}} = 1.6$ Hz, 1H, Ar-*H*), 7.74 (d, $J_{\text{H-H}} = 8.1$ Hz, 1H, Ar-*H*), 7.53 (d, $J_{\text{H-H}} = 1.9$ Hz, 1H, Ar-*H*), 7.22 (dd, $J_{\text{H-H}} = 8.4, 1.6$ Hz, 1H, Ar-*H*), 7.09 (dd, $J_{\text{H-H}} = 8.1, 2.1$ Hz, 1H, Ar-*H*), 6.69 (m, 2H, Ar-*H*), 2.14 (s, 3H, Ar- CH_3), 1.95 (m, 1H, CHMe_2), 1.89 (s, 3H, Ar- CH_3), 1.69 (d, $J_{\text{H-H}} = 7.3$ Hz, 3H, CHMe_2), 1.46 (d, $J_{\text{H-H}} = 7.3$ Hz, 3H, CHMe_2), 1.39 (s, 12H, CH_3 on Bpin), 1.28 (s, 6H, CH_3 on Bpin), 1.23 (m, 1H, CHMe_2), 1.14 (d, $J_{\text{H-H}} = 7.3$ Hz, 3H, CHMe_2), 1.06 (s, 6H, CH_3 on Bpin), 0.72 (d, $J_{\text{H-H}} = 7.3$ Hz, 3H, CHMe_2), -14.98 (d, $J_{\text{Rh-H}} = 30$ Hz, 1H, Ir-*H*). Selected ^1H - ^{29}Si DQF (400 MHz, C_6D_6) data for Ir-*H*: δ -14.98 (d, $J_{\text{Rh-H}} = 30$ Hz). The $J_{\text{Si-H}}$ value was too small to be determined (<1 Hz). $^{13}\text{C}\{^1\text{H}\}$ NMR (126 MHz, C_6D_6): δ 153.5 (d, $J = 2.0$ Hz, 2-position at the quinoline fragment), 150.6, 148.7, 146.8, 144.9, 137.0, 136.0, 135.7, 135.1, 130.1, 130.0, 128.8, 128.6, 125.1, 121.9 (15 Ar-C), 84.5 (C_{quart} , Bpin on N), 80.79, 80.78 (2 C_{quart} , Bpin on Ir), 26.5, 26.1, 25.8, 24.6, 21.2, 21.1 (d, $J = 1.4$ Hz), 21.0, 20.7, 20.3, 20.1, 18.6 (d, $J = 2.3$ Hz, $\text{Si}(\text{CHMe}_2)_2$), 17.7 (d, $J = 4.4$ Hz, $\text{Si}(\text{CHMe}_2)_2$) (12 aliphatic C, 2 Ar- CH_3 + 6 for *i*Pr + 4 for CH_3 on Bpin). $^{29}\text{Si}\{^1\text{H}\}$ NMR (79 MHz, C_6D_6): 54.9 (d, $J_{\text{Rh-Si}} = 52$ Hz). ^{11}B NMR (128 MHz, C_6D_6): 41.3 (N-*B*), 23.8 (Ir-*B*). Anal. Calcd for $\text{C}_{35}\text{H}_{53}\text{B}_2\text{N}_2\text{O}_4\text{RhSi}$: C, 58.51; H, 7.44. Found: C, 58.39; H, 7.60.



Figure 3-6. Left: Removal of all volatiles before filtration. Right: Filtration through a fritted funnel.

Representative procedure for attempted catalysis of DHBTA. To a J. Young NMR tube in an Ar-filled glovebox, a 0.0125 M stock solution of **301** in C_6D_6 (80 μ L, 1.0 μ mol) was added, followed by 0.20 mL of neat C_6D_6 . Then, HBpin (29 μ L, 0.20 mmol) was added via microsyringe. The tube was shaken and the contents were allowed to react for 3 min. After this, 4-ethynyltoluene (13 μ L, 0.10 mmol) was dissolved in 0.20 mL C_6D_6 . This solution was added in four parts in one-minute intervals. After addition of HBpin, the solution changed colors from dark blue to yellow-brown, and this mixture was allowed to react at RT. After 3 d, analysis by 1H NMR spectroscopy revealed 43% *trans*- $CH_3-C_6H_4-CH=CH-Bpin$, 30% *gem*- $CH_3-C_6H_4-CH(Bpin)=CH_2$, 5% *cis*- $CH_3-C_6H_4-CH=CH-Bpin$, and 22% 4-ethynyltoluene. All volatiles were removed *in vacuo* and redissolved in $CDCl_3$, and the 1H NMR (500 MHz, $CDCl_3$) spectral data of alkenylboronates were in agreement with those reported in the literature.^{168,169} 1H NMR (500 MHz, $CDCl_3$): *Trans*- $CH_3-C_6H_4-CH=CH-Bpin$: δ 7.40 (d, $J_{H-H} = 8.0$ Hz, 2H, Ar-*H*), 7.38 (d, $J_{H-H} = 19$ Hz, 1H, alkenyl-*H*), 7.15 (d, $J_{H-H} = 8.0$ Hz, 2H, Ar-*H*), 6.12 (d, $J_{H-H} =$

19 Hz, 1H, alkenyl-*H*), 2.35 (s, 3H, Ar-*CH*₃), 1.32 (s, 12H, *CH*₃ on Bpin). *Gem*-*CH*₃-C₆H₄-CH(Bpin)=CH₂: δ 7.39 (d, *J*_{H-H} = 8.0 Hz, 2H, Ar-*H*), 7.13 (d, *J*_{H-H} = 8.0 Hz, 2H, Ar-*H*), 6.06 (d, *J*_{H-H} = 3.0 Hz, 1H, alkenyl-*H*), 6.02 (d, *J*_{H-H} = 3.0 Hz, 1H, alkenyl-*H*), 2.34 (s, 3H, Ar-*CH*₃), 1.33 (s, 12H, *CH*₃ on Bpin). *Cis*-CH₃-C₆H₄-CH=CH-Bpin: δ 7.47 (d, *J*_{H-H} = 8.0 Hz, 2H, Ar-*H*), 7.19 (d, *J*_{H-H} = 15 Hz, 1H, alkenyl-*H*), 7.12 (d, *J*_{H-H} = 8.0 Hz, 2H, Ar-*H*), 5.54 (d, *J*_{H-H} = 15 Hz, alkenyl-*H*), 2.36 (s, 3H, Ar-*CH*₃), 1.31 (s, 12H, *CH*₃ on Bpin).

Catalytic reaction of 301 with C₆H₆ and HBpin. To a J. Young NMR tube in an Ar-filled glovebox, a 0.010 M stock solution of **301** in C₆H₆ was added (400 μL, 0.0040 mmol). To this, HBpin (12 μL, 0.080 mmol) was added. After 2 min, the dark blue solution became yellow/brown. The NMR tube was sealed and taken out of the glovebox to place in an 80 °C oil bath to heat for three days. The reaction mixture was then transferred into a Schlenk flask, with pentane and CH₂Cl₂ used to rinse the NMR tube. The solvent was removed under vacuum, and the solid residue was dissolved in CDCl₃. PhBpin formation was confirmed by both ¹H and ¹³C NMR spectroscopic analysis.¹⁷⁰ The quaternary carbon atom attached to boron was not observed in the ¹³C NMR spectrum due to low intensity. ¹H NMR (300 MHz, CDCl₃) of PhBpin: δ 7.81 (d, *J*_{H-H} = 7.9 Hz, 2H, Ar-*H*), 7.46 (m, 1H, Ar-*H*), 7.37 (m, 2H, Ar-*H*), 1.35 (s, 12H, *CH*₃ on Bpin). ¹³C{¹H} NMR (75 MHz, CDCl₃) of PhBpin: δ 134.9, 131.4, 127.8, 83.9 (*C*_{quart}, Bpin), 25.0 (*CH*₃, Bpin).

Catalytic reaction of 301 with C₆H₆ and B₂pin₂. To a J. Young NMR tube in an Ar-filled glovebox, B₂pin₂ (10 mg, 0.041 mmol) was added. To this, a 0.010 M stock

solution of **301** in C₆H₆ was added (400 μL, 0.0040 mmol). The NMR tube was sealed and taken out of the glovebox to place in an 80 °C oil bath to heat for three days. The dark blue solution became brown. The reaction mixture was then transferred into a Schlenk flask, with pentane and CH₂Cl₂ used to rinse the NMR tube. The solvent was removed under vacuum, and the solid residue was dissolved in CDCl₃. PhBpin formation was confirmed by both ¹H and ¹³C NMR spectroscopic analysis.

Catalytic reaction of 301 with C₆D₆ and HBpin. To a J. Young NMR tube in an Ar-filled glovebox, a 0.0125 M stock solution of **301** in C₆D₆ was added (80 μL, 0.0010 mmol) followed by 266 μL of neat C₆D₆. To this, hexamethylbenzene and HBpin (200 μL of 0.25 M hexamethylbenzene/ 0.50 M HBpin stock solution in C₆D₆, 0.050 mmol for hexamethylbenzene and 0.10 mmol for HBpin) was added in once. The NMR tube was sealed and taken out of the glovebox to place in an 80 °C oil bath, and the reaction progress was monitored by ¹H NMR spectroscopy. After 48 h, 27% yield (based on HBpin) of D₅-PhBpin was determined on ¹H NMR measurement by the ratio of integration of methyl signals of Bpin to methyl signals of hexamethylbenzene.

Catalytic reaction of 301 with C₆D₆ and B₂pin₂. To a J. Young NMR tube in an Ar-filled glovebox, a 0.0125 M stock solution of **301** in C₆D₆ was added (80 μL, 0.0010 mmol) followed by 251 μL of neat C₆D₆. To this, hexamethylbenzene and B₂pin₂ (200 μL of 0.25 M hexamethylbenzene/ 0.250 M B₂pin₂ stock solution in C₆D₆, 0.050 mmol for hexamethylbenzene and 0.050 mmol for B₂pin₂) was added in once. The NMR tube was sealed and taken out of the glovebox to place in an 80 °C oil bath, and the reaction progress was monitored by ¹H NMR spectroscopy. After 48 h, 7% yield (based on Bpin

equivalent of B₂pin₂) of D₅-PhBpin was determined on ¹H NMR measurement by the ratio of integration of methyl signals of Bpin to methyl signals of hexamethylbenzene.

Catalytic reaction of 302-x with C₆D₆ and HBpin. To a J. Young NMR tube in an Ar-filled glovebox, a 0.0125 M stock solution of **302-x** in C₆D₆ was added (80 μL, 0.0010 mmol) followed by 266 μL of neat C₆D₆. To this, hexamethylbenzene and HBpin (200 μL of 0.25 M hexamethylbenzene/ 0.500 M HBpin stock solution in C₆D₆, 0.050 mmol for hexamethylbenzene and 0.10 mmol for HBpin) was added in once. The NMR tube was sealed and taken out of the glovebox to place in an 80°C oil bath and the reaction progress was monitored by ¹H NMR spectroscopy. After 48 h, 33% yield (based on HBpin) of D₅-PhBpin was determined on ¹H NMR measurement by the ratio of integration of methyl signals of Bpin to methyl signals of hexamethylbenzene.

Catalytic reaction of 302-x with C₆D₆ and B₂pin₂. To a J. Young NMR tube in an Ar-filled glovebox, a 0.0125 M stock solution of **302-x** in C₆D₆ was added (80 μL, 0.0010 mmol). To this, hexamethylbenzene and B₂pin₂ (200 μL of 0.25 M hexamethylbenzene/ 0.250 M B₂pin₂ stock solution in C₆D₆, 0.050 mmol for hexamethylbenzene and 0.050 mmol for B₂pin₂) was added in once, followed by 251 μL of neat C₆D₆. The NMR tube was sealed and taken out of the glovebox to place in an 80°C oil bath, and the reaction progress was monitored by ¹H NMR spectroscopy. After 48 h, 5% yield (based on Bpin equivalent of B₂pin₂) of D₅-PhBpin was determined on ¹H NMR measurement by the ratio of integration of methyl signals of Bpin to methyl signals of hexamethylbenzene.

Decomposition of 302-x in C₆D₆. 302-x (25 mg, 0.035 mmol) was dissolved in 0.5 mL C₆D₆ to result in a yellow solution in a J. Young tube. The solution was analyzed by ¹H and ¹¹B{¹H} spectroscopy immediately. The solution color turned green gradually. After 6 h at RT, analysis by ¹H NMR spectroscopy indicated roughly equal amount of HBpin (δ 0.98) and C₆D₅Bpin (δ 1.10) formation. HBpin (δ 28.2) and C₆D₅Bpin (δ 31.0) were also observed in the ¹¹B{¹H} NMR spectrum. The identity of HBpin was further confirmed by the ¹¹B NMR spectrum that showed a doublet at 28.2 ppm (J_{H-B} = 170 Hz).¹⁷¹

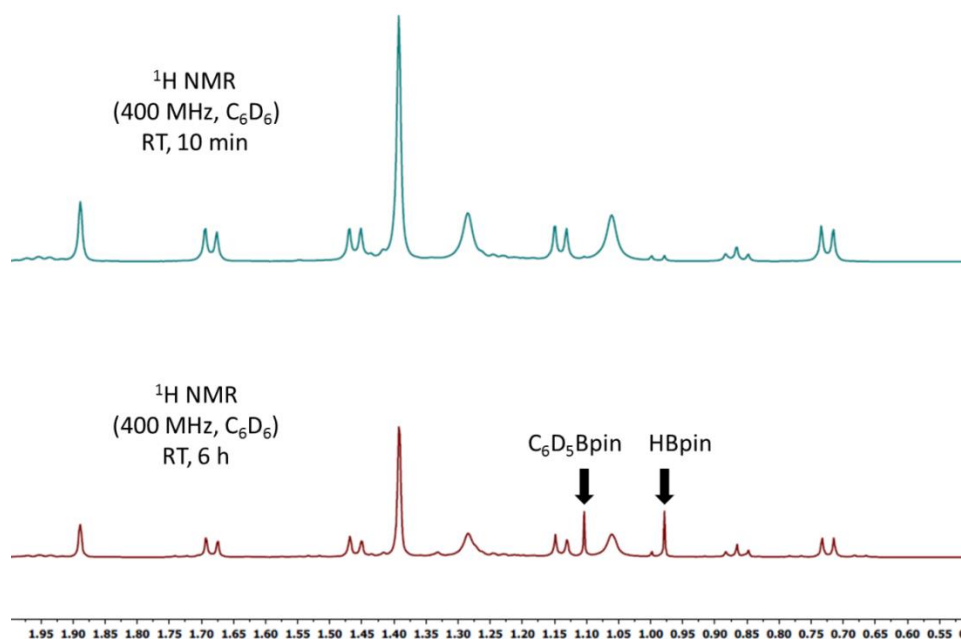


Figure 3-7. ¹H NMR spectra of 302-x in C₆D₆ after RT 10 min (top) and RT 6 h (bottom).

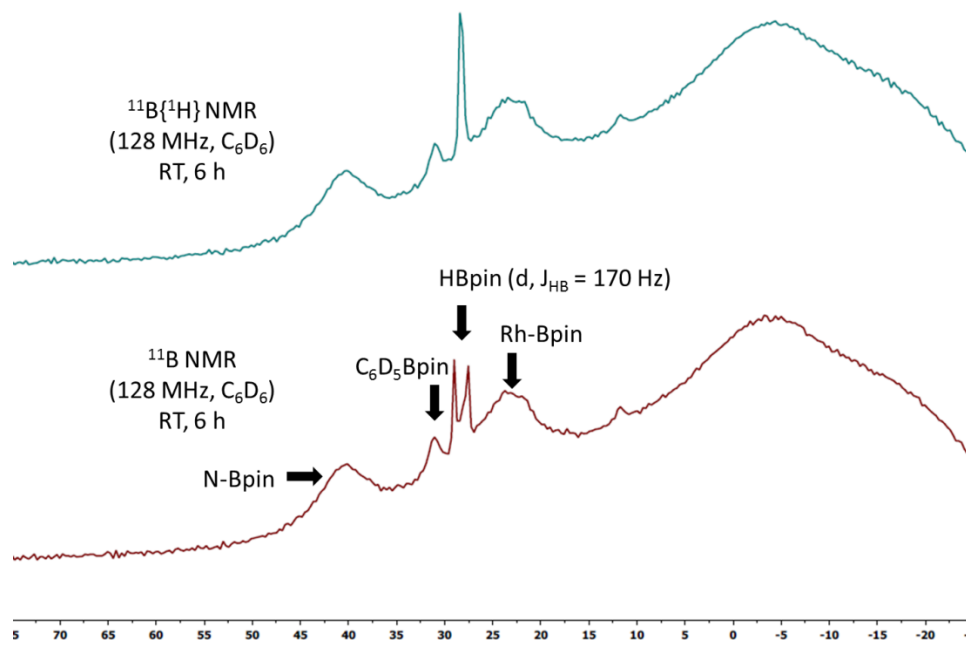


Figure 3-8. $^{11}\text{B}\{^1\text{H}\}$ NMR (top) and ^{11}B NMR (bottom) spectra of **302-x** in C_6D_6 after RT 6 h.

Decomposition of 302-x in cyclohexane- d_{12} . **302-x** (5 mg, 0.007 mmol) was dissolved in 0.5 mL cyclohexane- d_{12} to result in a light yellow solution in a J. Young tube. The solution was analyzed by ^1H and $^{11}\text{B}\{^1\text{H}\}$ spectroscopy immediately. The solution color turned darker gradually. After 6 h at RT, analysis by ^1H NMR spectroscopy indicated HBpin (δ 1.18) formation. HBpin (δ 28.4) was also observable in the $^{11}\text{B}\{^1\text{H}\}$ NMR spectrum, and the identity of HBpin was further confirmed by the ^{11}B NMR spectrum that showed a doublet at 28.4 ppm ($J_{\text{H-B}} = 170$ Hz).

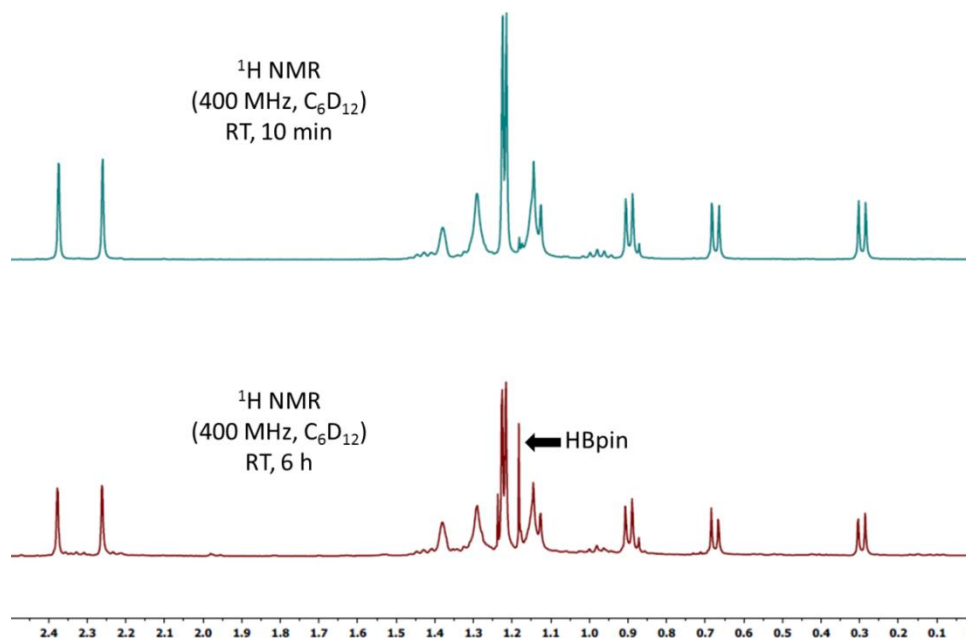


Figure 3-9. ¹H NMR spectra of **302-x** in C₆D₁₂ after RT 10 min (top) and RT 6 h (bottom).

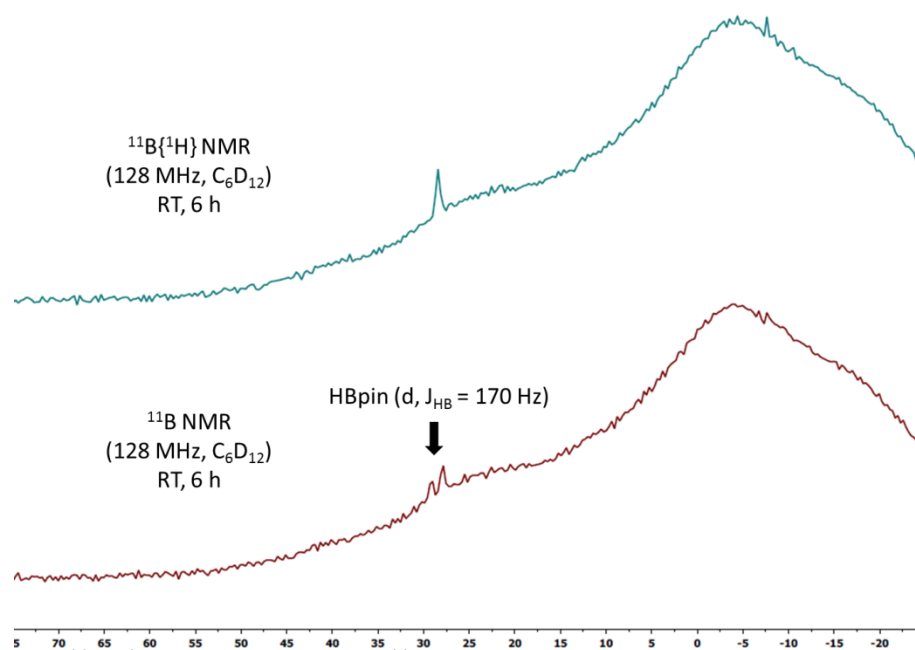


Figure 3-10. ¹¹B{¹H} NMR (top) and ¹¹B NMR (bottom) spectra of **302-x** in C₆D₁₂ after RT 6 h. The signals of **302-x** were not observable due to its low solubility in C₆D₁₂.

X-Ray data collection, solution, and refinement for 301. A Leica MZ 75 microscope was used to identify a suitable dark-blue multifaceted crystal with dimensions (max, intermediate, and min; in mm) $0.41 \times 0.27 \times 0.12$ from a representative sample of crystals of the same habit. The crystal mounted on a nylon loop was then placed in a cold nitrogen stream (Oxford) maintained at 110 K. A BRUKER GADDS X-ray (three-circle) diffractometer was employed for crystal screening, unit cell determination, and data collection. The goniometer was controlled using the FRAMBO software.¹⁵⁰

The sample was optically centered with the aid of a video camera such that no translations were observed as the crystal was rotated through all positions. The detector was set at 5.0 cm from the crystal sample. The X-ray radiation employed was generated from a Cu sealed X-ray tube ($K_{\alpha} = 1.5418 \text{ \AA}$ with a potential of 40 kV and a current of 40 mA) fitted with a graphite monochromator in the parallel mode (175 mm collimator with 0.5 mm pinholes). A total of 180 data frames were taken at widths of 0.5° with an exposure time of 15 s. These reflections were used to determine the unit cell using Cell_Now.¹⁵⁰ A suitable cell was found and refined by nonlinear least-squares and Bravais lattice procedures.

Integrated intensity information for each reflection was obtained by reduction of the data frames with SAINTplus.¹⁵⁰ The integration method employed a three-dimensional profiling algorithm and all data were corrected for Lorentz and polarization factors, as well as for crystal decay effects. Finally the data was merged and scaled to produce a suitable data set. SADABS¹⁵⁰ was employed to correct the data for absorption effects.

The structure was solved in the monoclinic P21/n space group using XS¹⁵¹ (incorporated in SHELXTL). All non-hydrogen atoms were refined with anisotropic thermal parameters. The hydrogen atoms were placed in idealized positions and refined using riding model. Two alkenyl-hydrogens in the cyclooctene fragment and Rh-*H* were assigned from Q peaks near the expected positions and refined. The structure was refined (weighted least-squares refinement on F²) to convergence. The presence of Rh-*H* is also indicated both by ¹H and ¹H-²⁹Si DQF NMR spectroscopic data.

X-Ray data collection, solution, and refinement for 302-x. A Leica MZ 75 microscope was used to identify a suitable yellowish block with very well defined faces with dimensions (max, intermediate, and min) 0.3 mm x 0.2 mm x 0.18 mm from a representative sample of crystals of the same habit. The crystal mounted on a nylon loop was then placed in a cold nitrogen stream (Oxford) maintained at 110 K.

A BRUKER APEX 2 X-ray (three-circle) diffractometer was employed for crystal screening, unit cell determination, and data collection. The goniometer was controlled using the APEX2 software suite, v2008-6.0.¹⁵⁰ The sample was optically centered with the aid of a video camera such that no translations were observed as the crystal was rotated through all positions. The detector was set at 6.0 cm from the crystal sample (APEX2, 512x512 pixel). The X-ray radiation employed was generated from a Mo sealed X-ray tube ($K_{\alpha} = 0.70173\text{\AA}$ with a potential of 40 kV and a current of 40 mA) fitted with a graphite monochromator in the parallel mode (175 mm collimator with 0.5 mm pinholes).

180 data frames were taken at widths of 0.5° . These reflections were used in the auto-indexing procedure to determine the unit cell. A suitable cell was found and refined by nonlinear least squares and Bravais lattice procedures. The unit cell was verified by examination of the $h k l$ overlays on several frames of data. No super-cell or erroneous reflections were observed. After careful examination of the unit cell, a standard data collection procedure was initiated using omega scans.

Integrated intensity information for each reflection was obtained by reduction of the data frames with the program APEX2.¹⁵⁰ The integration method employed a three dimensional profiling algorithm and all data were corrected for Lorentz and polarization factors, as well as for crystal decay effects. Finally the data was merged and scaled to produce a suitable data set. The absorption correction program SADABS¹⁵⁰ was employed to correct the data for absorption

Systematic reflection conditions and statistical tests of the data suggested the space group $P2_1/c$. A solution was obtained readily using SHELXTL (XS).¹⁵¹ Hydrogen atoms were placed in idealized positions and were set riding on the respective parent atoms. All non-hydrogen atoms were refined with anisotropic thermal parameters. Solvent molecules which could not be identified or modeled to a disordered known solvent were found. Thermal ellipsoids of the solvent molecules suggested partial occupancy and / or significant disorder. Eventually the solvent were SQUEEZED using PLATON.¹⁵⁰ The results indicated 62 electrons, and a volume of 352.2 \AA^3 . Since we could not recognize the nature of solvent or its disorder, the formula and the density reported in the CIF file does not represent the actual values. Absence of additional symmetry and voids were

confirmed using PLATON (ADDSYM).¹⁵⁰ The structure was refined (weighted least squares refinement on F^2) to convergence.^{151,172} Although the Rh-*H* ligand couldn't be located in the crystal structure confidently, its presence is indicated both by ¹H and ¹H-²⁹Si DQF NMR spectroscopic data.

CHAPTER IV

DEHYDROGENATIVE BORYLATION OF TERMINAL ALKYNES BY PNP

PINCER COMPLEXES OF IRIDIUM

4.1 Introduction

In the chapter 2, we presented the first example of DHBTA catalyzed by SiNN Ir complexes (Figure 4-1).¹³⁷ The reaction is chemoselective and can be performed under very mild conditions with alkyl-, aryl- and silyl- terminal alkynes in high yield. The origins of the excellent chemoselectivity and high activity are still unknown. Moreover, it is unclear whether all the structural factors of the specific SiNN ligand are essential for DHBTA. Later, in the study of Rh analogues of the Ir-DHBTA catalyst, an unusual double non-innocence of the SiNN ligand was observed (chapter 3). Besides the flexible Si-H moiety, the amido nitrogen can reversibly accept a boryl group from the metal.

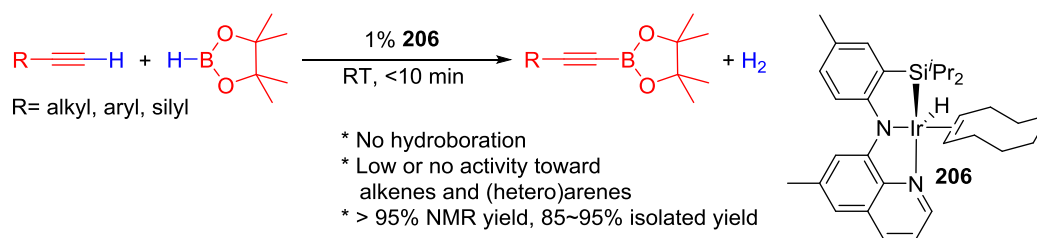


Figure 4-1. DHBTA catalyzed by **206**.

Inspired by the chemistry of the SiNN Rh complexes, one possible mechanism of DHBTA involving boryl transfer to and from the center amido group of the ligand backbone is depicted in the section 2-3. From the DFT studies and the phenomenon we observed in the SiNN Rh complexes, the N_(amido) donor seems to play the central role in DHBTA. Here we report the performance of a series of related ligands in DHBTA and

lead to the discovery of a new highly active catalyst **415-Ir-COE**, synthesis and characterization of the possible intermediates in DHBTA.

4.2 Results and discussion

4.2.1 Synthesis and screening of ligands for DHBTA

In light of the success of **206** in DHBTA, we decided to examine a series of ligands that systematically varied some of the SiNN features (Figure 4-2). From **401-H** to **405-H** and **1-F**, we preserved the central amido donor and the quinoline fragment but removed the silyl side arm (**401-H**) or replaced it with other hemilabile donors (**402-H** to **405-H** and **1F**). For **406-H** and **407-H**, the silane segment and the central amido donor are maintained; however, the quinoline moiety was eliminated (**406-H**) or substituted with a phosphine donor (**407-H**). We also included the PNP ligand (**408-H**) and the PCP/POCOP ligands (**409-H** to **410-H**) because these are common pincers with a rich history of C-H activation chemistry with Ir.^{3,51,173,174} The examination of related isopropyl PCP/POCOP ligand (**411-H** and **412-H**) is still undergoing at the time of this writing.

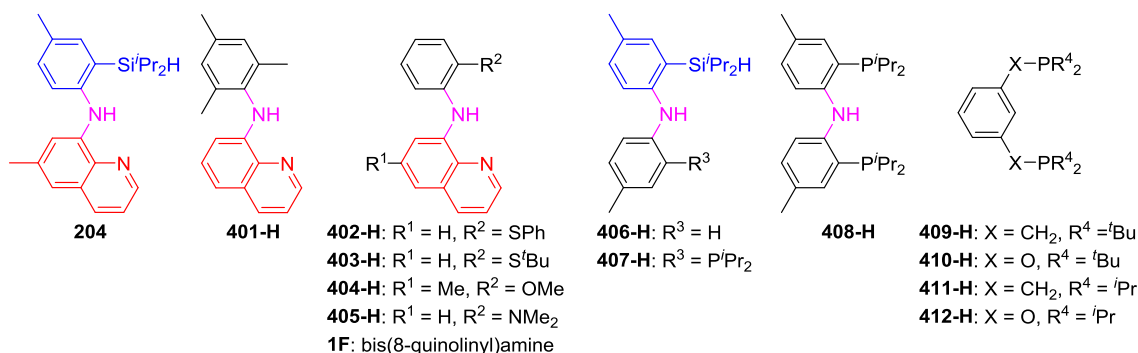
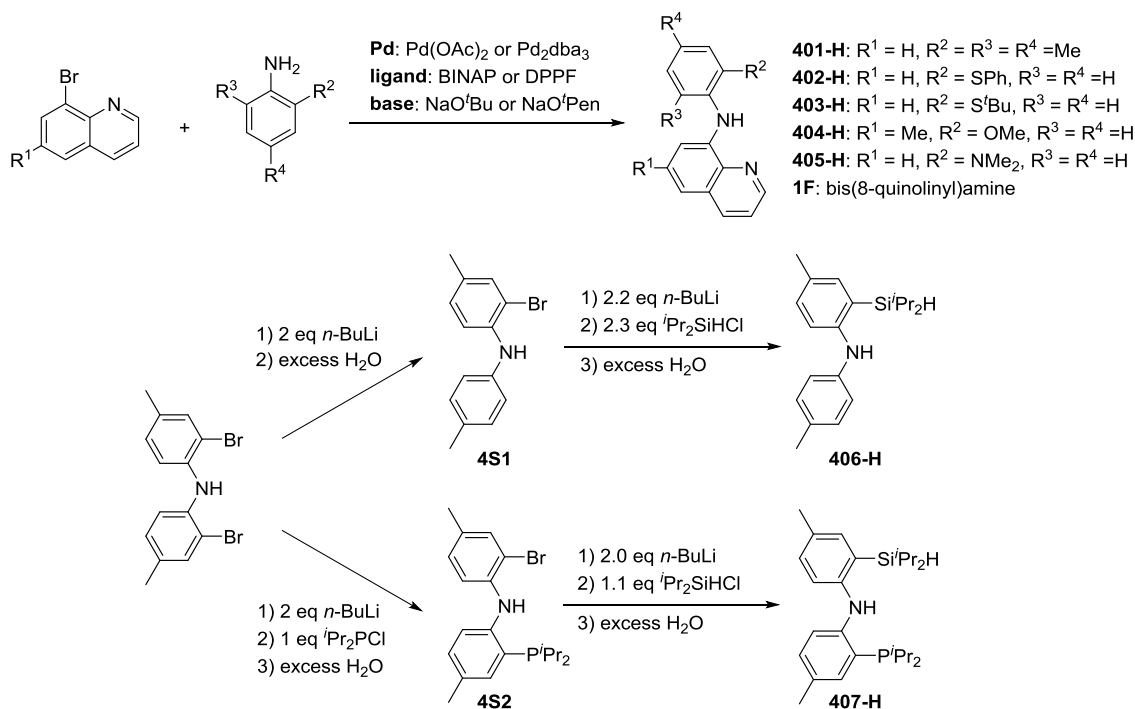


Figure 4-2. General strategy of ligand screening for DHBTA.

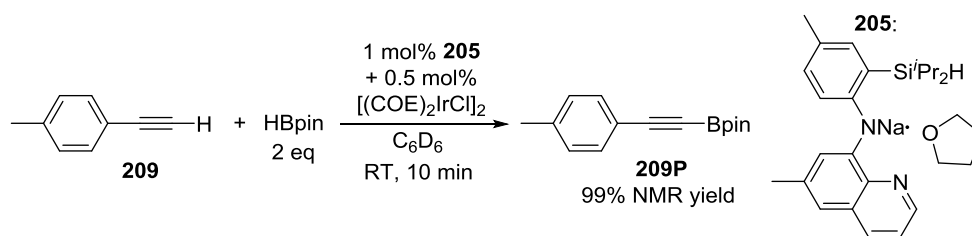
The syntheses of ligands used in the screening of DHBTA are shown in Scheme 4-1. Quinoline derivatives (i.e. **401-H**,¹²⁴ **402-H**, **403-H**, **404-H**, **405-H**,¹⁸ **1F**¹⁸) could be readily synthesized *via* Buchwald-Hartwig coupling from 8-bromoquinoline with various anilines or 8-aminoquinoline. The synthesis of **4S1** is adapted from our previous synthesis of **4S2**.¹⁷⁵ The dilithiation of bis(2-bromo-4-methylphenyl)amine with 2 equivalents of *n*-BuLi followed by aqueous workup and column chromatography produced **4S1** in 86% yield. Treatment of **4S1** with *n*-BuLi, followed by addition of ⁱPr₂SiHCl and work up gave **406-H** in 73% yield. The new SiNP ligand **407-H** was first prepared by Alyson Christopher in our group from **4S2** through a similar protocol.



Scheme 4-1. Synthesis of ligands used in screening DHBTA.

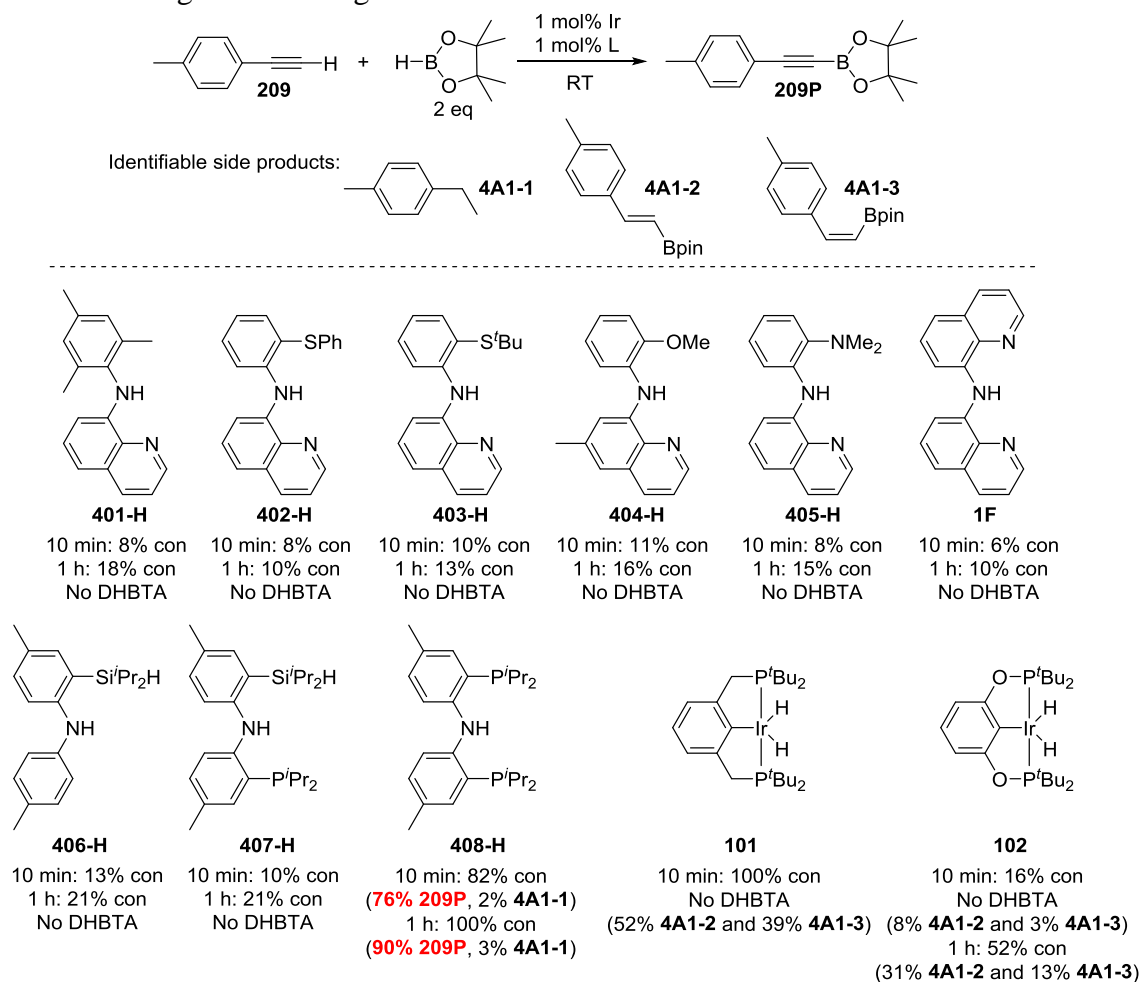
We demonstrated before that DHBTA could be carried out by generating **206** *in situ* from the reaction between **205** and [(COE)₂IrCl]₂ (Scheme 4-2).¹³⁷ Therefore, ligands

with central amido donors (**401-H** to **408-H** and **1F**) were deprotonated with 1 equivalent of $\text{NaN}(\text{SiMe}_3)_2$ and mixed with 0.5 equivalent of $[(\text{COE})_2\text{IrCl}]_2$. We assumed generation of the corresponding Ir cyclooctene complexes analogous to **206** *in situ* and these mixtures were used to test DHBTA. For PCP/POCOP ligands (**409-H** and **410-H**), we directly took the iridium dihydride complexes (**101**¹⁷⁶ and **102**¹⁷⁷) to examine DHBTA.



Scheme 4-2. DHBTA catalyzed by **206** generating *in situ* from **205**.

1 mol% Ir catalyst was tested in the reaction between 4-ethynyltoluene (**209**) and 2 equivalent of HBpin. The results are summarized in Table 4-1. None of the ligands tested showed any DHBTA reactivity except for **408-H**. In general, sluggish and nonselective hydrogenation and hydroboration were observed for **401-H** to **407-H** and **1F**. For PCP/POCOP iridium complexes (**101** and **102**), a mixture of *trans*-alkenylboronate (**4A1-2**) and *cis*-alkenylboronate (**4A1-3**) were observed as major products. Interestingly, the use of **408-H** gave 76% alkynylboronate **209P** after 10 min at ambient temperature and 90% yield after 1 h. About 3% 4-ethyltoluene (**4A1-1**) was also formed from hydrogenation which was not detected in the reactions catalyzed by SiNN Ir complexes.

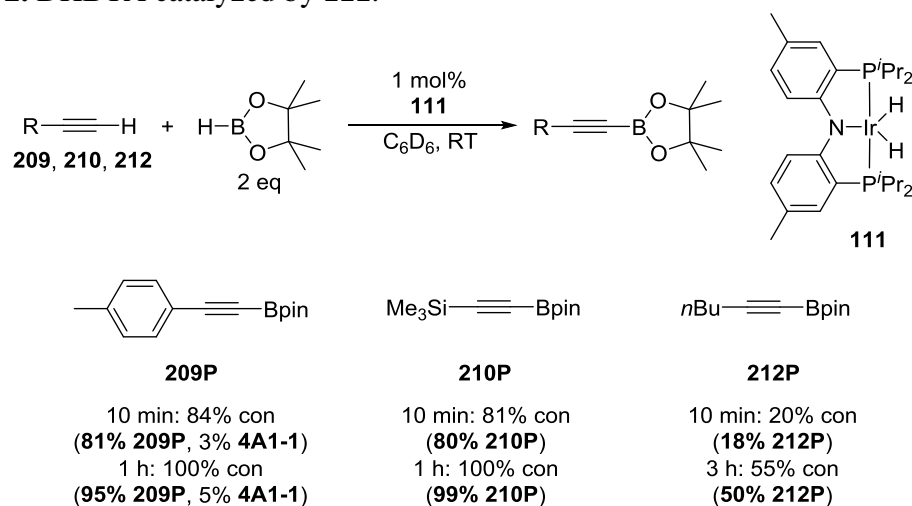
Table 4-1. Ligand screening in DHBTA.

For **401-H** to **408-H** and **1F**: In the following order, the ligand (0.0010 mmol), NaN(TMS)₂ (0.0010 mmol), [(COE)₂IrCl]₂ (0.00050 mmol) and HBpin (0.20 mmol) were mixed in C₆D₆ in a J. Young tube. 4-ethynyltoluene (0.10 mmol) was then added in 4 portions with 1 min intervals and the mixture was allowed to stand at ambient temperature for 10 min (see experimental for details). For **101** and **102**: The iridium complex (0.0010 mmol) and HBpin (0.20 mmol) were mixed in C₆D₆ in a J. Young tube. 4-ethynyltoluene (0.10 mmol) was then added in 4 portions with 1 min intervals and the mixture was allowed to stand at ambient temperature for 10 min (see experimental for details).

111 also gave the same result in the test reaction,¹⁵⁰ so we used **111** for the further DHBTA studies. 4-Ethynyltoluene (**209**), trimethylsilylacetylene (**210**), and 1-hexyne

(**212**) were chosen as model substrates for aromatic, silyl, and aliphatic terminal alkynes respectively (Table 4-2). In general, using **111** gave lower yields than **206** after 10 min at RT. For **209** and **210**, DHBTA was finished in 1 h and gave excellent yields. When using **111** as the catalyst, a small amount of the hydrogenation product **4A1-1** was also observed. The catalytic activity of **111** towards **212** was significantly slower than **209** and **210** and only achieved 50% yield after 3 h.

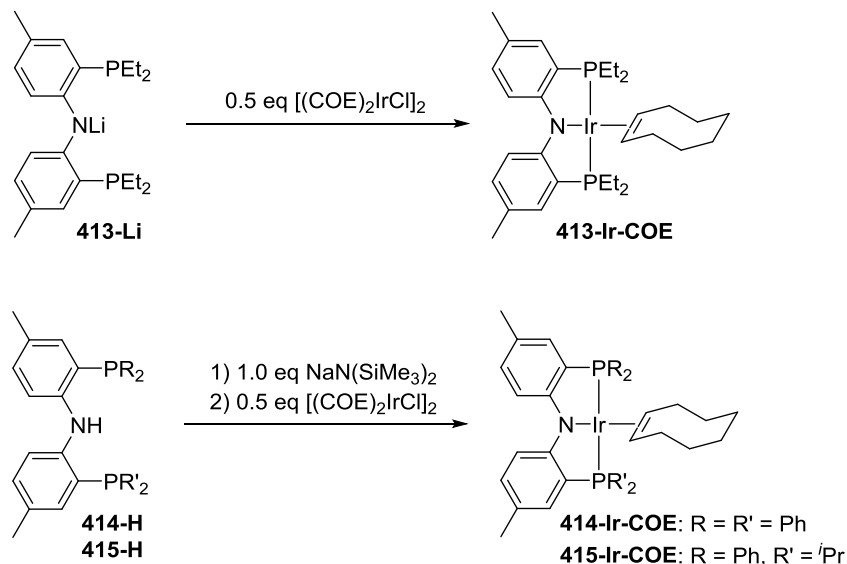
Table 4-2. DHBTA catalyzed by **111**.



4.2.2 Testing of (PNP)Ir complexes with various phosphine substituents

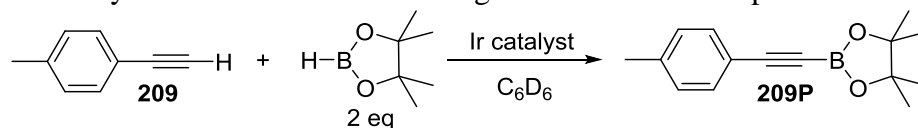
We were encouraged by the activity shown by the PNP ligand **408-H**. The PNP framework is readily modifiable, thus we selected several PNP ligands with different steric and electronic properties to install onto iridium (Scheme 4-3) for testing in DHBTA. The synthesis of **413-H** was recently reported by our group.¹⁷⁸ **413-H** was liquid and proved very difficult to purify; however, the Li derivative (**413-Li**) could be

isolated in a pure form in 56% yield. **413-Li** was then reacted with 0.5 equivalent of $[(\text{COE})_2\text{IrCl}]_2$ to yield **413-Ir-COE**. **414-Ir-COE**¹⁷⁹ and **415-Ir-COE** were synthesized *via* one-pot reactions by deprotonation of neutral ligands and treatment with $[(\text{COE})_2\text{IrCl}]_2$.



Scheme 4-3. Synthesis of (PNP)Ir(COE) complexes.

The newly synthesized (PNP)Ir(COE) complexes (**413-Ir-COE**, **414-Ir-COE**, **415-Ir-COE**), **111**, and the previously reported **206** were all tested in DHBTA by using **209** as the model substrate. The results were summarized in Table 4-3. Under 1 mol% catalyst loading, **413-Ir-COE**, **415-Ir-COE**, **111**, as well as **206** gave excellent yields at ambient temperature, whereas **414-Ir-COE** did not (entry 4). When the catalyst loading was lowered to 0.25%, **206** gave 43% yield after 1 h (entry 6) and the yield did not increase with longer reaction times.

Table 4-3. Catalytic results for DHBTA using various PNP Ir complexes and **206**.

Entry	Catalyst	Loading (mol%)	Time	Con. (%)	Yield (%)	Note
1	206	1	10 min	100	99	
2	111	1	1 h	100	95	10 min: 81% yield
3	413-Ir-COE	1	10 min	100	97	
4	414-Ir-COE	1	10 min	27	21	
5	415-Ir-COE	1	10 min	100	97	
6	206	0.25	1 h	44	43	10 min: 37% yield
7	111	0.25	4 h	100	90	10 min: 34% yield
8	413-Ir-COE	0.25	2 h	100	82	10 min: 45% yield
9	415-Ir-COE	0.25	10 min	100	92	
10	415-Ir-COE	0.05	2 h	100	85	
11	415-Ir-COE	0.025	8 h	100	85	10 min: 13% yield
12	415-Ir-COE	0.025	1 h ^a	100	84	
13	415-Ir-COE	0.01	2 h ^a	77	65	

The iridium complex and HBpin (0.20 mmol) were mixed in C_6D_6 in a J. Young tube. **209** (0.10 mmol) was then added in 4 portions with 1 min intervals and the mixture was allowed to stand at ambient temperature (see experimental for details).^a 60 °C.

415-Ir-COE showed superior reactivity to **111** and **413-Ir-COE** that gave 92% yield in 10 min. The reaction rate could be promoted by heating to 60 °C (entry 11 and 12) without significant yield loss and gave remarkable turnover number (~3400) with 0.025 mol% catalyst loading. The highest turnover number **415-Ir-COE** could achieve

was 6500 (entry 13), though under incomplete conversion at 0.01 mol% loading. In terms of chemoselectivity, using **206** in the DHBTA gave **209P** as the product exclusively; 2 to 10% of hydrogenation product **4A1-1** was observed in all (PNP)Ir complexes catalyzed reactions as the major side products (Figure 4-3).

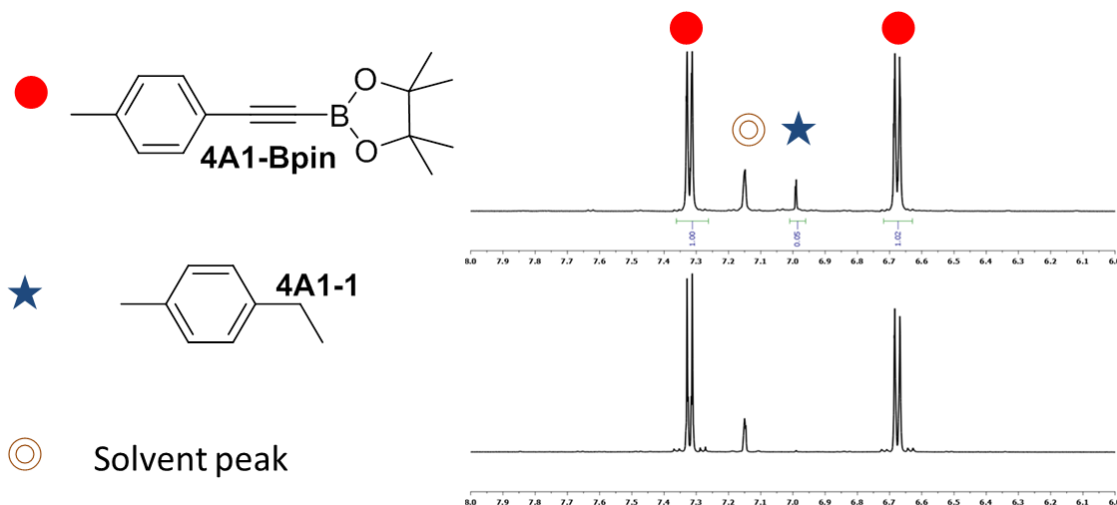
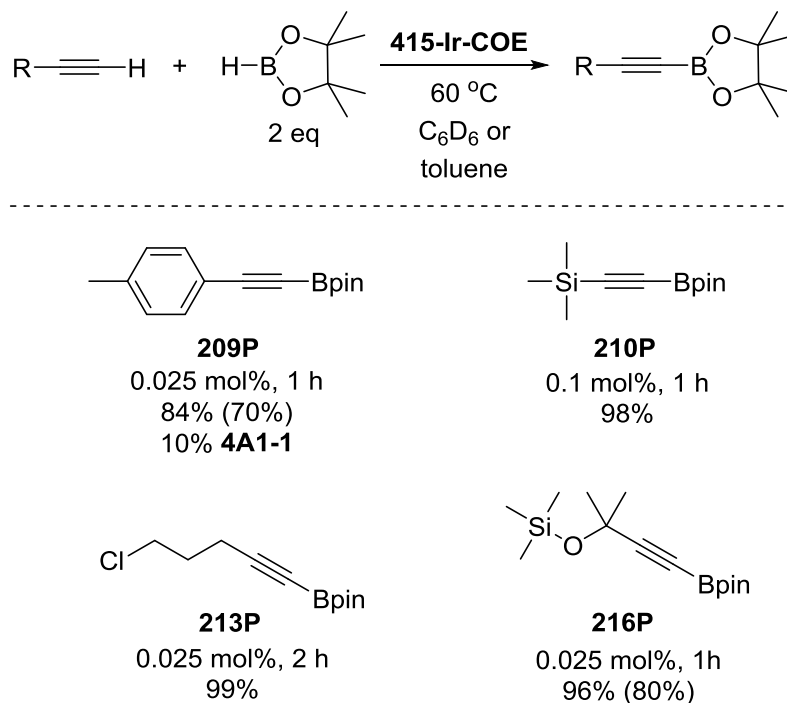


Figure 4-3. Partial ^1H NMR spectra of DHBTA reaction mixtures catalyzed by a) 1 mol% **413-Ir-COE** (entry 3 in Table 4-3) and b) 1 mol% **206** (entry 1 in Table 4-3).

To further explore the catalytic reactivity of **415-Ir-COE**, **209**, **210**, 5-chloro-1-pentyne (**213**) and 3-methyl-3-trimethylsiloxy-1-butyne (**216**) were chosen as model substrates for aromatic, silyl, aliphatic terminal alkynes and propargyl ethers respectively (Table 4-4). 84-99% NMR yields were obtained for all four substrates with 0.025 to 0.1 mol% loading of **415-Ir-COE** as the catalyst, and the alkynylboronate products (**209P** and **216P**) in the preparative-scale reactions could be easily purified by recrystallization and isolated in good yield. A mercury test¹⁸⁰ was performed with 0.025 mol% **415-Ir-COE** loading and **209** as substrate. No significant yield changes were

observed for either **209P** or the major side-product **4A1-1** which suggests that the catalysis is homogeneous.

Table 4-4. DHBTA of representative terminal alkynes catalyzed by **415-Ir-COE**.



^a **415-Ir-COE** and HBpin (0.20 mmol) were mixed in C_6D_6 in a J. Young tube. Alkyne (0.10 mmol) was then added in 4 portions with 1 min intervals at RT and the mixture was heated at 60 °C (see experimental for details). ^b NMR yield. ^c Yields in parentheses are isolated yields in preparative-scale (10 mmol alkyne) reactions that used toluene as the solvent instead of C_6D_6 .

4.2.3 Synthesis of proposed intermediates in DHBTA

In order to understand the reaction mechanism and the origin of chemoselectivity in DHBTA catalyzed by (PNP)Ir systems, (^{Me}PNP^{iPr})Ir (**408-Ir**) system was chosen for the further studies. The C_{2v} -symmetric ligand structure of **408-Ir** system leads to nice signals

in the ^{31}P NMR spectrum that are easy to track and a lot of $(^{\text{Me}}\text{PNP}^{\text{iPr}})\text{Ir}$ chemistry is also already known.^{51,173,174} We decided to independently synthesize possible intermediates in DHBTA by reacting $(^{\text{Me}}\text{PNP}^{\text{iPr}})\text{Ir}$ precursors with HBpin, terminal alkynes, and alkynylboronates (Figure 4-4) and examining them in both stoichiometric and catalytic reactions.

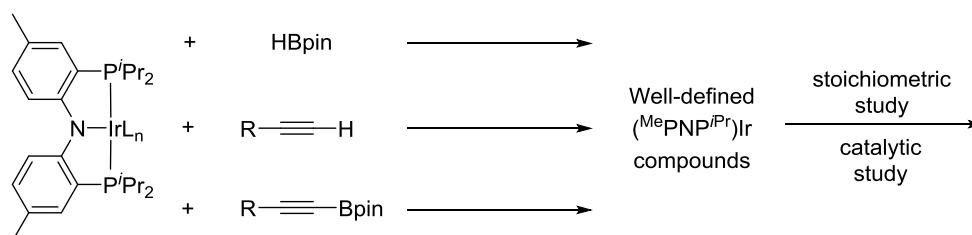
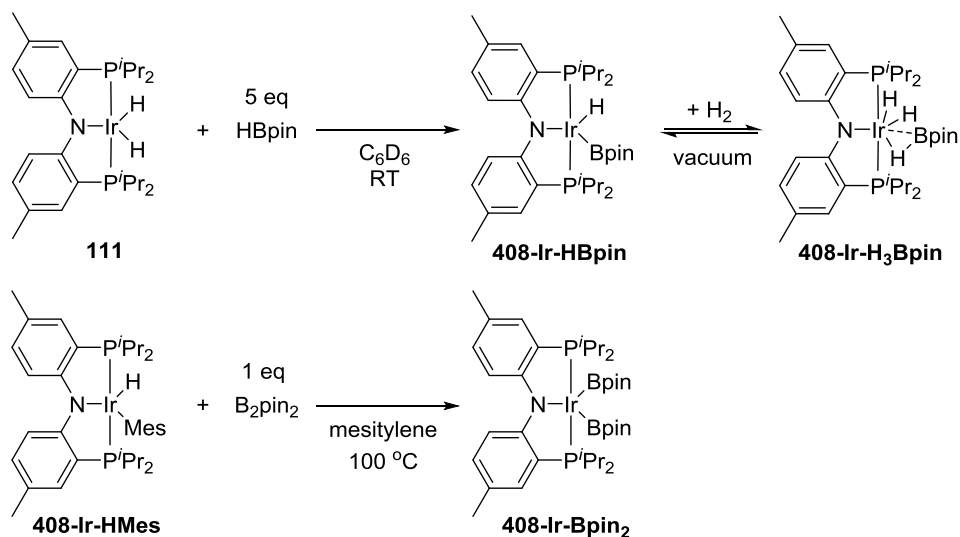


Figure 4-4. Strategy of examining possible intermediates in DHBTA.

In our original report, we showed the iridium diboryl complex **207** can be synthesized by reacting **206** with 5 equivalents of HBpin;¹³⁷ and isolated **207** exhibited the same catalytic activity as **206**. Treating **111** with 5 equivalents of HBpin, however, led to a mixture of **408-Ir-H₃Bpin** and **408-Ir-HBpin** and in equilibrium with free H₂ (top, Scheme 4-4). Because the reaction of **111** with HBpin did not yield **408-Ir-Bpin₂**, we employed an alternative route of heating **408-Ir-HMes**, a good synthon for $(^{\text{Me}}\text{PNP}^{\text{iPr}})\text{Ir}$,¹⁷³ with 1 equivalent of B₂pin₂ to get **408-Ir-Bpin₂** in 83% isolated yield (bottom, Scheme 4-4).



Scheme 4-4. The synthesis of **408-Ir-HBpin** and its equilibrium with **408-Ir-H₃Bpin** (top). The synthesis of **408-Ir-Bpin₂** (bottom).

In the 1H NMR spectrum, **408-Ir-HBpin** exhibited an up-field signal at -19.8 ppm (t, 1H, $J_{P-H} = 8.4$ Hz), and the peak sharpened upon ^{11}B decoupling (Figure 4-5, left) which suggests that this proton interacted with a boron atom of the boryl. In contrast, **408-Ir-H₃Bpin** displayed two broad up-field signals at -5.3 (1H, $\omega_{1/2} = 60$ Hz) and -12.4 (2H, $\omega_{1/2} = 64$ Hz) ppm in the 1H NMR spectrum at ambient temperature. Only the peak at -5.3 ppm ($\omega_{1/2} = 35$ Hz) sharpened upon ^{11}B decoupling (Figure 4-5, right), but the width of the peak at -12.4 ppm remained unchanged that we can unambiguously assign the peak at -5.3 ppm to the proton associated with a boron atom. The up-field signals of **408-Ir-H₃Bpin** can be further resolved *via* variable temperature (VT) 1H NMR analysis (Figure 4-6) that displayed three distinct peaks (-5.39, -9.43, -15.35 ppm) at 213K. From the data of $^1H\{^{11}B\}$ and VT 1H NMR spectroscopy, **408-Ir-H₃Bpin** is best described as an *exo*- σ -borane dihydride complex.¹⁸¹

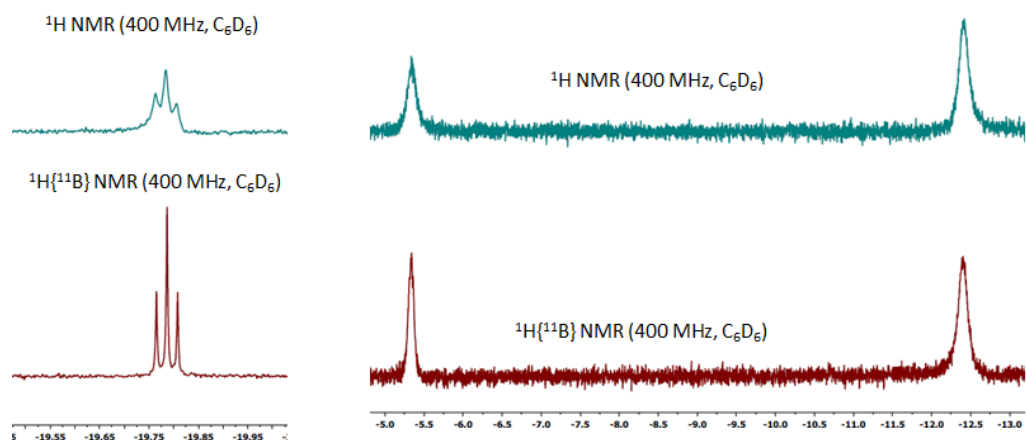


Figure 4-5. The upfield region of ^1H and $^1\text{H}\{^{11}\text{B}\}$ NMR spectrum (400 MHz, C_6D_6) of **408-Ir-HBpin** (left) and **408-Ir-H₃Bpin** (right).

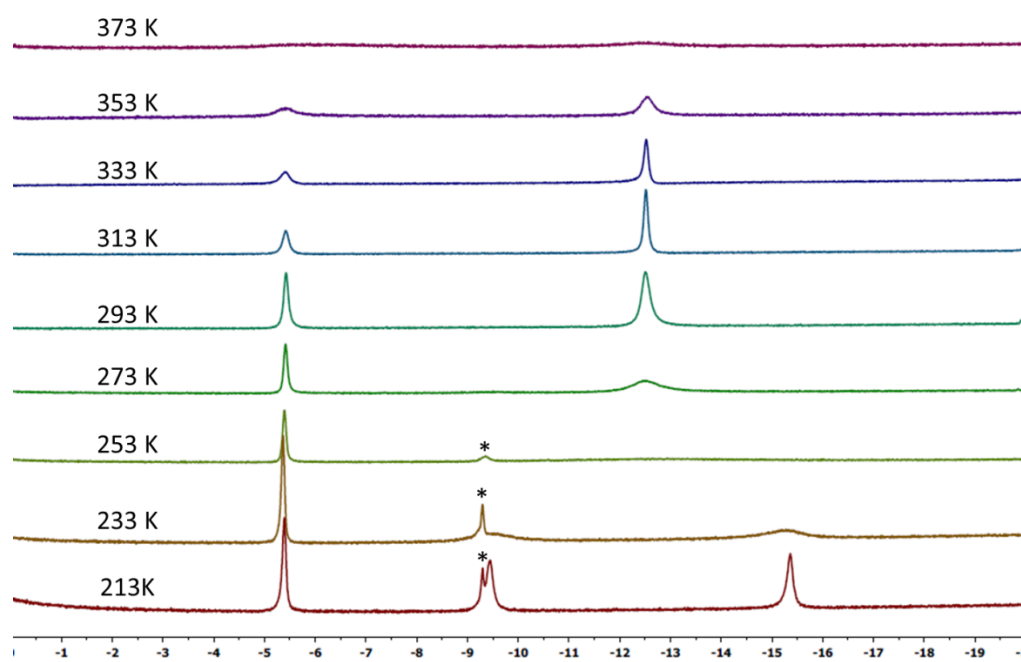
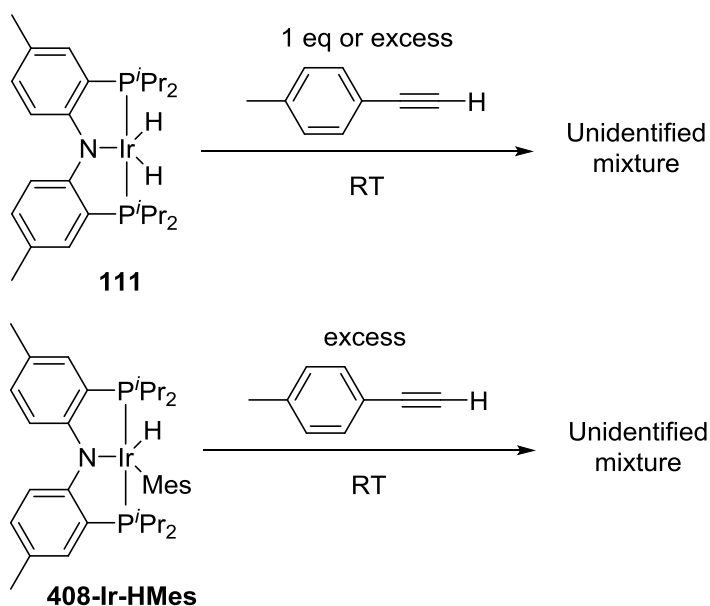


Figure 4-6. Partial (upfield region) ^1H NMR spectrum (500 MHz, $\text{toluene-}d_8$) of **408-Ir-H₃Bpin** as a function of temperature. Small amount of unidentified impurity (marked with asterisks) was shown near -9.2 ppm.

The attempts to obtain a well-defined terminal alkyne complex have been unsuccessful so far. Reacting **408-Ir-H₂** or **408-Ir-HMes** with one equivalent or excess of **209** under various conditions all led to mixtures of unidentified products that have resisted our attempts at isolation and separation (Scheme 4-5). The phenomenon might be related to the fact that Rh analog **129** has been shown to be an alkyne dimerization catalyst⁵⁵ and PCP/POCOP iridium complexes reacted alkynes to form a variety of allene or enyne complexes.^{54,182}



Scheme 4-5. Unsuccessful attempts of making terminal alkyne related complexes.

Before attempting to make an alkynylboronate complex, we considered the possible structures of (^{Me}PNP^{iPr})Ir with an alkynylboronate, and therefore did DFT calculations on the three conceivable isomers for (^{Me}PNP^{iPr})Ir with **209P**: the alkynylboronate π -complex, **408-Ir-p-tol**; the vinylidene complex, **408-Ir-v-tol**; and the alkynyl boryl

complex, **408-Ir-ynlBpin-tol** (Figure 4-7). **408-Ir-v-tol** was calculated to be the lowest energy isomer, with **408-Ir-p-tol** and **408-Ir-ynlBpin-tol** lying 3.4 and 7.7 kcal/mol higher in energy, respectively.

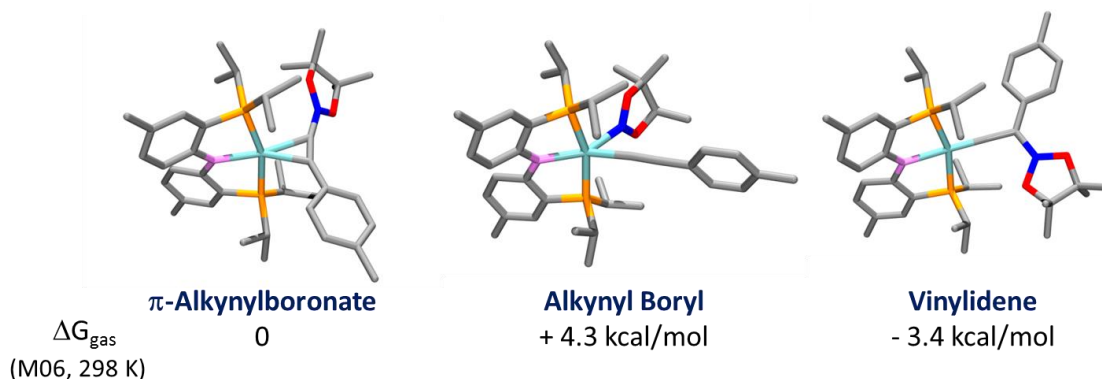
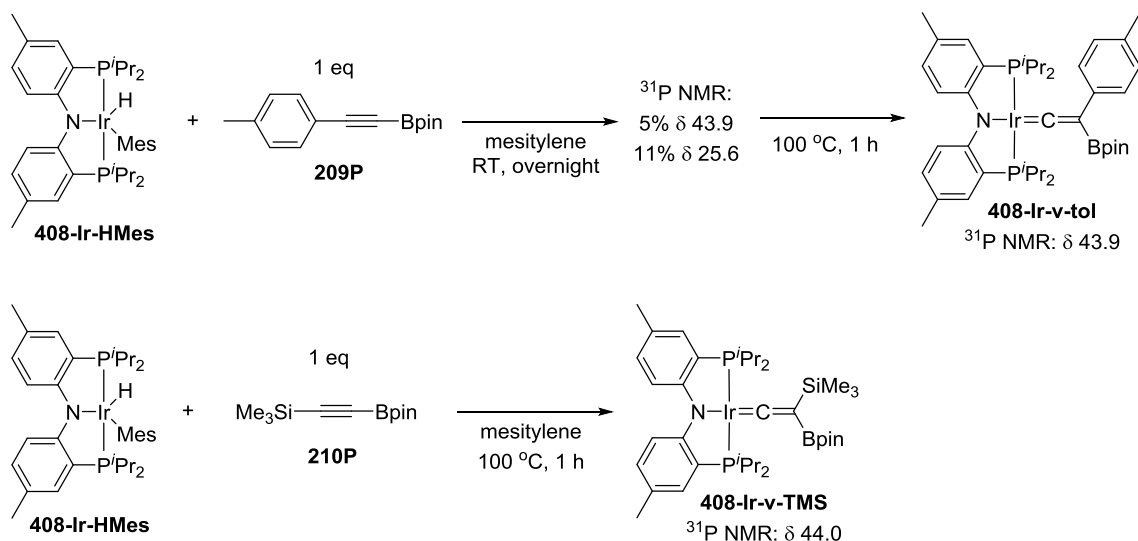


Figure 4-7. DFT calculation of three possible isomers of $(^{\text{Me}}\text{PNP}^{\text{iPr}})\text{Ir} + \mathbf{209P}$.

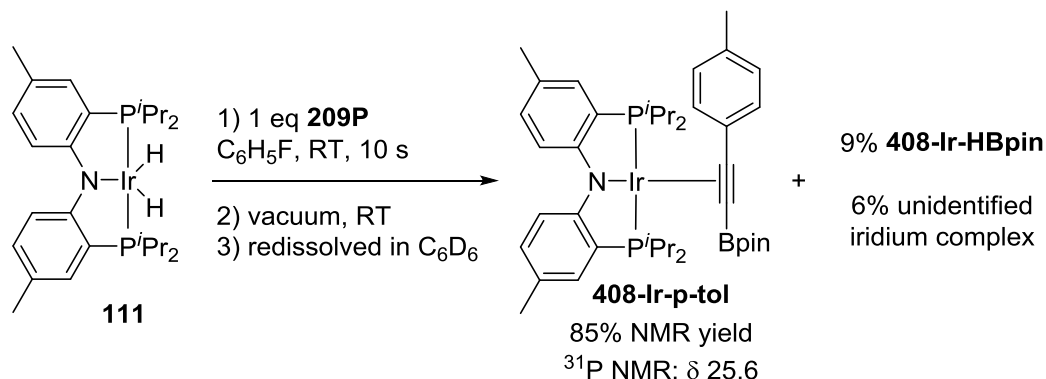
Mixing **408-Ir-HMes** with one equivalent of **209P** at ambient temperature overnight led to two products which appeared at 43.9 (5%) and 25.6 (11%) ppm respectively in the ^{31}P NMR spectrum (Scheme 4-6, top), and further heating the mixture at 100 °C for 1 h cleanly converted all iridium complexes to a single product that resonated at 43.9 ppm in the ^{31}P NMR spectrum, which was isolated and identified as **408-Ir-v-tol**. The Me_3Si substituted vinylidene analog **408-Ir-v-TMS** was also characterized without isolation by using **210P** as the reactant (Scheme 4-6, bottom). The vinylidene resonances were observed at 282.8 and 269.3 ppm in the ^{13}C NMR spectrum as expected for **408-Ir-v-tol** and **408-Ir-v-TMS** respectively.¹⁸³ The result is consistent with the DFT prediction of **408-Ir-v-tol** as the thermodynamically favored isomer.



Scheme 4-6. Synthesis of vinylidene complexes **408-Ir-v-tol** and **408-Ir-v-TMS**.

Conversion of osmium boryl alkynyl complexes to vinylideneboronate esters has been observed by Esteruelas and López,¹⁸⁴ thus we expected other kinetically stable intermediates to **408-Ir-v-tol** should be obtained if a suitable (^{Me}CNP^{iPr})Ir precursor was reacted with **209P** at milder conditions. We first attempted to mix **111** with **209P** then removed all volatiles immediately. The residue was redissolved in C₆D₆ and analyzed by ¹H and ³¹P NMR spectroscopy. The major product was assigned as an alkynylboronate π-complex **408-Ir-p-tol** (Scheme 4-7), and its phosphine signal in the ³¹P NMR spectrum was appeared at 25.6 ppm which was identical to the observed intermediate in the synthesis of **408-Ir-v-tol**. We also observed 9% of **408-Ir-HBpin** formation indicates that C_{sp}-B bond cleavage is facile and the quantity of **408-Ir-HBpin** would increase over the longer reaction times. The assignment of **408-Ir-p-tol** was supported by its aromatic proton signals of the 2,6-positions on **209P** in the ¹H NMR spectrum were shifted downfield significantly to 8.28 ppm which is characteristic of internal

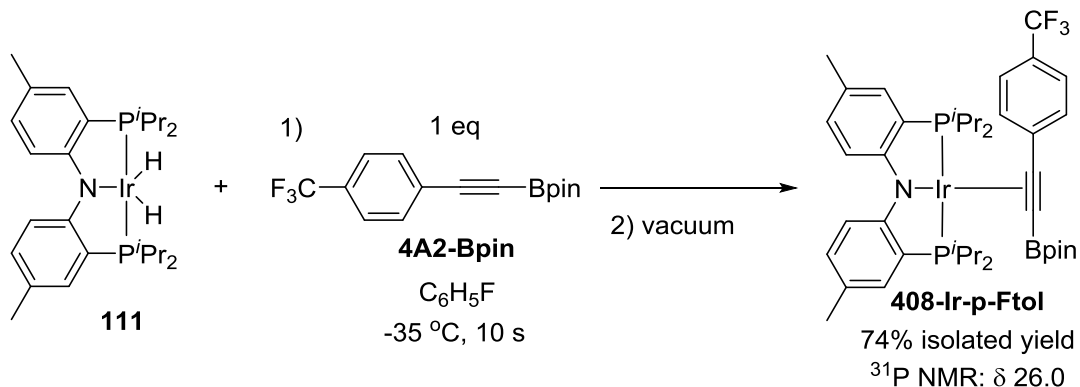
aromatic alkyne π -complexes.^{182,185,186} However, the isomerization from **408-Ir-p-tol** to **408-Ir-v-tol** at ambient temperature (about 50% after 15 h) prevented the isolation of pure **408-Ir-p-tol**.



Scheme 4-7. Synthesis of **408-Ir-p-tol**.

We surmised that a more electron-poor alkyne should be thermodynamically less predisposed to form a vinylidene,¹⁸³ so the rearrangement should be retarded by decreasing the electron density of the triple bond due to both a ground state and a transition state effect. To examine the postulation, we replaced **209** with **4A2-Bpin** as the reactant and mixed with pre-cooled **111** at -35 °C. We were able to isolate **408-Ir-p-Ftol** as red-orange solid in 74% yield (Scheme 4-8). To the best of our knowledge, this is the first alkynylboronate π -complex that has been isolated and characterized. ^{31}P NMR spectroscopic analysis showed a singlet at 26.1 ppm, which was close to **408-Ir-p-tol**. Consistent with our proposal, the conversion of **408-Ir-p-Ftol** to the vinylidene complex, **408-Ir-v-Ftol** is significantly slower (about 5% after 15 h) than **408-Ir-p-tol** at ambient temperature. Like **408-Ir-p-tol**, the aromatic proton signals of the 2,6-positions on **4A2-Bpin** in **408-Ir-p-Ftol** were also downfield shift to 8.22 ppm in the 1H NMR spectrum.

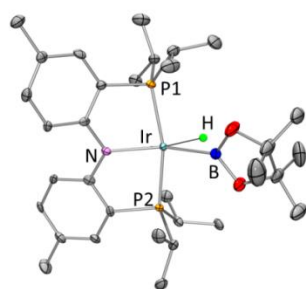
In the ^{13}C NMR spectrum, the carbon signal of alkynyl-C ($\underline{\text{C}}\equiv\text{C-B}$) in **408-Ir-p-Ftol** (δ 105.7) was slightly downfield shift than in free **4A2-Bpin**.



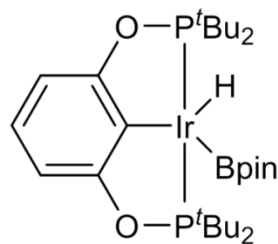
Scheme 4-8. Synthesis of **408-Ir-p-Ftol**.

4.2.4 X-ray diffraction and density functional theory studies of **408-Ir-HBpin**, **408-Ir-Bpin**₂, **408-Ir-v-tol**, and **408-Ir-p-Ftol**

The solid-state structure of **408-Ir-HBpin** is shown in Figure 4-8 (left). To reinforce the X-ray studies, especially with respect to the location of the Ir-H and compare with analogous **410-Ir-HBpin** (right) reported by Heinekey et al,¹⁸¹ Dr. Jia Zhou also performed density functional theory (DFT) analysis in the gas phase using the M06 functional. Based on the DFT results, the degree of B-H bond activation is larger in **408-Ir-HBpin** than in **410-Ir-HBpin** that is depicted by the shorter Ir-B and Ir-H bond distance and longer B-H bond distance in **408-Ir-HBpin**.



408-Ir-HBpin



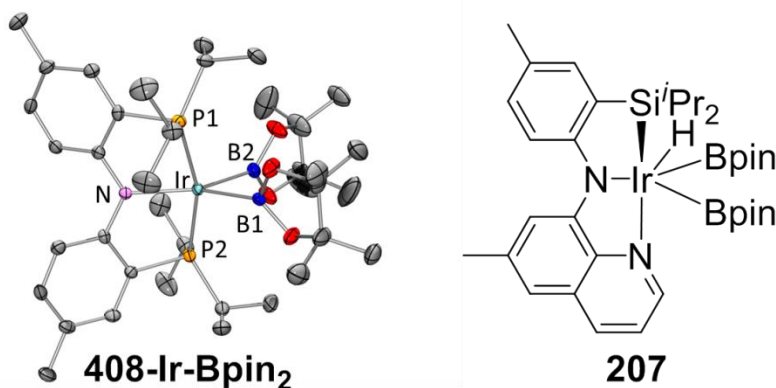
410-Ir-HBpin

	408-Ir-HBpin (X-ray)	408-Ir-HBpin (DFT)	410-Ir-HBpin (X-ray)	410-Ir-HBpin (DFT)
Ir-H	1.69(4)	1.639	1.56(6)	1.706
Ir-B	2.049(6)	2.033	2.082(5)	2.114
H-B	1.788	1.608	1.47(6)	1.406
B-Ir-H	56.1(15)	50.5	45(2)	41.5

Figure 4-8. ORTEP drawing (50% probability ellipsoids) of **408-Ir-HBpin** (top left) showing selected atom labeling and depiction of **410-Ir-HBpin** (top right). Hydrogen atoms are omitted for clarity in the ORTEP drawing, except for the hydride on the Ir atom. The selected bond distances (Å) and angles (deg) for **408-Ir-HBpin** and **410-Ir-HBpin** are summarized in the table at bottom.

The structure of **408-Ir-Bpin₂** can be described as Y-shaped five-coordinate where the Y was defined by N_(amido) and two boryls (Figure 4-9, top left) with an acute B-Ir-B angle (68.2°). The Y-shaped geometry is exactly expected for a five-coordinate d⁶ complex^{134,135} when the equatorial plane contains a single good π-donor (N_(amido)) and two strong σ-donors (two boryls). Two Ir-boryls are shown almost the same metrics and the Ir-B distances are similar to the analogous Ir-Bpin distances reported in the literature (2.02–2.07 Å).^{68,137} In general, all parameters of bond distances and bond angles on the equatorial plane are very close to the previous reported **207** (top right).¹³⁷

The B...B distance of 2.29 Å is too long for boron-boron interaction thus **408-Ir-Bpin₂** should be viewed as an Ir(III) diboryl complex.



	408-Ir-Bpin₂	207
Ir-B	2.034(4), 2.048(4)	2.062(6), 2.069(5)
Ir-N(amido)	2.078(3)	2.073(4)
N(amido)-Ir-B	144.1(1), 147.1(1)	146.2(2), 147.0(2)
B-Ir-B	68.2(2)	66.5(2)

Figure 4-9. ORTEP drawing (50% probability ellipsoids) of **408-Ir-Bpin₂** (top left) showing selected atom labeling and depiction of **207** (top right). Hydrogen atoms are omitted for clarity in the ORTEP drawing. The selected bond distances (Å) and angles (deg) for **408-Ir-Bpin₂** and **207** are summarized in the table at bottom.

X-ray quality crystals of **408-Ir-v-tol** and **408-Ir-p-Ftol** were grown from fluorobenzene/pentane and the solid structures are shown in Figure 4-10. The structure of **408-Ir-v-tol** and **408-Ir-p-Ftol** can be described as having a slightly distorted square planar geometry. For **408-Ir-v-tol**, C2-C1-Ir bond angle (178.2°) is very close to 180° which is the character of a typical vinylidene complex.¹⁸³ The Ir-C1 and C1-C2 bond lengths of 1.807 and 1.334 Å, respectively, are similar to the analogous distances in the [(Ph₂PCH₂SiMe₂)₂N]Ir=C=CH₂ vinylidene complex reported by Fryzuk.¹⁸⁷ In the

structure of **408-Ir-p-Ftol**, **4A2-Bpin** is bound to iridium through a unsymmetrical η^2 fashion (Ir-C1: 2.165 Å, Ir-C2: 2.101 Å) which is similar to other square planar Ir(I) alkyne complexes.^{182,188,189} Both the elongation of C≡C bond (1.304 Å) and the bending of C≡C-C_{ipso} (147.5°) and C≡C-B (161.9°) away from 180° indicate back-donation from the iridium center to the π^* orbitals of C≡C bond.^{41,190}

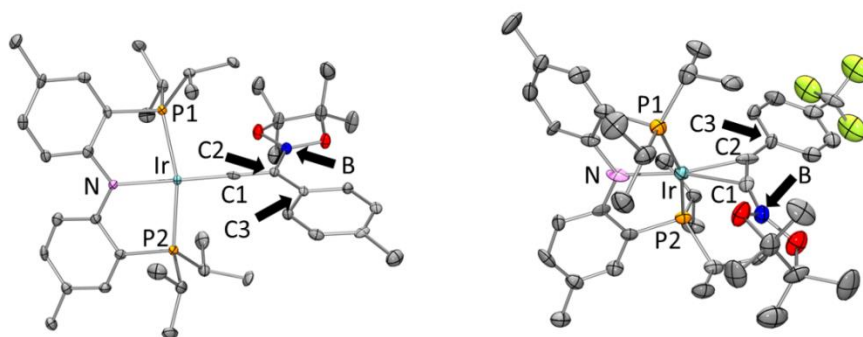
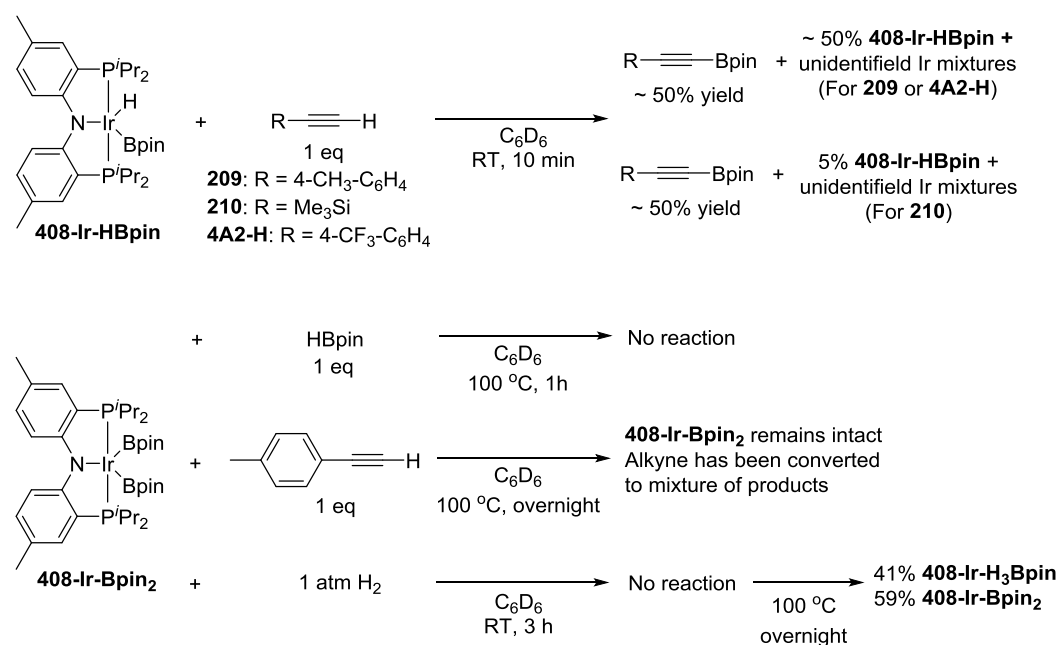


Figure 4-10. ORTEP drawings (50% probability ellipsoids) of **408-Ir-v-tol** (left) and **408-Ir-p-Ftol** (right) showing selected atom labeling and hydrogen atoms are omitted for clarity. For 10-Ir-v-tol, one of two molecules in the asymmetric unit is shown, and a non-coordinated fluorobenzene molecule is omitted for **408-Ir-p-Ftol**. Selected bond distances (Å) and angles (deg) for **408-Ir-v-tol**: Ir-C1, 1.807(4); C1-C2, 1.334(5); P2-Ir1-P1, 164.84(3); C2-C1-Ir, 178.2(3); C1-C2-C3, 120.1(3); C1-C2-B 113.1(3); C3-C2-B, 126.8(3). Selected bond distances (Å) and angles (deg) for **408-Ir-p-Ftol**: Ir-C1, 2.165(11); Ir-C2, 2.101(12); C1-C2, 1.301(15); C1-C2-C3, 147.5(11); B-C1-C2, 161.9(11).

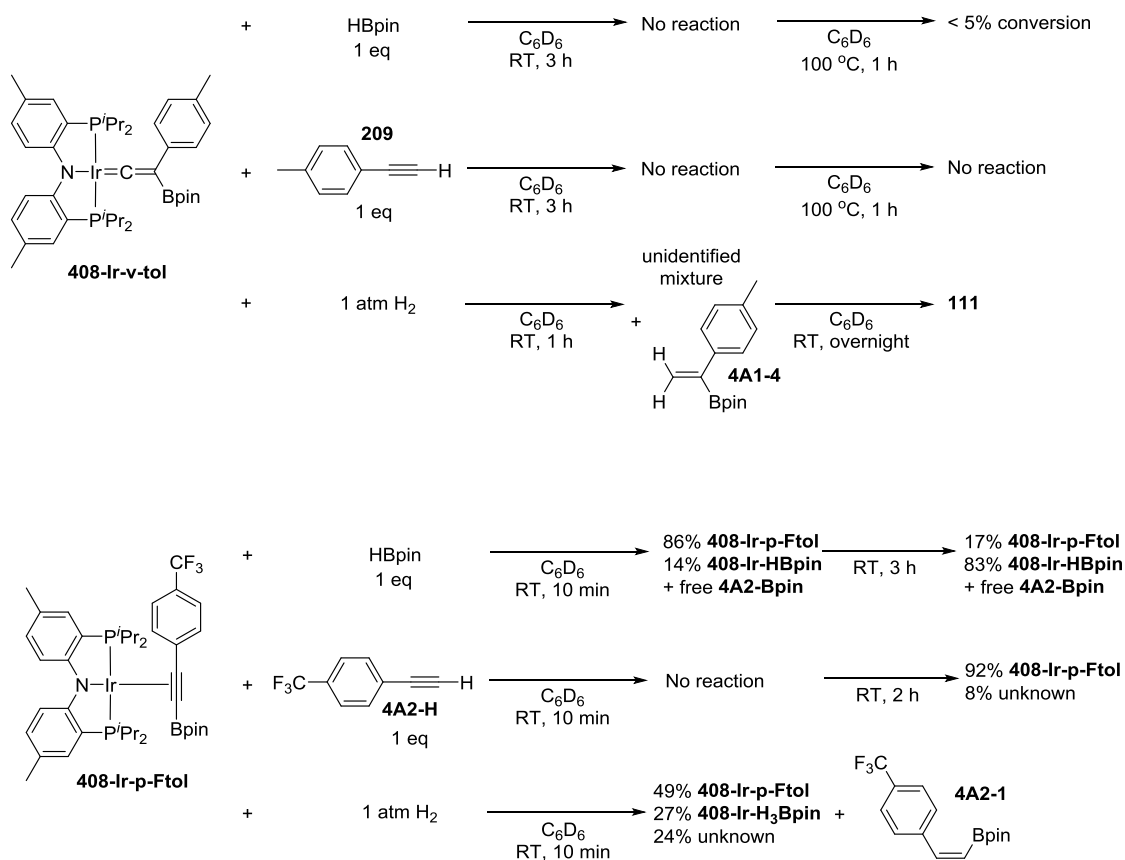
4.2.5 Stoichiometric reactions of (^{Me}PNP^{iPr})Ir complexes

To examine the possible roles that four new isolated (^{Me}PNP^{iPr})Ir complexes played in DHBTA, these compounds were tested with the three components in DHBTA: A terminal alkyne (substrate), HBpin (substrate), and H₂ (by-product). **408-Ir-HBpin** was reacted with three different terminal alkynes to study the boryl transfer ability: **209**, **210** and **4A2-H** (Scheme 4-9, top). After 10 min at ambient temperature, approximately

50% yield of the corresponding alkynylboronates was observed in ^1H NMR spectrum for all three substrates. The amount of alkynylboronate did not increase with longer reaction times; however, other side reactions such as hydrogenation occurred. By ^{31}P NMR spectroscopic analysis, different degrees of unreacted **408-Ir-HBpin** were observed along with multiple phosphorus containing species formed but could not be assigned at this stage. Surprisingly, **408-Ir-Bpin₂** was inert to all three major components in DHBTA: HBpin, terminal alkyne and H_2 (Scheme 4-9, bottom) in stoichiometric reactions at ambient temperature. ^{31}P NMR spectroscopic analysis showed **408-Ir-Bpin₂** was the only observable phosphorus containing compound in each reaction mixture. Only heating of **408-Ir-Bpin₂** under 1 atm H_2 at $100\text{ }^\circ\text{C}$ overnight led to 41% **408-Ir-H₃Bpin** formation.



Scheme 4-9. Boryl transfer from **408-Ir-HBpin** to terminal alkynes (top) and reactivities of **408-Ir-Bpin₂**.



Scheme 4-10. Reactivities of **408-Ir-v-tol** (top) and **408-Ir-p-Ftol** (bottom).

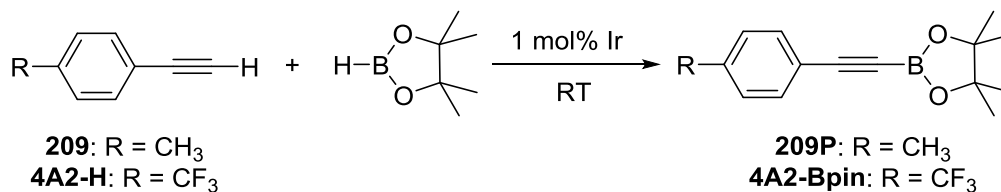
408-Ir-v-tol was stable toward to both HBpin and **209** at ambient temperature (Scheme 4-10, top). On the other hand, treating **408-Ir-v-tol** with H₂ quickly resulted in *gem*-alkenylboronate (**4A1-4**) formation and unidentified iridium compounds in 1 h at ambient temperature. After overnight, **111** was the only observable species by ³¹P NMR spectroscopic analysis. Treating **408-Ir-p-Ftol** with 1 equivalent of HBpin at ambient temperature slowly and cleanly leads to **408-Ir-HBpin** formation (Scheme 4-10, bottom); meanwhile, equal amount of free **4A2-Bpin** was observed in the ¹H NMR spectrum. The reaction between **408-Ir-p-Ftol** and **4A2-H** was relatively sluggish that no noticeable

change after 10 min, and only made 8% conversion after 2 h at ambient temperature based on analysis by ^{31}P NMR spectroscopy. Exposing **408-Ir-p-Ftol** under 1 atm H_2 quickly yielded 27% **408-Ir-H₃Bpin** and 24% unknown iridium species in 10 min, and the formation of **408-Ir-H₃Bpin** proved the $\text{C}_{\text{sp}}\text{-B}$ bond cleavage is effortless again. *Cis*-alkenylboronate (**4A2-1**) was also observed as the hydrogenation product of **4A2-Bpin**.

4.2.6 Catalytic results for DHBTA using various ($^{\text{Me}}\text{PNP}^{\text{iPr}}$)Ir complexes

Table 4-5 summarizes the results when newly synthesized ($^{\text{Me}}\text{PNP}^{\text{iPr}}$)Ir compounds, along with **408-Ir-H₂** were tested in DHBTA. When **111** was treated with excess HBpin, yellow mixture of **408-Ir-HBpin** and **408-Ir-H₃Bpin** immediately formed before addition of alkyne. Not surprisingly, comparable yield and hydrogenation side-product (**4A1-1**) ratio was observed when isolated **408-Ir-HBpin** was used instead of **111** (entry 1 and 2). **408-Ir-p-Ftol** also gave very similar performance on **4A2-H** to **111** (entry 5 and 6). In contrast, **408-Ir-Bpin₂** showed no DHBTA after the first 10 min (entry 3) and only gave 37% **209P** after 3 h indicating **408-Ir-Bpin₂** is clearly not in the DHBTA catalytic cycle. The inertness of **408-Ir-Bpin₂** in the DHBTA was correlated with its poor reactivity in the previous stoichiometric reactions. Finally, **408-Ir-v-tol** also showed poor reactivity (entry 4) eliminating involvement of alkenylboronate formation through vinylidene intermediates in the mechanism.

Table 4-5. Catalytic results for DHBTA using various (^{Me}PNP^{iPr})Ir complexes.



Entry	Ir catalyst	Alkyne	DHBTA Yield (10 min)	Note
1	111	209	81% (16% 209 , 3% 4A1-1)	95% after 1 h (5% 4A1-1)
2	408-Ir-HBpin	209	82% (16% 209 , 2% 4A1-1)	96% after 1 h (4% 4A1-1)
3	408-Ir-Bpin₂	209	0% (all 209)	37% after 3 h
4	408-Ir-v-tol	209	17% (80% 209)	85% after 1 h
5	111	4A2-H	45%	65% after 1 h
6	408-Ir-p-Ftol	4A2-H	49%	64% after 1 h

4.3 Conclusion

Through ligand screening, we have shown the discovery of new DHBTA catalysts supported by various PNP ligands. Using the unsymmetric PNP supported iridium complex **415-Ir-COE** TONs of 6500 was achieved. Good to excellent yields were obtained under mild conditions for aryl-, silyl-, and alkyl-substituted terminal alkynes. Unlike the strict chemoselectivity in the (SiNN)Ir system, <10% hydrogenation products are observed as the main side-products in all the (PNP)Ir systems.

Several ^{Me}PNP^{iPr} iridium complexes analogous to intermediates in the original proposed DHBTA catalytic cycle have been synthesized and tested in both stoichiometric and catalytic reactions. The vinylidene (**408-Ir-v-tol**) and diboryl (**408-**

Ir-Bpin₂) complexes are inert to both terminal alkynes and HBpin, plus their poor performance in DHBTA that we could rule them out of the catalytic cycle of the (^{Me}PNP^{iPr})Ir system. The inactivity of **408-Ir-Bpin**₂ is in contrast to analogous (SiNN)Ir(Bpin)₂ **207** which might imply that a diboryl structure is not essential for successful DHBTA. On the other hand, hydride boryl (**408-Ir-HBpin**) and alkynylboronate π -complex (**408-Ir-p-Ftol**) show nearly identical performance to **111**. Further organic application using **415-Ir-COE** and related kinetic studies are in progress.

4.4 Experimental

General Considerations. Unless specified otherwise, all manipulations were performed under an Ar atmosphere using standard Schlenk line or glovebox techniques. Toluene, fluorobenzene, THF, Et₂O, pentane, C₆D₆ were dried over NaK/Ph₂CO/18-crown-6, distilled or vacuum transferred and stored over molecular sieves in an Ar-filled glovebox. Mesitylene, CH₂Cl₂, CD₂Cl₂ and CDCl₃ were dried with and then distilled from CaH₂ and stored over molecular sieves in an Ar-filled glove box. **206**,¹³⁷ **401-H**,¹²⁴ 2-*tert*-butylmercaptoaniline,¹⁹¹ 8-bromo-6-methylquinoline,¹³⁷ **405-H**,¹⁸ **1F**,¹⁸ **4S2**,¹⁷⁵ bis(2-bromo-4-methylphenyl)amine,¹⁹² **111**,⁵¹ **408-Ir-HMes**,⁵¹ **101**,¹⁷⁶ **102**,¹⁷⁷ **414-H**,¹⁹³ **415-H**,¹⁷⁸ **209P**,¹³⁷ **210P**¹³⁷ were prepared according to published procedures. (Me₃Si)₂O and alkynes were deoxygenated by three freeze-pump-thaw cycles prior to use. All other chemicals were used as received from commercial vendors. NMR spectra were recorded on a Varian Inova 300, Mercury 300 (¹H NMR, 299.952 MHz; ¹³C NMR, 75.421 MHz; ³¹P NMR, 121.42 MHz), Varian Inova 400 (¹H NMR, 399.535 MHz; ¹¹B NMR, 128.185 MHz; ¹³C NMR, 100.465 MHz; ²⁹Si NMR, 79.366 MHz) and NMRS 500 (¹H NMR,

499.703 MHz; ^{19}F NMR, 469.854 MHz; ^{13}C NMR, 125.697 MHz; ^{31}P NMR, 202.283 MHz) spectrometer. For ^1H and ^{13}C NMR spectra, the residual solvent peak was used as an internal reference (^1H NMR: δ 7.15 for C_6D_6 , 5.32 for CD_2Cl_2 , 7.24 for CDCl_3 ; ^{13}C NMR: δ 128.06 for C_6D_6 , 53.84 for CD_2Cl_2 , 77.16 for CDCl_3). For ^{29}Si NMR, spectra were referenced externally to $\delta = 0$ ppm by using Me_4Si . For ^{11}B NMR, spectra were referenced externally to $\delta = 0$ ppm by using $\text{BF}_3 \cdot \text{Et}_2\text{O}$. For ^{19}F NMR, spectra were referenced externally to $\delta = -78.5$ ppm by using CF_3COOH . For ^{31}P NMR, spectra were referenced externally to $\delta = 0$ ppm by using 85% H_3PO_4 . Mass spectrometric analyses were carried out by the Texas A&M University Laboratory for Biological Mass Spectrometry (LBMS). Elemental analyses were performed by CALI Labs, Inc. (Parsippany, NJ).

Note: In ^{13}C NMR spectra of alkynylboronates and vinylidenes, quaternary carbon atoms attached to boron were usually not observed due to low intensity.

Computational details. All computations were carried out with the Gaussian09 program.¹⁴⁵ All of the geometries were fully optimized at the M06¹⁴⁶ level of theory. The Stuttgart basis set and the associated effective core potential (ECP) was used for Ir atom, and an all-electron 6-311G(d,p) basis set was used for the other atoms. The harmonic vibrational frequency calculations were performed to ensure that a minimum was obtained.

Synthesis of 402-H. In an Ar-filled glove box, $\text{Pd}_2(\text{dba})_3$ (180 mg, 0.196 mmol) and BINAP (245 mg, 0.393 mmol) were transferred to a 25 mL PTFE-valved gas-tight flask and dissolved in 5 mL toluene. After stirring 3 min, 8-bromoquinoline (1.25 mL,

9.58 mmol) and 2-aminophenyl phenyl sulfide (2.35 g, 11.7 mmol) was added to the mixture and stirred for 1 min. Sodium *tert*-butoxide (1.39 g, 14.5 mmol) was then added to the solution with 5 mL toluene to assist in transfer. The flask was taken outside the glovebox and heated at 115 °C for 4 d. After allowing the mixture to cool to ambient temperature, 0.5 mL of H₂O was added to quench the reaction and then the volatiles were removed *in vacuo*. The residue was redissolved with CH₂Cl₂ and filtered through Celite. The volatiles of filtrate were removed *in vacuo* and the residue was purified *via* column chromatography (1:10 ethyl acetate/hexanes on silica; Rf of **402-H**: 0.58; Rf of 2-aminophenyl phenyl sulfide: 0.48). The volatiles of the eluate were removed *in vacuo* to get yellow solid. Its ¹H NMR spectroscopic analysis indicated >97% purity. Yield: 2.39 g (76%). ¹H NMR (500 MHz, CDCl₃): δ 8.91 (br s, 1H, N-*H*), 8.65 (m, 1H, Ar-*H*), 7.98 (d, J_{H-H} = 8.0 Hz, 1H, Ar-*H*), 7.68 (d, J_{H-H} = 8.0 Hz, 1H, Ar-*H*), 7.51 (d, J_{H-H} = 8.0 Hz, 1H, Ar-*H*), 7.46 (d, J_{H-H} = 8.0 Hz, 1H, Ar-*H*), 7.30 (m, 3H, Ar-*H*), 7.25 (m, 2H, Ar-*H*, overlapping with the solvent peak), 7.14 (m, 3H, Ar-*H*), 7.04 (m, 1H, Ar-*H*), 6.91 (m, 1H, Ar-*H*). ¹³C{¹H} NMR (126 MHz, CDCl₃): δ 147.7, 143.2, 139.3, 139.2, 136.2, 136.1, 136.0, 129.8, 129.1, 129.0, 128.9, 127.0, 126.3, 123.4, 121.8, 121.6, 117.9, 117.5, 108.9. HRMS (ESI) calcd. for C₂₁H₁₇N₂S (M+H)⁺: 329.1112. Found: 329.1107.

Synthesis of 403-H. In an Ar-filled glove box, Pd₂(dba)₃ (22 mg, 0.024 mmol) and BINAP (31 mg, 0.050 mmol) were transferred to a 25 mL PTFE-valved gas-tight flask and dissolved in 3 mL toluene. After stirring 3 min, 8-bromoquinoline (350 μL, 2.68 mmol) and 2-*tert*-butylmercaptoaniline (434 μL, 2.39 mmol) was added to the mixture and stirred for 1 min. Sodium *tert*-butoxide (361 mg, 3.75 mmol) was then added to the

solution with 2 mL toluene to assist in transfer. The flask was taken outside the glovebox and heated at 115 °C for 3 d. After allowing the mixture to cool to ambient temperature, 0.5 mL of H₂O was added to quench the reaction and then the volatiles were removed *in vacuo*. The residue was purified *via* flash column chromatography (1:10 ethyl acetate/hexanes on silica). The volatiles of the eluate were removed *in vacuo* to get yellow oil. Its ¹H NMR spectroscopic analysis indicated >98% purity. Yield: 339 mg (46%). ¹H NMR (500 MHz, C₆D₆): δ 10.18 (br s, 1H, N-*H*), 8.59 (d, J_{H-H} = 4.0 Hz, 1H, Ar-*H*), 7.67 (t, J_{H-H} = 8.0 Hz, 2H, Ar-*H*), 7.59 (d, J_{H-H} = 8.0 Hz, 1H, Ar-*H*), 7.53 (d, J_{H-H} = 8.0 Hz, 1H, Ar-*H*), 7.19 (t, J_{H-H} = 8.0 Hz, 1H, Ar-*H*), 7.13 (d, J_{H-H} = 8.0 Hz, 1H, Ar-*H*), 6.99 (d, J_{H-H} = 8.0 Hz, 1H, Ar-*H*), 6.76 (m, 2H, Ar-*H*), 1.27 (s, 9H, SC(CH₃)₃). ¹³C {¹H} NMR (126 MHz, C₆D₆): δ 147.9, 146.1, 140.7, 140.1, 139.8, 135.9, 130.6, 129.4, 127.5, 122.0, 121.7, 120.6, 117.5, 116.7, 108.5, 47.5 (SC(CH₃)₃), 31.1 (SC(CH₃)₃). HRMS (ESI) calcd. for C₁₉H₂₁N₂S (M+H)⁺: 309.1425. Found: 309.1437.

Synthesis of 404-H. In an Ar-filled glove box, 8-bromo-6-methylquinoline (532 mg, 2.40 mmol), 2-methoxyaniline (356 mg, 2.89 mmol) and BINAP (24 mg, 0.038 mmol) were transferred to a 25 mL PTFE-valved gas-tight flask and dissolved in 1.5 mL toluene. After stirring for 1 min, Pd(OAc)₂ (5.7 mg, 0.025 mmol Pd) and 0.5 mL toluene were added and stirred for 3 min. Sodium *tert*-pentoxide (379 mg, 3.44 mmol) was then added to the solution with 2 mL toluene to assist in transfer. The flask was taken outside the glovebox and heated at 120 °C for 3 d. All the volatiles were removed *in vacuo* and the residue was purified *via* column chromatography (1:8 ethyl acetate/hexanes on silica) to yield yellow oil. Its ¹H NMR spectroscopic analysis indicated >98% purity. Yield:

565 mg (89%). ^1H NMR (500 MHz, CDCl_3): δ 8.75 (dd, $J_{\text{H-H}} = 4.0, 1.5$ Hz, 1H), 8.50 (s, 1H, N-*H*), 7.99 (dd, $J_{\text{H-H}} = 8.0, 1.5$ Hz, 1H, Ar-*H*), 7.69 (d, $J_{\text{H-H}} = 8.0$ Hz, 1H, Ar-*H*), 7.42 (s, 1H, Ar-*H*), 7.36 (dd, $J_{\text{H-H}} = 8.0, 4.0$ Hz, 1H, Ar-*H*), 6.99 (m, 4H, Ar-*H*), 3.94 (s, 3H, OCH_3), 2.48 (s, 3H, Ar- CH_3). $^{13}\text{C}\{^1\text{H}\}$ NMR (126 MHz, CDCl_3): δ 150.3, 146.8, 139.5, 138.1, 137.3, 135.5, 131.6, 129.1, 121.7, 121.4, 120.7, 117.5, 116.0, 110.9, 110.2, 55.8 (OCH_3), 22.5 (Ar- CH_3). HRMS (ESI) calcd. for $\text{C}_{17}\text{H}_{17}\text{N}_2\text{O}$ ($\text{M}+\text{H}$) $^+$: 265.1341. Found: 265.1332.

Synthesis of 4S1. In an Ar-filled glovebox, bis(2-bromo-4-methylphenyl)amine (8.03 g, 22.6 mmol) was dissolved in 80 mL Et_2O in a 250 mL Schlenk flask. The flask was then taken outside of glovebox, connected to a Schlenk line and maintained an Ar atmosphere, and placed in a -45 °C dry ice/acetone cooling bath to result in a slurry. *n*-BuLi (18.1 mL of 2.5 M solutions in hexanes, 45.3 mmol) was added dropwise over the course of 30 min *via* syringe. The solution color turned to yellow and then white precipitate formed. After addition of *n*-BuLi, the solution was left to stir at -45 °C for 30 min further and the mixture was allowed to warm to room temperature. After stirring at room temperature for 1 h, the flask was placed in a 0 °C ice bath and water (3.0 mL, 166 mmol) was slowly added in 1 min *via* syringe. The volatiles were removed *in vacuo* to result in yellow liquid with white precipitate. TLC analysis revealed that the liquid contained ~90% of desired product and ~10% di-4-tolylamine. The liquid part was purified *via* column chromatography (hexanes on silica, R_f of 4S1: 0.61, R_f of di-4-tolylamine: 0.13). The volatiles of eluate were removed to get slightly yellow liquid. Its ^1H NMR spectroscopic analysis indicated >98% purity. Yield: 5.39 g (86%). ^1H NMR

(500 MHz, C₆D₆): δ 7.22 (s, 1H, Ar-*H*), 7.05 (d, J_{H-H} = 8.0 Hz, 2H, Ar-*H*), 6.88 (d, J_{H-H} = 8.0 Hz, 2H, Ar-*H*), 6.80 (d, J_{H-H} = 8.0 Hz, 1H, Ar-*H*), 6.68 (d, J_{H-H} = 8.0 Hz, 1H, Ar-*H*), 5.80 (br s, 1H, N-*H*), 2.10 (s, 3H, Ar-CH₃), 1.93 (s, 3H, Ar-CH₃). ¹³C{¹H} NMR (126 MHz, C₆D₆): δ 140.2, 140.0, 133.6, 132.0, 130.5, 130.2, 129.1, 120.9, 116.3, 112.5, 20.8 (Ar-CH₃), 20.1 (Ar-CH₃).

Synthesis of 406-H. In an Ar-filled glovebox, **4S1** (1.00 g, 3.62 mmol) was dissolved in 20 mL Et₂O in a 50 mL Schlenk flask. *n*-BuLi (3.19 mL of 2.5 M solutions in hexanes, 7.98 mmol) was added dropwise over the course of 10 min *via* syringe. The solution color turned from colorless to yellow and then white precipitate formed. After addition of *n*-BuLi, the solution was left to stir at ambient temperature for 2 h further, and ⁱPr₂SiHCl (1.42 mL, 8.32 mmol) was then added dropwise over the course of 10 min. The solution was left to stir at ambient temperature for 15 h. The flask was then taken outside of glovebox, 5 mL 1M HCl_(aq) was added to the flask and the solution was left to stir at ambient temperature for 2 h. NaHCO₃ was added to neutralize the solution and remove all volatiles *in vacuo*. The liquid part of the residue was purified through column chromatography (hexane on silica, R_f of **406-H**: 0.39). The volatiles of eluate were removed to get colorless liquid. Its ¹H NMR spectroscopic analysis indicated >98% purity. Yield: 827 mg (73%). ¹H NMR (500 MHz, C₆D₆): δ 7.35 (s, 1H, Ar-*H*), 7.27 (d, J_{H-H} = 8.5 Hz, 1H, Ar-*H*), 6.96 (d, J_{H-H} = 8.5 Hz, 1H, Ar-*H*), 6.93 (d, J_{H-H} = 8.5 Hz, 2H, Ar-*H*), 6.84 (d, J_{H-H} = 8.5 Hz, 2H, Ar-*H*), 5.64 (br s, 1H, N-*H*), 4.26 (t, J_{Si-H} = 178 Hz, J_{H-H} = 3.5 Hz, 1H, Si-*H*), 2.16 (s, 3H, Ar-CH₃), 2.12 (s, 3H, Ar-CH₃), 1.19 (m, 2H, CHMe₂), 1.08 (d, J_{H-H} = 7.5 Hz, 6H, CHMe₂), 1.03 (d, J_{H-H} = 7.5 Hz, 6H, CHMe₂).

$^{13}\text{C}\{^1\text{H}\}$ NMR (126 MHz, C_6D_6): δ 147.2, 142.7, 137.8, 131.7, 130.9, 130.2, 129.7, 125.2, 120.0, 117.7, 20.9 (Ar- CH_3), 20.7 (Ar- CH_3), 19.3 (CHMe_2), 19.1 (CHMe_2), 11.3 (CHMe_2). ^{29}Si NMR (79 MHz, C_6D_6): δ 0.6 (d, $J_{\text{Si-H}} = 178$ Hz). HRMS (ESI) calcd. for $\text{C}_{20}\text{H}_{30}\text{NSi}$ ($\text{M}+\text{H}$) $^+$: 312.2148. Found: 312.2139.

Synthesis of 407-H. A 100 mL Schlenk flask was charged with **4S2** (515 mg, 1.31 mmol), diethyl ether (20 mL), and a stir bar. *n*-BuLi (1.10 mL of 2.5 M solutions in hexanes, 2.75 mmol) was added drop-wise *via* syringe to a stirring solution. Stirred was continued for 1 h and then $^i\text{Pr}_2\text{SiHCl}$ (250 μL , 1.46 mmol) was added slowly *via* syringe. The solution became a murky yellow color. The reaction mixture was then stirred for 12 h and prior to being quenched with degassed H_2O (50 μL). The volatiles were then removed *in vacuo* and the resulting residue was dissolved in pentane and filtered through Celite. All volatiles were removed *in vacuo* to yield white solid. Its ^1H NMR spectroscopic analysis indicated 95% purity. Yield: 479 mg (85%). The material was further recrystallized from pentane prior testing its catalytic reactivity in DHBTA. ^1H NMR (500 MHz, C_6D_6): δ 7.48 (m, 2H, Ar-*H*), 7.37 (d, $J_{\text{H-H}} = 8.2$ Hz, 1H, Ar-*H*), 7.19 (dd, $J_{\text{H-H}} = 8.4$ Hz, $J_{\text{P-H}} = 5.0$ Hz, 1H, Ar-*H*), 7.13 (s, 1H, N-*H*), 6.97 (dd, $J_{\text{H-H}} = 8.2$, 2.0 Hz, 1H, Ar-*H*), 6.88 (dd, $J_{\text{H-H}} = 8.4$, 2.0 Hz, 1H, Ar-*H*), 4.46 (t, $J_{\text{Si-H}} = 183$ Hz, $J_{\text{H-H}} = 4.0$ Hz, 1H, Si-*H*), 2.18 (s, 3H, Ar-*Me*), 2.17 (s, 3H, Ar-*Me*), 1.97 (m, 2H, $\text{P}(\text{CHMe}_2)_2$), 1.47 (m, 2H, $\text{Si}(\text{CHMe}_2)_2$), 1.21 (d, $J_{\text{H-H}} = 7.4$ Hz, 6H, $\text{Si}(\text{CHMe}_2)_2$), 1.15 (d, $J_{\text{H-H}} = 7.4$ Hz, 6H, $\text{Si}(\text{CHMe}_2)_2$), 1.11 (dd, $J_{\text{P-H}} = 15$ Hz, $J_{\text{H-H}} = 7.0$ Hz, 6H, $\text{P}(\text{CHMe}_2)_2$), 0.98 (dd, $J_{\text{P-H}} = 12$ Hz, $J_{\text{H-H}} = 7.0$ Hz, 6H, $\text{P}(\text{CHMe}_2)_2$). $^{13}\text{C}\{^1\text{H}\}$ NMR (126 MHz, C_6D_6): δ 149.1 (d, $J_{\text{C-P}} = 19$ Hz), 147.0, 138.6, 138.6, 133.5, 133.5, 131.6, 131.5, 131.0, 121.0, 120.4 (d, $J_{\text{P-C}} =$

15 Hz), 115.7, 23.6 (d, $J_{P-C} = 10$ Hz, $P(CHMe_2)_2$), 20.9 (Ar-CH₃), 20.8 (Ar-CH₃), 20.4, (d, $J_{P-C} = 19$ Hz, $P(CHMe_2)_2$), 19.6 (Si(CHMe₂)₂), 19.5 (Si(CHMe₂)₂), 19.2 (d, $J_{P-C} = 9.0$ Hz, $P(CHMe_2)_2$), 11.6 (Si(CHMe₂)₂). ³¹P{¹H} NMR (202 MHz, C₆D₆): δ -15.4. ²⁹Si NMR (79 MHz, C₆D₆): δ 5.2 (d, $J_{H-Si} = 183$ Hz). HRMS (ESI) calcd. for C₂₆H₄₃NPSi (M+H)⁺: 428.2902. Found: 428.2908.

Ligand screening of DHBTA. For central amido donor ligands (401-H to 408-H and 1F): In an Ar-filled glove box, stock solution of a ligand (40 μL of 0.025 M stock solution in C₆D₆, 0.0010 mmol) and sodium bis(trimethylsilyl)amide (40 μL of 0.025 M stock solution in C₆D₆, 0.0010 mmol) were mixed in a vial for 10 s. [(COE)₂IrCl]₂ (40 μL of 0.0125 M stock solution in C₆D₆, 0.00050 mmol) was added to the vial and mixed for 10 s, and the mixture was then transferred to a J. Young tube. Pinacolborane stock solution (200 μL of 1.0 M pinacolborane stock solution in C₆D₆, 0.20 mmol) was added to the J. Young tube. 4-ethynyltoluene (**209**)/1,4-dioxane (200 μL of 0.50 M 4-ethynyltoluene (**209**)/ 0.35 M 1,4-dioxane stock solution in C₆D₆, 0.10 mmol for 4-ethynyltoluene and 0.070 mmol for 1,4-dioxane) was then added in 4 portions with 1 min intervals. The J. Young tube was taken outside, after 10 min, reaction yield was determined on ¹H NMR measurement by using 1,4-dioxane as internal standard. The reagent ratio was calibrated through the integration ratio from a ¹H NMR spectrum of a sample obtained by mixing 100 μL of the pinacolborane stock solution and 100 μL 4-ethynyltoluene (**209**)/1,4-dioxane stock solution in 0.3 mL C₆D₆ in another J. Young tube without adding other reagents. **For central aryl donor ligands (101 and 102):** In an Ar-filled glove box, stock solution of an iridium complex (80 μL

of 0.0125 M stock solution in C₆D₆, 0.0010 mmol) was transferred to a J. Young tube. Pinacolborane stock solution (200 μL of 1.0 M pinacolborane stock solution in C₆D₆, 0.20 mmol) was added to the J. Young tube. 4-ethynyltoluene (**209**)/1,4-dioxane (200 μL of 0.50 M 4-ethynyltoluene / 0.35 M 1,4-dioxane stock solution in C₆D₆, 0.10 mmol for 4-ethynyltoluene (**209**) and 0.070 mmol for 1,4-dioxane) was then added in 4 portions with 1 min intervals. The J. Young tube was taken outside, after 10 min, reaction yield was determined on ¹H NMR measurement by using 1,4-dioxane as internal standard. The reagent ratio was calibrated through the integration ratio from a ¹H NMR spectrum of a sample obtained by mixing 100 μL of the pinacolborane stock solution and 100 μL 4-ethynyltoluene (**209**)/1,4-dioxane stock solution in 0.3 mL C₆D₆ in another J. Young tube without adding other reagents.

4A1-1. ¹H NMR (500 MHz, C₆D₆): δ 7.00 (s, 4H, Ar-*H*), 2.46 (q, J_{H-H} = 7.6 Hz, 2H, Ar-CH₂CH₃), 2.14 (s, 3H, Ar-CH₃), 1.10 (t, J_{H-H} = 7.6 Hz, 3H, Ar-CH₂CH₃).

4A1-2. ¹H NMR (500 MHz, C₆D₆): δ 7.75 (d, J_{H-H} = 18 Hz, 1H, alkenyl-*H*), 7.27 (d, J_{H-H} = 8.0 Hz, 2H, Ar-*H*), 6.85 (d, J_{H-H} = 8.0 Hz, 2H, Ar-*H*), 6.42 (d, J_{H-H} = 18 Hz, 1H, alkenyl-*H*), 2.01 (s, 3H, Ar-CH₃), 1.12 (s, 12H, CH₃ on Bpin).

4A1-3. ¹H NMR (500 MHz, C₆D₆): δ 7.61 (d, J_{H-H} = 8.0 Hz, 2H, Ar-*H*), 7.17 (d, J_{H-H} = 15 Hz, 1H, alkenyl-*H*), 7.00 (d, J_{H-H} = 8.0 Hz, 2H, Ar-*H*), 5.78 (d, J_{H-H} = 15 Hz, 1H, alkenyl-*H*), 2.09 (s, 3H, Ar-CH₃), 1.06 (s, 12H, CH₃ on Bpin).

413-Li. In a 100 mL Schlenk flask under Ar atmosphere, bis(2-bromo-4-methylphenyl)amine (1.31 g, 3.69 mmol) was dissolved in 30 mL of Et₂O. The solution was placed in freezer for 2 h at -35 °C. *n*-BuLi (5.00 mL of 2.5 M solution in hexanes,

12.5 mmol) was added and the solution was stirred overnight after which some white precipitate was observed. The solution was cooled to $-35\text{ }^{\circ}\text{C}$ in freezer for 1 h, then Et_2PCl (1.66 mL, 13.6 mmol) was added. The mixture immediately became bright yellow-orange gradually fading to a light yellow. After 3 h, the reaction was quenched with 200 μL degassed $\text{H}_2\text{O}/\text{MeOH}$ 1:1 soln. Solution was stirred for 20 min, then volatiles were removed. Product was extracted with Et_2O then filtered over Celite yielding a pale yellow solution. Volatiles were reduced leaving a yellow oil. The oil was diluted in pentane then filtered over Celite, and all volatiles were removed *in vacuo*. 10 mL pentane was added to dissolve the residue, and *n*-BuLi (1.8 mL of 2.5 M solution in hexanes, 4.5 mmol) was added dropwise in 5 min. The solution color turned bright yellow immediately and fine yellow powder formed. The solution was stirred 1 h at RT and filtered through a fritted funnel. The yellow powder was washed with cold pentane and dried *in vacuo*. Yield: 785 mg (56%). ^1H NMR (500 MHz, C_6D_6): δ 7.03 (dd, 2H, $J_{\text{H-H}} = 8.5\text{ Hz}$, $J_{\text{P-H}} = 5.5\text{ Hz}$, Ar-*H*), 6.99 (m, 2H, Ar-*H*), 6.93 (dd, 2H, $J_{\text{H-H}} = 8.5, 2.0\text{ Hz}$, Ar-*H*), 2.24 (s, 6H, Ar- CH_3), 1.48 (m, 4H, $-\text{CH}_2\text{CH}_3$), 1.19 (m, 4H, $-\text{CH}_2\text{CH}_3$), 0.88 (m, 12H, $-\text{CH}_2\text{CH}_3$). $^{13}\text{C}\{^1\text{H}\}$ NMR (126 MHz, C_6D_6): δ 167.2 (m), 132.3, 131.4, 126.1, 126.0, 125.5, 20.7, 19.8 (br), 10.6, 10.5. $^{31}\text{P}\{^1\text{H}\}$ NMR (202 MHz, C_6D_6): δ -26.9 (br).

413-Ir-COE. $[(\text{COE})_2\text{IrCl}]_2$ (130 mg, 0.145 mmol) was dissolved in 2 mL fluorobenzene in a 25 mL Schlenk flask and resulted an orange suspension. Solution of **413-Li** (109 mg, 0.288 mmol) in 1 mL PhF was added dropwise in 30 s and the mixture turned clear deep orange. After 10 min, the solution was filtered through Celite and removed all volatiles *in vacuo*. 5 mL pentane was added to the flask and used a spatula

to dislodge the orange powder from the walls of the flask. The solution was vigorously stirred for 1 h and filtered through a fritted funnel. The powder was washed by cold pentane and dried *in vacuo* to yield orange solid. Yield: 125 mg (64%). ^1H NMR (500 MHz, C_6D_6): δ 7.82 (d, $J_{\text{H-H}} = 8.0$ Hz, 2H, Ar-*H*), 6.85 (m, 4H, Ar-*H*), 2.72 (m, 2H, alkenyl-*H* on COE), 2.39 (m, 2H), 2.21 (s, 6H, Ar- CH_3) 1.89 (m, 2H), 1.59 (m, 16H), 1.00 (m, 12H, $\text{P}(\text{CH}_2\text{CH}_3)_2$). $^{13}\text{C}\{^1\text{H}\}$ NMR (126 MHz, C_6D_6): δ 164.4, 131.7, 130.6, 128.6, 126.2, 115.5, 42.6, 33.1 (t, $J_{\text{P-C}} = 3.8$ Hz), 32.9, 27.4, 22.9 (br), 20.4, 17.7 (br), 9.2. $^{31}\text{P}\{^1\text{H}\}$ NMR (121 MHz, C_6D_6): δ 19.6 (d, $J = 15$ Hz). Anal. Calcd for $\text{C}_{30}\text{H}_{46}\text{IrNP}_2$: C, 53.39; H, 6.87. Found: C, 53.25; H, 6.83.

414-Ir-COE. 414-H (175 mg, 0.310 mmol) and $\text{NaN}(\text{TMS})_2$ (57 mg, 0.31 mmol) were dissolved in 10 mL toluene in a 50 mL Schlenk flask to result in a yellow solution. $[(\text{COE})_2\text{IrCl}]_2$ (138 mg, 0.154 mmol) in 5 mL toluene was added to the flask dropwise in 3 min interval. Solution color turned orange during the addition. After 1 h, the solution was filtered through Celite and silica gel, and all volatiles were removed *in vacuo*. 5 mL Et_2O was added to the flask and used a spatula to scratch the film on the wall to result orange powder. The solution was vigorously stirred for 1 h and filtered through a fritted funnel. The powder was washed by cold Et_2O and dried *in vacuo* to yield an orange solid. Its ^1H NMR spectroscopic analysis indicated >95% purity. Yield: 199 mg (74%). The material was further recrystallized from $\text{CH}_2\text{Cl}_2/\text{Et}_2\text{O}$ prior testing its catalytic reactivity in DHBTA. The ^1H NMR (500 MHz, C_6D_6) spectral data were in agreement with those reported in the literature. ^{179}H NMR (400 MHz, CD_2Cl_2): δ 7.82 (br, 8H, Ar-*H*), 7.43 (m, 12H, Ar-*H*), 7.34 (dt, $J_{\text{H-H}} = 8.5$ Hz, $J_{\text{P-H}} = 2.7$ Hz, 2H, Ar-*H*),

6.92 (td, $J_{P-H} = 4.8$ Hz, $J_{H-H} = 1.8$ Hz, 2H, Ar-*H*), 6.83 (dd, $J_{H-H} = 8.5$, 1.8 Hz, 2H, Ar-*H*), 2.62 (m, 2H, alkenyl-*H* on COE), 2.12 (s, 6H, Ar- CH_3), 1.76 (m, 2H), 1.20 (m, 2H), 1.08 (m, 2H), 0.94 (m, 2H), 0.78 (m, 4H). $^{13}C\{^1H\}$ NMR (100 MHz, CD_2Cl_2): δ 161.8, 134.2 (br, 4C), 133.1, 131.9, 130.3, 128.6 (t, $J_{P-C} = 4.6$ Hz, 4C), 127.1 (t, $J_{P-C} = 3.4$ Hz), 115.1, 50.1, 32.2, 31.7 (t, $J_{P-C} = 3.4$ Hz), 26.6, 20.2. $^{31}P\{^1H\}$ NMR (121 MHz, CD_2Cl_2): δ 28.1 (br).

415-Ir-COE. 415-H (202 mg, 0.406 mmol) and $NaN(TMS)_2$ (74 mg, 0.41 mmol) were dissolved in 10 mL toluene in a 50 mL Schlenk flask to result in a yellow solution. $[(COE)_2IrCl]_2$ (182 mg, 0.203 mmol) in 5 mL toluene was added to the flask dropwise in 3 min interval. Solution color turned orange during the addition. After 1 h, the solution was filtered through Celite and silica gel, and all volatiles were removed in vacuo. 5 mL Et_2O was added to the flask and used a spatula to scratch the film on the wall to result orange powder. The solution was vigorously stirred for 1 h and filtered through a fritted funnel. The powder was washed by cold Et_2O and dried *in vacuo* to yield orange solid. Its 1H NMR spectroscopic analysis indicated >95% purity. Yield: 223 mg (69%). The material was further recrystallized from CH_2Cl_2/Et_2O prior testing its catalytic reactivity in DHBTA. 1H NMR (500 MHz, C_6D_6): δ 8.13 (br, 4H, Ar-*H*), 7.61 (dd, $J_{H-H} = 8.5$ Hz, $J_{P-H} = 5.0$ Hz, 1H, Ar-*H*), 7.46 (dd, $J_{H-H} = 8.5$ Hz, $J_{P-H} = 4.0$ Hz, 1H, Ar-*H*), 7.12 (d, $J_{H-H} = 8.5$ Hz, 1H, Ar-*H*), 7.03 (m, 6H, Ar-*H*), 6.92 (d, $J_{H-H} = 8.5$ Hz, 1H, Ar-*H*), 6.74 (d, $J_{H-H} = 8.5$ Hz, 1H, Ar-*H*), 6.69 (d, $J_{H-H} = 8.5$ Hz, 1H, Ar-*H*), 3.48 (br, 2H, alkenyl-*H* on COE), 2.40 (m, 2H), 2.18 (m, 5H, included Ar- CH_3), 2.04 (s, 3H, Ar- CH_3), 1.61 (m, 2H), 1.42 (m, 2H), 1.33 (dvt, $J = 14$, 7.0 Hz, 6H, $CHMe_2$), 1.13 (m, 8H, included

CHMe₂), 1.00 (br, 2H). ¹³C{¹H} NMR (75 MHz, C₆D₆): δ 164.3 (dd, J_{P-C} = 16, 4.8 Hz), 162.5 (dd, J_{P-C} = 18, 3.4 Hz), 136.4 (d, J = 7.8 Hz), 135.9 (d, J_{P-C} = 7.8 Hz), 135.0 (d, J_{P-C} = 9.5 Hz), 132.7, 131.9, 131.6, 129.8, 128.2, 126.4 (d, J_{P-C} = 6.5 Hz), 126.0 (d, J_{P-C} = 6.5 Hz), 123.1 (d, J_{P-C} = 3.8 Hz), 122.5 (d, J_{P-C} = 3.8 Hz), 116.7 (d, J_{P-C} = 9.4 Hz), 114.3 (d, J_{P-C} = 9.1 Hz), 44.4, 32.8, 32.4 (d, J_{P-C} = 5.4 Hz), 27.1, 24.0 (d, J_{P-C} = 22 Hz), 20.5, 20.3, 18.8, 17.5. ³¹P{¹H} NMR (202 MHz, C₆D₆): δ 31.2 (d, J_{P-P} = 360 Hz), 27.2 (d, J_{P-P} = 360 Hz). Anal. Calcd for C₄₀H₅₀IrNP₂: C, 60.13; H, 6.31. Found: C, 59.91; H, 6.27.

General procedure for the NMR-scale dehydrogenative borylation of alkynes (Table 4-3). In an Ar-filled glove box, stock solution of an iridium complex (80 μL of **X** mM stock solution in C₆D₆, **Y** mmol; **1 mol%**: X = 12.5, Y = 1.0 × 10⁻³; **0.25 mol%**: X = 3.1, Y = 2.5 × 10⁻⁴; **0.05 mol%**: X = 0.62, Y = 5.0 × 10⁻⁵; **0.025 mol%**: X = 0.31, Y = 2.5 × 10⁻⁵; **0.01 mol%**: X = 0.125, Y = 1.0 × 10⁻⁵) was transferred to a J. Young tube. Pinacolborane stock solution (200 μL of 1.0 M pinacolborane stock solution in C₆D₆, 0.20 mmol) was added to the J. Young tube. 4-ethynyltoluene/1,4-dioxane (200 μL of 0.50 M 4-ethynyltoluene / 0.35 M 1,4-dioxane stock solution in C₆D₆, 0.10 mmol for 4-ethynyltoluene and 0.070 mmol for 1,4-dioxane) was then added in 4 portions with 1 min intervals. The J. Young tube was taken outside, the reaction yield was determined on ¹H NMR measurement by using 1,4-dioxane as internal standard. The reagent ratio was calibrated through the integration ratio from a ¹H NMR spectrum of a sample obtained by mixing 100 μL of the pinacolborane stock solution and 100 μL 4-ethynyltoluene/1,4-dioxane stock solution in 0.3 mL C₆D₆ in another J. Young tube without adding other reagents.

General procedure for the NMR-scale DHBTA catalyzed by 415-Ir-COE (Table 4-4). In an Ar-filled glove box, stock solution of **415-Ir-COE** (80 μL of **X** mM stock solution in C_6D_6 , **Y** mmol; **0.1 mol%**: $X = 1.25$, $Y = 1.0 \times 10^{-4}$; **0.025 mol%**: $X = 0.31$, $Y = 2.5 \times 10^{-5}$) was transferred to a J. Young tube. Pinacolborane stock solution (200 μL of 1.0 M pinacolborane stock solution in C_6D_6 , 0.20 mmol) was added to the J. Young tube. Alkyne/1,4-dioxane (200 μL of 0.50 M alkyne / 0.35 M 1,4-dioxane stock solution in C_6D_6 , 0.10 mmol for alkyne and 0.070 mmol for 1,4-dioxane) was then added in 4 portions with 1 min intervals. The J. Young tube was taken outside, the reaction yield was determined on ^1H NMR measurement by using 1,4-dioxane as internal standard. The reagent ratio was calibrated through the integration ratio from a ^1H NMR spectrum of a sample obtained by mixing 100 μL of the pinacolborane stock solution and 100 μL alkyne/1,4-dioxane stock solution in 0.3 mL C_6D_6 in another J. Young tube without adding other reagents. The ^1H NMR spectral data of alkynylboronates were in agreement with those reported in the literature.¹³⁷

General procedure for the preparative-scale DHBTA catalyzed by 415-Ir-COE (Table 4-4). In an Ar-filled glove box, **415-Ir-COE** (200 μL of 0.0125 M stock solution in C_6D_6 , 0.0025 mmol) and pinacolborane (2.90 mL, 20.0 mmol) were dissolved in 15 mL toluene to form a light yellow solution in a 100 mL PTFE-valved gas-tight flask. After stirring 3 min at ambient temperature, alkyne (10.0 mmol) was then added dropwise in 30 s. Solution color remained light yellow and bubbles evolved slowly which indicated H_2 generation. After all alkyne was added, the flask was taken out glovebox and heated to 60 $^\circ\text{C}$. After 1 h, the flask was allowed to cool to ambient

temperature and taken into the glove box. The solution was transferred to a 100 mL Schlenk flask and removed all volatiles *in vacuo*. The crude product was redissolved in pentane and placed in a -35 °C freezer for overnight. The next day the solid was collected, washed with cold pentane, and dried *in vacuo*. The decanted solution was combined with the washings, and the volatiles were removed *in vacuo*. The residue was then redissolved in pentane, placed in the freezer and collected in the same manner to yield the second fraction.

209P. White solid, yield: 1.70 g (70%).

216P. White solid, yield: 2.25 g (80%).

Synthesis of 408-Ir-HBpin. In a Ar-filled glove box, **111** (505 mg, 0.811 mmol) was dissolved in 5 mL fluorobenzene in a 25 mL Schlenk flask and pinacolborane (140 μ L, 0.965 mmol) was added. The solution color turned from orange to yellow immediately. After 5 min, all volatiles were removed *in vacuo* to result in yellow sticky fiber-like solid (see Figure 4-11). The residue was redissolved in 1 mL pentane and removed all volatiles *in vacuo*. The residue was dissolved in 1 mL hexamethyldisiloxane then placed in a -35 °C freezer for 2 d. The solution was decanted and yellow solid was dried *in vacuo*. (Note: The synthesis on a smaller scale resulted difficulty to isolate product due to its high solubility in hexamethyldisiloxane.) Yield: 321 mg (53%). ^1H NMR (500 MHz, C_6D_6): δ 7.79 (d, $J_{\text{H-H}} = 8.5$ Hz, 2H, Ar-*H*), 7.05 (s, 2H, Ar-*H*), 6.86 (d, $J_{\text{H-H}} = 8.5$ Hz, 2H, Ar-*H*), 3.11 (m, 2H, CHMe_2), 2.27 (m, 2H, CHMe_2), 2.22 (s, 6H, Ar- CH_3), 1.34 (dvt, $J = 14$, 7.0 Hz, 6H, CHMe_2), 1.28 (dvt, $J = 14$, 7.0 Hz, 6H, CHMe_2), 1.24 (dvt, $J = 14$, 7.0 Hz, 6H, CHMe_2), 1.12 (s, 12H, CH_3 on Bpin), 1.03 (dvt, $J = 14$, 7.0

Hz, 6H, CHMe_2), -19.82 (t, $J_{\text{P-H}} = 8.4$ Hz, 1H, Ir- H). $^{13}\text{C}\{^1\text{H}\}$ NMR (126 MHz, C_6D_6): δ 164.4 (t, $J_{\text{P-C}} = 11$ Hz), 133.1, 131.7, 126.0 (t, $J_{\text{P-C}} = 3.1$ Hz), 124.3 (t, $J_{\text{P-C}} = 20$ Hz), 115.8 (t, $J_{\text{P-C}} = 5.3$ Hz), 81.2 (C_{quart} , Bpin), 24.7 (CH_3 , Bpin), 24.5 (t, $J_{\text{P-C}} = 15$ Hz), 24.0 (t, $J_{\text{P-C}} = 15$ Hz), 20.1, 19.5 (t, $J_{\text{P-C}} = 3.0$ Hz), 18.8, 18.7 (t, $J_{\text{P-C}} = 2.2$ Hz), 16.4. $^{31}\text{P}\{^1\text{H}\}$ NMR (121 MHz, C_6D_6): δ 51.8. $^{11}\text{B}\{^1\text{H}\}$ NMR (128 MHz, C_6D_6): δ 26.4. Anal. Calcd for $\text{C}_{32}\text{H}_{53}\text{BIrNO}_2\text{P}_2$: C, 51.33; H, 7.14. Found: C, 51.24; H, 7.31.



Figure 4-11. Left: Fiber-like **408-Ir-HBpin**; Right: **408-Ir-HBpin** after recrystallization from hexamethyldisiloxane.

Observation of 408-Ir-H₃Bpin. In a Ar-filled glove box, **408-Ir-HBpin** (20 mg, 0.027 mmol) was dissolved in 0.5 mL C_6D_6 (toluene- d_8 was used instead for variable-temperature NMR analysis) in a J. Young tube. The tube was taken out and degassed by three freeze-pump-thaw cycles and back-filled with H_2 (1 atm, excess). After 10 min at RT, the tube was taken up for NMR analysis. ^1H NMR (400 MHz, C_6D_6): δ 7.78 (d, $J_{\text{H-H}} = 8.5$ Hz, 2H, Ar- H), 6.98 (s, 2H, Ar- H), 6.77 (d, $J_{\text{H-H}} = 8.5$ Hz, 2H, Ar- H), 2.81 (m, 2H, CHMe_2), 2.22 (s, 6H, Ar- CH_3), 2.00 (m, 2H, CHMe_2), 1.31 (dvt, $J = 14, 7.0$ Hz, 6H, CHMe_2), 1.23 (dvt, $J = 14, 7.0$ Hz, 6H, CHMe_2), 1.17 (dvt, $J = 14, 7.0$ Hz, 6H, CHMe_2), 1.07 (s, 12H, CH_3 on Bpin), 1.04 (dvt, $J = 14, 7.0$ Hz, 6H, - CHMe_2), -5.35 (br s, 1H, $\omega_{1/2}$

= 60 Hz), -12.40 (br s, 2H, $\omega_{1/2}$ = 64 Hz). Selected $^1\text{H}\{^{11}\text{B}\}$ NMR data (400 MHz, C_6D_6): -5.35 (br s, 1H, $\omega_{1/2}$ = 35 Hz), -12.40 (br s, 2H, $\omega_{1/2}$ = 64 Hz). Selected ^1H NMR data (293 K, 500 MHz, toluene- d_8): -5.43 (br s, 1H), -12.51 (br s, 2H). Selected ^1H NMR data (213 K, 500 MHz, toluene- d_8): -5.39 (br s, 1H), -9.43 (br s, 1H), -15.35 (br s, 1H). $^{31}\text{P}\{^1\text{H}\}$ NMR (202 MHz, C_6D_6): δ 40.8. $^{11}\text{B}\{^1\text{H}\}$ NMR (128 MHz, C_6D_6): δ 32.9.

Synthesis of 408-Ir-Bpin₂. In an Ar-filled glove box, **408-Ir-HMes** (133 mg, 0.180 mmol) and B_2pin_2 (46 mg, 0.18 mmol) were transferred to a 10 mL PTFE-valved gas-tight flask and dissolved in 0.5 mL mesitylene. The flask was taken outside the glovebox and heated at 100 °C for 1 h. The solution color turned from brown to yellow gradually and yellow crystals formed. After allowing the mixture to cool to ambient temperature, the flask was taken into glovebox. Et_2O was added to the flask to assist transferring the solution to a 25 mL Schlenk flask, and then the volatiles were removed *in vacuo*. The residue was redissolved in CH_2Cl_2 /pentane mixture, and the flask was then placed in a -35 °C freezer for overnight. The next day the solid was collected and washed with cold pentane and dried under vacuum to get yellow solid. The decanted solution was combined with the washings, and the volatiles were removed *in vacuo*. The residue was then redissolved in CH_2Cl_2 /pentane, placed in the freezer and collected in the same manner to yield the second fraction. Combined yield: 130 mg (83%). ^1H NMR (500 MHz, C_6D_6): δ 7.57 (d, $J_{\text{H-H}}$ = 8.5 Hz, 2H, Ar-*H*), 6.96 (s, 2H, Ar-*H*), 6.84 (d, $J_{\text{H-H}}$ = 8.5 Hz, 2H, Ar-*H*), 2.93 (m, 4H, CHMe_2), 2.23 (s, 6H, Ar- CH_3), 1.48 (dvt, J = 14, 7.0 Hz, 12H, CHMe_2), 1.19 (dvt, J = 14, 7.0 Hz, 12H, CHMe_2), 1.18 (s, 24H, CH_3 on Bpin). $^{13}\text{C}\{^1\text{H}\}$ NMR (126 MHz, CDCl_3): δ 161.9 (t, $J_{\text{P-C}}$ = 9.2 Hz), 132.8, 130.8, 125.2 (t, $J_{\text{P-C}}$

= 3.5 Hz), 124.2 (t, $J_{P-C} = 20$ Hz), 114.6 (t, $J_{P-C} = 4.5$ Hz), 81.6 (C_{quart} , Bpin), 25.7 (CH_3 , Bpin), 23.8 (br), 20.6, 19.0 (br), 17.0. $^{31}\text{P}\{^1\text{H}\}$ NMR (202 MHz, C_6D_6): δ 46.4. $^{11}\text{B}\{^1\text{H}\}$ NMR (128 MHz, CDCl_3): δ 28.5. Anal. Calcd for $\text{C}_{38}\text{H}_{64}\text{B}_2\text{IrNO}_4\text{P}_2$: C, 52.18; H, 7.38. Found: C, 52.28; H, 7.24. See Figure 4-12 for colors of different boryl complexes.



Figure 4-12. From top to bottom: **408-Ir-H₃Bpin**, **408-Ir-Bpin₂**, **408-Ir-HBpin** in C_6D_6 .

Attempt of making terminal alkyne related complexes (1). **111** (14 mg, 0.023 mmol) was dissolved in 0.5 mL PhF in a 10 mL Schlenk flask and followed by **209** (226 μL of 0.1 M stock solution in C_6D_6 , 0.0226 mmol). After 10 s at RT, all volatiles were removed *in vacuo*. The residue was redissolved in C_6D_6 and analysis by ^{31}P spectroscopy revealed 36% **111** and 64% unidentified mixtures: 6% unknown **4U-1-A** (δ 40.3), 32% unknown **4U-1-B** (δ 29.7), 26% unknown **4U-1-C** (δ 28.6).

Attempt of making terminal alkyne related complexes (2). **111** (10 mg, 0.018 mmol) was dissolved in 0.5 mL C_6D_6 in a J. Young tube and followed by **209** (11 μL , 0.087 mmol). After 10 min at RT, analysis by ^{31}P spectroscopy revealed 36% unknown **4U-2-A** (δ 37.5), 36% unknown **4U-2-B** (δ 30.4), 28% unknown **4U-2-C** (δ 28.3).

Attempt of making terminal alkyne related complexes (3). **408-Ir-HMes** (12 mg, 0.016 mmol) was dissolved in 0.5 mL mesitylene in a J. Young tube and followed by **209** (32 μ L of 0.5 M stock solution in mesitylene, 0.016 mmol). After 1 d at RT, analysis by ^{31}P spectroscopy revealed 58% **408-Ir-HMes** and 42% unidentified mixtures: 6% unknown **4U-3-A** (δ 48.4), 5% unknown **4U-3-B** (δ 37.3), 16% unknown **4U-3-C** (δ 29.9), 4% unknown **4U-3-D** (δ 29.1), and 11% unknown **4U-3-E** (δ 28.2).

Observation of 408-Ir-v-tol and 408-Ir-p-tol. In a Ar-filled glove box, **408-Ir-HMes** (15 mg, 0.021 mmol) and **209P** (210 μ L of 0.1 M stock solution in mesitylene, 0.021 mmol) was dissolved in 300 μ L mesitylene in a J. Young tube. After overnight, ^{31}P NMR spectroscopic analysis revealed formation of two products: 5% **408-Ir-v-tol** and 11% **408-Ir-p-tol**.

Synthesis of 408-Ir-v-tol. In a Ar-filled glove box, **408-Ir-HMes** (118 mg, 0.160 mmol) and **209** (39 mg, 0.16 mmol) was dissolved in 1.0 mL mesitylene in a J. Young tube. The tube was taken out of then placed in a 100 $^{\circ}\text{C}$ oil bath for 1 h. The J. Young tube was allowed to cool to ambient temperature and brought into a glove box. The solution was transferred to a 25 mL Schlenk flask with fluorobenzene to assist. All volatiles were removed *in vacuo*. The residue was redissolved in PhF/pentane, and the flask was then placed in a -35 $^{\circ}\text{C}$ freezer for overnight. The next day the solid was collected and washed with cold pentane and dried under vacuum to get brick red solid. The decanted solution was combined with the washings, and the volatiles were removed *in vacuo*. The residue was then redissolved in PhF/pentane, placed in the freezer and collected in the same manner to yield the second fraction. Combined yield: 70 mg (51%).

^1H NMR (500 MHz, C_6D_6): δ 8.19 (d, $J = 8.5$ Hz, 2H, Ar-*H*), 7.67 (d, $J_{\text{H-H}} = 8.5$ Hz, 2H, Ar-*H*), 7.15 (d, $J_{\text{H-H}} = 8.5$ Hz, 2H, Ar-*H*, overlapping with the solvent peak), 7.06 (s, 2H, Ar-*H*), 6.83 (d, $J_{\text{H-H}} = 8.5$ Hz, 2H, Ar-*H*), 2.58 (m, 4H, CHMe_2), 2.21 (s, 6H, Ar- CH_3), 1.38 (m, 12H, CHMe_2), 1.18 (m, 24H, CHMe_2 and CH_3 on Bpin). $^{13}\text{C}\{^1\text{H}\}$ NMR (126 MHz, C_6D_6): δ 282.8 (t, $J_{\text{P-C}} = 10$ Hz, Ir=C), 163.4 (t, $J_{\text{P-C}} = 11$ Hz), 133.0, 132.6, 131.8, 129.0, 127.0 (t, $J_{\text{P-C}} = 3.0$ Hz), 126.8, 124.8 (t, $J_{\text{P-C}} = 21$ Hz), 120.9, 116.6 (t, $J_{\text{P-C}} = 7.0$ Hz), 82.0 (C_{quart} , Bpin), 26.4 (t, $J_{\text{P-C}} = 15$ Hz), 25.1 (CH_3 , Bpin), 21.1, 20.4, 19.4, 18.5. (Note: In ^{13}C NMR spectra, the quaternary carbon atom attached to boron was not observed.) $^{31}\text{P}\{^1\text{H}\}$ NMR (202 MHz, C_6D_6): δ 43.9. $^{11}\text{B}\{^1\text{H}\}$ NMR (128 MHz, C_6D_6): δ 22.5. Anal. Calcd for $\text{C}_{41}\text{H}_{59}\text{BIrNO}_2\text{P}_2$: C, 57.07; H, 6.89. Found: C, 57.18; H, 6.89.

Synthesis of 408-Ir-v-TMS. In a Ar-filled glove box, **408-Ir-HMes** (52 mg, 0.070 mmol) and **210P** (16 mg, 0.070 mmol) was dissolved in 0.5 mL mesitylene in a J. Young tube. The tube was left at RT overnight. ^{31}P NMR spectroscopic analysis revealed that 60% conversion to **408-Ir-v-TMS** and no observable intermediate. The tube was then placed in a 100 °C oil bath for 1 h. ^{31}P NMR spectroscopic analysis revealed >90% conversion to **408-Ir-v-TMS**. The tube was brought in a glove box and the solution was transferred to a 25 mL Schlenk flask. All volatiles were removed *in vacuo* to yield a red oil, and attempts on recrystallization of residue was failed. The residue was taken up in C_6D_6 for NMR analysis. ^1H NMR (500 MHz, C_6D_6): δ 7.66 (d, $J_{\text{H-H}} = 8.5$ Hz, 2H, Ar-*H*), 7.04 (s, 2H, Ar-*H*), 6.81 (d, $J_{\text{H-H}} = 8.5$ Hz, 2H, Ar-*H*), 2.70 (m, 2H, CHMe_2), 2.60 (m, 2H, CHMe_2), 2.22 (s, 6H, Ar- CH_3), 1.48 (dvt, $J = 14, 7.0$ Hz, 6H, CHMe_2), 1.42 (dvt, $J = 14, 7.0$ Hz, 6H, CHMe_2), 1.27 (dvt, $J = 14, 7.0$ Hz, 6H, CHMe_2), 1.18 (dvt, $J = 14, 7.0$

Hz, 6H, CHMe₂), 1.10 (s, 12H, CH₃ on Bpin), 0.49 (s, 9H, CH₃ on TMS). ¹³C{¹H} NMR (126 MHz, C₆D₆): δ 269.3 (t, J_{P-C} = 8.8 Hz, Ir=C), 163.8 (t, J_{P-C} = 11 Hz), 132.9, 131.8, 126.0 (t, J_{P-C} = 3.3 Hz), 124.4 (t, J_{P-C} = 21 Hz), 116.3 (t, J_{P-C} = 5.1 Hz), 81.7 (C_{quart}, Bpin), 26.7 (t, J_{P-C} = 15 Hz), 26.6 (t, J_{P-C} = 15 Hz), 24.9 (CH₃, Bpin), 20.5, 19.7, 19.6, 18.6, 18.5, 1.2 (SiMe₃). (Note: In ¹³C NMR spectra, the quaternary carbon atom attached to boron was not observed.) ³¹P{¹H} NMR (202 MHz, C₆D₆): δ 44.0. ¹¹B{¹H} NMR (128 MHz, C₆D₆): δ 21.6.

Synthesis of 408-Ir-p-tol. In an Ar-filled glove box, **111** (34 mg, 0.054 mmol) was dissolved in 1 mL fluorene in a 25 mL Schlenk flask and stock solution of **209P** (540 μL of 0.1 M stock solution in C₆D₆, 0.054 mmol) was added to the solution, and the solution color turned red-orange immediately. After 10 s, all volatiles were removed *in vacuo*. The residue was taken up in C₆D₆ for NMR analysis. ³¹P NMR spectroscopic analysis revealed 85% π complex, 9% **408-Ir-HBpin** and 6% unidentified species. ¹H NMR (300 MHz, C₆D₆): δ 8.28 (d, J_{H-H} = 8.1 Hz, 2H, Ar-H), 7.76 (d, J_{H-H} = 8.1 Hz, 2H, Ar-H), 6.99 (d, J_{H-H} = 8.1 Hz, 2H, Ar-H), 6.90 (s, 2H, Ar-H), 6.86 (d, J_{H-H} = 8.1 Hz, 2H, Ar-H), 2.60 (m, 2H, CHMe₂), 2.20 (m, 8H, Ar-CH₃ of PNP and CHMe₂), 2.00 (s, 3H, Ar-CH₃ of alkynylboronate), 1.41 (dvt, J = 14, 7.0 Hz, 6H, CHMe₂), 1.20 (m, 24H, CH₃ on Bpin and -CHMe₂), 0.94 (dvt, J = 14, 7.0 Hz, 6H, CHMe₂). ³¹P{¹H} NMR (121 MHz, C₆D₆): δ 25.6.

Synthesis of 4-CF₃-C₆H₄-C≡C-Bpin (4A2-Bpin). The procedure was adapted from previous reported synthesis.¹³⁷ In an Ar-filled glove box, **206** (14 mg, 0.020 mmol) and pinacolborane (580 μL, 4.00 mmol) were dissolved in 4 mL PhF in a 50 mL Schlenk

flask. After stirring 3 min at ambient temperature, 4-CF₃-C₆H₄-C≡C-H (**4A2-H**, 326 μL, 2.00 mmol) in 3 mL PhF was then added dropwise in 5 min. Bubbles evolved immediately which indicated H₂ generation. After all alkyne was added, the mixture was stirred for 5 min and then the volatiles were removed *in vacuo*. The residue was recrystallized in PhF/pentane in a -35 °C freezer. After overnight, the solution was decanted and the solid was washed with 1 mL pentane three times. The solid was dried *in vacuo* to yield off-white crystal. Yield: 441 mg (74%). ¹H NMR (500 MHz, C₆D₆): δ 7.11 (d, J_{H-H} = 8.5 Hz, 2H, Ar-H), 6.97 (d, J_{H-H} = 8.5 Hz, 2H, Ar-H), 1.02 (s, 12H, -CH₃ on Bpin). ¹³C{¹H} NMR (126 MHz, C₆D₆): δ 132.8, 130.8 (q, J_{F-C} = 33 Hz), 126.1, 125.4 (q, J_{F-C} = 3.8 Hz), 124.4 (q, J_{F-C} = 270 Hz, CF₃), 100.0 (br, C≡C-B), 84.4 (C_{quart}, Bpin), 24.7 (CH₃, Bpin). ¹⁹F NMR (470 MHz, C₆D₆): δ -63.7. ¹¹B{¹H} NMR (128 MHz, C₆D₆): δ 24.4.

Synthesis of 408-Ir-p-Ftol. In an Ar-filled glove box, **111** (204 mg, 0.327 mmol) was dissolved in 2 mL fluorobenzene in a 25 mL Schlenk flask. The flask was placed in a -35 °C freezer for 2 h. **4A2-Bpin** (97 mg, 0.33 mmol) was added to the solution, and the solution color turned red-orange immediately. After 10 s, all volatiles were removed *in vacuo*. (Note: Longer reaction times would result in more **408-Ir-HBpin** formation.) 3 mL pentane was added to the flask and used a spatula to scratch the film on the wall to result red-orange powder. The solution was vigorously stirred for 10 min and then placed in a -35 °C freezer for overnight. The next day the solution part was separated and 3 mL pentane was added to the flask. The solution with suspension was filtered through a fritted funnel. The solid was washed with pentane and dried under vacuum to

get red-orange solid. Yield: 221 mg (74%). ^1H NMR (500 MHz, C_6D_6): δ 8.22 (d, $J_{\text{H-H}} = 8.5$ Hz, 2H, Ar-*H*), 7.71 (d, $J_{\text{H-H}} = 8.5$ Hz, 2H, Ar-*H*), 7.39 (d, $J_{\text{H-H}} = 8.5$ Hz, 2H, Ar-*H*), 6.87 (s, 2H, Ar-*H*), 6.84 (d, $J_{\text{H-H}} = 8.5$ Hz, 2H, Ar-*H*), 2.54 (m, 2H, CHMe_2), 2.19 (s, 6H, Ar- CH_3), 2.08 (m, 2H, CHMe_2), 1.33 (dvt, $J = 14, 7.0$ Hz, 6H, CHMe_2), 1.19 (s, 12H, CH_3 on Bpin), 1.14 (dvt, $J = 14, 7.0$ Hz, 12H, CHMe_2), 0.87 (dvt, $J = 14, 7.0$ Hz, 6H, CHMe_2). $^{13}\text{C}\{^1\text{H}\}$ NMR (100 MHz, CD_2Cl_2): δ 164.4 (t, $J_{\text{P-C}} = 9.4$ Hz), 132.6, 131.3, 131.0, 130.1, 127.6 (q, $J_{\text{F-C}} = 32$ Hz), 126.7 (t, $J_{\text{P-C}} = 3.1$ Hz), 125.4 (q, $J_{\text{F-C}} = 3.8$ Hz), 125.2 (q, $J_{\text{F-C}} = 270$ Hz, CF_3), 124.8 (t, $J_{\text{P-C}} = 20$ Hz), 114.7 (t, $J_{\text{P-C}} = 4.8$ Hz), 105.7 ($\text{C}\equiv\text{C-B}$), 83.5 (C_{quart} , Bpin), 25.0 (CH_3 , Bpin), 24.1 (t, $J_{\text{P-C}} = 13$ Hz), 23.5 (t, $J_{\text{P-C}} = 13$ Hz), 20.3, 18.6, 18.4, 17.6, 17.1. $^{31}\text{P}\{^1\text{H}\}$ NMR (202 MHz, C_6D_6): δ 26.1. $^{11}\text{B}\{^1\text{H}\}$ NMR (128 MHz, C_6D_6): δ 25.5. ^{19}F NMR (470 MHz, C_6D_6): δ 62.9. Anal. Calcd for $\text{C}_{41}\text{H}_{56}\text{BF}_3\text{IrNO}_2\text{P}_2$: C, 53.71; H, 6.16. Found: C, 53.73; H, 6.29.

Reaction of 408-Ir-HBpin with 4-ethynyltoluene. **408-Ir-HBpin** (14 mg, 0.019 mmol) and stock solution of 4-ethynyltoluene (190 μL of 0.1 M stock solution in C_6D_6 , 0.019 mmol) was dissolved in 0.3 mL C_6D_6 in a J. Young tube. After 10 min at RT, analysis by ^{31}P NMR spectroscopy revealed 56% **408-Ir-HBpin**, 16% unknown A (δ 48.8), 14% unknown B (δ 29.5), 14% unknown C (δ 28.7). ~45% Bpin converted to 4-Me- $\text{C}_6\text{H}_4\text{-C}\equiv\text{C-Bpin}$ based on analysis by ^1H NMR spectroscopy. The amount of 4-Me- $\text{C}_6\text{H}_4\text{-C}\equiv\text{C-Bpin}$ did not increase for the longer reaction time, and other side reactions such as hydrogenation occurred.

Reaction of 408-Ir-HBpin with 4- $\text{CF}_3\text{-C}_6\text{H}_4\text{-C}\equiv\text{C-H}$. **408-Ir-HBpin** (11 mg, 0.014 mmol) and stock solution of 4-ethynyltoluene (28 μL of 0.5 M stock solution in

C₆D₆, 0.014 mmol) was dissolved in 0.4 mL C₆D₆ in a J. Young tube. After 10 min at RT, analysis by ³¹P NMR spectroscopy revealed 52% **408-Ir-HBpin**, 23% unknown A' (δ 49.2), 14% unknown B' (δ 28.9), 14% unknown C' (δ 28.5), and 3% **408-Ir-p-Ftol**. ~50% Bpin converted to 4-CF₃-C₆H₄-C≡C-Bpin based on analysis by ¹H NMR spectroscopy. The amount of 4-CF₃-C₆H₄-C≡C-Bpin did not increase for the longer reaction time, and other side reactions such as hydrogenation occurred.

Reaction of 408-Ir-HBpin with TMS-C≡C-H. **408-Ir-HBpin** (11 mg, 0.014 mmol) and stock solution of trimethylsilylacetylene (28 μL of 0.5 M stock solution in C₆D₆, 0.014 mmol) was dissolved in 0.4 mL C₆D₆ in a J. Young tube. After 10 min at RT, analysis by ³¹P NMR spectroscopy revealed 5% **408-Ir-HBpin**, 33% unknown A'' (δ 48.7), 44% unknown B'' (δ 44.6), 14% unknown C'' (δ 41.0), 6% unknown D'' (δ 39.3) and 3% unknown E'' (δ 34.5). ~50% Bpin converted to TMS-C≡C-Bpin based on analysis by ¹H NMR spectroscopy.

Reaction of 408-Ir-Bpin₂ with pinacolborane. **408-Ir-Bpin₂** (13 mg, 0.015 mmol) and stock solution of pinacolborane (15 μL of 1.0M stock solution in C₆D₆, 0.015 mmol) was dissolved in 0.5 mL C₆D₆ in a J. Young tube. The mixture was heated at 100 °C overnight, analysis by ¹H and ³¹P NMR spectroscopy revealed that only unreacted **408-Ir-Bpin₂** and pinacolborane were present.

Reaction of 408-Ir-Bpin₂ with 4-ethynyltoluene. **408-Ir-Bpin₂** (12 mg, 0.014 mmol) and stock solution of 4-ethynyltoluene (27 μL of 0.50M stock solution in C₆D₆, 0.014 mmol) was dissolved in 0.5 mL C₆D₆ in a J. Young tube. After 3 h at RT, analysis by ¹H and ³¹P NMR spectroscopy revealed that only unreacted **408-Ir-Bpin₂** and 4-

ethynyltoluene were present. The mixture was heated at 100 °C overnight, **408-Ir-Bpin₂** was still intact based on the analysis by ³¹P NMR spectroscopy, but 4-ethynyltoluene was consumed to yield a mixture of products.

Reaction of 408-Ir-Bpin₂ with H₂. **408-Ir-Bpin₂** (10 mg, 0.012 mmol) was dissolved in 0.5 mL C₆D₆ in a J. Young tube. The tube was degassed by three freeze-pump-thaw cycles and back-filled with H₂ (1 atm, excess). After 3 h at RT, analysis by ¹H and ³¹P NMR spectroscopy revealed that only unreacted **408-Ir-Bpin₂** and H₂ were present. The mixture was heated at 100 °C overnight, and there was 59% **408-Ir-Bpin₂** and 41% **408-Ir-H₃Bpin** based on the analysis by ³¹P NMR spectroscopy.

Reaction of 408-Ir-v-tol with H₂. **408-Ir-v-tol** (10 mg, 0.011 mmol) was dissolved in 0.5 mL C₆D₆ in a J. Young tube. The tube was degassed by three freeze-pump-thaw cycles and back-filled with H₂ (1 atm, excess). After 1 h at RT, 80% **408-Ir-v-tol** was converted to several unknown products (no observable signals in ³¹P NMR) and H₂C=C(4-Me-C₆H₄)(Bpin) based on the analysis by ¹H NMR spectroscopy. After RT overnight, **111** was the only observable species in ³¹P NMR spectroscopy analysis. Selected NMR data for H₂C=C(4-Me-C₆H₄)(Bpin). ¹H NMR (500 MHz, C₆D₆): δ 6.39 (d, J = 3.0 Hz, 1H, alkenyl-*H*), 6.15 (d, J = 3.0 Hz, 1H, alkenyl-*H*), 1.05 (s, 12H, -CH₃ on Bpin).

Reaction of 408-Ir-v-tol with pinacolborane. **408-Ir-v-tol** (12 mg, 0.014 mmol) and stock solution of pinacolborane (14 μL of 1.0M stock solution in C₆D₆, 0.014 mmol) was dissolved in 0.5 mL C₆D₆ in a J. Young tube. After 3 h at RT, analysis by ¹H and ³¹P NMR spectroscopy revealed that only unreacted **408-Ir-v-tol** and pinacolborane were

present. The mixture was heated at 100 °C for 1 h, <5% decomposition of **408-Ir-v-tol** was observed by ¹H NMR spectroscopy analysis and **408-Ir-v-tol** remained the only observable species in the ³¹P NMR spectrum.

Reaction of 408-Ir-v-tol with 4-CH₃-C₆H₄-C≡C-H. **408-Ir-v-tol** (11 mg, 0.013 mmol) and stock solution of 4-ethynyltoluene (26 μL of 0.50M stock solution in C₆D₆, 0.013 mmol) was dissolved in 0.5 mL C₆D₆ in a J. Young tube. After 3 h at RT and 1 h at 100 °C, analysis by ¹H and ³¹P NMR spectroscopy revealed that only unreacted **408-Ir-v-tol** and 4-ethynyltoluene were present. After 15 h at 100 °C, <5% decomposition of **408-Ir-v-tol** was observed by ¹H NMR spectroscopy analysis and **408-Ir-v-tol** remained the only observable species in the ³¹P NMR spectrum.

Reaction of 408-Ir-p-Ftol with H₂. **408-Ir-p-Ftol** (10 mg, 0.011 mmol) was dissolved in 0.5 mL C₆D₆ in a J. Young tube. The tube was degassed by three freeze-pump-thaw cycles and back-filled with H₂ (1 atm, excess). The solution color turned lighter orange gradually. After 10 min at RT, there were 49% **408-Ir-p-Ftol**, 27% **408-Ir-H₃Bpin**, and 24% unknown (δ 31.1) based on the analysis by ³¹P NMR spectroscopy.

Reaction of 408-Ir-p-Ftol with pinacolborane. **408-Ir-p-Ftol** (11 mg, 0.011 mmol) and stock solution of pinacolborane (22 μL of 0.5 M stock solution in C₆D₆, 0.011 mmol) was dissolved in 0.5 mL C₆D₆ in a J. Young tube. After 10 min at RT, there were 14% **408-Ir-HBpin** and 86% **408-Ir-p-Ftol** based on the analysis by ³¹P NMR spectroscopy. After 4 h at RT, there were 83% **408-Ir-HBpin** and 17% **408-Ir-p-Ftol** based on the analysis by ³¹P NMR spectroscopy, and analysis by ¹H NMR spectroscopy

revealed that only free 4-CF₃-C₆H₄-C≡C-Bpin, free pinacolborane, **408-Ir-HBpin**, **408-Ir-p-Ftol** were present.

Reaction of 408-Ir-p-Ftol with 4-CF₃-C₆H₄-C≡C-H. **408-Ir-p-Ftol** (10 mg, 0.011 mmol) and stock solution of 4-CF₃-C₆H₄-C≡C-H (22 μL of 0.50M stock solution in C₆D₆, 0.011 mmol) was dissolved in 0.5 mL C₆D₆ in a J. Young tube. After 10 min at RT, analysis by ¹H and ³¹P NMR spectroscopy revealed that only unreacted **408-Ir-p-Ftol** and 4-ethynyltoluene were present. After 2 h at RT, analysis by ¹H NMR spectroscopy revealed 8% free 4-CF₃-C₆H₄-C≡C-Bpin and 92% **408-Ir-p-Ftol** were present as alkynylboronate related species.

General procedure for the NMR-scale dehydrogenative borylation of alkynes (Table 4-5). In an Ar-filled glove box, stock solution of iridium catalyst (80 μL of 0.0125 M stock solution in C₆D₆, 0.0010 mmol) and pinacolborane stock solution (200 μL of 1.0 M pinacolborane stock solution in C₆D₆, 0.20 mmol) were mixed in a J. Young tube. Alkyne/1,4-dioxane (200 μL of 0.50 M alkyne/ 0.35 M 1,4-dioxane stock solution in C₆D₆, 0.10 mmol for alkyne and 0.070 mmol for 1,4-dioxane) was then added in 4 portions with 1 min intervals. The J. Young tube was taken outside, after 10 min, reaction yield was determined on ¹H NMR measurement by using 1,4-dioxane as internal standard. The reagent ratio was calibrated through the integration ratio from a ¹H NMR spectrum of a sample obtained by mixing 100 μL of the pinacolborane stock solution and 100 μL alkyne/1,4-dioxane stock solution in 0.3 mL C₆D₆ in another J. Young tube without adding iridium catalyst.

X-Ray data collection, solution, and refinement for 408-Ir-HBpin. A Leica MZ 75 microscope was used to identify a suitable yellow block with very well defined faces with dimensions (max, intermediate, and min) 0.65 mm x 0.55 mm x 0.30 mm from a representative sample of crystals of the same habit. The crystal mounted on a nylon loop was then placed in a cold nitrogen stream (Oxford) maintained at 110 K. A BRUKER GADDS X-ray (three-circle) diffractometer was employed for crystal screening, unit cell determination, and data collection. The goniometer was controlled using the FRAMBO software, v.4.1.05.¹⁵⁰ The sample was optically centered with the aid of a video camera such that no translations were observed as the crystal was rotated through all positions. The detector was set at 5.0 cm from the crystal sample. The X-ray radiation employed was generated from a Cu sealed X-ray tube ($K_{\alpha} = 1.5418 \text{ \AA}$ with a potential of 40 kV and a current of 40 mA) fitted with a graphite monochromator in the parallel mode (175 mm collimator with 0.5 mm pinholes). 180 data frames were taken at widths of 0.5° . These reflections were used to determine the unit cell using Cell_Now.¹⁵⁰ The unit cell was verified by examination of the $h k l$ overlays on several frames of data. No super-cell or erroneous reflections were observed. After careful examination of the unit cell, an extended data collection procedure (26 sets) was initiated using omega and phi scans. Integrated intensity information for each reflection was obtained by reduction of the data frames with APEX2.¹⁵⁰ The integration method employed a three dimensional profiling algorithm and all data were corrected for Lorentz and polarization factors, as well as for crystal decay effects. Finally the data was merged and scaled to produce a suitable data set. SADABS¹⁵⁰ was employed to correct the data for absorption effects. Systematic

reflection conditions and statistical tests indicated the space group $P21/c$. A solution was obtained readily using SHELXTL (SHELXS).¹⁵¹ Hydrogen atoms were placed in idealized positions and were refined using riding model. All non-hydrogen atoms were refined with anisotropic thermal parameters. The hydride on iridium was assigned from a Q peak near the expected position and refined. The presence of Ir- H is also indicated both by ^1H NMR spectroscopic data. The structure was refined (weighted least squares refinement on F^2) to convergence.^{151,172} Platon¹⁵⁰ was used to verify the absence of additional symmetry.

X-Ray data collection, solution, and refinement for 408-Ir-Bpin₂. A yellow, multi-faceted block of suitable size (0.80 x 0.70 x 0.45 mm) was selected from a representative sample of crystals of the same habit using an optical microscope and mounted onto a nylon loop. Low temperature (110 K) X-ray data were obtained on a Bruker APEXII CCD based diffractometer (Mo sealed X-ray tube, $K_{\alpha} = 0.71073 \text{ \AA}$). All diffractometer manipulations, including data collection, integration and scaling were carried out using the Bruker APEXII software.¹⁵⁰ An absorption correction was applied using SADABS.¹⁵⁰ The space group was determined on the basis of systematic absences and intensity statistics and the structure was solved by direct methods and refined by full-matrix least squares on F^2 . The structure was solved in the monoclinic $P21/c$ space group using XS¹⁵¹ (incorporated in SHELXTL). All non-hydrogen atoms were refined with anisotropic thermal parameters. All hydrogen atoms were placed in idealized positions and refined using riding model. The structure was refined (weighted least squares refinement on F^2) and the final least-squares refinement converged.

X-Ray data collection, solution, and refinement for 408-Ir-v-tol. A Leica MZ 75 microscope was used to identify a suitable red block with very well defined faces with dimensions (max, intermediate, and min) 0.08 mm x 0.02 mm x 0.02 mm from a representative sample of crystals of the same habit. The crystal mounted on a nylon loop was then placed in a cold nitrogen stream (Oxford) maintained at 110 K. A BRUKER GADDS X-ray (three-circle) diffractometer was employed for crystal screening, unit cell determination, and data collection. The goniometer was controlled using the FRAMBO software, v.4.1.05.¹⁵⁰ The sample was optically centered with the aid of a video camera such that no translations were observed as the crystal was rotated through all positions. The detector was set at 5.0 cm from the crystal sample. The X-ray radiation employed was generated from a Cu sealed X-ray tube ($K_{\alpha} = 1.5418 \text{ \AA}$ with a potential of 40 kV and a current of 40 mA) fitted with a graphite monochromator in the parallel mode (175 mm collimator with 0.5 mm pinholes). 180 data frames were taken at widths of 0.5° . These reflections were used to determine the unit cell using Cell_Now.¹⁵⁰ The unit cell was verified by examination of the $h k l$ overlays on several frames of data. No super-cell or erroneous reflections were observed. After careful examination of the unit cell, an extended data collection procedure (26 sets) was initiated using omega and phi scans. Integrated intensity information for each reflection was obtained by reduction of the data frames with APEX2.¹⁵⁰ The integration method employed a three dimensional profiling algorithm and all data were corrected for Lorentz and polarization factors, as well as for crystal decay effects. Finally the data was merged and scaled to produce a suitable data set. SADABS¹⁵⁰ was employed to correct the data for absorption effects. Systematic

reflection conditions and statistical tests indicated the space group $P-1$. A solution was obtained readily ($Z' = 2$; $Z = 4$) using SHELXTL (SHELXS).¹⁵¹ Hydrogen atoms were placed in idealized positions and were refined using riding model. All non-hydrogen atoms were refined with anisotropic thermal parameters. Elongated thermal ellipsoids on (O1-O2-C36 to C41) group suggested disorder which was modeled successfully between two positions. Restraints and constraints were used to keep the bond distances, angles, and the thermal ellipsoids meaningful.¹⁵⁰ The structure was refined (weighted least squares refinement on F^2) to convergence.^{151,172} Platon⁴⁸ was used to verify the absence of additional symmetry; however it suggested presence of 50 \AA^3 voids with no ($0 \text{ e}^-/\text{\AA}^3$) electrons in them, which agreed with the difference map showing no electron density in the voids.

X-Ray data collection, solution, and refinement for 408-Ir-p-Ftol. A Leica MZ 75 microscope was used to identify a suitable orange block with very well defined faces with dimensions (max, intermediate, and min) 0.23 mm x 0.21 mm x 0.13 mm from a representative sample of crystals of the same habit. The crystal mounted on a nylon loop was then placed in a cold nitrogen stream (Oxford) maintained at 110 K. A BRUKER GADDS X-ray (three-circle) diffractometer was employed for crystal screening, unit cell determination, and data collection. The goniometer was controlled using the FRAMBO software, v.4.1.05.¹⁵⁰ The sample was optically centered with the aid of a video camera such that no translations were observed as the crystal was rotated through all positions. The detector was set at 5.0 cm from the crystal sample. The X-ray radiation employed was generated from a Cu sealed X-ray tube ($K_\alpha = 1.5418 \text{ \AA}$ with a potential of 40 kV

and a current of 40 mA) fitted with a graphite monochromator in the parallel mode (175 mm collimator with 0.5 mm pinholes). 180 data frames were taken at widths of 0.5° . These reflections were used to determine the unit cell using Cell_Now.¹⁵⁰ The unit cell was verified by examination of the $h k l$ overlays on several frames of data. No super-cell or erroneous reflections were observed. After careful examination of the unit cell, a standard data collection procedure (9 sets) was initiated using omega and phi scans. Integrated intensity information for each reflection was obtained by reduction of the data frames with APEX2.¹⁵⁰ The integration method employed a three dimensional profiling algorithm and all data were corrected for Lorentz and polarization factors, as well as for crystal decay effects. Finally the data was merged and scaled to produce a suitable data set. SADABS¹⁵⁰ was employed to correct the data for absorption effects. Systematic reflection conditions and statistical tests indicated the space group $P2_1/n$. A solution was obtained readily using SHELXTL (SHELXS).¹⁵¹ A molecule of fluorobenzene was found solvated. Hydrogen atoms were placed in idealized positions and were refined using riding model. All non-hydrogen atoms were refined with anisotropic thermal parameters. Thermal ellipsoids indicated fluorobenzene and CF_3 groups were disordered. While the latter disorder was successfully modeled the former could be only modeled only with strong restraints / constraints. The structure was refined (weighted least squares refinement on F^2) to convergence.^{150,151,172} Platon⁴⁸ was used to verify the absence of additional symmetry and voids.

CHAPTER V

DEHYDROGENATIVE DIBORATION OF ALKYNYLBORONATES CATALYZED BY SINN IRIIDIUM COMPLEXES³

5.1 Introduction

Multisubstituted olefins are important structural motifs in drugs, natural products, and functional materials.^{194,195} Chemists have developed many methodologies to synthesize multisubstituted olefins in a stereocontrolled fashion.^{194,195} Among these methodologies, selective Suzuki-Miyaura coupling of multiborylated alkenes appeared as an attractive route.¹⁹⁶⁻¹⁹⁹ Multiborylated alkenes are relatively harmless and stable starting materials that undergo Suzuki-Miyaura coupling with high selectivity and yields. Syntheses of multiborylated alkenes are summarized in Figure 5-1.

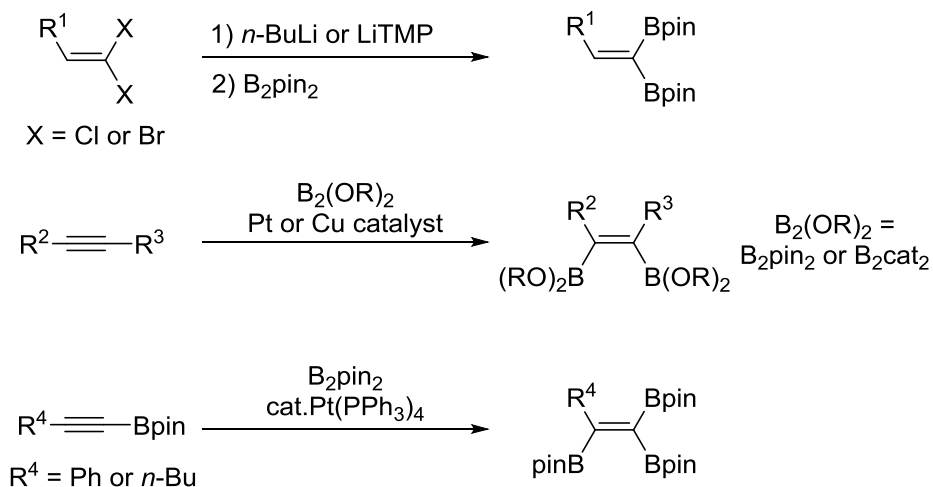


Figure 5-1. Syntheses of 1,1-diborylalkenes (top), 1,2-*cis*-diborylalkenes (middle) and triborylalkenes (bottom).

³ In this chapter, all DFT calculations are done by Dr. Jia Zhou.

Traditionally, 1,1-diborylalkene was made from *gem*-diboration of 1,1-dichloro- or 1,1-dibromoalkenes through Li-halide exchange and then reaction with bis(pinacolato)diboron (B_2pin_2) (Figure 5-1, top).^{200,201} On the other hand, 1,2-*cis*-diborylalkenes are more widely used building blocks that are readily available from diboration of terminal or internal alkynes (Figure 5-1, middle). Since the discovery of diboration of alkynes by Suzuki, Miyaura and co-workers in 1993,²⁰² the methodology²⁰³ has been extensively studied. These reactions utilize B_2pin_2 and bis(catecholato)diboron (B_2cat_2) as the typical boron reagents and are usually catalyzed by platinum^{202,204-210} or copper²¹¹⁻²¹³ complexes. Syntheses of triborylalkene were relatively rare and only two examples have been reported which employ platinum-catalyzed diboration of alkynylboronates (Figure 5-1, bottom).²¹⁴

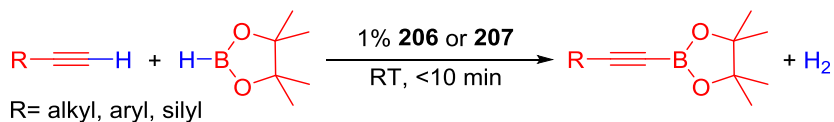


Figure 5-2. DHBTA catalyzed by (SiNN)Ir complexes.

In the Chapter 2, we demonstrated the first example of dehydrogenative borylation of terminal alkynes (DHBTA) catalyzed by a SiNN pincer cyclooctene iridium complex (Figure 5-2).¹³⁷ The reaction was highly chemoselective leading to alkynylboronates in excellent yields. This motivated us to explore the potential to further borylate alkynylboronates in a one-pot reaction. Here we report the discovery of a new selective dehydrogenative diboration of alkynylboronates. The independent synthesis and

characterization of the possible catalytic intermediates in the diboration will also be described.

5.2 Results and discussion

5.2.1 Discovery and optimization of dehydrogenative diboration of alkynylboronates

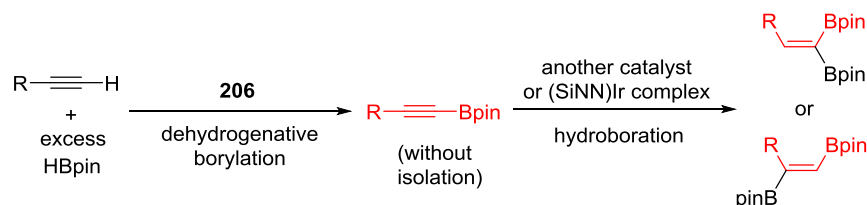
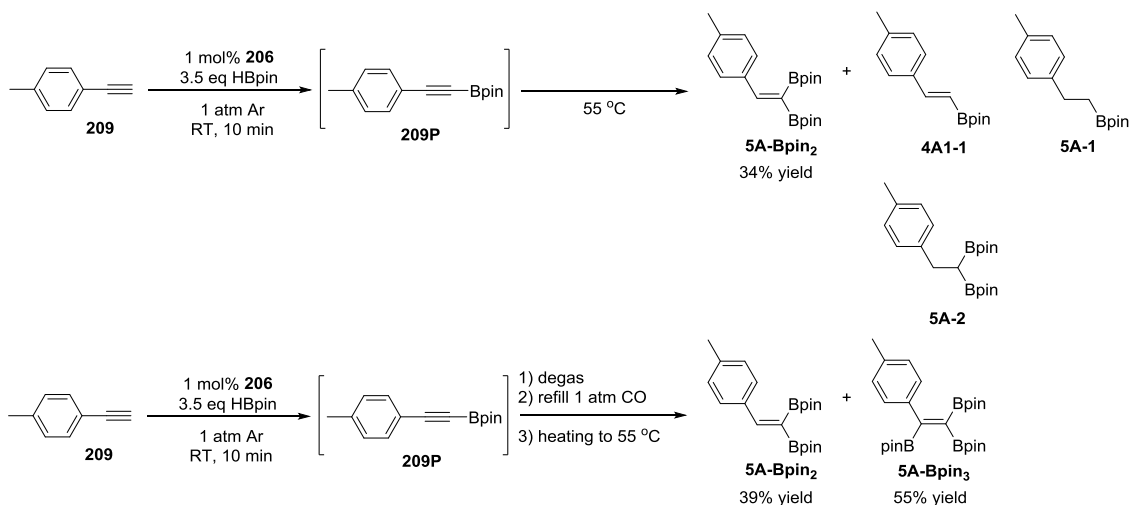


Figure 5-3. Original idea of one-pot synthesis of diborylalkenes.

Originally inspired by the success of **206** in DHBTA, we set out to evaluate the potential to develop a one-pot synthesis that could combine DHBTA and hydroboration (Figure 5-3). Ideally after successful DHBTA, hydroboration can be performed in *syn*-addition fashion to alkynylboronates to yield 1,1-*gem*-diborylalkenes or 1,2-*trans*-diborylalkenes. 4-Ethynyltoluene (**209**) was chosen as the model substrate. According to the previous DHBTA protocol, **209** was first reacted with 3.5 equivalents of pinacolborane to cleanly yield **209P**. Hydroboration was first attempted, simply from heating up the reaction mixture at 55 °C. However, after 24 h, multiple hydrogenation and hydroboration products were observed (Scheme 5-1, top) including 34% yield of *gem*-diborylalkene (**5A-Bpin₂**). Degassing the reaction mixtures and refilling with 1 atm Ar before heating still resulted in a similar product distribution. Surprisingly, heating at 55 °C under 1 atm CO, the DHBTA mixture produced only two major products: 34% yield of **5A-Bpin₂**, and 55% yield of a new triborylalkene product, **5A-Bpin₃** (Scheme 5-1, bottom) after heating at 55 °C for 8 h. The product ratio did not change even with

additional heating. The formation of the unexpected product, **5A-Bpin₃**, can be viewed as the result of diboration of **209P**. Although diboration of alkynes is well-known in the literature,²⁰³ we believe this is the first diboration of alkynes using dialkoxyborane as the boron reagent and losing dihydrogen as the by-product.

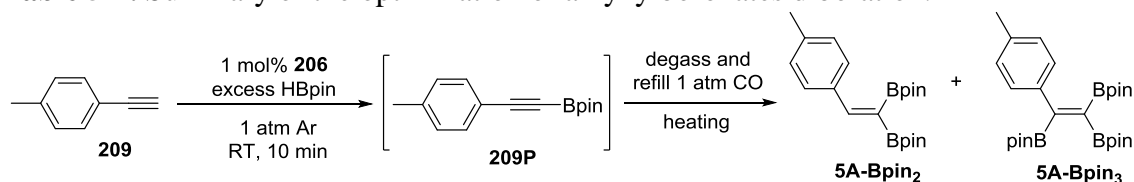


Scheme 5-1. Attempts at further borylation of alkynylboronates.

After the discovery of this unusual diboration, we started to examine factors to optimize the yield of triborylalkenes and the results are summarized in Table 5-1. The product ratio between **5A-Bpin₂** and **5A-Bpin₃** did not change significantly when fluorobenzene (entry 2) or THF (entry 3) was selected as the solvent. Heating the reaction mixture at 80 °C led to slightly higher **5A-Bpin₂** yield, however, the amount of other side products also increased (entry 4). We surmised that increasing the equivalents and concentration of HBpin should favor **5A-Bpin₃** formation. By increasing the amount of HBpin to 5 equivalents and reducing the solvent volume, the yield of **5A-Bpin₃** was achieved an impressive 88% (entry 5). Finally, the reaction could also be carried out in

neat HBpin and the product ratio of **5A-Bpin₃** to **5A-Bpin₂** was further improved to about 20 (entry 6). Considering the cost of HBpin and the small yield improvement from entry 5 to entry 6, the conditions of entry 5 were selected for the subsequent substrate scope examination.

Table 5-1. Summary of the optimization of alkynylboronates diboration.



Entry	Eq. of HBpin	Conc. of HBpin (M)	Solvent	Temp	Time	5A-Bpin₂	5A-Bpin₃
1	3.5	0.56	C ₆ D ₆	55 °C	8 h	39%	55%
2	3.5	0.56	PhF	55 °C	8 h	45%	50%
3 ^a	3.5	0.56	THF	55 °C	8 h	26%	43%
4	3.5	0.56	C ₆ D ₆	80 °C	3 h	52%	32%
5	5.0	3.0	PhF	55 °C	18 h	7%	88%
6	10	6.3	neat	55 °C	18 h	5%	91%

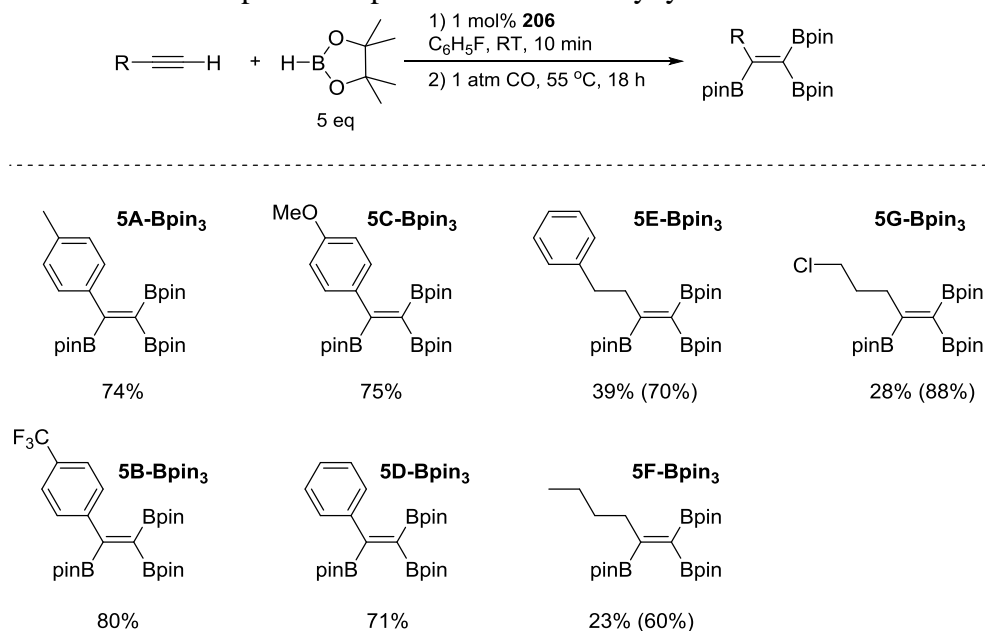
^a 26% **209P**.

5.2.2 Substrate scope of one-pot dehydrogenative diboration of alkynylboronates

Various terminal alkynes were subjected to explore the scope of the one-pot synthesis of triborylalkenes catalyzed by **206**, and the results are summarized in Table 5-2. Generally after removal of volatiles, the pentane insoluble triborylalkenes can be

easily separated by suspending the mixture in pentane and filtering through a fritted funnel. 70 - 80% isolated yields were obtained for all aromatic alkynes regardless of whether electron-donating or electron-withdrawing groups were present (**5A-Bpin₃** – **5D-Bpin₃**). Good to fair NMR yields were observed for aliphatic alkynes (**5E-Bpin₃** – **5G-Bpin₃**), however, the isolated yields were significantly lower than aromatic alkynes. We found the solubility of aliphatic triborylalkenes in pentane to be much higher which was responsible for low isolated yields. Use of other solvent with even poorer solvating power than pentane, like 2,2-dimethylbutane is under investigation to help with the isolation of products.

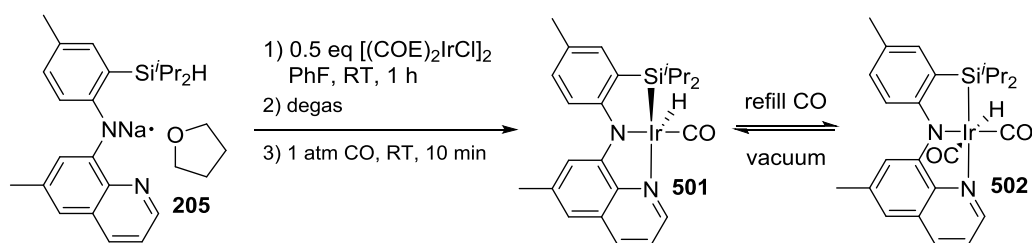
Table 5-2. Substrate scope of one-pot diboration of alkynylboronates.^{a,b,c}



^a **206** (0.020 mmol) and HBpin (10 mmol) were dissolved in PhF in a PTFE-valved gas-tight flask. Alkyne (2.00 mmol) was then added in 4 portions with 1 min intervals at RT. After 10 min, the mixture was degassed, refilled with 1 atm CO and heated at 55 °C for 18 h (see experimental for details). ^b Isolated yield. ^c Yields in parentheses are NMR yield.

5.2.3 Independent synthesis of (SiNN)Ir(CO) and its equilibrium with (SiNN)Ir(CO)₂

Since the diboration of alkynylboronates took place under CO atmosphere, we wanted to examine the reaction of the starting catalyst **206** with CO in the absence of alkynes and HBpin. Treating the *in-situ* generated **206** from **205** and [(COE)₂IrCl]₂ with 1 atm CO at ambient temperature led to an equilibrium mixture of the monocarbonyl adduct **501** and bis(carbonyl) adduct **502** (Scheme 5-2). We were able to isolate **501** as a brown solid in 92% yield.



Scheme 5-2. The synthesis of **501** and its equilibrium with **502**.

In the ¹H NMR spectrum, **501** showed an up-field Ir-H signal at -15.52 ppm, and no signal for Ir-H was observed in the ¹H-²⁹Si DQF spectrum, which suggests that this proton has no interaction with the silicon atom. On the other hand, the Ir-H signal of **502** displayed a more downfield position (-6.1 ppm) presumably because the hydride is *trans*- to a carbonyl. In the ¹H-²⁹Si DQF spectrum, a small Si-H coupling constant (*J*_{Si-H} = 2.1 Hz) was observed which suggested **502** should be viewed as a silyl hydride complex.^{128,131} The existence of CO in both complexes is supported by the corresponding absorption peaks at 1977 cm⁻¹ for **501**, and 2057 and 2007 cm⁻¹ for **502** in the IR analysis.

An X-ray quality crystal of **501** was grown from CH₂Cl₂/pentane and the solid structures are shown in Figure 5-4 (top). To assist the X-ray studies, especially the location of the Ir-H, density functional theory (DFT) calculations were carried out on **501** in the gas phase using the M06 functional (Figure 5-4, bottom). The positions of nonhydrogen atoms from the experimental XRD determination were closely reproduced in the DFT calculated structure. The longer calculated Si-H distance in **501** (2.183 Å) versus **206** (2.007 Å) and **207** (1.889 Å) is in agreement with no observable Si-H coupling, and J_{Si-H} values of 8 and 32 Hz, respectively. Both the calculated Si-H distance and the J_{Si-H} of **501** are outside of the range for a Si-H bonding interaction, hence **501** can be confidently viewed as an d⁶-Ir(III) silyl hydride complex.^{128,131}

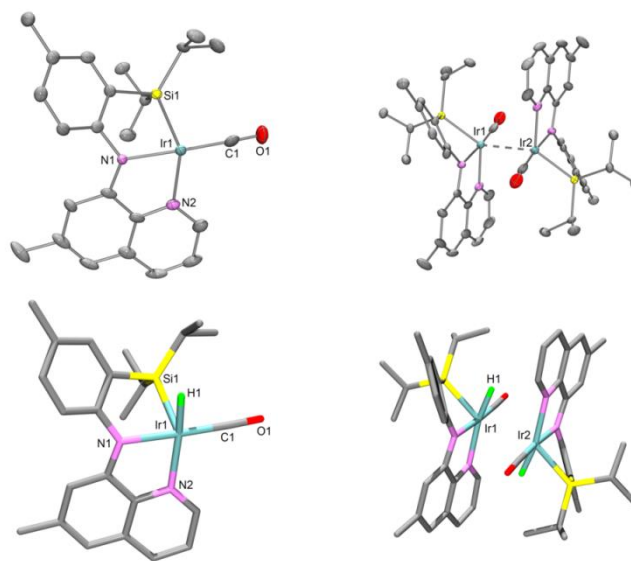


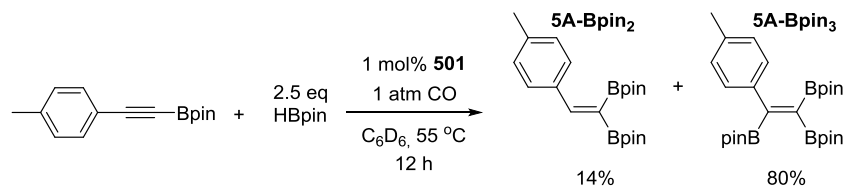
Figure 5-4. ORTEP drawing¹²⁹ (50% probability ellipsoids) of **501** (top) showing selected atom labeling, and drawing of the DFT-calculated structures of **501** (bottom). Hydrogen atoms are omitted for clarity, except for the hydride on the Ir atom. Selected bond distances (Å) and angles (deg) for **501**, with DFT-derived metrics in square brackets: Ir1-Si1, 2.3366(15) [2.376]; Si1-H, [2.183]; Ir1-H1, [1.592]; Ir2-H1, [3.117]; Ir1-Ir2, 2.9074(8) [3.046]; Si1-Ir1-N2, 124.89(11) [127.51]; Si1-Ir1-H1, [63.17]; Ir1-C1-O1, 176.1(5) [177.75].

Interestingly, **501** forms a dimer structure in the solid state with a 2.907 Å distance between two iridium centers. No π - π stacking is observed and the hydrides are clearly terminal (Ir1-H1: 1.592 Å; Ir2-H1: 3.117 Å), ruling out the possibility of a hydride-bridged dimer. Many examples of d^{10} - d^{10} and d^8 - d^8 dimers,²¹⁵⁻²²⁰ most commonly with Pd(II) and Pt(II) can be found in the literature, and unsupported d^8 - d^8 interactions have also been reported.^{221,222} The M...M distances in the d^8 - d^8 dimers supported by bridging ligands are usually in the range of 2.7-3.2 Å,^{223,224} and the M...M distances in the unsupported d^8 - d^8 dinuclear complexes are 2.8-3.1 Å.^{221,222} However, the d^6 - d^6 interaction has not been observed to the best of our knowledge. 5-coordinate d^6 complexes usually require a certain degree of steric protection of the open coordination site, and that would prevent the possible formation of a d^6 - d^6 interaction. **501** is unique in that its square pyramidal base is almost perfectly flat, so two iridium centers can approach each other to ~ 3.0 Å, which is the common M...M distance for these types of interactions.^{221,222} It is still not clear whether or not the dimer persists in solution and experiments like diffusion-ordered NMR might be helpful for elucidating the status of **501** in solution.

5.2.4 Examination of isolated **501** and other CO complex in the borylation

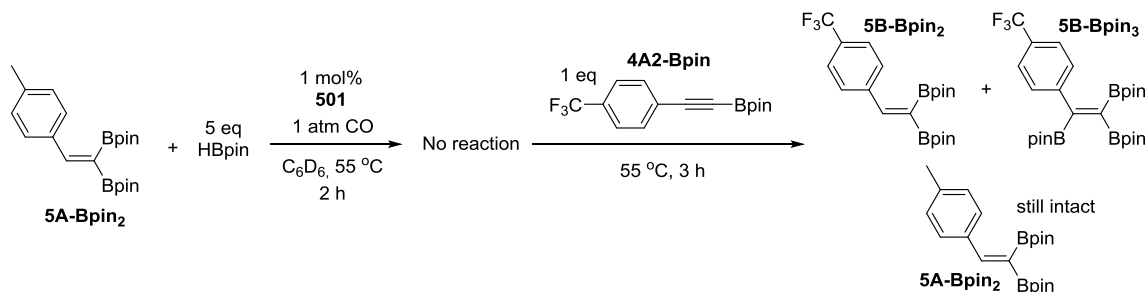
To examine the possible role of **501** in the diboration of alkynylboronates, we first tested **501** in the reaction between isolated **209P** and HBpin under 1 atm CO (Scheme 5-3). 80% yield of **5A-Bpin₃** and 14% yield of **5A-Bpin₂** were observed by ¹H NMR spectrum after 12 h. The observation of two major products, **5A-Bpin₃** and **5A-Bpin₂**, was consistent with the results observed from one-pot synthesis reactions but with

slightly different product ratio. This suggested **501** acts as the actual entry point into the catalytic cycle of the diboration.



Scheme 5-3. Borylation of **209P** with HBpin catalyzed by **501**.

During the optimization of diboration, we found the product ratio of *gem*-diborylalkenes and triborylalkenes did not change once all the alkynylboronates were consumed. It seems triborylalkenes are not generated from alkynylboronates via *gem*-diborylalkenes. To further prove this point, we independently synthesized a *gem*-diborylalkene **5A-Bpin₂** via a recently published protocol.²²⁵

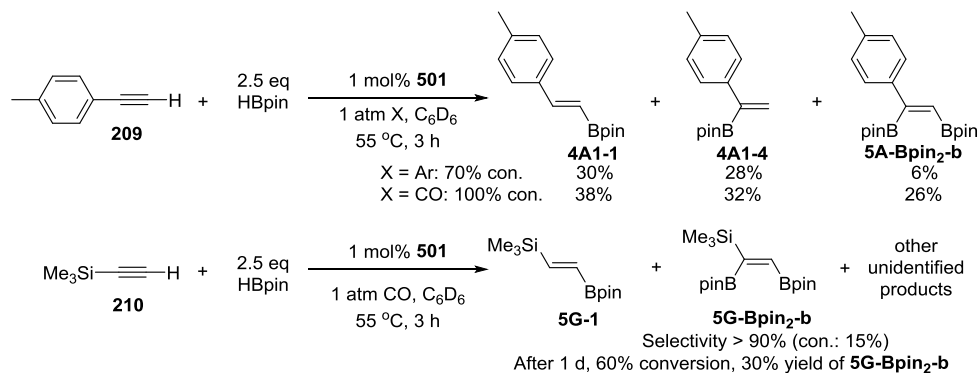


Scheme 5-4. Borylation of **5A-Bpin₂** with HBpin catalyzed by **501**.

Treating **5A-Bpin₂** with 5 equivalents of HBpin and 3 mol% **501** under 1 atm CO, resulted in no observable change in the ¹H NMR spectrum after 2 h at 55 °C (Scheme 5-4). To ensure a trace amount of impurity in **5A-Bpin₂** does not interfere with the reaction, 1 equivalent of **4A2-Bpin** was added to the mixture, which was then degassed and heated at 55 °C. After 3 h, ¹H NMR spectroscopic analysis revealed all **4A2-Bpin** was

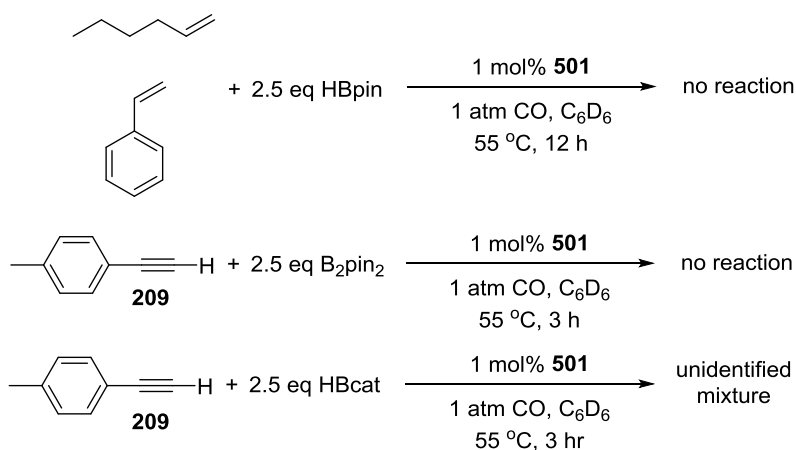
converted to **5B-Bpin₂** and **5B-Bpin₃**, with **5A-Bpin₂** was still remained intact. The results unambiguously proved a free *gem*-diborylalkene is not an intermediate to a triborylalkene.

501 was also tested in the reactions between terminal alkynes and HBpin. Using 1 mol% of **501**, **209** was reacted with 2.5 equivalents of HBpin under 1 atm argon (Scheme 5-5, top). After 3 h at 55 °C, 70% conversion was observed with two major products: **4A1-1** and **4A1-4** in about 1:1 ratio, with a trace amount of **5A-Bpin₂-b**. Under 1 atm CO, the reaction was completed in 3 h and gave higher yields of **5A-Bpin₂-b**. The reaction can also be carried out with only 0.1 mol% **501**. 100% conversion of **209** and similar product distributions were observed after 15 h at 55 °C. No significant product ratio change was observed when using 10 equivalents of HBpin or switching the solvent to CH₃CN or THF. Remarkably, greater than 90% selectivity of diboration product **5G-Bpin₂-b** was observed after 3 h when trimethylsilylacetylene (**210**) was used as the substrate (Scheme 5-5, bottom). However, the reaction was sluggish, and whole the ratio of other products increased. 60% conversion and 30% yield of **5G-Bpin₂-b** was observed after 1 d.



Scheme 5-5. Borylation of terminal alkynes with HBpin catalyzed by **501**.

In contrast to the reactivity with terminal alkynes, no reaction was observed between HBpin with 1-hexene or styrene in the presence of 1 mol % **501** (Scheme 5-6, top). B₂pin₂ also did not react with **209** under the same conditions (Scheme 5-6, middle). Heating HBcat with **209** in the presence of 1 mol % **501** at 55 °C for 15 h, at least eight unidentified products were observed based on Ar-CH₃ signals in the ¹H NMR spectrum (Scheme 5-6, bottom).



Scheme 5-6. Control experiments.

5.2.5 Observation of irreproducible borylation in the blank reaction

When we performed the control experiments of **209P** with HBpin in the absence of **501**, irreproducible 5~40% conversion of **209P** to **5A-Bpin₂** and **5A-Bpin₃** was occasionally observed after 15 h at 55 °C. This phenomenon aroused our attention and made us contemplate whether or not iridium contaminants on the glassware were active. For example, active iridium species might covalently bond to J. Young tubes or form nanoparticles deposits that cannot be washed out with acetone. After repeatedly cleaning both J. Young tubes and caps with more vigorous solutions, like base bath (KOH/EtOH),

aqua regia (HCl/HNO₃), and Piranha solution (H₂O₂/H₂SO₄), no conversion was observed for the control reactions. Also, no reaction was observed when using J. Young tubes that were never in contact with iridium species. The identity of the active species is still not clear at this stage. Further control reactions with mercury tests, examination of iridium powder and a carbonyl cluster, Ir₄(CO)₁₂, are currently under investigation.

5.3 Mechanistic considerations

Although the nature of the catalytic species is still not clear, a generic catalytic cycle (using “[Ir]” to represent the unidentified iridium catalyst) for explaining different borylation products is postulated in Figure 5-5. The status of [Ir] at each step is unknown. The catalytic cycle starts from an alkyne and HBpin binding to the iridium center and reacting to yield hydride alkenyl complexes **505-a** or **505-b**. Normal hydroboration products, an *E*-alkenylboronate or a *gem*-alkenylboronate, are obtained after reductive elimination and **503** would be regenerated. The hydride alkenyl complexes **505-a** or **505-b** could also react with another equivalent of HBpin to lose H₂ and form a boryl alkenyl complex **506**, followed by reductive elimination to yield a dehydrogenative diboration product, 1,2-*cis*-diborylalkene. A triborylalkene can be obtained through the same sequence, starting from an alkynylboronate instead. This proposed mechanism not only rationalizes the formation of different products but also explains why the higher diboration product ratios are observed when using more equivalents of HBpin.

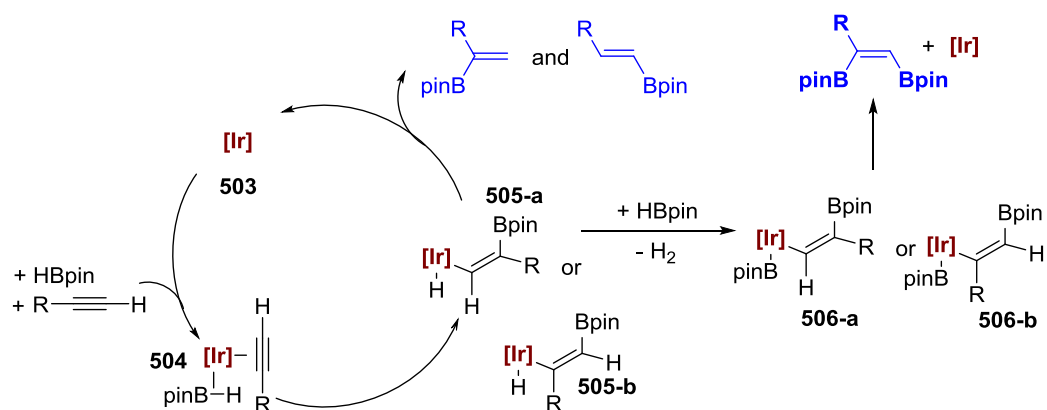


Figure 5-5. Proposed mechanism for diboration.

5.4 Conclusion

In this chapter, we described the development of a convenient one-pot synthesis of triborylalkenes directly from terminal alkynes. The process consisted of a DHBTA and a novel dehydrogenative diboration. Good isolated yields were obtained for various aromatic alkynes, but the yields for aliphatic alkynes were lower mainly due to solubility issues during isolation attempts. The carbonyl complex **501** has been independently synthesized from **206** and has shown to possess the ability to catalyze diboration. Preliminary mechanistic studies suggested the triborylalkenes are not obtained from borylation of free diborylalkenes. Further experiments are needed to elucidate the details of the catalytic mechanism.

5.5 Experimental

General Considerations. Unless specified otherwise, all manipulations were performed under an Ar atmosphere using standard Schlenk line or glovebox techniques. Toluene, fluorobenzene, THF, diethyl ether, pentane, C₆D₆ were dried over NaK/Ph₂CO/18-crown-6, distilled or vacuum transferred and stored over molecular

sieves in an Ar-filled glovebox. CH_2Cl_2 , CD_2Cl_2 and CDCl_3 were dried with and then distilled from CaH_2 and stored over molecular sieves in an Ar-filled glove box. **5A-Bpin**²²⁵ was prepared according to published procedures. Alkynes were deoxygenated by three freeze-pump-thaw cycles prior to use. All other chemicals were used as received from commercial vendors. Pinacolborane was purchased from Sigma-Aldrich in the Sure/Seal form. NMR spectra were recorded on a Varian Inova 300, Mercury 300 (^1H NMR, 299.952 MHz; ^{13}C NMR, 75.421 MHz), Varian Inova 400 (^1H NMR, 399.535 MHz; ^{11}B NMR, 128.185 MHz; ^{29}Si NMR, 79.366 MHz) and NMRS 500 (^1H NMR, 499.703 MHz; ^{13}C NMR, 125.697 MHz) spectrometer. ^1H - ^{29}Si double quantum filter (DQF)¹⁴⁴ experiments on compounds **501** and **502** were performed on Varian Inova 400. Chemical shifts are reported in δ (ppm). For ^1H and ^{13}C NMR spectra, the residual solvent peak was used as an internal reference (^1H NMR: δ 7.15 for C_6D_6 , 5.32 for CD_2Cl_2 , 7.24 for CDCl_3 ; ^{13}C NMR: δ 128.06 for C_6D_6 , 53.84 for CD_2Cl_2 , 77.16 for CDCl_3). For ^{29}Si NMR, spectra were referenced externally to $\delta = 0$ ppm by using Me_4Si . For ^{11}B NMR, spectra were referenced externally to $\delta = 0$ ppm by using $\text{BF}_3 \cdot \text{Et}_2\text{O}$. Elemental analyses were performed by CALI Labs, Inc. (Parsippany, NJ).

Note: In ^{13}C NMR spectra of triborylalkenes, quaternary carbon atoms attached to boron were usually not observed due to low intensity.

Computational details. All computations were carried out with the Gaussian09 program.¹⁴⁵ All of the geometries were fully optimized at the M06¹⁴⁶ level of theory. The Stuttgart basis set and the associated effective core potential (ECP) was used for Ir atom, and an all-electron 6-311G(d,p) basis set was used for the other atoms. The harmonic

vibrational frequency calculations were performed to ensure that a minimum was obtained.

Reaction of 209 and HBpin catalyzed by 206. Stock solution of **206** (64 μ L of 0.0125 M stock solution in C_6D_6 , 0.00080 mmol) and pinacolborane stock solution (280 μ L of 1.0 M stock solution in C_6D_6 , 0.28 mmol) were mixed in a J. Young tube. **209**/1,4-dioxane (160 μ L of 0.50 M **209**/0.35 M 1,4-dioxane stock solution in C_6D_6 , 0.080 mmol for **209** and 0.056 mmol for 1,4-dioxane) was then added in 4 portions with 1 min intervals. After 10 min, the J. Young tube was taken outside and heated at 55 $^{\circ}C$. After 24 h, analysis by 1H NMR spectroscopy revealed all **209** has been consumed and showed 34% yield of **5A-Bpin₂**. Other hydrogenation and/or hydroboration products including **4A1-1**, **5A-1**, and **5A-2** were observed. Selective 1H NMR (500 MHz, C_6D_6) data for **5A-Bpin₂**: δ 8.15 (s, 1H, alkenyl-*H*). Selective 1H NMR (500 MHz, C_6D_6) data for **4A1-1**: δ 6.40 (d, $J_{H-H} = 18$ Hz, 1H, alkenyl-*H*). Selective 1H NMR (500 MHz, C_6D_6) data for **5A-1**: δ 2.84 (t, $J_{H-H} = 8.0$ Hz, 1H, $CH_2-CH_2(Bpin)$). Selective 1H NMR (500 MHz, C_6D_6) data for **5A-2**: δ 3.20 (d, $J_{H-H} = 8.0$ Hz, 1H, $CH_2-CH(Bpin)_2$).

Reaction of 209 and HBpin catalyzed by 206 then degassed and treated with 1 atm CO. Stock solution of **206** (64 μ L of 0.0125 M stock solution in C_6D_6 , 0.00080 mmol) and pinacolborane stock solution (280 μ L of 1.0 M stock solution in C_6D_6 , 0.28 mmol) were mixed in a J. Young tube. **209**/1,4-dioxane (160 μ L of 0.50 M **209**/0.35 M 1,4-dioxane stock solution in C_6D_6 , 0.080 mmol for **209** and 0.056 mmol for 1,4-dioxane) was then added in 4 portions with 1 min intervals. After 10 min, the J. Young tube was taken outside and degassed by three freeze-pump-thaw cycles, and the tube was refilled

with 1 atm CO. The tube was heated at 55 °C. After 8 h, analysis by ¹H NMR spectroscopy revealed all **209** has been consumed and showed 39% yield of **5A-Bpin₂** and 55% yield of **5A-Bpin₃**.

Reaction of 209 and HBpin catalyzed by 206 then degassed and treated with 1 atm Ar. Stock solution of **206** (64 μL of 0.0125 M stock solution in C₆D₆, 0.00080 mmol) and pinacolborane stock solution (280 μL of 1.0 M stock solution in C₆D₆, 0.28 mmol) were mixed in a J. Young tube. **209**/1,4-dioxane (160 μL of 0.50 M **209**/0.35 M 1,4-dioxane stock solution in C₆D₆, 0.080 mmol for **209** and 0.056 mmol for 1,4-dioxane) was then added in 4 portions with 1 min intervals. The J. Young tube was taken outside, after 10 min, the tube was degassed by three freeze-pump-thaw cycles and refilled with 1 atm argon. The tube was heated at 55 °C. After 24 h, analysis by ¹H NMR spectroscopy revealed all **209** has been consumed and showed 31% yield of **5A-Bpin₂**. Other hydrogenation and/or hydroboration products including **4A1-1**, **5A-1**, and **5A-2** were observed.

Reaction catalyzed by 206 then degassed and treated with 1 atm CO in various solvents. Stock solution of **206** (64 μL of 0.0125 M stock solution in C₆D₆, 0.00080 mmol) and pinacolborane stock solution (280 μL of 1.0 M stock solution in THF or fluorobenzene, 0.28 mmol) were mixed in a J. Young tube. **209**/1,4-dioxane (160 μL of 0.50 M 4-ethynyltoluene/0.35 M 1,4-dioxane stock solution in THF or fluorobenzene, 0.080 mmol for **209** and 0.056 mmol for 1,4-dioxane) was then added in 4 portions with 1 min intervals. The J. Young tube was taken outside, after 10 min, the tube was degassed by three freeze-pump-thaw cycles and refilled with 1 atm CO. The tube was

heated at 55 °C. After 8 h, a drop of solution was transferred to another J. Young tube followed by 0.5 mL C₆D₆. The reaction yield was determined by ¹H NMR spectroscopy based on the integration of Ar-CH₃.

Reaction of 209 and 5 equivalents of HBpin catalyzed by 206. **206** (4.0 mg, 0.0060 mmol), 1,4-dioxane (30 μL, 0.35 mmol), pinacolborane (435 μL, 3.00 mmol) were dissolved in 0.5 mL fluorobenzene in a 25 mL PTFE-valved gas-tight flask. **209** (76 μL, 0.60 mmol) was added dropwise in 1 min. After 10 min, the flask was brought outside glovebox, degassed by three freeze-pump-thaw cycles, and refilled 1 atm CO. The flask was heated at 55 °C. After 18 h, 0.5 mL C₆D₆ was added to the flask to dissolve all the mixtures. The solution was analyzed by ¹H NMR spectroscopy and showed 7% yield of **5A-Bpin₂** and 88% yield of **5A-Bpin₃**.

Reaction of 209 in neat HBpin catalyzed by 206. **206** (3.3 mg, 0.0050 mmol), 1,4-dioxane (30 μL, 0.35 mmol), pinacolborane (726 μL, 5.00 mmol) were added in a 25 mL PTFE-valved gas-tight flask. **209** (63 μL, 0.50 mmol) was added dropwise in 1 min. After 10 min, the flask was brought outside glovebox, degassed by three freeze-pump-thaw cycles, and refilled 1 atm CO. The flask was heated at 55 °C. After 18 h, 0.5 mL C₆D₆ was added to the flask to dissolve all the mixtures. The solution was analyzed by ¹H NMR spectroscopy and showed 5% yield of **5A-Bpin₂** and 91% yield of **5A-Bpin₃**.

General procedure for the preparative-scale dehydrogenative borylation of alkynes. In an Ar-filled glove box, **206** (13 mg, 0.020 mmol) and pinacolborane (1.45 mL, 10.0 mmol) were mixed in a 25 mL PTFE-valved gas-tight flask. After stirring 3 min at ambient temperature, alkyne (2.00 mmol) in 1.0 mL fluorobenzene was then

added dropwise in 1 min. Bubbles evolved immediately which indicated H₂ generation. After all alkyne was added, the mixture was stirred for 5 min. The flask was then degassed via two freeze-pump-thaw cycles and refilled 1 atm CO. The solution color turned from indigo to orange. The flask was heated at 55 °C for 18 h and the mixture was allowed to cool to ambient temperature. 5 mL Et₂O was added to the flask to assist in transferring to a 50 mL Schlenk flask, and all volatiles were removed *in vacuo*. 10 mL pentane was added to the flask and sonicated for 20 min. The solution was filtered through a fritted funnel, and the solid was washed with cold pentane and dried *in vacuo*. The decanted solution was combined with the washings, and the volatiles were removed *in vacuo*. The residue was then redissolved pentane, placed in the freezer and collected in the same manner to yield the second fraction.

5A-Bpin₃. White solid, isolated yield: 729 mg (74%). ¹H NMR (500 MHz, CDCl₃): δ 7.17 (d, J_{H-H} = 8.0 Hz, 2H, Ar-*H*), 7.01 (d, J_{H-H} = 8.0 Hz, 2H, Ar-*H*), 2.28 (s, 3H, Ar-CH₃), 1.28 (s, 12H, -CH₃ on Bpin), 1.25 (s, 12H, -CH₃ on Bpin), 1.08 (s, 12H, -CH₃ on Bpin). ¹³C{¹H} NMR (126 MHz, CDCl₃): δ 142.5, 136.3, 128.4, 127.8, 83.9 (C_{quart}, Bpin), 83.5 (C_{quart}, Bpin), 83.2 (C_{quart}, Bpin), 25.1 (CH₃, Bpin), 25.0 (CH₃, Bpin), 24.7 (CH₃, Bpin), 21.3 (Ar-CH₃). ¹¹B NMR (128 MHz, CDCl₃): δ 29.9. HRMS (MALDI) calcd. for C₂₇H₄₄B₃O₆ (M+H)⁺: 497.3417. Found: 497.3391.

5B-Bpin₃. White solid, isolated yield: 884 mg (80%). ¹H NMR (500 MHz, CDCl₃): δ 7.47 (d, J_{H-H} = 8.0 Hz, 2H, Ar-*H*), 7.33 (d, J_{H-H} = 8.0 Hz, 2H, Ar-*H*), 1.30 (s, 12H, -CH₃ on Bpin), 1.24 (s, 12H, -CH₃ on Bpin), 1.04 (s, 12H, -CH₃ on Bpin). ¹³C{¹H} NMR (126 MHz, CDCl₃): δ 149.1, 128.7 (q, J_{F-C} = 32 Hz), 128.2, 124.7 (q, J_{F-C} = 3.7 Hz),

124.6 (q, $J_{F-C} = 270$ Hz), 84.3 (C_{quart} , Bpin), 83.8 (C_{quart} , Bpin), 83.6 (C_{quart} , Bpin), 25.1 (CH_3 , Bpin), 24.9 (CH_3 , Bpin), 24.6 (CH_3 , Bpin). ^{19}F NMR (470 MHz, $CDCl_3$): δ -63.3. ^{11}B NMR (128 MHz, $CDCl_3$): δ 29.9. HRMS (MALDI) calcd. for $C_{27}H_{41}B_3F_3O_6$ (M+H) $^+$: 551.3134. Found: 551.3127.

5C-Bpin₃. White solid, isolated yield: 763 mg (75%). 1H NMR (500 MHz, $CDCl_3$): δ 7.21 (d, $J_{H-H} = 8.0$ Hz, 2H, Ar-*H*), 6.75 (d, $J_{H-H} = 8.0$ Hz, 2H, Ar-*H*), 3.75 (s, 3H, Ar-*OCH*₃), 1.27 (s, 12H, -*CH*₃ on Bpin), 1.25 (s, 12H, -*CH*₃ on Bpin), 1.09 (s, 12H, -*CH*₃ on Bpin). $^{13}C\{^1H\}$ NMR (126 MHz, $CDCl_3$): δ 158.9, 138.1, 129.1, 123.2, 83.9 (C_{quart} , Bpin), 83.5 (C_{quart} , Bpin), 83.2 (C_{quart} , Bpin), 55.3 (*OCH*₃), 25.04 (CH_3 , Bpin), 24.98 (CH_3 , Bpin), 24.7 (CH_3 , Bpin). ^{11}B NMR (128 MHz, $CDCl_3$): δ 30.4. HRMS (MALDI) calcd. for $C_{27}H_{44}B_3O_7$ (M+H) $^+$: 513.3366. Found: 513.3346.

5D-Bpin₃. White solid, isolated yield: 680 mg (71%). 1H NMR (500 MHz, $CDCl_3$): δ 7.21 (m, 5H, Ar-*H*), 1.30 (s, 12H, -*CH*₃ on Bpin), 1.27 (s, 12H, -*CH*₃ on Bpin), 1.08 (s, 12H, -*CH*₃ on Bpin). $^{13}C\{^1H\}$ NMR (126 MHz, $CDCl_3$): δ 145.4, 127.8, 127.7, 126.8, 84.0 (C_{quart} , Bpin), 83.5 (C_{quart} , Bpin), 83.3 (C_{quart} , Bpin), 25.04 (CH_3 , Bpin), 24.95 (CH_3 , Bpin), 24.7 (CH_3 , Bpin). ^{11}B NMR (128 MHz, $CDCl_3$): δ 29.9. HRMS (MALDI) calcd. for $C_{26}H_{42}B_3O_6$ (M+H) $^+$: 483.3241. Found: 483.3257.

5E-Bpin₃. White solid, isolated yield: 396 mg (39%). 1H NMR (500 MHz, $CDCl_3$): δ 7.24 (m, 4H, Ar-*H*), 7.14 (m, 1H, Ar-*H*), 2.66 (s, 4H, -*CH*₂-*CH*₂-), 1.30 (s, 12H, -*CH*₃ on Bpin), 1.26 (s, 12H, -*CH*₃ on Bpin), 1.24 (s, 12H, -*CH*₃ on Bpin). $^{13}C\{^1H\}$ NMR (126 MHz, $CDCl_3$): δ 143.7, 128.6, 128.2, 125.5, 83.8 (C_{quart} , Bpin), 83.4 (C_{quart} , Bpin), 83.1 (C_{quart} , Bpin), 40.3, 37.4, 25.1 (CH_3 , Bpin), 25.03 (CH_3 , Bpin), 24.97 (CH_3 , Bpin). ^{11}B

NMR (128 MHz, CDCl₃): δ 29.8. HRMS (MALDI) calcd. for C₂₈H₄₅B₃O₆Na (M+Na)⁺: 533.3401. Found: 533.3377.

5F-Bpin₃. Off-white solid, isolated yield: 197 mg (21%). ¹H NMR (500 MHz, CDCl₃): δ 2.35 (t, J = 7.5 Hz, 2H), 1.30 (m, 4H), 1.26 (s, 12H, -CH₃ on Bpin), 1.22 (s, 12H, -CH₃ on Bpin), 1.21 (s, 12H, -CH₃ on Bpin), 0.84 (t, J = 7.5 Hz, 3H). ¹³C{¹H} NMR (126 MHz, CDCl₃): δ 83.6 (C_{quart}, Bpin), 83.3 (C_{quart}, Bpin), 83.0 (C_{quart}, Bpin), 37.7, 32.9, 25.1 (CH₃, Bpin), 24.95 (CH₃, Bpin), 24.92 (CH₃, Bpin), 23.0, 14.2. ¹¹B NMR (128 MHz, CDCl₃): δ 30.1. HRMS (MALDI) calcd. for C₂₄H₄₅B₃O₆Na (M+Na)⁺: 485.3400. Found: 485.3423.

5G-Bpin₃. White solid, isolated yield: 268 mg (28%). ¹H NMR (500 MHz, CDCl₃): δ 3.48 (t, J = 7.5 Hz, 2H), 2.46 (t, J = 7.5 Hz, 2H), 1.85 (pentet, J = 7.5 Hz, 2H), 1.27 (s, 12H, -CH₃ on Bpin), 1.22 (s, 12H, -CH₃ on Bpin), 1.21 (s, 12H, -CH₃ on Bpin). ¹³C{¹H} NMR (126 MHz, CDCl₃): δ 83.9 (C_{quart}, Bpin), 83.4 (C_{quart}, Bpin), 83.2 (C_{quart}, Bpin), 45.4, 35.1, 33.6, 25.1 (CH₃, Bpin), 25.0 (CH₃, Bpin), 24.9 (CH₃, Bpin). ¹¹B NMR (128 MHz, CDCl₃): δ 30.0. HRMS (MALDI) calcd. for C₂₃H₄₂B₃ClO₆Na (M+Na)⁺: 505.2856. Found: 505.2854.

Synthesis of 501. In a Ar-filled glove box, **205** (514 mg, 1.12 mmol) and [(COE)₂IrCl]₂ (505 mg, 0.563 mmol) were allowed to dissolve in 10 mL of fluorobenzene in a 50 mL Schlenk flask. The solution turned black immediately, and then changed to deep blue over the next 10 min. After 1 h, 10 mL CH₂Cl₂ were added to the flask to assist in filtering the solution through Celite and then the solution was transferred to a 100 mL PTFE-valved gas-tight flask. The flask was degassed via freeze-

pump-thaw once and refilled 1 atm CO. The solution turned pink immediately which indicated **502** formation. After 10 min at RT, the flask was degassed again via freeze-pump-thaw once and refilled 1 atm CO. After 30 min at RT, the solution was filtered through Celite and removed all volatiles *in vacuo* to result brown powder. The flask was taken outside the glovebox and 10 mL pentane was added. The flask was taken to sonication for 20 min to disperse the powder and filtered through a fritted funnel. The brown powder was further washed with pentane and dried *in vacuo*. Yield: 602 mg (92%). ^1H NMR (500 MHz, CD_2Cl_2): δ 8.69 (m, 1H, Ar-*H*), 8.12 (m, 1H, Ar-*H*), 7.28 (dd, $J_{\text{H-H}} = 8.4, 4.8$ Hz, 1H, Ar-*H*), 6.98 (d, $J_{\text{H-H}} = 1.8$ Hz, 1H, Ar-*H*), 6.85 (dd, $J_{\text{H-H}} = 8.4, 1.8$ Hz, 1H, Ar-*H*), 6.77 (s, 1H, Ar-*H*), 6.46 (br s, 1H, Ar-*H*), 6.09 (br s, 1H, Ar-*H*), 2.28 (s, 3H, Ar- CH_3), 2.19 (s, 3H, Ar- CH_3), 1.61 (m, 1H, $\text{CH}(\text{Me})_2$), 1.07 (d, $J_{\text{H-H}} = 7.5$ Hz, 3H, $\text{CH}(\text{Me})_2$), 0.90 (d, $J_{\text{H-H}} = 7.5$ Hz, 3H, $\text{CH}(\text{Me})_2$), 0.70 (m, 1H, $\text{CH}(\text{Me})_2$), 0.45 (d, $J_{\text{H-H}} = 7.5$ Hz, 3H, $\text{CH}(\text{Me})_2$), 0.35 (d, $J_{\text{H-H}} = 7.5$ Hz, 3H, $\text{CH}(\text{Me})_2$), -15.52 (s, 1H, Ir-*H*). Selected ^1H - ^{29}Si DQF (400 MHz, CD_2Cl_2) data for Ir-*H*: Not observable. $^{13}\text{C}\{^1\text{H}\}$ NMR (126 MHz, CD_2Cl_2): δ 176.4, 160.0, 154.1, 149.5, 145.5, 144.0, 139.8, 137.3, 133.3, 131.8, 131.1, 128.1, 122.5, 121.9, 114.2, 114.0 (15 Ar-C + 1 CO), 22.2, 21.0, 20.6, 19.4, 19.1, 19.0, 17.8, 15.1 (8 aliphatic C: 2 Ar- CH_3 + 6 for Si^iPr_2). $^{29}\text{Si}\{^1\text{H}\}$ NMR (79 MHz, CD_2Cl_2): δ 34.1 (br s). IR (solid, cm^{-1}): 1977. Anal. Calcd for $\text{C}_{24}\text{H}_{29}\text{IrN}_2\text{OSi}$: C, 49.55; H, 5.02. Found: C, 49.39; H, 4.91.

Observation of 502. In a Ar-filled glove box, **501** (30 mg, 0.052 mmol) was dissolved in 0.5 mL CD_2Cl_2 in a J. Young tube. The tube was taken out and degassed by three freeze-pump-thaw cycles and back-filled with CO (1 atm, excess). The solution

color turned to pink immediately. After 10 min at RT, the tube was taken up for NMR analysis. ^1H NMR (500 MHz, CD_2Cl_2): δ 8.60 (m, 1H, Ar-*H*), 8.00 (m, 1H, Ar-*H*), 7.77 (d, $J_{\text{H-H}} = 8.4$ Hz, 1H, Ar-*H*), 7.53 (br s, 1H, Ar-*H*), 7.30 (dd, $J_{\text{H-H}} = 8.4, 4.8$ Hz, 1H, Ar-*H*), 7.13 (d, $J_{\text{H-H}} = 1.8$ Hz, 1H, Ar-*H*), 6.92 (dd, $J_{\text{H-H}} = 8.4, 1.8$ Hz, 1H, Ar-*H*), 6.58 (s, 1H, Ar-*H*), 2.36 (s, 3H, Ar- CH_3), 2.28 (s, 3H, Ar- CH_3), 1.63 (m, 1H, $\text{CH}(\text{Me})_2$), 1.25 (m, 4H, $\text{CH}(\text{Me})_2 + \text{CH}(\text{Me})_2$), 1.08 (d, $J_{\text{H-H}} = 7.5$ Hz, 3H, $\text{CH}(\text{Me})_2$), 1.04 (d, $J_{\text{H-H}} = 7.5$ Hz, 3H, $\text{CH}(\text{Me})_2$), 0.92 (d, $J_{\text{H-H}} = 7.5$ Hz, 3H, $\text{CH}(\text{Me})_2$), -6.10 (s, 1H, Ir-*H*). Selected ^1H - ^{29}Si DQF (400 MHz, CD_2Cl_2) data for Ir-*H*: -6.10 (d, $J_{\text{Si-H}} = 2.1$ Hz). $^{13}\text{C}\{^1\text{H}\}$ NMR (126 MHz, CD_2Cl_2): δ 174.1, 169.8, 158.2, 154.7, 149.0, 147.5, 140.1, 138.2, 137.3, 135.3, 132.0, 129.1, 128.3, 122.2, 115.1, 113.6, 111.5 (15 Ar-C + 2 CO), 22.3, 20.8, 20.7, 20.2, 19.7, 19.4, 18.0, 16.0 (8 aliphatic C: 2 Ar- $\text{CH}_3 + 6$ for Si^iPr_2). IR (CH_2Cl_2 , cm^{-1}): 2057, 2007.

Reaction of 209P with HBpin catalyzed by 501. **209P**/1,4-dioxane (80 μL of 1.0 M **209P**/0.35 M 1,4-dioxane stock solution in C_6D_6 , 0.080 mmol for **209P** and 0.028 mmol for 1,4-dioxane), pinacolborane (200 μL of 1.0 M stock solution in C_6D_6 , 0.200 mmol), and **501** (160 μL of 0.0050 M stock solution in C_6D_6 , 0.00080 mmol) were mixed in a J. Young tube. The tube was degassed by three freeze-pump-thaw cycles and back-filled with 1 atm CO. The tube was then heated at 55 $^\circ\text{C}$. After 12 h, analysis by ^1H NMR spectroscopy revealed all **209P** was consumed and mainly converted to **5B-Bpin₂** (14% yield) and **5B-Bpin₃** (80% yield).

Reaction of 5A-Bpin₂ with HBpin catalyzed by 501. **5A-Bpin₂** (14 mg, 0.037 mmol), 1,4-dioxane (10 μL , 0.12 mmol), pinacolborane (180 μL of 1.0 M stock solution

in C₆D₆, 0.180 mmol), and **501** (80 μ L of 0.0125 M stock solution in C₆D₆, 0.001 mmol) were dissolved in 0.3 mL C₆D₆ in a J. Young tube. The tube was degassed by three freeze-pump-thaw cycles and back-filled with 1 atm CO. The tube was then heated at 55 °C. After 2 h, analysis by ¹H NMR spectroscopy revealed only unreacted **5A-Bpin₂** and pinacolborane. **4A2-Bpin** (11 mg, 0.037 mmol) was added to the tube. The tube was degassed by three freeze-pump-thaw cycles and back-filled with 1 atm CO. The tube was then heated at 55 °C. After 3 h, analysis by ¹H NMR spectroscopy revealed all **4A2-Bpin** was consumed and converted to **5B-Bpin₂** and **5B-Bpin₃**. The integration of CH₃ on Bpin of **5A-Bpin₂** remained by using 1,4-dioxane as the internal standard.

Reaction of 4-ethynyltoluene and HBpin catalyzed by 501 under Ar. **501** (80 μ L of 0.00625 M stock solution in CH₂Cl₂, 0.00050 mmol) was transferred to a 10 mL Schlenk flask and removed all volatiles *in vacuo*. 0.2 mL C₆D₆ was added to dissolve **501** and transferred the solution to a J. Young tube. Pinacolborane (18 μ L, 0.13 mmol) and 4-ethynyltoluene (6 μ L, 0.05 mmol) were added to the J. Young tube followed by 0.2 mL C₆D₆. After 30 min at ambient temperature, analysis by ¹H NMR revealed only that unreacted pinacolborane and 4-ethynyltoluene were present. The solution was heated at 55 °C for 3 h, analysis by ¹H NMR spectroscopy revealed 70% conversion of 4-ethynyltoluene. **4A1-1** (30% yield) and **4A1-4** (28% yield) were observed as the major products with 6% of **5A-Bpin_{2-b}**. Selective ¹H NMR (500 MHz, C₆D₆) data for **4A1-4**: δ 6.23 (d, J_{H-H} = 3.2 Hz, 1H, alkenyl-*H*), 6.06 (d, J_{H-H} = 3.2 Hz, 1H, alkenyl-*H*). Selective ¹H NMR (500 MHz, C₆D₆) data for **5A-Bpin_{2-b}**: δ 6.48 (s, 1H, alkenyl-*H*).

Reaction of 4-ethynyltoluene and HBpin catalyzed by 501 under CO. **501** (80 μL of 0.00625 M stock solution in CH_2Cl_2 , 0.00050 mmol) was transferred to a 10 mL Schlenk flask and removed all volatiles *in vacuo*. 0.2 mL C_6D_6 was added to dissolve **501** and transferred the solution to a J. Young tube. Pinacolborane (18 μL , 0.13 mmol) and 4-ethynyltoluene (6 μL , 0.05 mmol) were added to the J. Young tube followed by 0.2 mL C_6D_6 . The tube was degassed by three freeze-pump-thaw cycles and back-filled with 1 atm CO. The tube was then heated at 55 $^\circ\text{C}$. After 3 h, analysis by ^1H NMR spectroscopy revealed 100% conversion of 4-ethynyltoluene. **4A1-1** (38% yield), **4A1-4** (32% yield), and **5A-Bpin₂-b** (26% yield) were observed as the major products.

Reaction of 4-ethynyltoluene and HBpin catalyzed by 0.1 mol% 501 under CO. **501** (8 μL of 0.00625 M stock solution in CH_2Cl_2 , 0.00005 mmol) was transferred to a 10 mL Schlenk flask and removed all volatiles *in vacuo*. 0.2 mL C_6D_6 was added to dissolve **501** and transferred the solution to a J. Young tube. Pinacolborane (18 μL , 0.13 mmol) and 4-ethynyltoluene (6 μL , 0.05 mmol) were added to the J. Young tube followed by 0.2 mL C_6D_6 . The tube was degassed by three freeze-pump-thaw cycles and back-filled with 1 atm CO. The tube was then heated at 55 $^\circ\text{C}$. After 15 h, analysis by ^1H NMR spectroscopy revealed 100% conversion of 4-ethynyltoluene. **4A1-1** (42% yield), **4A1-4** (34% yield), and **5A-Bpin₂-b** (20% yield) were observed as the major products.

Reaction of 4-ethynyltoluene and large excess HBpin catalyzed by 501 under CO. **501** (80 μL of 0.00625 M stock solution in CH_2Cl_2 , 0.00050 mmol) was transferred to a 10 mL PTFE-valved gas-tight flask and all volatiles were removed all *in vacuo*. Pinacolborane (73 μL , 0.50 mmol) and **209** (6 μL , 0.05 mmol) were added into the flask.

The flask was brought outside the glovebox, degassed by three freeze-pump-thaw cycles, and refilled 1 atm CO. The flask was heated at 55 °C for 3 h and allowed to cool to ambient temperature. The flask was brought in the glovebox, and 20 μL of the solution was transferred to a J. Young tube followed by 0.5 mL C_6D_6 . ^1H NMR spectroscopic analysis showed 100% conversion of 4-ethynyltoluene. **4A1-1** (36% yield), **4A1-4** (25% yield), and **5A-Bpin₂-b** (40% yield) were observed as the major products.

Borylation of 209 in different solvents. **501** (80 μL of 0.00625 M stock solution in CH_2Cl_2 , 0.00050 mmol) was transferred to a 10 mL Schlenk flask and removed all volatiles *in vacuo*. 0.2 mL of the specific solvent was added to dissolve **501** and transferred the solution to a J. Young tube. Pinacolborane (18 μL , 0.13 mmol) and **209** (6 μL , 0.05 mmol) were added to the J. Young tube followed by 0.2 mL of the specific solvent. The tube was degassed by three freeze-pump-thaw cycles, and refilled 1 atm CO. The tube was heated at 55 °C for 15 h and allowed to cool to ambient temperature. The tube was brought in the glovebox, and 20 μL of the solution was transferred to a J. Young tube. 0.5 mL C_6D_6 was added to the J. Young tube, and ^1H NMR spectroscopic analysis was used to determine the yield by the ratio of integration of alkenyl-*H*. The results are summarized in Table 5-3.

Table 5-3. Borylation of **209** in different solvents.

Solvent	Conversion	Yield of 4A1-1	Yield of 4A1-4	Yield of 5A-Bpin₂-b
CH_3CN	76%	36%	23%	9%
THF	100%	44%	27%	24%

Reaction of olefins and HBpin catalyzed by 501 under CO. **501** (80 μL of 0.00625 M stock solution in CH_2Cl_2 , 0.00050 mmol) was transferred to a 10 mL Schlenk flask and removed all volatiles *in vacuo*. 0.2 mL C_6D_6 was added to dissolve **501** and transferred the solution to a J. Young tube. Pinacolborane (18 μL , 0.13 mmol) and olefin (0.05 mmol of 1-hexene or styrene) were added to the J. Young tube followed by 0.2 mL C_6D_6 . The solution was heated at 55 $^\circ\text{C}$ for 15 h, analysis by ^1H NMR spectroscopy revealed only unreacted olefin and HBpin were present.

Reaction of 4-ethynyltoluene and B_2pin_2 catalyzed by 501 under CO. **501** (80 μL of 0.00625 M stock solution in CH_2Cl_2 , 0.00050 mmol) was transferred to a 10 mL Schlenk flask and removed all volatiles *in vacuo*. 0.2 mL C_6D_6 was added to dissolve **501** and transferred the solution to a J. Young tube. Bis(pinacolato)diboron (B_2pin_2 , 32 mg, 0.13 mmol) and 4-ethynyltoluene (6 μL , 0.05 mmol) were added to the J. Young tube followed by 0.2 mL C_6D_6 . The tube was degassed by three freeze-pump-thaw cycles, and refilled 1 atm CO. The solution was then heated at 55 $^\circ\text{C}$ for 3 h, analysis by ^1H NMR revealed that only unreacted B_2pin_2 and 4-ethynyltoluene were present.

Reaction of 4-ethynyltoluene and HBcat catalyzed by 501 under CO. **501** (80 μL of 0.00625 M stock solution in CH_2Cl_2 , 0.00050 mmol) was transferred to a 10 mL Schlenk flask and removed all volatiles *in vacuo*. 0.2 mL C_6D_6 was added to dissolve **501** and transferred the solution to a J. Young tube. Catecholborane (HBcat, 13 μL , 0.13 mmol) and 4-ethynyltoluene (6 μL , 0.05 mmol) were added to the J. Young tube followed by 0.2 mL C_6D_6 . The tube was degassed by three freeze-pump-thaw cycles, and refilled 1 atm CO. The solution was then heated at 55 $^\circ\text{C}$ for 3 h, analysis by ^1H

NMR spectroscopy revealed that at least 8 products were present based on the signals of Ar-CH₃.

Reaction of trimethylsilylacetylene and HBpin catalyzed by 501 under CO. 501 (80 μ L of 0.00625 M stock solution in CH₂Cl₂, 0.00050 mmol) was transferred to a 10 mL Schlenk flask and removed all volatiles *in vacuo*. 0.2 mL C₆D₆ was added to dissolve **501** and transferred the solution to a J. Young tube. Pinacolborane (18 μ L, 0.13 mmol) and trimethylsilylacetylene (**210**) (7 μ L, 0.05 mmol) were added to the J. Young tube followed by 0.2 mL C₆D₆. The tube was degassed by three freeze-pump-thaw cycles, and refilled 1 atm CO. The solution was then heated at 55 °C for 3 h, analysis by ¹H NMR spectroscopy revealed 15% conversion based on trimethylsilylacetylene and >90% product selectivity for *cis*-diborylalkene **5G-Bpin₂-b**. ¹H NMR (500 MHz, C₆D₆) data for **5G-Bpin₂-b**: δ 6.95 (s, 1H, alkenyl-*H*), 1.22 (s, 12H, CH₃ on Bpin), 1.08 (s, 12H, CH₃ on Bpin), 0.20 (s, 9H, CH₃ on Me₃Si). After 55 °C for 1 d, analysis by ¹H NMR spectroscopy revealed 60% conversion and 30% yield for **5G-Bpin₂-b**. The mixtures of other products included *trans*-alkenylboronate **5G-1** formation were observed. Selective ¹H NMR (500 MHz, C₆D₆) data for **5G-1**: δ 7.49 (d, J_{H-H} = 21 Hz, 1H, alkenyl-*H*), 6.58 (d, J_{H-H} = 21 Hz, 1H, alkenyl-*H*). After 55 °C for 2 d, analysis by ¹H NMR spectroscopy revealed the ratio of other product increased but not **5G-Bpin₂-b**.

Reaction of 209P with HBpin without any added catalyst. Pinacolborane (54 μ L, 0.37 mmol) and **209P** (18 mg, 0.074 mmol) were dissolved in 0.5 mL C₆D₆ in a J. Young tube. After 18 h at 55 °C, analysis by ¹H NMR spectroscopy revealed that only unreacted pinacolborane and **209P** were present.

X-Ray data collection, solution, and refinement for 501. A black, multi-faceted block of suitable size (0.46 x 0.35 x 0.30 mm) was selected from a representative sample of crystals of the same habit using an optical microscope and mounted onto a nylon loop. Low temperature (110 K) X-ray data were obtained on a Bruker APEXII CCD based diffractometer (Mo sealed X-ray tube, $K_{\alpha} = 0.71073 \text{ \AA}$). All diffractometer manipulations, including data collection, integration and scaling were carried out using the Bruker APEXII software.¹⁵⁰ An absorption correction was applied using SADABS.¹⁵⁰ The space group was determined on the basis of systematic absences and intensity statistics and the structure was solved by direct methods and refined by full-matrix least squares on F^2 . The structure was solved in the triclinic P-1 space group using XS¹⁵¹ (incorporated in SHELXTL). All non-hydrogen atoms were refined with anisotropic thermal parameters. All hydrogen atoms were placed in idealized positions and refined using riding model. The structure was refined (weighted least squares refinement on F^2) and the final least-squares refinement converged.

CHAPTER VI

SYNTHESIS OF PNP IRIDIUM TRIFLATE COMPLEXES

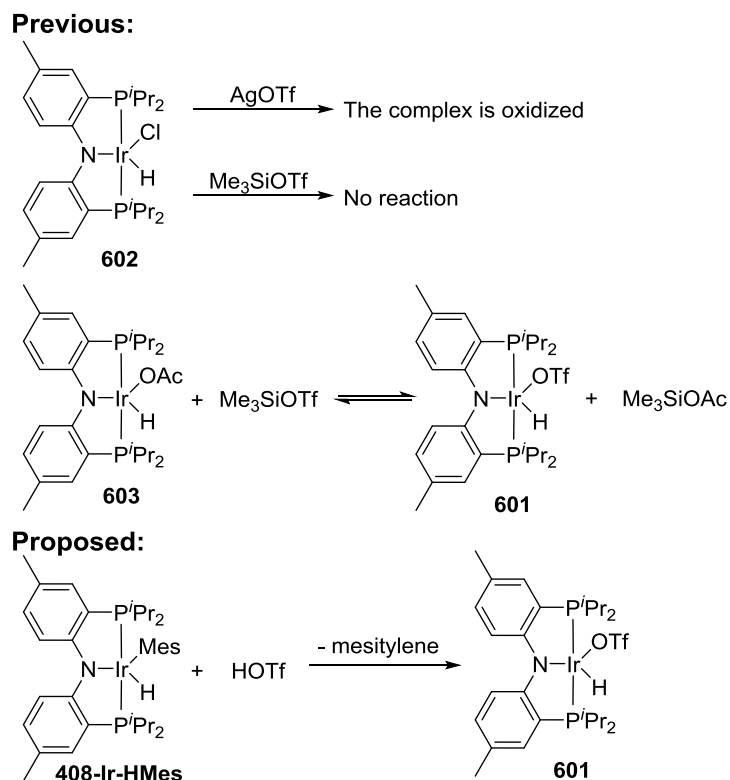
6.1 Introduction

Electrophilic iridium complexes have shown their great ability to activate strong bonds, such as C(sp³)-H bonds of alkanes,²²⁶⁻²²⁸ C(sp²)-H bonds of arenes,^{226,229} N-H bonds^{5,230,231} and C-O bonds.²³² They also serve as strong Lewis acids to catalyze reactions, for example: olefin polymerization,²³³ Nazarov cyclization,²³³⁻²³⁶ Diels-Alder reaction,²³⁴ and others.^{237,238} In the Ozerov group, we have a long history of studies of bond activation mediated by well-defined iridium pincer complexes.^{5,51,173,174,239} In this chapter, we describe the approach to synthesize a highly electrophilic iridium complex supported by a PNP pincer ligand, (PNP)Ir(H)(OTf) (**601**) and its equilibrium with ether solvents. The reaction of **601** with diamine or bipyridine ligands will also be discussed.

6.2 Results and discussion

6.2.1 Synthesis of (PN(H)P)Ir(H)(OTf)₂

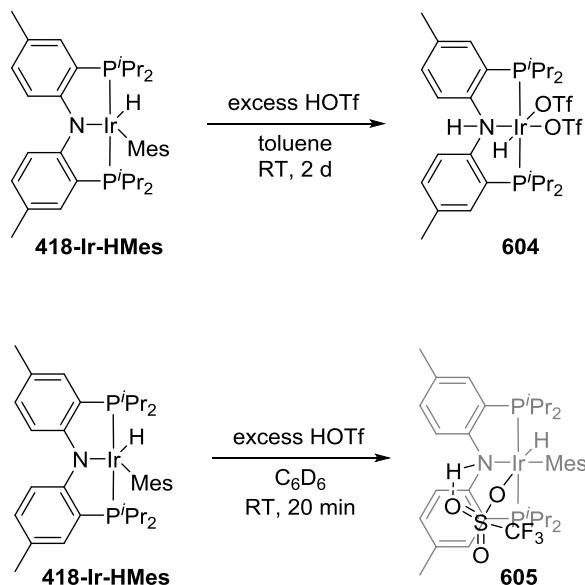
In the previous work by Dr. Zhu in our group,²⁴⁰ we attempted to synthesize (PNP)Ir(H)(OTf) (**601**) via substitution reaction of (PNP)Ir(H)(Cl) (**602**, Scheme 6-1) but unsuccessfully. Reaction of (PNP)Ir(H)(OAc) (**603**) with Me₃SiOTf resulted in the equilibrium with **601** and Me₃SiOAc; however, **601** could not be isolated in the pure form because the equilibrium mixture reverted to **603** under vacuum. (PNP)Ir(H)(Mes) (**408-Ir-HMes**) has been used as “(PNP)Ir” equivalent by losing mesitylene in the previous study,¹⁷³ hence we proposed another approach to **601** via protonation of **408-Ir-HMes** with HOTf to prevent the equilibrium issue.



Scheme 6-1. Previous attempts to **601**²⁴⁰ and proposed alternative synthesis.

Treating **408-Ir-HMes** with excess of HOTf in toluene after 2 d at RT did not lead to **601** but instead yielded the bis-triflic acid adduct of the (PNP)Ir fragment **604** (PN(H)P)Ir(H)(OTf)₂ in excellent yield (Scheme 6-2). The reaction was proposed to proceed through an intermediate **605**, which was observed through treating **408-Ir-HMes** with excess HOTf in C₆D₆. After 20 min at RT, analysis by ³¹P NMR spectroscopy showed a major signal at δ 36.9, and a hydride signal at δ -34.02 (t, J_{P-H} = 15 Hz) with a peak corresponding to N-H at δ 9.96 in the ¹H NMR spectrum. The coordination environments of PNP iridium hydride complexes can be disclosed by the hydride chemical shift. In general, we would expect very upfield shifts if the hydride

were *trans* to an empty site (δ -45.6 for **602**). The hydride chemical shift of **605** (-34) suggesting the hydride is not *trans* to an empty site. Also, the N-H chemical shift is consistent with hydrogen bonding with triflate, so we propose the triflate in **605** as bridging NH and iridium center.



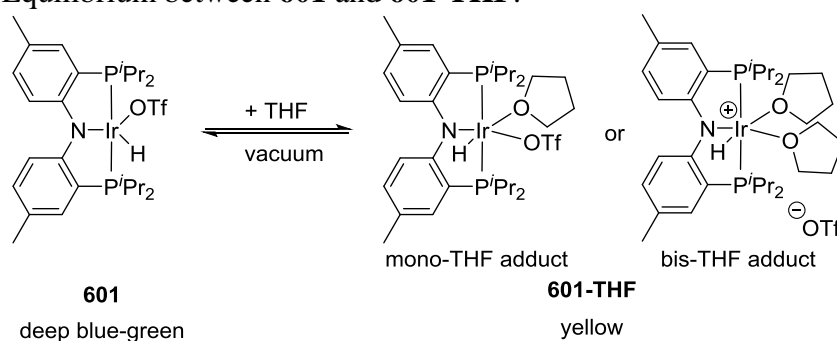
Scheme 6-2. Synthesis of **604** and observation of **605**.

6.2.2 Synthesis and characterization of (PNP)Ir(H)(OTf)

Although **601** was not directly obtained from **418-Ir-HMes** by protonation, the product **604** can be seen as “**601** + HOTf”. We then sought a suitable base to selectively neutralize one equivalent of HOTf in **604** to yield **601**. By reacting **604** with Et_3N , (PNP)Ir(H)₂ and (PNP)Ir(D)(C₆D₅) were observed as major products. (PNP)Ir(H)₂ was formed possibly from Et_3N bound to [(PNP)Ir(H)]⁺ and followed by β -H elimination.^{241,242} NaH suspension in THF could successfully neutralize one equivalent of HOTf in **604** to yield **601**, however, the strong binding of THF to **601** made the full

removal of THF impossible. Even under prolonged high-vacuum, THF residue was still observable in the ^1H NMR spectrum. Since **601** is a coordinatively unsaturated $16 e^-$ Ir(III) complex, it is reasonable to postulate THF would bind to the iridium center in **601** through the lone pair on the oxygen atom to form a THF adduct **601-THF**. The equilibrium between **601** and THF adduct **601-THF** was monitored by the chemical shift difference between two methine peaks and the hydride signal in the ^1H NMR spectrum (Table 6-1).

Table 6-1. Equilibrium between **601** and **601-THF**.^a

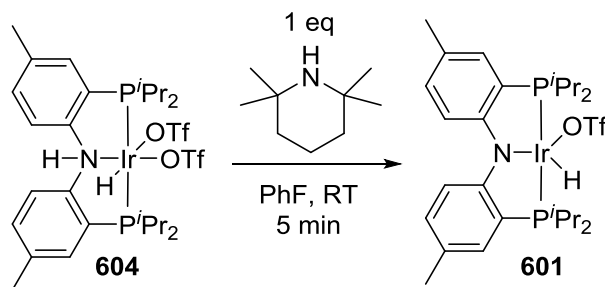


Entry	Eq of THF	^1H NMR of CHMe_2 (ppm)	Difference of CHMe_2 (ppm)	^1H NMR of Ir-H (ppm)	^{31}P NMR (ppm)
1	0 ^b	2.48, 3.22	0.74	-45.5	46.9
2	0.25	2.53, 3.16	0.63	-43.7	44.7
3	0.8	2.56, 3.06	0.50	-40.2	40.3
4	2.0	2.64, 2.94	0.30	-36.2	35.3
5	20	2.70, 2.83	0.13	-32.3	30.4

^a C_6D_6 was used as the solvent. ^b From the experiment that using 2,2,6,6-tetramethylpiperidine as the base, see experimental for the details.

Based on the spectroscopic data, we cannot rule out the involvement of a bis THF monocation. Notably, the cationic iridium bis acetone adduct $[\text{Ir}(\text{H})_2(\text{PPh}_3)_3(\text{acetone})_2](\text{BF}_4)$ has been characterized by Crabtree.²²⁸ Performing the neutralization with NaH in Et₂O resulted in the similar solvent coordination problem, and using the NaH/PhF reaction system led to multiple unidentified compounds.

Since coordination solvents are generally needed for solvation of inorganic bases, we turned our interest back to organic bases. Besides previously used Et₃N, pyridine usually shows strong coordination ability to the coordinatively unsaturated complexes. Hence 2,6-lutidine or 2,2,6,6,-tetramethylpiperidine are preferred because the steric bulk near the nitrogen atoms diminishes their ability to coordinate. By utilizing the 2,2,6,6,-tetramethylpiperidine as the base in PhF, we could neutralize 1 eq. of HOTf in **604** to obtain **601** in the most “naked” form (Scheme 6-3). Nevertheless, the low crystallinity of **601** made all the attempts to isolate pure form of **601** unsuccessful. During the prolonged work up process, **601** would unavoidably react with trace amount of coordination solvent or moisture from extra operations.



Scheme 6-3. Synthesis of **601** from **604**.

The H-D exchange rate of **601** with C_6D_6 was measured at room temperature and showed first-order kinetics (Figure 6-1). The half-life of **601** (7.3 h) was about 50% of **602** (15 h) that we reported earlier.⁵ Recently, the Grubbs group reported **111** catalyzed H-D exchange reaction between aromatic compounds and tertiary silanes and D_2O or C_6D_6 (Figure 6-2, top).²⁴³ The mechanism (Figure 6-2, bottom) was proposed through exchanging Ir-H to Ir-D through oxidative addition/reductive elimination with deuterated solvents, and the deuterium in Ir-D was transferred to substrates through the same oxidative addition/reductive elimination process. Other precedents for similar hydrides undergoing H/D exchange were also reported in the literatures.²⁴⁴⁻²⁴⁸

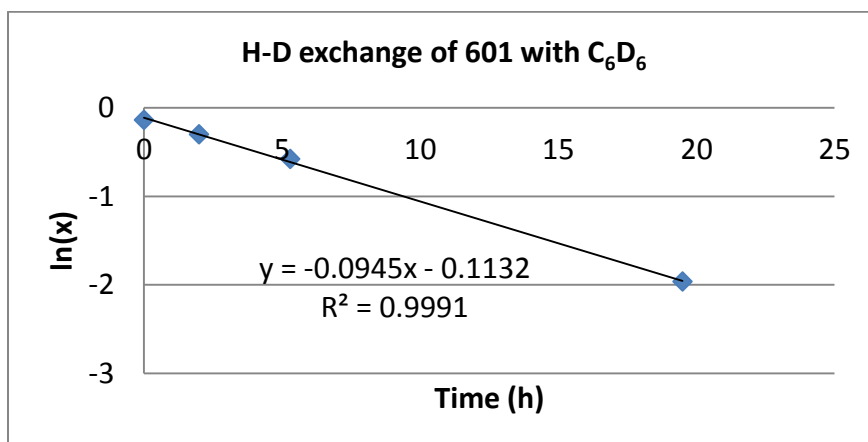
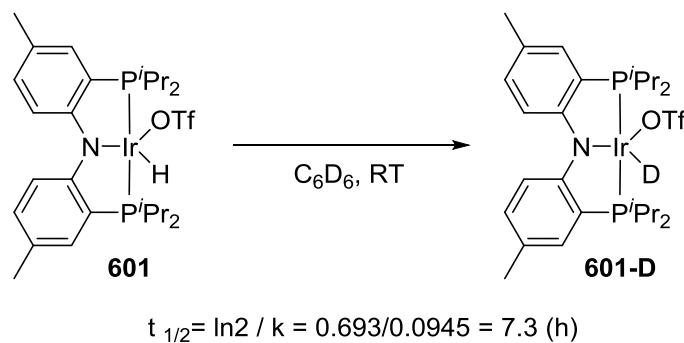


Figure 6-1. H-D exchange rate measurement of **601**.

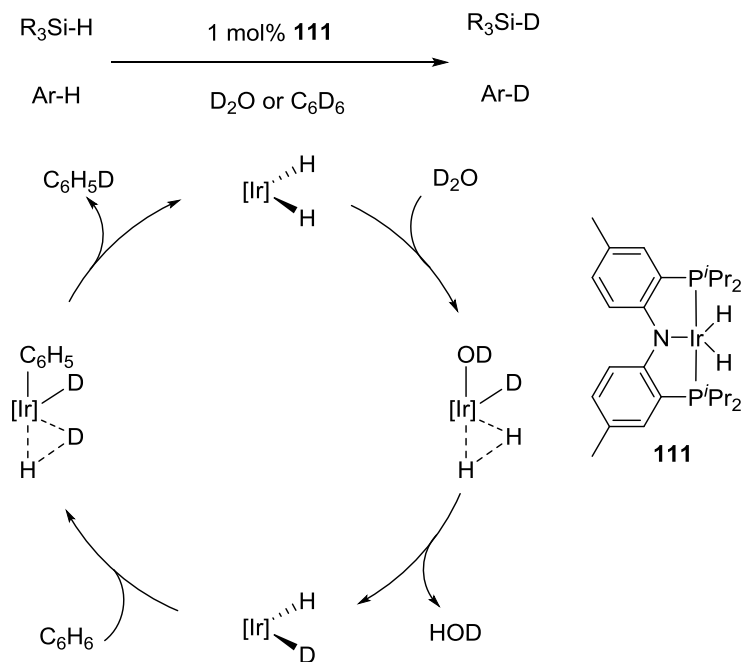
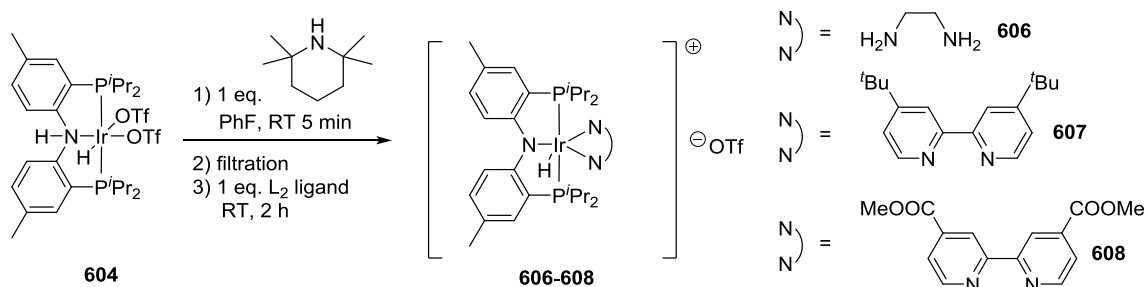


Figure 6-2. Catalytic H-D exchange reaction and proposed mechanism by Grubbs.²⁴³

6.2.3 Synthesis and characterization of $[(PNP)Ir(H)(L_2)](OTf)$

We also wanted to examine the reactions between coordinatively unsaturated **601** and L_2 type ligands. **601** generated *in situ* could readily react with one equivalent of ethylenediamine or bipyridine ligands to form the 6-coordinate $[(PNP)Ir(H)(L_2)](OTf)$ type complexes **606-608** in good yields (Scheme 6-4). The light yellow **606**, and olive-green **607** and **608** are insoluble in pentane that can be easily separated by suspending the mixture in pentane and filtering through a fritted funnel. Comparing to **602**, the hydride peaks of **606-608** in the 1H NMR spectra shift downfield from -45 to -17 - -20 ppm which is similar to the trend observed by Dr. Lei Fan for a series of 6-coordinate $(PNP)Ir(H)(Ar)(py)$ complexes.²⁴⁹ The ethylenediamine or bipyridine ligands also showed desymmetrization after coordination to the iridium center in the 1H NMR spectra.



Scheme 6-4. Synthesis of **606-608**.

6.3 Conclusion

In this chapter, the synthesis of **601** through selective neutralization of **604** was described. The H-D exchange rate of **601** was slightly faster than the previously reported **602**. The equilibrium between **601** and ether solvents was observed, however, the attempts to isolate pure form of **601** were unsuccessful. On the other hand, **601** generated *in situ* could react with diamine or bipyridine ligands to form stable 18 e⁻ Ir(III) triflate salts.

6.4 Experimental

General Considerations. Unless specified otherwise, all manipulations were performed under an Ar atmosphere using standard Schlenk line or glovebox techniques. Toluene, fluorobenzene, THF, diethyl ether, pentane, C₆D₆ were dried over NaK/Ph₂CO/18-crown-6, distilled or vacuum transferred and stored over molecular sieves in an Ar-filled glovebox. CH₂Cl₂, CD₂Cl₂ and CDCl₃ were dried with and then distilled from CaH₂ and stored over molecular sieves in an Ar-filled glove box. All other chemicals were used as received from commercial vendors. NMR spectra were recorded on a Varian Inova 300, Mercury 300 (¹H NMR, 299.952 MHz; ¹³C NMR, 75.421 MHz), Varian Inova 400 (¹H NMR, 399.535 MHz; ¹¹B NMR, 128.185 MHz and NMRS 500

(^1H NMR, 499.703 MHz; ^{13}C NMR, 125.697 MHz) spectrometer. Chemical shifts are reported in δ (ppm). For ^1H and ^{13}C NMR spectra, the residual solvent peak was used as an internal reference (^1H NMR: δ 7.15 for C_6D_6 , 5.32 for CD_2Cl_2 , 7.24 for CDCl_3 ; ^{13}C NMR: δ 128.06 for C_6D_6 , 53.84 for CD_2Cl_2 , 77.16 for CDCl_3). For ^{11}B NMR, spectra were referenced externally to $\delta = 0$ ppm by using $\text{BF}_3 \cdot \text{Et}_2\text{O}$. For ^{19}F NMR, spectra were referenced externally to $\delta = 0$ ppm by using CF_3COOH . For ^{31}P NMR, spectra were referenced externally to $\delta = 0$ ppm by using 85% H_3PO_4 . Elemental analyses were performed by CALI Labs, Inc. (Parsippany, NJ).

(PN(H)P)Ir(H)(OTf)₂ (604). **408-Ir-HMes** (2.01 g, 2.72 mmol) was dissolved in 20 mL toluene in a 100 mL PTFE-cap gas-tight flask, upon stirring, HOTf (4.0 mL of 2.0 M stock solution in Et_2O , 8.0 mmol) was added to the mixture. The flask was capped and the solution was stirred at ambient temperature. Solution color turned from deep brown to light yellow gradually, during the time, white fine powder precipitated out. After 2 d, the solution was filtered through a fritted funnel, and the white powder was washed with Et_2O and dried *in vacuo*. Yield: 2.26 g (90%). ^1H NMR (500 MHz, CDCl_3): δ 10.84 (s, 1H, N-H), 7.52 (s, 2H, Ar-H), 7.10 (d, JH-H = 8.0 Hz, 2H, Ar-H), 6.99 (d, JH-H = 8.0 Hz, 2H, Ar-H), 3.34 (m, 2H, CHMe_2), 2.92 (m, 2H, CHMe_2), 2.43 (s, 6H, Ar-Me), 1.66 (dvt, J = 14, 7.0 Hz, 6H, CHMe_2), 1.48 (dvt, J = 14, 7.0 Hz, 6H, CHMe_2), 1.33 (dvt, J = 14, 7.0 Hz, 6H, CHMe_2), 0.86 (dvt, J = 14, 7.0 Hz, 6H, CHMe_2), -31.02 (t, $J_{\text{P-H}} = 15$ Hz, 1H, Ir-H). $^{31}\text{P}\{^1\text{H}\}$ NMR (121 MHz, CDCl_3): δ 31.8. Anal. Calcd for $\text{C}_{28}\text{H}_{42}\text{F}_6\text{IrNO}_6\text{P}_2\text{S}_2$: C, 36.52; H, 4.60. Found: C, 36.63; H, 4.79.

Observation of 605. 604 (10 mg, 0.014 mmol) was placed in a J. Young tube followed by HOTf (100 μ L of 0.56 M stock solution in Et₂O, 0.056 mmol) and 0.5 mL C₆D₆. After 20 min, analysis by ³¹P NMR spectroscopy revealed ~80% **606** formation (δ 36.9). Selected ¹H NMR data of **605** (300 MHz, C₆D₆): δ 9.96 (s, 1H, N-*H*), -34.02 (t, J_{P-H} = 15 Hz, 1H, Ir-*H*).

Equilibrium between 601 and 601-THF. 601 (22 mg, 0.024 mmol) was suspended in 1 mL THF in a 10 mL Schlenk flask. NaH (5 mg, 0.21 mmol) was added to the solution, and the solution color turned to yellow immediately. After 10 min, all volatiles were removed *in vacuo*. The residue was redissolved in pentane and filtered through Celite. All volatiles of filtrate were removed *in vacuo* and redissolved in 0.5 mL C₆D₆ and the solution was taken up for NMR analysis. 0.25 eq THF (compared to 602) was observed in the ¹H NMR spectrum. Different amount of THF (overall 0.8 eq, 2.0 eq, 20 eq) was then added to the J. Young tube and the solution was taken up for ¹H and ³¹P NMR analysis.

(PNP)Ir(H)(OTf) (601). 604 (11 mg, 0.012 mmol) was suspended in 1 mL PhF in a 10 mL Schlenk flask. 2,2,6,6-Tetramethylpiperidine (33 μ L of 0.36 M stock solution in pentane, 0.012 mmol) was added to the solution, and the solution color turned to deep blue-green immediately. After 5 min, all volatiles were removed *in vacuo*. The residue was redissolved in pentane and filtered through Celite. All volatiles of filtrate were removed *in vacuo* and redissolved in 0.5 mL C₆D₆. All volatiles were removed *in vacuo*, redissolved in 0.5 mL C₆D₆, and the solution was taken up for NMR analysis. ¹H NMR (300 MHz, C₆D₆): δ 7.66 (dt, J = 8.6, 2.0 Hz, 2H, Ar-*H*), 6.91 (m, 2H, Ar-*H*), 6.62 (dd, J

= 8.6, 2.0 Hz, 2H, Ar-*H*), 3.22 (m, 2H, CHMe₂), 2.48 (m, 2H, CHMe₂), 2.13 (s, 6H, Ar-CH₃), 1.31 (dvt, J = 14, 7.0 Hz, 6H, CHMe₂), 1.20 (dvt, J = 14, 7.0 Hz, 6H, CHMe₂), 1.01 (dvt, J = 14, 7.0 Hz, 6H, CHMe₂), 0.90 (dvt, J = 14, 7.0 Hz, 6H, CHMe₂), -45.45 (t, J = 12 Hz, 1H, Ir-*H*). ³¹P{¹H} NMR (121 MHz, C₆D₆): δ 46.9. ¹⁹F NMR (282 MHz, C₆D₆): δ -77.4.

Kinetic studies of 601 in H-D exchange. **604** (11 mg, 0.012 mmol) was suspended in 1 mL PhF in a 10 mL Schlenk flask. 2,2,6,6-Tetramethylpiperidine (33 μL of 0.36 M stock solution in pentane, 0.012 mmol) was added to the solution, and the solution color turned to deep blue-green immediately. After 5 min, all volatiles were removed *in vacuo*. The residue was redissolved in pentane and filtered through Celite. All volatiles of filtrate were removed *in vacuo* and redissolved in 0.5 mL C₆D₆. All volatiles were removed *in vacuo*, redissolved in 0.5 mL C₆D₆. The solution was left at ambient temperature and the integration of Ir-*H* was monitored by ¹H NMR spectroscopy.

Synthesis of 606. **604** (101 mg, 0.110 mmol) was suspended in 3 mL fluorobenzene in a 10 mL Schlenk flask. 2,2,6,6-Tetramethylpiperidine (19 μL, 0.11 mmol) was added to the solution, and the solution color turned to deep blue-green immediately. After 5 min, all volatiles were removed *in vacuo*. 3 mL pentane was added to the flask and used a spatula to scratch the solid on the wall, and all volatiles were removed *in vacuo*. The residue was redissolved in pentane and filtered through Celite. All volatiles of filtrate were removed *in vacuo* and redissolved in 3 mL fluorobenzene. Ethylenediamine (8 μL, 0.12 mmol) was added to the solution. The solution color turned from deep blue-green to yellow immediately. After 2 h, all volatiles were removed *in*

vacuo. 5 mL pentane was added to the flask and used a spatula to scratch the film on the wall to result light yellow powder. The suspension was stirred vigorously for 2 h and filtered through a fritted funnel. The light yellow solid was washed with pentane and dried *in vacuo*. Yield: 73 mg (80%). ^1H NMR (500 MHz, C_6D_6): δ 7.46 (d, $J_{\text{H-H}} = 8.5$ Hz, 2H, Ar-*H*), 6.85 (s, 2H, Ar-*H*), 6.64 (d, $J_{\text{H-H}} = 8.5$ Hz, 2H, Ar-*H*), 4.25 (s, 2H), 3.11 (s, 2H), 2.82 (m, 2H), 2.61 (s, 2H), 2.51 (s, 2H), 2.16 (m, 8H, included Ar- CH_3), 1.16 (m, 12H, CHMe_2), 1.06 (dvt, $J = 14, 7.0$ Hz, 6H, CHMe_2), 0.87 (dvt, $J = 14, 7.0$ Hz, 6H, CHMe_2), -21.18 (t, $J_{\text{P-H}} = 16$ Hz, 1H, Ir-*H*). $^{13}\text{C}\{^1\text{H}\}$ NMR (126 MHz, CDCl_3): δ 161.3 (t, $J_{\text{P-C}} = 8.8$ Hz), 131.2, 131.0, 125.6 (t, $J_{\text{P-C}} = 3.6$ Hz), 121.9 (t, $J_{\text{P-C}} = 25$ Hz), 120.7 (q, $J_{\text{F-C}} = 320$ Hz, C on OTf), 116.0 (m), 51.6, 44.8, 26.8 (t, $J_{\text{P-C}} = 17$ Hz), 24.7 (t, $J_{\text{P-C}} = 13$ Hz), 20.5, 18.8, 18.7, 18.6, 18.4 (m). $^{31}\text{P}\{^1\text{H}\}$ NMR (202 MHz, C_6D_6): δ 23.7. ^{19}F NMR (470 MHz, C_6D_6): δ -78.8. Anal. Calcd for $\text{C}_{29}\text{H}_{49}\text{F}_3\text{IrN}_3\text{O}_3\text{P}_2\text{S}$: C, 41.92; H, 5.94. Found: C, 42.12; H, 5.79.

Synthesis of 607. 604 (110 mg, 0.119 mmol) was suspended in 3 mL fluorobenzene in a 10 mL Schlenk flask. 2,2,6,6-Tetramethylpiperidine (21 μL , 0.123 mmol) was added to the solution, and the solution color turned to deep blue-green immediately. After 5 min, all volatiles were removed *in vacuo*. 3 mL pentane was added to the flask and used a spatula to scratch the solid on the wall, and all volatiles were removed *in vacuo*. The residue was redissolved in pentane and filtered through Celite. All volatiles of filtrate were removed *in vacuo* and redissolved in 3 mL fluorobenzene. 4,4'-Di-*tert*-butyl-2,2'-dipyridyl (30 mg, 0.11 mmol) was added to the solution. The solution color turned from deep blue-green to brown gradually. After 2 h, all volatiles

were removed *in vacuo*. 5 mL pentane was added to the flask and used a spatula to scratch the film on the wall to result olive-green powder. The suspension was stirred vigorously for 2 h and filtered through a fritted funnel. The olive-green solid was washed with pentane and dried *in vacuo*. Yield: 95 mg (77%). ^1H NMR (500 MHz, CDCl_3): δ 9.15 (d, $J_{\text{H-H}} = 6.0$ Hz, 1H, Ar-*H*), 8.42 (m, 3H, Ar-*H*), 7.54 (d, $J_{\text{H-H}} = 8.6$ Hz, 2H, Ar-*H*), 7.42 (dd, $J_{\text{H-H}} = 6.0, 1.8$ Hz, 1H, Ar-*H*), 7.32 (dd, $J_{\text{H-H}} = 6.0, 1.8$ Hz, 1H, Ar-*H*), 6.81 (m, 4H, Ar-*H*), 2.35 (m, 4H, CHMe_2), 2.21 (s, 6H, Ar- CH_3), 1.46 (s, 9H, ^tBu on bipyridine), 1.40 (s, 9H, ^tBu on bipyridine), 1.11 (dvt, $J = 14, 7.0$ Hz, 6H, CHMe_2), 1.01 (dvt, $J = 14, 7.0$ Hz, 6H, CHMe_2), 0.40 (dvt, $J = 14, 7.0$ Hz, 6H, CHMe_2), 0.27 (dvt, $J = 14, 7.0$ Hz, 6H, CHMe_2), -18.29 (t, $J_{\text{P-H}} = 16$ Hz, 1H, Ir-*H*). $^{13}\text{C}\{^1\text{H}\}$ NMR (126 MHz, CDCl_3): δ 164.4, 163.9, 160.7 (t, $J_{\text{P-C}} = 8.5$ Hz), 158.4, 157.4, 157.1, 150.4, 131.8, 131.2, 126.3 (t, $J_{\text{P-C}} = 3.8$ Hz), 125.2, 123.6, 121.7, 121.3, 121.2 (q, $J_{\text{F-C}} = 320$ Hz, C on OTf), 121.1 (t, $J_{\text{P-C}} = 24$ Hz), 116.6 (t, $J_{\text{P-C}} = 4.6$ Hz), 36.0, 35.9, 30.55, 30.52, 27.6 (t, $J_{\text{P-C}} = 18$ Hz), 25.9 (t, $J_{\text{P-C}} = 13$ Hz), 20.5, 18.4, 18.2, 17.7, 17.4. $^{31}\text{P}\{^1\text{H}\}$ NMR (202 MHz, C_6D_6): δ 23.3. ^{19}F NMR (470 MHz, C_6D_6): δ -78.2. Anal. Calcd for $\text{C}_{45}\text{H}_{65}\text{F}_3\text{IrN}_3\text{O}_3\text{P}_2\text{S}$: C, 52.01; H, 6.30. Found: C, 52.24; H, 6.27.

Synthesis of 608. 604 (101 mg, 0.110 mmol) was suspended in 3 mL fluorobenzene in a 10 mL Schlenk flask. 2,2,6,6-Tetramethylpiperidine (19 μL , 0.11 mmol) was added to the solution, and the solution color turned to deep blue-green immediately. After 5 min, all volatiles were removed *in vacuo*. 3 mL pentane was added to the flask and used a spatula to scratch the solid on the wall, and all volatiles were removed *in vacuo*. The residue was redissolved in pentane and filtered through Celite.

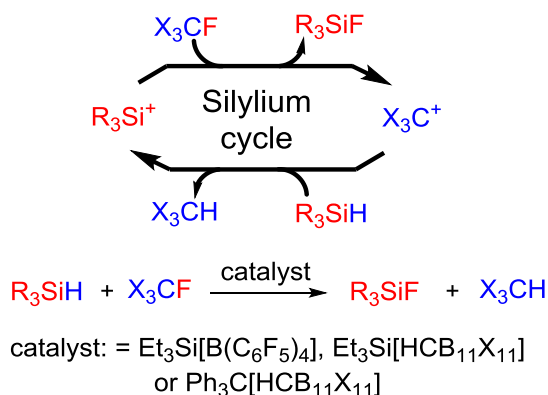
All volatiles of filtrate were removed *in vacuo* and redissolved in 3 mL fluorobenzene. (8 μ L, 0.12 mmol) was added to the solution. The solution color turned from deep blue-green to yellow immediately. After 2 h, all volatiles were removed *in vacuo*. 5 mL pentane was added to the flask and used a spatula to scratch the film on the wall to result light yellow powder. The suspension was stirred vigorously for 2 h and filtered through a fritted funnel. The olive-green solid was washed with pentane and dried *in vacuo*. Yield: 92 mg (80%). ^1H NMR (500 MHz, CDCl_3): δ 9.63 (d, $J_{\text{H-H}} = 5.8$ Hz, 1H, Ar-*H*), 9.15 (m, 2H, Ar-*H*), 8.77 (d, $J_{\text{H-H}} = 5.8$ Hz, 1H, Ar-*H*), 8.06 (dd, $J_{\text{H-H}} = 5.8, 1.6$ Hz, 1H, Ar-*H*), 7.90 (dd, $J_{\text{H-H}} = 5.8, 1.6$ Hz, 1H, Ar-*H*), 7.56 (d, $J_{\text{H-H}} = 8.5$ Hz, 2H, Ar-*H*), 6.86 (d, $J_{\text{H-H}} = 8.5$ Hz, 2H, Ar-*H*), 6.79 (s, 2H, Ar-*H*), 4.10 (s, 3H, CO_2Me), 4.07 (s, 3H, CO_2Me), 2.43 (m, 4H, CHMe_2), 2.21 (s, 6H, Ar-*Me*), 1.13 (dvt, $J = 14, 7.0$ Hz, 6H, CHMe_2), 1.05 (dvt, $J = 14, 7.0$ Hz, 6H, CHMe_2), 0.39 (dvt, $J = 14, 7.0$ Hz, 6H, CHMe_2), 0.23 (dvt, $J = 14, 7.0$ Hz, 6H, CHMe_2), -17.79 (t, $J_{\text{P-H}} = 16$ Hz, Ir-*H*). $^{31}\text{P}\{^1\text{H}\}$ NMR (202 MHz, CDCl_3): δ 24.7. ^{19}F NMR (470 MHz, CDCl_3): δ -78.5.

CHAPTER VII
DESIGN AND SYNTHESIS OF HIGHLY ELECTROPHILIC TRIARYLMETHYL
CATION PRECURSORS

7.1 Introduction

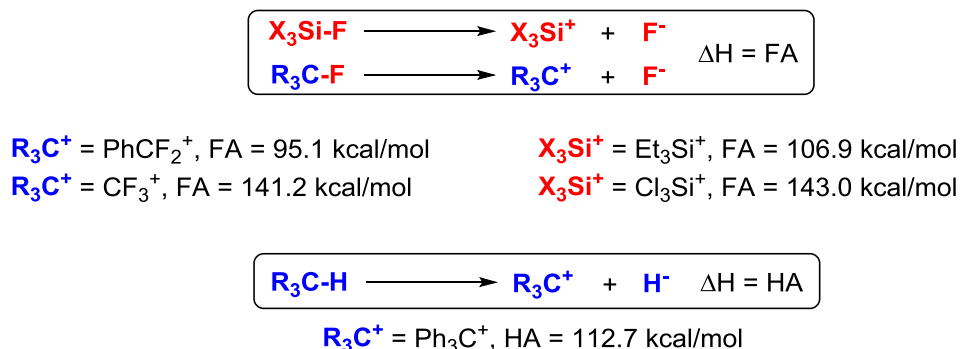
Carbon-fluorine bonds are among the most inert functionalities in organic chemistry.²⁵⁰ The inertness can be explained by both thermodynamic and kinetic aspects: Thermodynamically, the C-F bond is the strongest single bond to carbon;²⁵⁰⁻²⁵² kinetically, organofluorine compounds are poor ligands to metal complexes and unlikely to undergo oxidative addition.²⁵⁰⁻²⁵² As poor leaving groups, S_N2 nucleophilic substitution is sluggish with fluorides.⁶¹ The activation of C-F bonds is especially motivated by the environmental impact. Chlorofluorocarbons (freons or CFC), hydrofluorocarbons (partially fluorinated alkanes, HFC), and perfluorocarbons (perfluoroalkanes, PFC), have been depicted as “super-greenhouse gases” due to their extremely high global warming potential and long life-time.²⁵³

In 2005, our group reported catalytic hydrodefluorination (HDF) of C(sp³)-F bonds at room temperature using [Et₃Si][B(C₆F₅)₄] as the catalyst.²⁵⁴ The reactivity and durability of silylium cations were later improved by applying carboranes as the counterions.²⁵⁵ The HDF mediated by silyliums is proposed to follow the catalytic cycle shown in Scheme 7-1. The silylium cations abstract the fluoride of organofluorine compounds to generate silyl fluorides and carbocations. The carbocations gain hydrides from silanes to yield alkanes and regenerate silylium cations to complete the catalytic cycle.



Scheme 7-1. Silylium mediated C-F bond activations.

Typically using trialkylsilane, HDF was successfully performed for a variety of organofluorine substrates. Slower rates were observed when the degree of fluorination increased, and the perfluoroalkanes are totally unreactive. To seek out the more powerful HDF catalyst, a theoretical study of hydride and fluoride affinities of carbenium and silylium cations was conducted in cooperation with Prof. Gusev.²⁵⁶ From the study, the fluoride abstraction from perfluorinated substrates by the commonly used trialkylsilylium cations was shown to be thermodynamically disfavored (Scheme 7-2, top), explaining the observed inactivity of perfluoroalkanes in HDF.



Scheme 7-2. Representative values of fluoride (FA) and hydride (HA) affinities, all values were calculated in chlorobenzene.

On the other hand, the high fluoride affinities of chlorine-substituted silylium cations suggested they would be made be strong candidates for the next generation of HDF catalysts. However, these chlorine-substuted silylium cations also have high hydride affinities which prevent them from being generated by reacting corresponding silanes with the plain trityl cation (Ph_3C^+ , Scheme 7-2, bottom). Intrigued by the computational results, abstraction of hydrides from chlorosilanes would be more favorable by utilizing more electrophilic triarylmethyl cation reagents.

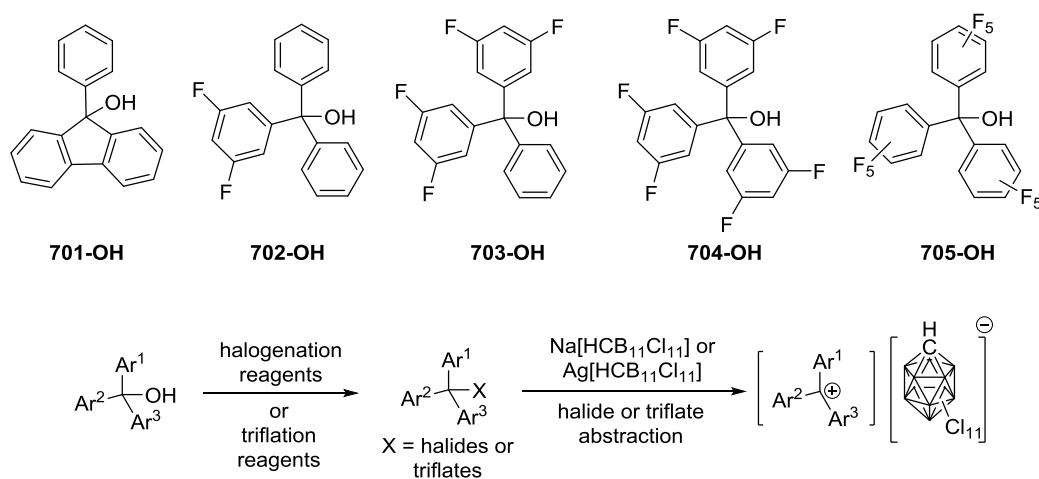
The value of making new triarylmethyl cations is also relevant in organometallic chemistry²⁵⁷⁻²⁵⁹ because trityl salts are regularly used in hydride abstraction of metal hydride complexes to generate coordinatively unsaturated species that are active in catalysis such as hydrogenation and polymerization. The use of trityl cations as strong oxidants to oxidize transition metal complexes has also been reported.²⁶⁰ In this chapter, we illustrate the synthesis of the selected triarylmethanol and triarylmethyl chloride bearing electron withdrawing groups. The attempts to generate highly electrophilic triarylmethyl cations are also shown.

7.2 Results and discussion

7.2.1 Design and synthesis of triarylmethanols

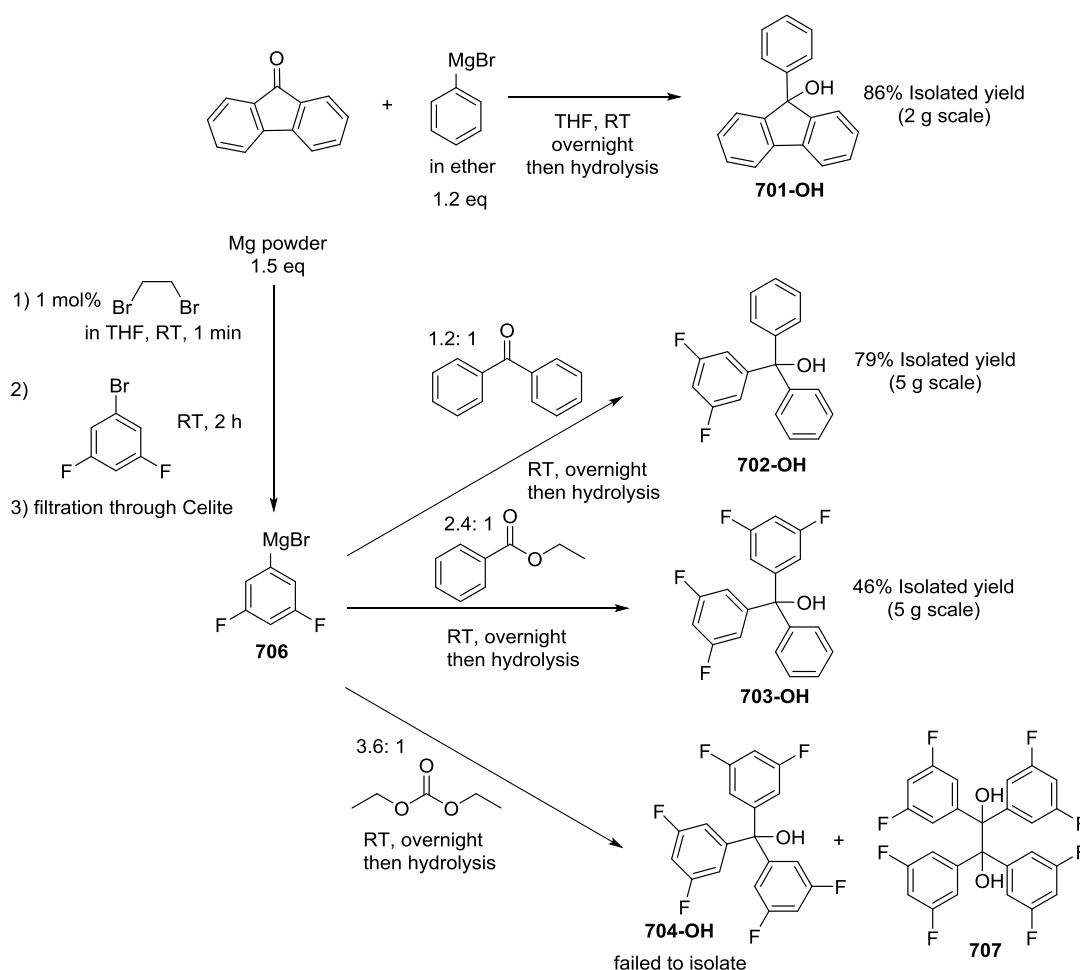
We selected five triarylmethanols as the starting target molecules (Scheme 7-3, top). The structure of **701-OH**²⁶¹ is closest to triphenylmethanol. Since our goal was to synthesize new electrophilic triarylmethyl carborane reagents and use them to generate silylium cations, the stability and coordination ability of electron withdrawing substituents on triarylmethyl precursors towards to silylium cations was taken into

consideration. Among common electron withdrawing groups, $-\text{CF}_3$ is reactive with a silylium cation,²⁵⁴ and $-\text{CN}$ or $-\text{NO}_2$ show strong coordination that diminish the silylium character.²⁶² Hence fluorine substitutions are preferred because their inertness and weaker coordination ability compared to other halogen substitutions.^{263,264} From **702-OH** to **704-OH**, the numbers of *m*-F substituents increase on triphenylmethanols from 2 to 6. *Meta*-fluorine substitutions are favored because they serve as the strong electron withdrawing groups by the inductive effect and no opposite resonance effect that occurs when fluorine are on *ortho*- or *para*- positions.²⁶⁵ Finally, perfluorotriphenylmethanol **705-OH** was chosen as the precursor to the most electrophilic triarylmethyl cation.^{266,267} The general strategy of making triarylmethyl carboranes is shown at the bottom of Scheme 7-3. First, converting the selected triarylmethanols to triarylmethyl halides or triarylmethyl triflates, and the halides or triflates could be abstracted either by sodium carborane or silver carborane.



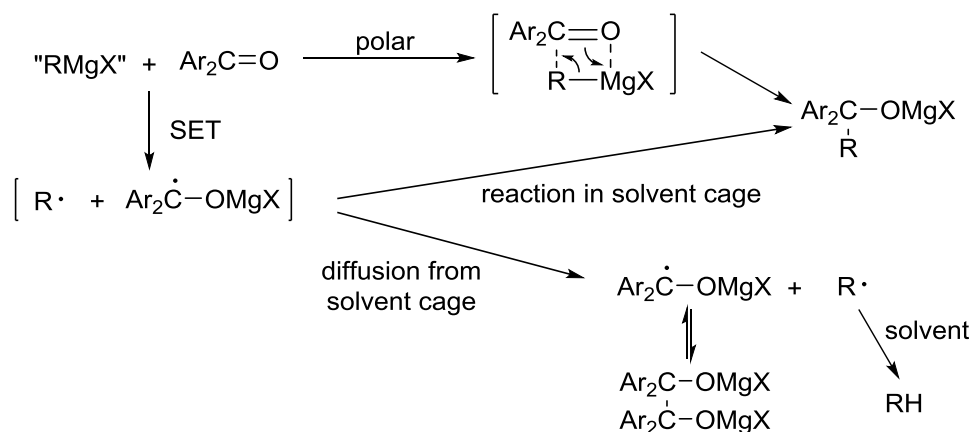
Scheme 7-3. Objective triarylmethanol (top) and strategy of making triarylmethyl carboranes (bottom).

701-OH was synthesized in good yield from fluorenone and commercially available PhMgBr solution (Scheme 7-4).²⁶⁸ For the syntheses of **702-OH** and **703-OH**, the Grignard reagent **706** was prepared from 3,5-difluorobromobenzene and Mg powder in THF (*Caution*: The solid or concentrated form of fluorine-containing Grignard reagents might be potentially explosive so dryness or concentration of the Grignard reagent solution should be prevented before quenching), and the THF solution of **706** was then reacted with benzophenone or ethyl benzoate to yield **702-OH** or **703-OH**.



Scheme 7-4. Synthesis of **701-OH** to **704-OH**.

Notably, the removal of excess Mg powder before reacting **706** with carbonyl compounds is essential to prevent pinacol coupling reaction²⁶⁹ as the side reaction. The attempt to make **704-OH** through **706** with diethyl carbonate in the same protocol, however, led to significant amount of diol **707** as the side product and failed to isolate **704-OH**. The formation of **707** can be explained as the result of single electron transfer (SET) reaction that shows in the Scheme 7-5.²⁷⁰ The reactions between a Grignard reagent and a ketone compound is generally been taught that undergoing through the polar mechanism (Scheme 7-5, top).⁶¹ The nucleophilic R group in the Grignard reagent attacks carbonyl carbon leads to a magnesium alkoxide, and after aqueous work-up, alcohol is obtained by hydrolyzing the magnesium-oxygen bond.



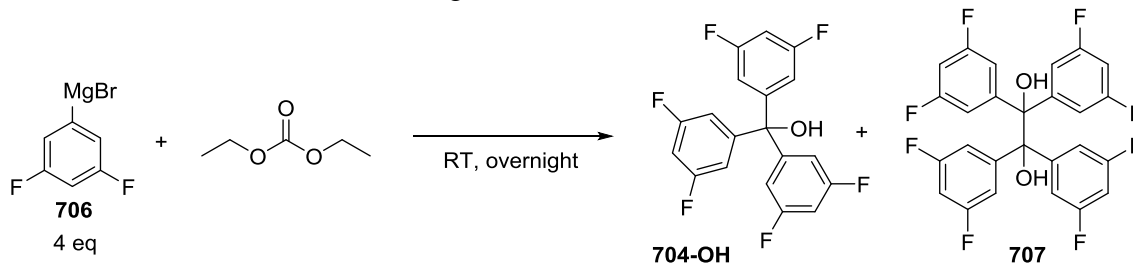
Scheme 7-5. Polar and SET pathways for the reaction between Grignard reagents and ketone compounds.

A Grignard reagent could also react with a ketone compound through the SET pathway (Scheme 7-5, bottom) and lead to an ion pair. If the ketyl radical of an ion pair diffuse from the solvent cage and undergo dimerization then a diol would be obtained after hydrolysis. The factors result in diol products from various Grignard reagents with

ketone compounds have been extensively studied by Ashby and Walling.²⁷⁰⁻²⁷² Based on the experimental results, four ways to reduce the diol formation were identified: 1) Using high purity Mg (impurities like Fe would increase SET^{270,271}); 2) Using less coordinating solvents; 3) Adding anion radical scavengers; 4) Reducing the reaction rate.

Performing the reaction at a lower temperature or using Mg from different sources did not lead to significant product ratio change. The ratio of **704-OH** to **707** can be improved by pairing THF with other less polar solvents (Table 7-1). The lower the polarity of the co-solvent (Snyder polarity index²⁷³: THF, 4.2; Et₂O, 2.8; toluene, 2.3; pentane, 0), the higher yield of **704-OH** was obtained. However, the scalability of the reaction was restricted by the poor solubility of the **706** in pentane.

Table 7-1. Solvent effect in making of **704-OH**.



Solvent	704-OH : 707 ^a
THF	78:22
THF/Et ₂ O (1:4)	86:14
THF/toluene (1:4)	91:9
THF/pentane (1:4)	95:5

^a The product ratio was determined by ¹⁹F NMR spectroscopy.

Several syntheses were described for **705-OH** in the literature.^{267,274} We found the Li-Br exchange of C₆F₅Br with *n*-BuLi at -78 °C followed by reaction with diethyl carbonate at -25 °C led to good yield of **705-OH** (Figure 7-1). We attempted to apply the procedure to make **704-OH** that using 3,5-difluorobromobenzene instead of C₆F₅Br, and >90% NMR yield was indicated by ¹⁹F NMR spectroscopy. However, the high solubility of **704-OH** in all organic solvents even pentane prevented the isolation of **704-OH**.

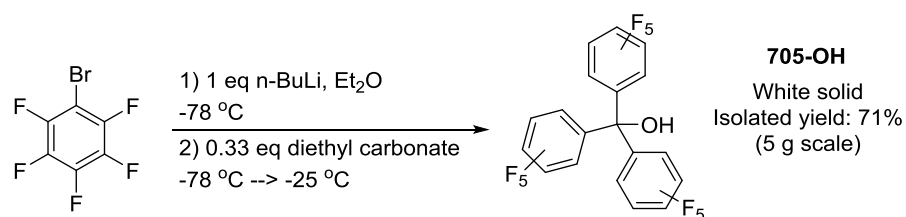
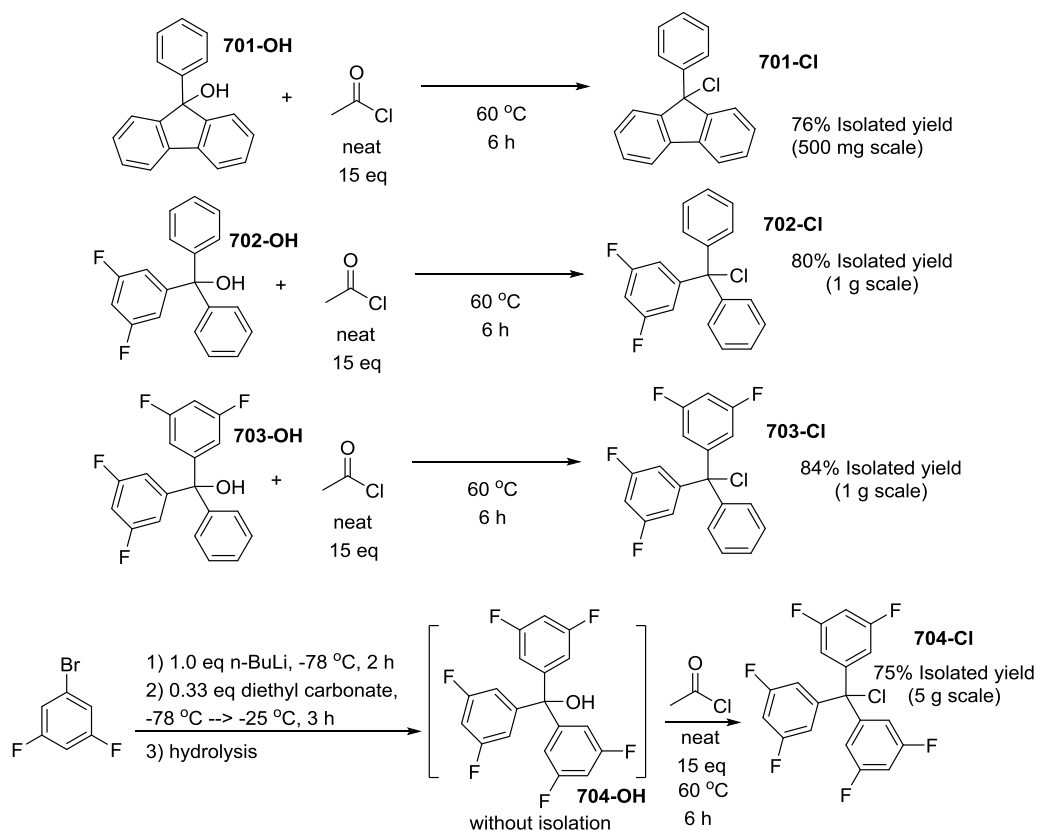


Figure 7-1. Synthesis of **705-OH**.

7.2.2 Synthesis of triarylmethyl chlorides

SOCl₂ and acetyl chloride are commonly used for converting triarylmethanol to triarylmethyl chloride.^{265,275-278} Heating **701-OH** to **703-OH** in neat acetyl chloride at 60 °C overnight can yield corresponding triarylmethyl chloride **701-Cl** to **703-Cl** in good yields (Scheme 7-6). For **704-OH**, which was hard to isolate in the pure form, the reaction mixture from 3,5-difluorobromobenzene + *n*-BuLi + diethyl carbonate could be directly treated with acetyl chloride and **704-Cl** was isolated in 75% yield in a one pot reaction.



Scheme 7-6. Synthesis **701-Cl** to **704-Cl**.

Heating **705-OH** with acetyl chloride yielded triarylmethyl acetate **705-OAc** instead of triarylmethyl chloride (Figure 7-2), as indicated by the characteristic peak of the acetyl at δ 2.15 (CH_3COO) in the ^1H NMR spectrum and δ 169.1 (CH_3COO) in the ^{13}C NMR spectrum. **705-OH** was unreactive toward to SOCl_2 or $\text{HCl}_{(\text{aq})}$, and it also remained intact after treating with HOTf, Tf_2O or $(\text{CF}_3\text{CO})_2\text{O}$ with or without a base.

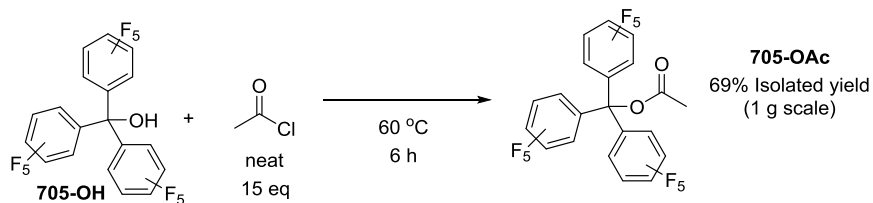
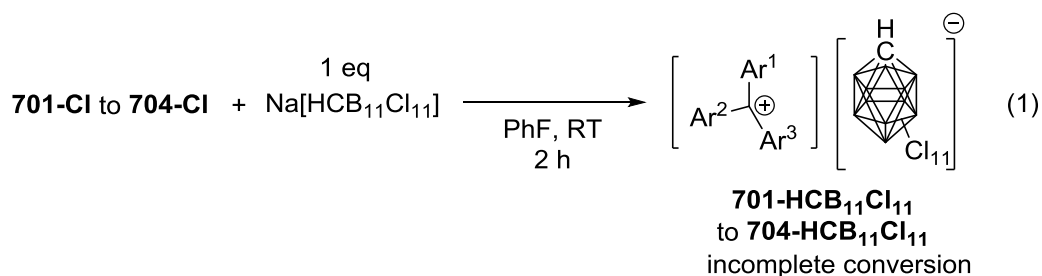


Figure 7-2. Synthesis of **705-OAc**.

7.2.3 Attempt to synthesize triarylmethyl carboranes and triarylmethyl triflates

Abstraction of the chloride from the plain trityl chloride, Ph_3CCl was achieved by using $\text{Na}[\text{HCB}_{11}\text{Cl}_{11}]$ to cleanly yield $[\text{Ph}_3\text{C}][\text{HCB}_{11}\text{Cl}_{11}]$.²⁷⁹ Analogous to this procedure, **704-Cl** was mixed with 1 eq of $\text{Na}[\text{HCB}_{11}\text{Cl}_{11}]$ in PhF, and the solution turned red immediately which indicated the corresponding triarylmethyl cation formation. However, analysis by ^{19}F NMR spectroscopy only showed 19% conversion of **704-Cl** after workup. The reaction of **701-Cl** to **703-Cl** with 1 eq of $\text{Na}[\text{HCB}_{11}\text{Cl}_{11}]$ in PhF also led to incomplete conversion (Scheme 7-7). No reaction was observed when performing the reaction between **702-Cl** and $\text{Na}[\text{HCB}_{11}\text{Cl}_{11}]$ in CD_3CN . We also attempted to synthesize triarylmethyl triflate from triarylmethyl chloride. Mixing **701-Cl** and **702-Cl** with Me_3SiOTf resulted no reaction at room temperature and led to multiple products upon heating at 70°C . No observable change was observed for **703-Cl** and **704-Cl** with Me_3SiOTf even heating at 70°C .



Scheme 7-7. Attempt of synthesis of triarylmethyl carboranes.

The chloride abstraction of triarylmethyl chlorides by sodium carboranes or the triflate exchange reactions did not proceed completely and cleanly that might be explained by the high Lewis acidity of corresponding triarylmethyl cations. The

employment of stronger halide abstraction reagents such like silylium or silver carboranes in the reactions will be reasonable options in the future work.

7.3 Conclusion

In this chapter, the syntheses of various triarylmethanols and triarylmethyl chlorides bearing electron-withdrawing groups have been described. The percentage of the diol side product in making triarylmethanol was proved to decreased when using less polar solvents. Perfluorotriptylmethanol was inert to most chlorination and triflation reagents except acetyl chloride that led to perfluorotriptyl acetate. The attempts of abstraction of chlorides from the new triarylmethyl chlorides by sodium carboranes were unsuccessful so far.

7.4 Experimental

General Considerations. Unless specified otherwise, all manipulations were performed under an Ar atmosphere using standard Schlenk line or glovebox techniques. Toluene, fluorobenzene, THF, diethyl ether, pentane, C₆D₆ were dried over NaK/Ph₂CO/18-crown-6, distilled or vacuum transferred and stored over molecular sieves in an Ar-filled glovebox. CH₂Cl₂ and CDCl₃ were dried with and then distilled from CaH₂ and stored over molecular sieves in an Ar-filled glove box. **701-OH** was prepared according to published procedures.²⁶⁸ All other chemicals were used as received from commercial vendors. NMR spectra were recorded on a Varian Inova 300, Mercury 300 (¹H NMR, 299.952 MHz; ¹³C NMR, 75.421 MHz), Varian Inova 400 (¹H NMR, 399.535 MHz) and NMRS 500 (¹H NMR, 499.703 MHz; ¹³C NMR, 125.697 MHz; ¹⁹F NMR, 469.854 MHz) spectrometer. Chemical shifts are reported in δ (ppm).

For ^1H and ^{13}C NMR spectra, the residual solvent peak was used as an internal reference (^1H NMR: δ 7.15 for C_6D_6 , 7.24 for CDCl_3 ; ^{13}C NMR: δ 128.06 for C_6D_6 , 77.16 for CDCl_3 , 29.84 for $(\text{CD}_3)_2\text{CO}$). For ^{19}F NMR, spectra were referenced externally to $\delta = -78.5$ ppm by using CF_3COOH .

Synthesis of 702-OH. In an Ar-filled glove box, magnesium powder (954 mg, 39.2 mmol), 1,2-dibromoethane (25 μL , 0.29 mmol) and 60 mL THF were transferred to a 250 mL Schlenk flask. After stirring 10 min, 3,5-difluorobromobenzene (3.00 mL, 26.1 mmol) was slowly added in 3 portions in 15 min intervals over the course of 45 min. During that time, the solution color turned from colorless to yellow which indicated the Grignard reaction occurred. The solution temperature increased significantly and boiling was observed. (Note: Pause the addition of 3,5-difluorobromobenzene if the solution begin to boil too violently.) After addition all of 3,5-difluorobromobenzene, the solution was left to stir at RT overnight. The solution was then filtered through Celite to get rid of excess magnesium. A solution of benzophenone (3.77 g, 20.7 mmol) in 10 mL THF was added to the flask dropwise over 1 min. The solution was left to stir at RT overnight. The flask was brought out of glovebox and quenched with 80 mL 1 M $\text{HCl}_{(\text{aq})}$. The solution color turned from dark brown to yellow. The organic layer was separated and the water layer was extracted with 100 mL of hexanes twice. The organic layer was combined and dried with anhydrous MgSO_4 . The solution was filtered through Celite and dried *in vacuo* to yield a yellow oil. The oil was triturated by pentane and sonicated. White powder formed and precipitated, and the solution was filtered through a fritted funnel. The white powder was washed with cold pentane and dried *in vacuo*. Yield: 4.85 g

(79%). The ^1H and ^{13}C NMR spectral data were in agreement with those reported in the literature.²⁸⁰

Synthesis of 703-OH. In an Ar-filled glove box, magnesium powder (1.82 g, 75.0 mmol), 1,2-dibromoethane (45 μL , 0.52 mmol) and 60 mL THF were transferred to a 250 mL Schlenk flask. After stirring 10 min, 3,5-difluorobromobenzene (5.76 mL, 50.0 mmol) was slowly added in 3 portions in 15 min intervals over the course of 45 min. During that time, the solution color turned from colorless to yellow which indicated the Grignard reaction occurred. The solution temperature increased significantly and boiling was observed. (Note: Pause the addition of 3,5-difluorobromobenzene if the solution begin to boil too violently.) After addition all of 3,5-difluorobromobenzene, the solution was left to stir at RT overnight. The solution was then filtered through Celite to get rid of excess magnesium. Ethyl benzoate (3.00 mL, 21.0 mmol) was added to the flask dropwise over 1 min. The solution was left to stir at RT overnight. The flask was brought out of glovebox and quenched with 80 mL 1 M $\text{HCl}_{(\text{aq})}$. The solution color turned from dark brown to yellow. The organic layer was separated and the water layer was extracted with 100 mL of hexanes twice. The organic layer was combined and dried with anhydrous MgSO_4 . The solution was filtered through Celite and dried *in vacuo* to yield a yellow oil. The oil was triturated by pentane and sonicated. White powder formed and precipitated, and the solution was filtered through a fritted funnel. The white powder was washed with cold pentane and dried *in vacuo*. Yield: 3.24 g (46%). The ^1H and ^{13}C NMR spectral data were in agreement with those reported in the literature.²⁶⁵

Examination of solvent effect in making of 704-OH. In an Ar-filled glove box, magnesium powder (737 mg, 30.3 mmol), 1,2-dibromoethane (20 μ L, 0.23 mmol) and 20 mL THF were transferred to a 100 mL Schlenk flask. After stirring 10 min, 3,5-difluorobromobenzene (2.30 mL, 20.0 mmol) was slowly added in 5 portions in 10 min intervals over the course of 50 min. During that time, the solution color turned from colorless to yellow which indicated the Grignard reaction occurred. The solution temperature increased significantly and boiling was observed. (Note: Pause the addition of 3,5-difluorobromobenzene if the solution begin to boil too violently.) After addition all of 3,5-difluorobromobenzene, the solution was left to stir at RT 1h. The solution was then filtered through Celite to get rid of excess magnesium and the filtrate was divided to 4 portions equally (~11.5 mL for each portion). Every portion was diluted with 46 mL specific solvent: THF, Et₂O, toluene, pentane. Diethyl carbonate (150 μ L, 1.24 mmol) was then added to every portion. After RT 4 h, a drop of the solution was quenched with H₂O and extracted with CDCl₃. The CDCl₃ solution was then examined by ¹⁹F NMR spectroscopy.

Synthesis of 705-OH. In an Ar-filled glovebox, pentafluorobromobenzene (12.4 g, 50.0 mmol) was dissolved in 100 mL Et₂O in a 250 mL Schlenk flask. The flask was taken outside the glovebox, connected to a Schlenk line while maintain an Ar atmosphere, and placed in a -78 °C dry ice/acetone cooling bath. *n*-BuLi (20.0 mL of 2.5 M solution in hexanes, 50.0 mmol) was slowly added to the solution over the course of 10 min via syringe. The mixture was left to stir at -78 °C. After 2 h, diethyl carbonate (2.00 mL, 16.5 mmol) was added to the mixture over the course of 1 min via syringe and

allowed to warm to -25 °C (a cooling bath made with dry ice/ethanol : ethylene glycol = 3:7). After 3 h, 2 M HCl_(aq) was added to quench the reaction. The organic layer was extracted with hexanes and dried over anhydrous MgSO₄. The hexanes solution was filtered through Celite and dried *in vacuo* to yield slightly yellow crude product. The crude product was redissolved in hot hexanes and placed in a -35 °C freezer. After overnight, the solid was collected and redissolved in hot hexanes and placed in a -35 °C freezer. After overnight, the white solid was collected and dried *in vacuo*. Yield: 6.19 g (71%). ¹H NMR (500 MHz, CDCl₃): δ 4.24 (m, 1H, -OH). ¹⁹F NMR (470 MHz, CDCl₃): -141.1 (6F), -152.1 (3F), -161.3 (6F).

Synthesis of 701-Cl. **701-OH** (505 mg, 1.95 mmol) was dissolved in acetyl chloride (2.5 mL, 35 mmol) in a 25 mL PTFE-valved gas-tight flask. The flask was heated at 65 °C overnight and allowed to cool to ambient temperature. The solution was transferred to a 25 mL Schlenk flask with CH₂Cl₂ to assist. After removing all volatiles *in vacuo*, the residues were redissolved in hexanes then filtered through Celite. The volatiles of filtrate were removed *in vacuo* and the crude product was recrystallized from hexanes to yield white solid. Yield: 413 mg (76%). The ¹H and ¹³C NMR spectral data were in agreement with those reported in the literature.²⁶¹

Synthesis of 702-Cl. **702-Cl** was prepared through the same procedure as **701-Cl** but used **702-OH** as the starting material instead of **701-OH** to yield white solid. Yield: 80%. ¹H NMR (500 MHz, CDCl₃): δ 7.32 (m, 6H), 7.21 (m, 4H), 6.78 (m, 3H). ¹³C{¹H} NMR (126 MHz, (CD₃)₂CO): δ 163.3 (dd, J_{F-C} = 247, 13 Hz), 150.5 (t, J_{F-C} = 8.8 Hz), 144.9, 130.1, 129.3, 129.0, 113.7 (m), 104.3 (t, J_{F-C} = 26 Hz), 80.9 (m, Ar₃C).

Synthesis of 703-Cl. **703-Cl** was prepared through the same procedure as **701-Cl** but used **703-OH** as the starting material instead of **701-OH** to yield white solid. Yield: 84%. ^1H NMR (500 MHz, CDCl_3): δ 7.32 (m, 6H), 7.21 (m, 4H), 6.78 (m, 3H). $^{13}\text{C}\{^1\text{H}\}$ NMR (126 MHz, $(\text{CD}_3)_2\text{CO}$): δ 163.3 (dd, $J_{\text{F-C}} = 247, 13$ Hz), 150.5 (t, $J_{\text{F-C}} = 8.8$ Hz), 144.9, 130.1, 129.3, 129.0, 113.7 (m), 104.3 (t, $J_{\text{F-C}} = 26$ Hz), 80.9 (m, Ar_3C).

Synthesis of 704-Cl. In an Ar-filled glovebox, 3,5-difluorobromobenzene (9.64 g, 50.0 mmol) was dissolved in 100 mL Et_2O in a 250 mL Schlenk flask. The flask was taken outside the glovebox, connected to a Schlenk line while maintain an Ar atmosphere, and placed in a -78 °C dry ice/acetone cooling bath. *n*-BuLi (20.0 mL of 2.5 M solution in hexanes, 50.0 mmol) was slowly added to the solution over the course of 10 min via syringe. The mixture was left to stir at -78 °C. After 3 h, diethyl carbonate (2.00 mL, 16.5 mmol) was added to the mixture over the course of 1 min via syringe and allowed to warm to -25 °C (a cooling bath made with dry ice/ethanol : ethylene glycol = 3:7). After 3 h, 2 M $\text{HCl}_{(\text{aq})}$ was added to quench the reaction. The organic layer was extracted with hexanes and dried over anhydrous MgSO_4 . The hexanes solution was filtered through Celite and dried *in vacuo* to yield a yellow viscous oil. The oil was further dried *in vacuo* at 60 °C for 2 h. Acetyl chloride (25 mL, 350 mmol) was added to dissolve the oil and transferred to a 100 mL PTFE-cap gas-tight flask. The solution was placed in a 65 °C oil bath. After 1 d, the flask was allowed to cool to ambient temperature, and all volatiles were removed *in vacuo* to yield off-white solid. Pentane was added to the flask and sonicated. The solution was filtered through a fritted funnel, and the white powder was washed with cold pentane and dried *in vacuo*. Yield: 4.33 g

(68%). ^1H NMR (500 MHz, CDCl_3): δ 7.32 (m, 6H), 7.21 (m, 4H), 6.78 (m, 3H). $^{13}\text{C}\{^1\text{H}\}$ NMR (126 MHz, $(\text{CD}_3)_2\text{CO}$): δ 163.3 (dd, $J_{\text{F-C}} = 247, 13$ Hz), 150.5 (t, $J_{\text{F-C}} = 8.8$ Hz), 144.9, 130.1, 129.3, 129.0, 113.7 (m), 104.3 (t, $J_{\text{F-C}} = 26$ Hz), 80.9 (m, Ar_3C). ^{19}F NMR (470 MHz, CD_3CN): -110.1.

Synthesis of 705-OAc. **705-OH** (1.06 g, 2.01 mmol) was dissolved in acetyl chloride (3.0 mL, 42 mmol) in a 25 mL PTFE-valved gas-tight flask. The flask was heated at 65 °C overnight and allowed to cool to ambient temperature. The solution was transferred to a 25 mL Schlenk flask with CH_2Cl_2 to assist. After removing all volatiles *in vacuo*, the residues were redissolved in hexanes then filtered through Celite. The volatiles of filtrate were removed *in vacuo* and the crude product was recrystallized from hexanes to yield white solid. Yield: 738 mg (67%). ^1H NMR (500 MHz, CDCl_3): δ 2.15 (s, 3H, CH_3COO). $^{13}\text{C}\{^1\text{H}\}$ NMR (126 MHz, CDCl_3): δ 169.1 (CH_3COO), 145.0 (m), 141.8 (m), 137.8 (m), 113.3 (m), 76.0 (m, Ar_3C), 21.2 (CH_3COO). ^{19}F NMR (470 MHz, CDCl_3): 138.8 (6F), 152.1 (3F), 161.7 (6F).

Attempt of making triarylmethyl chloride from 705-OH. **705-OH** (1.00 g, 1.89 mmol) was mixed with SOCl_2 (2.0 mL, 28 mmol) in a 10 mL PTFE-valved gas tight flask. The flask was heated at 65 °C overnight and allowed to cool to ambient temperature. An aliquot was dissolved in CDCl_3 and analyzed by ^1H and ^{19}F NMR spectroscopy revealed only unreacted **705-OH** was presented.

Attempt of making triarylmethyl chloride from 705-OH with $\text{HCl}_{(\text{aq})}$. **705-OH** (113 mg, 0.213 mmol) was mixed with 35% $\text{HCl}_{(\text{aq})}$ (1.0 mL, 9.6 mmol) in a 10 mL

Schlenk flask. After 1 h at RT, an aliquot was dissolved in CDCl_3 and analyzed by ^{19}F NMR spectroscopy revealed only unreacted **705-OH** was presented.

Attempt of making triarylmethyl triflate from 705-OH with Tf_2O . **705-OH** (25 mg, 0.047 mmol) and Tf_2O (12 μL , 0.071 mmol) was dissolved in 0.5 mL C_6D_6 in a J. Young tube and was heated to 70 $^\circ\text{C}$. After 15 h, the solution was analyzed by ^{19}F NMR spectroscopy and showed only unreacted **705-OH**.

Attempt of making triarylmethyl triflate from 705-OH with Tf_2O and K_2CO_3 . **705-OH** (33 mg, 0.062 mmol) and K_2CO_3 (25 mg, 0.18 mmol) were mixed in 2 mL CH_3CN in a 10 mL Schlenk flask, and Tf_2O (16 μL , 0.095 mmol) was added to the solution. After 1 h at RT, the solution was analyzed by ^{19}F NMR spectroscopy and showed an unidentified mixture.

Attempt of making triarylmethyl triflate from 705-OH with Tf_2O and pyridine. **705-OH** (24 mg, 0.045 mmol) and pyridine (10 μL , 0.124 mmol) were dissolved in 0.5 mL C_6D_6 in a J. Young tube, and Tf_2O (12 μL , 0.071 mmol) was added to the solution. The tube was heated to 70 $^\circ\text{C}$. After 2 d, the solution was analyzed by ^{19}F NMR spectroscopy and showed only unreacted **705-OH**.

Attempt of making triarylmethyl triflate from 705-OH with Me_3SiOTf . **705-OH** (33 mg, 0.061 mmol) and trimethylsilyl triflate (Me_3SiOTf , 15 μL , 0.083 mmol) were dissolved in 0.5 mL C_6D_6 in a J. Young tube and the tube was heated to 70 $^\circ\text{C}$. After 2 d, the solution was analyzed by ^{19}F NMR spectroscopy and showed only unreacted **705-OH**.

Attempt of making triarylmethyl trifluoroacetate from 705-OH with TFAA. **705-OH** (307 mg, 0.579 mmol) and trifluoroacetic anhydride (TFAA, 400 μ L, 2.83 mmol) were dissolved in 3 mL Et₂O in a 25 mL PTFE-valved gas-tight flask. The flask was heated to 40 °C. After 15 h, the solution was allowed to cool to ambient temperature and the volatiles were removed *in vacuo*. The white solid was dissolved in CDCl₃ and showed only unreacted **705-OH** in the ¹⁹F NMR spectrum.

General procedures for attempts of making triarylmethyl carborane from triarylmethyl chloride (For 701-Cl to 704-Cl). Triarylmethyl chloride (~ 70 mg) and Na[HCB₁₁Cl₁₁] (1 eq) were placed in a 25 mL Schlenk flask, followed by 3 mL PhF. Solution color turned to red immediately. After 2 h, the mixture was filtered through a fine fritted funnel and removed all volatiles *in vacuo*. The residue was redissolved in CD₃CN and analyzed by ¹H and ¹⁹F NMR spectroscopies.

Attempt of making triarylmethyl carborane from 702-Cl in CD₃CN. **702-Cl** (9 mg, 0.03 mmol) and Na[HCB₁₁Cl₁₁] (15 mg, 0.03 mmol) were dissolved in 0.5 mL CD₃CN in a J. Young tube. No color change was observed after 4 h, and analysis by ¹H and ¹⁹F NMR spectroscopies revealed only unreacted **702-Cl** in the spectra.

General procedures for attempts of making triarylmethyl triflate by reacting Me₃SiOTf with triarylmethyl chloride (For 701-Cl to 704-Cl). Triarylmethyl chloride (~ 20 mg) and Me₃SiOTf (3.5 eq) were dissolved in a 0.5 mL C₆D₆ in a J. Young tube. After RT 20 min, the mixtures were analyzed by ¹H and ¹⁹F NMR spectroscopies. The tube was then heated at 70 °C overnight and then analyzed by ¹H and ¹⁹F NMR spectroscopies.

CHAPTER VIII

SUMMARY

This dissertation surveyed the C-H borylation mediated by group 9 pincer complexes, as well as the synthesis of iridium triflates and triarylmethyl species. We are reporting iridium and rhodium complexes featuring a new silyl-amido-quinoline tridentate SiNN pincer ligand. The geometry and presumably the electronic interactions in the M/Si/H triangle appear to be able to adapt in response to the changes in the metal coordination sphere. Besides the Si-H moiety, the new Rh complexes of the SiNN ligand uncovered the ligand's potential for unusual double non-innocence. For example, the amido nitrogen can reversibly accept a boryl group from the metal. Taken together, these two phenomena identify a ligand with an exceptional ability to reversibly adapt to events at the metal center.

The new iridium SiNN complexes are active catalysts for selective conversion of terminal alkynes into alkynylboronic esters via dehydrogenative C-H borylation (DHBTA) with pinacolborane. Optimization of the reactions conditions allowed us to achieve ca. 100 turnovers at ambient temperature in <10 min with aryl-, alkyl-, and silyl-substituted terminal alkynes. Later, through ligand screening, we discovered new DHBTA catalysts supported by various PNP ligands. Using the unsymmetric PNP supported iridium complex TONs of 6500 were achieved. Unlike the strict chemoselectivity in the (SiNN)Ir system, <10% hydrogenation products are observed as the main side-products in all the (PNP)Ir systems. Several ^{Me}PNPⁱPr iridium complexes analogous to intermediates in the original proposed DHBTA catalytic cycle have been

synthesized and tested in both stoichiometric and catalytic reactions. We also developed a convenient one-pot synthesis of triborylalkenes directly from terminal alkynes. The process consisted of a DHBTA and a novel dehydrogenative diboration. Further experiments are needed to elucidate the details of the catalytic mechanism.

The syntheses of PNP iridium triflate complexes were described, and while the equilibrium between (PNP)Ir(H)(OTf) and ether solvents is observed, the attempts to isolate pure form of (PNP)Ir(H)(OTf) were unsuccessful. On the other hand, (PNP)Ir(H)(OTf) generated *in situ* could react with diamine or bipyridine ligands to form stable 18 e⁻ Ir(III) triflate salts.

Finally, the syntheses of various triarylmethanols and triarylmethyl chlorides bearing electron-withdrawing groups have been described. Perfluorotriylmethanol was inert to most chlorination and triflation reagents except acetyl chloride that led to perfluorotriyl acetate. So far, attempts to abstract chloride from the new triarylmethyl chlorides by sodium carboranes were unsuccessful.

REFERENCES

- (1) Morales-Morales, D.; Jensen, C. M., Eds. *The Chemistry of Pincer Compounds*; Elsevier: Amsterdam, 2007.
- (2) Moulton, C. J.; Shaw, B. L. *J. Chem. Soc., Dalton Trans.* **1976**, 1020.
- (3) Choi, J.; MacArthur, A. H. R.; Brookhart, M.; Goldman, A. S. *Chem. Rev.* **2011**, *111*, 1761.
- (4) Gandelman, M.; Milstein, D. *Chem. Comm.* **2000**, 1603.
- (5) Ozerov, O. V.; Guo, C.; Papkov, V. A.; Foxman, B. M. *J. Am. Chem. Soc.* **2004**, *126*, 4792.
- (6) van der Boom, M. E.; Liou, S.-Y.; Ben-David, Y.; Shimon, L. J. W.; Milstein, D. *J. Am. Chem. Soc.* **1998**, *120*, 6531.
- (7) Kanzelberger, M.; Zhang, X.; Emge, T. J.; Goldman, A. S.; Zhao, J.; Incarvito, C.; Hartwig, J. F. *J. Am. Chem. Soc.* **2003**, *125*, 13644.
- (8) Lee, D. W.; Jensen, C. M.; Morales-Morales, D. *Organometallics* **2003**, *22*, 4744.
- (9) Tanaka, R.; Yamashita, M.; Nozaki, K. *J. Am. Chem. Soc.* **2009**, *131*, 14168.
- (10) Young, K. J. H.; Oxgaard, J.; Ess, D. H.; Meier, S. K.; Stewart, T.; Goddard, I. I. I. W. A.; Periana, R. A. *Chem. Comm.* **2009**, 3270.
- (11) Weng, W.; Chen, C.-H.; Foxman, B. M.; Ozerov, O. V. *Organometallics* **2007**, *26*, 3315.
- (12) Langer, R.; Leitus, G.; Ben-David, Y.; Milstein, D. *Angew. Chem. Int. Ed.* **2011**, *50*, 2120.
- (13) Morales-Morales, D.; Grause, C.; Kasaoka, K.; Redón, R.; Cramer, R. E.; Jensen, C. M. *Inorg. Chim. Acta* **2000**, *300–302*, 958.
- (14) Bedford, R. B.; Draper, S. M.; Noelle Scully, P.; Welch, S. L. *New J. Chem.* **2000**, *24*, 745.
- (15) Liang, L.-C.; Lin, J.-M.; Hung, C.-H. *Organometallics* **2003**, *22*, 3007.
- (16) Fan, L.; Foxman, B. M.; Ozerov, O. V. *Organometallics* **2004**, *23*, 326.

- (17) Fryzuk, M. D. *Can. J. Chem.* **1992**, *70*, 2839.
- (18) Peters, J. C.; Harkins, S. B.; Brown, S. D.; Day, M. W. *Inorg. Chem.* **2001**, *40*, 5083.
- (19) MacInnis, M. C.; MacLean, D. F.; Lundgren, R. J.; McDonald, R.; Turculet, L. *Organometallics* **2007**, *26*, 6522.
- (20) Okazaki, M.; Yamahira, N.; Minglana, J. J. G.; Tobita, H. *Organometallics* **2004**, *23*, 4531.
- (21) Okazaki, M.; Yamahira, N.; Minglana, J. J. G.; Komuro, T.; Ogino, H.; Tobita, H. *Organometallics* **2008**, *27*, 918.
- (22) Komuro, T.; Tobita, H. *Chem. Comm.* **2010**, *46*, 1136.
- (23) Klet, R. C.; VanderVelde, D. G.; Labinger, J. A.; Bercaw, J. E. *Chem. Comm.* **2012**, *48*, 6657.
- (24) Nguyen, A. I.; Blackmore, K. J.; Carter, S. M.; Zarkesh, R. A.; Heyduk, A. F. *J. Am. Chem. Soc.* **2009**, *131*, 3307.
- (25) Zarkesh, R. A.; Ziller, J. W.; Heyduk, A. F. *Angew. Chem. Int. Ed.* **2008**, *47*, 4715.
- (26) Koller, J.; Sarkar, S.; Abboud, K. A.; Veige, A. S. *Organometallics* **2007**, *26*, 5438.
- (27) Agapie, T.; Bercaw, J. E. *Organometallics* **2007**, *26*, 2957.
- (28) Crabtree, R. H.; Mihelcic, J. M.; Quirk, J. M. *J. Am. Chem. Soc.* **1979**, *101*, 7738.
- (29) Baudry, D.; Ephritikhine, M.; Felkin, H.; Holmes-Smith, R. *J. Chem. Soc., Chem. Commun.* **1983**, 788.
- (30) Felkin, H.; Fillebeen-Khan, T.; Gault, Y.; Holmes-Smith, R.; Zakrzewski, J. *Tetrahedron Lett.* **1984**, *25*, 1279.
- (31) Felkin, H.; Fillebeen-khan, T.; Holmes-Smith, R.; Yingrui, L. *Tetrahedron Lett.* **1985**, *26*, 1999.
- (32) Burk, M. J.; Crabtree, R. H.; McGrath, D. V. *J. Chem. Soc., Chem. Commun.* **1985**, 1829.

- (33) Burk, M. J.; Crabtree, R. H. *J. Am. Chem. Soc.* **1987**, *109*, 8025.
- (34) Aoki, T.; Crabtree, R. H. *Organometallics* **1993**, *12*, 294.
- (35) Maguire, J. A.; Goldman, A. S. *J. Am. Chem. Soc.* **1991**, *113*, 6706.
- (36) Maguire, J. A.; Petrillo, A.; Goldman, A. S. *J. Am. Chem. Soc.* **1992**, *114*, 9492.
- (37) Gupta, M.; Hagen, C.; Flesher, R. J.; Kaska, W. C.; Jensen, C. M. *Chem. Comm.* **1996**, 2083.
- (38) Göttker-Schnetmann, I.; White, P.; Brookhart, M. *J. Am. Chem. Soc.* **2004**, *126*, 1804.
- (39) Göttker-Schnetmann, I.; Brookhart, M. *J. Am. Chem. Soc.* **2004**, *126*, 9330.
- (40) Morales-Morales, D.; Redón, R.; Yung, C.; Jensen, C. M. *Inorg. Chim. Acta* **2004**, *357*, 2953.
- (41) Crabtree, R. H. *The Organometallic Chemistry of the Transition Metals*; Wiley: Hoboken, 2005.
- (42) Leeuwen, P. W. N. M. *Homogeneous Catalysis: Understanding the Art*; Kluwer: Dordrecht, 2004.
- (43) Rosen, B. M.; Quasdorf, K. W.; Wilson, D. A.; Zhang, N.; Resmerita, A.-M.; Garg, N. K.; Percec, V. *Chem. Rev.* **2010**, *111*, 1346.
- (44) Ishiyama, T.; Hartwig, J. *J. Am. Chem. Soc.* **2000**, *122*, 12043.
- (45) Wang, X.; Lane, B. S.; Sames, D. *J. Am. Chem. Soc.* **2005**, *127*, 4996.
- (46) Yanagisawa, S.; Sudo, T.; Noyori, R.; Itami, K. *J. Am. Chem. Soc.* **2006**, *128*, 11748.
- (47) Lewis, J. C.; Bergman, R. G.; Ellman, J. A. *Acc. Chem. Res.* **2008**, *41*, 1013.
- (48) Timpa, S. D.; Fafard, C. M.; Herbert, D. E.; Ozerov, O. V. *Dalton Trans.* **2011**, *40*, 5426.
- (49) Timpa, S. D.; Pell, C. J.; Ozerov, O. V. *J. Am. Chem. Soc.* **2014**, *136*, 14772.
- (50) Ben-Ari, E.; Gandelman, M.; Rozenberg, H.; Shimon, L. J. W.; Milstein, D. *J. Am. Chem. Soc.* **2003**, *125*, 4714.

- (51) Fan, L.; Parkin, S.; Ozerov, O. V. *J. Am. Chem. Soc.* **2005**, *127*, 16772.
- (52) Puri, M.; Gatard, S.; Smith, D. A.; Ozerov, O. V. *Organometallics* **2011**, *30*, 2472.
- (53) Zhu, Y.; Smith, D. A.; Herbert, D. E.; Gatard, S.; Ozerov, O. V. *Chem. Comm.* **2012**, *48*, 218.
- (54) Ghosh, R.; Zhang, X.; Achord, P.; Emge, T. J.; Krogh-Jespersen, K.; Goldman, A. S. *J. Am. Chem. Soc.* **2007**, *129*, 853.
- (55) Weng, W.; Guo, C.; Celenligil-Cetin, R.; Foxman, B. M.; Ozerov, O. V. *Chem. Comm.* **2006**, 197.
- (56) Pell, C. J.; Ozerov, O. V. *ACS Catal.* **2014**, *4*, 3470.
- (57) Semproni, S. P.; Hojilla Atienza, C. C.; Chirik, P. J. *Chem. Sci.* **2014**, *5*, 1956.
- (58) Brewster, J. H.; Negishi, E.-I. *Science* **1980**, *207*, 44.
- (59) Suzuki, A. *Angew. Chem. Int. Ed.* **2011**, *50*, 6722.
- (60) Hall, D. G. *Boronic Acids: Preparation and Applications in Organic Synthesis, Medicine and Materials*; 2 ed.; Wiley-VCH Verlag GmbH & Co. KGaA: Weinheim, 2011.
- (61) Vollhardt, K. P. C.; Schore, N. E. *Organic Chemistry: Structure and Function*; W. H. Freeman and Company: New York, 2003.
- (62) Beletskaya, I.; Pelter, A. *Tetrahedron* **1997**, *53*, 4957.
- (63) Trost, B. M.; Ball, Z. T. *Synthesis* **2005**, 853.
- (64) Mkhaliid, I. A. I.; Barnard, J. H.; Marder, T. B.; Murphy, J. M.; Hartwig, J. F. *Chem. Rev.* **2010**, *110*, 890.
- (65) Hartwig, J. F. *Chem. Soc. Rev.* **2011**, *40*, 1992.
- (66) Ishiyama, T.; Murata, M.; Miyaura, N. *J. Org. Chem.* **1995**, *60*, 7508.
- (67) Cho, J.-Y.; Tse, M. K.; Holmes, D.; Maleczka, R. E.; Smith, M. R. *Science* **2002**, *295*, 305.

- (68) Ishiyama, T.; Takagi, J.; Ishida, K.; Miyaura, N.; Anastasi, N. R.; Hartwig, J. F. *J. Am. Chem. Soc.* **2002**, *124*, 390.
- (69) Chen, H.; Hartwig, J. F. *Angew. Chem. Int. Ed.* **1999**, *38*, 3391.
- (70) Chen, H.; Schlecht, S.; Semple, T. C.; Hartwig, J. F. *Science* **2000**, *287*, 1995.
- (71) Murphy, J. M.; Lawrence, J. D.; Kawamura, K.; Incarvito, C.; Hartwig, J. F. *J. Am. Chem. Soc.* **2006**, *128*, 13684.
- (72) Brown, J. M.; Lloyd-Jones, G. C. *J. Am. Chem. Soc.* **1994**, *116*, 866.
- (73) Coapes, R. B.; Souza, F. E. S.; Thomas, R. L.; Hall, J. J.; Marder, T. B. *Chem. Comm.* **2003**, 614.
- (74) Ishiyama, T.; Ishida, K.; Takagi, J.; Miyaura, N. *Chem. Lett.* **2001**, *30*, 1082.
- (75) Olsson, V. J.; Szabó, K. J. *Angew. Chem. Int. Ed.* **2007**, *46*, 6891.
- (76) Boller, T. M.; Murphy, J. M.; Hapke, M.; Ishiyama, T.; Miyaura, N.; Hartwig, J. F. *J. Am. Chem. Soc.* **2005**, *127*, 14263.
- (77) Tamura, H.; Yamazaki, H.; Sato, H.; Sakaki, S. *J. Am. Chem. Soc.* **2003**, *125*, 16114.
- (78) Vanchura, I. I. B. A.; Preshlock, S. M.; Roosen, P. C.; Kallepalli, V. A.; Staples, R. J.; Maleczka, J. R. E.; Singleton, D. A.; Smith, I. I. M. R. *Chem. Comm.* **2010**, *46*, 7724.
- (79) Boebel, T. A.; Hartwig, J. F. *J. Am. Chem. Soc.* **2008**, *130*, 7534.
- (80) Ito, J.-i.; Kaneda, T.; Nishiyama, H. *Organometallics* **2012**, *31*, 4442.
- (81) Brück, A.; Gallego, D.; Wang, W.; Irran, E.; Driess, M.; Hartwig, J. F. *Angew. Chem. Int. Ed.* **2012**, *51*, 11478.
- (82) Chianese, A. R.; Mo, A.; Lampland, N. L.; Swartz, R. L.; Bremer, P. T. *Organometallics* **2010**, *29*, 3019.
- (83) Obligacion, J. V.; Semproni, S. P.; Chirik, P. J. *J. Am. Chem. Soc.* **2014**, *136*, 4133.
- (84) Hanh Nguyen, D.; Perez-Torrente, J. J.; Lomba, L.; Victoria Jimenez, M.; Lahoz, F. J.; Oro, L. A. *Dalton Trans.* **2011**, *40*, 8429.

- (85) Nguyen, D. H.; Pérez-Torrente, J. J.; Jiménez, M. V.; Modrego, F. J.; Gómez-Bautista, D.; Lahoz, F. J.; Oro, L. A. *Organometallics* **2013**, *32*, 6918.
- (86) Anaby, A.; Butschke, B.; Ben-David, Y.; Shimon, L. J. W.; Leitius, G.; Feller, M.; Milstein, D. *Organometallics* **2014**, *33*, 3716.
- (87) Fang, H.; Choe, Y.-K.; Li, Y.; Shimada, S. *Chem. Asian J.* **2011**, *6*, 2512.
- (88) Crudden, Cathleen M.; Edwards, D. *Eur. J. Org. Chem.* **2003**, *2003*, 4695.
- (89) Burgess, K.; Ohlmeyer, M. J. *Chem. Rev.* **1991**, *91*, 1179.
- (90) Vogels, C. M.; Westcott, S. A. *Curr. Org. Chem.* **2005**, *9*, 687.
- (91) Zhang, L.; Peng, D.; Leng, X.; Huang, Z. *Angew. Chem.* **2013**, *125*, 3764.
- (92) Balaraman, E.; Gnanaprakasam, B.; Shimon, L. J. W.; Milstein, D. *J. Am. Chem. Soc.* **2010**, *132*, 16756.
- (93) Obligacion, J. V.; Chirik, P. J. *Org. Lett.* **2013**, *15*, 2680.
- (94) Zhang, L.; Zuo, Z.; Leng, X.; Huang, Z. *Angew. Chem. Int. Ed.* **2014**, *53*, 2696.
- (95) Geier, S. J.; Westcott, S. A. *Rev. Inorg. Chem.* **2014**, DOI: 10.1515/revic-2014-0008.
- (96) Selander, N.; Willy, B.; Szabó, K. J. *Angew. Chem. Int. Ed.* **2010**, *49*, 4051.
- (97) Takaya, J.; Kirai, N.; Iwasawa, N. *J. Am. Chem. Soc.* **2011**, *133*, 12980.
- (98) Kirai, N.; Iguchi, S.; Ito, T.; Takaya, J.; Iwasawa, N. *Bull. Chem. Soc. Jpn.* **2013**, *86*, 784.
- (99) Gunanathan, C.; Hölscher, M.; Pan, F.; Leitner, W. *J. Am. Chem. Soc.* **2012**, *134*, 14349.
- (100) Sun, C.; Liu, M.; Sun, H.; Hang, F.; Sun, N.; Chen, D. *Int. J. Quant. Chem.* **2014**, DOI: 10.1002/qua.24791.
- (101) Sebelius, S.; Olsson, V. J.; Szabó, K. J. *J. Am. Chem. Soc.* **2005**, *127*, 10478.
- (102) Selander, N.; Kipke, A.; Sebelius, S.; Szabó, K. J. *J. Am. Chem. Soc.* **2007**, *129*, 13723.

- (103) Selander, N.; Szabó, K. J. *J. Org. Chem.* **2009**, *74*, 5695.
- (104) Brown, J. M.; Lloyd-Jones, G. C. *J. Chem. Soc., Chem. Commun.* **1992**, 710.
- (105) Nguyen, P.; Blom, H. P.; Westcott, S. A.; Taylor, N. J.; Marder, T. B. *J. Am. Chem. Soc.* **1993**, *115*, 9329.
- (106) Hartwig, J. F. In *Organotransition Metal Chemistry: from Bonding to Catalysis*; University Science Books: Sausalito: 2009, p 852.
- (107) Jiao, J.; Nishihara, Y. *J. Organomet. Chem.* **2012**, 721–722, 3.
- (108) Castanet, A.-S.; Colobert, F.; Schlama, T. *Org. Lett.* **2000**, *2*, 3559.
- (109) Ogawa, D.; Li, J.; Suetsugu, M.; Jiao, J.; Iwasaki, M.; Nishihara, Y. *Tetrahedron Lett.* **2013**, *54*, 518.
- (110) Gandon, V.; Leca, D.; Aechtner, T.; Vollhardt, K. P. C.; Malacria, M.; Aubert, C. *Org. Lett.* **2004**, *6*, 3405.
- (111) Huang, J.; Macdonald, S. J. F.; Harrity, J. P. A. *Chem. Comm.* **2009**, 436.
- (112) Barluenga, J.; Barrio, P.; Riesgo, L.; López, L. A.; Tomás, M. *J. Am. Chem. Soc.* **2007**, *129*, 14422.
- (113) Deloux, L.; Skrzypczak-Jankun, E.; Cheesman, B. V.; Srebnik, M.; Sabat, M. *J. Am. Chem. Soc.* **1994**, *116*, 10302.
- (114) Renaud, J.; Graf, C.-D.; Oberer, L. *Angew. Chem. Int. Ed.* **2000**, *39*, 3101.
- (115) Hussain, M. M.; Li, H.; Hussain, N.; Ureña, M.; Carroll, P. J.; Walsh, P. J. *J. Am. Chem. Soc.* **2009**, *131*, 6516.
- (116) Auvinet, A.-L.; Harrity, J. P. A. *Angew. Chem. Int. Ed.* **2011**, *50*, 2769.
- (117) Hussain, M. M.; Hernández Toribio, J.; Carroll, P. J.; Walsh, P. J. *Angew. Chem. Int. Ed.* **2011**, *50*, 6337.
- (118) Nishihara, Y.; Okada, Y.; Jiao, J.; Suetsugu, M.; Lan, M.-T.; Kinoshita, M.; Iwasaki, M.; Takagi, K. *Angew. Chem. Int. Ed.* **2011**, *50*, 8660.
- (119) Brown, H. C.; Bhat, N. G.; Srebnik, M. *Tetrahedron Lett.* **1988**, *29*, 2631.
- (120) van der Boom, M. E.; Milstein, D. *Chem. Rev.* **2003**, *103*, 1759.

- (121) O'Murchu, C. *Synthesis* **1989**, 880.
- (122) Stradiotto, M.; Furdala, K. L.; Tilley, T. D. *Chem. Comm.* **2001**, 1200.
- (123) Wada, K.; Mizutani, T.; Kitagawa, S. *J. Org. Chem.* **2003**, 68, 5123.
- (124) Liu, D.; Luo, Y.; Gao, W.; Cui, D. *Organometallics* **2010**, 29, 1916.
- (125) Butler, J. L.; Gordon, M. *J. Heterocycl. Chem.* **1975**, 12, 1015.
- (126) Zysman-Colman, E.; Arias, K.; Siegel, J. S. *Can. J. Chem.* **2009**, 87, 440.
- (127) Using *n*-BuLi for both the deprotonation of NH and the lithium/halogen exchange did not lead to successful silylation.
- (128) Corey, J. Y. *Chem. Rev.* **2011**, 111, 863.
- (129) ORTEP plots were created using Ortep-3 for Windows. Farugia, L. *J. Appl. Crystallogr.* **1997**, 30, 565.
- (130) McBee, J. L.; Escalada, J.; Tilley, T. D. *J. Am. Chem. Soc.* **2009**, 131, 12703.
- (131) Nikonov, G. I. *Adv. Organomet. Chem.* **2005**, 53, 217.
- (132) Alcaraz, G.; Sabo-Etienne, S. *Coord. Chem. Rev.* **2008**, 252, 2395.
- (133) Liskey, C. W.; Wei, C. S.; Pahls, D. R.; Hartwig, J. F. *Chem. Comm.* **2009**, 5603.
- (134) Riehl, J. F.; Jean, Y.; Eisenstein, O.; Pelissier, M. *Organometallics* **1992**, 11, 729.
- (135) Lam, W. H.; Shimada, S.; Batsanov, A. S.; Lin, Z.; Marder, T. B.; Cowan, J. A.; Howard, J. A. K.; Mason, S. A.; McIntyre, G. J. *Organometallics* **2003**, 22, 4557.
- (136) Tucker, C. E.; Davidson, J.; Knochel, P. *J. Org. Chem.* **1992**, 57, 3482.
- (137) Lee, C.-I.; Zhou, J.; Ozerov, O. V. *J. Am. Chem. Soc.* **2013**, 135, 3560.
- (138) Zhou, J. L., C.-I.; Ozerov, O. V. *manuscript in preparation*.
- (139) Lee, C.-I.; Hirscher, N. A.; Zhou, J.; Bhuvanesh, N.; Ozerov, O. V. *submitted*.
- (140) Herde, J. L.; Lambert, J. C.; Senoff, C. V.; Cushing, M. A. *Inorganic Syntheses* **1974**, 15, 18.

- (141) Ojima, I.; Vu, A. T.; Lee, S.-Y.; McCullagh, J. V.; Moralee, A. C.; Fujiwara, M.; Hoang, T. H. *J. Am. Chem. Soc.* **2002**, *124*, 9164.
- (142) Clavier, H.; Nolan, S. P. *Chem. Eur. J.* **2007**, *13*, 8029.
- (143) Schelwies, M.; Moser, R.; Dempwolff, A. L.; Rominger, F.; Helmchen, G. *Chem. Eur. J.* **2009**, *15*, 10888.
- (144) Braun, S.; Kalinowski, H.-O.; Berger, S.; VCH: Weinheim, 1996.
- (145) Frisch, M. J.; Trucks, G. W.; Schlegel, H. B.; Scuseria, G. E.; Robb, M. A.; Cheeseman, J. R.; Scalmani, G.; Barone, V.; Mennucci, B.; Petersson, G. A.; Nakatsuji, H.; Caricato, M.; Li, X.; Hratchian, H. P.; Izmaylov, A. F.; Bloino, J.; Zheng, G.; Sonnenberg, J. L.; Hada, M.; Ehara, M.; Toyota, K.; Fukuda, R.; Hasegawa, J.; Ishida, M.; Nakajima, T.; Honda, Y.; Kitao, O.; Nakai, H.; Vreven, T.; Montgomery Jr., J. A.; Peralta, J. E.; Ogliaro, F.; Bearpark, M. J.; Heyd, J.; Brothers, E. N.; Kudin, K. N.; Staroverov, V. N.; Kobayashi, R.; Normand, J.; Raghavachari, K.; Rendell, A. P.; Burant, J. C.; Iyengar, S. S.; Tomasi, J.; Cossi, M.; Rega, N.; Millam, N. J.; Klene, M.; Knox, J. E.; Cross, J. B.; Bakken, V.; Adamo, C.; Jaramillo, J.; Gomperts, R.; Stratmann, R. E.; Yazyev, O.; Austin, A. J.; Cammi, R.; Pomelli, C.; Ochterski, J. W.; Martin, R. L.; Morokuma, K.; Zakrzewski, V. G.; Voth, G. A.; Salvador, P.; Dannenberg, J. J.; Dapprich, S.; Daniels, A. D.; Farkas, Ö.; Foresman, J. B.; Ortiz, J. V.; Cioslowski, J.; Fox, D. J.; Gaussian, Inc.: Wallingford, CT, USA, 2009.
- (146) Zhao, Y.; Truhlar, D. *Theor. Chem. Acc.* **2008**, *120*, 215.
- (147) Gazić Smilović, I.; Casas-Arcé, E.; Roseblade, S. J.; Nettekoven, U.; Zanotti-Gerosa, A.; Kovačević, M.; Časar, Z. *Angew. Chem. Int. Ed.* **2012**, *51*, 1014.
- (148) Li, Y.; Asadi, A.; Perrin, D. M. *J. Fluorine Chem.* **2009**, *130*, 377.
- (149) Molander, G. A.; Ellis, N. M. *J. Org. Chem.* **2008**, *73*, 6841.
- (150) See experimental for details.
- (151) Sheldrick, G. *Acta Crystallogr. A* **2008**, *64*, 112.
- (152) Preshlock, S. M.; Ghaffari, B.; Maligres, P. E.; Krska, S. W.; Maleczka, R. E.; Smith, M. R. *J. Am. Chem. Soc.* **2013**, *135*, 7572.
- (153) Poverenov, E.; Milstein, D. *Organometallic Pincer Chemistry*; Springer Berlin Heidelberg: Berlin, 2013, p 21.
- (154) Chirik, P. J. *Inorg. Chem.* **2011**, *50*, 9737.

- (155) Osakada, K.; Sarai, S.; Koizumi, T.-A.; Yamamoto, T. *Organometallics* **1997**, *16*, 3973.
- (156) Esteruelas, M. A.; Oliván, M.; Vélez, A. *Inorg. Chem.* **2013**, *52*, 12108.
- (157) Delpech, F.; Sabo-Etienne, S.; Donnadieu, B.; Chaudret, B. *Organometallics* **1998**, *17*, 4926.
- (158) Montiel-Palma, V.; Munoz-Hernandez, M. A.; Ayed, T.; Barthelat, J.-C.; Grellier, M.; Vendier, L.; Sabo-Etienne, S. *Chem. Comm.* **2007**, 3963.
- (159) Takaya, J.; Iwasawa, N. *Organometallics* **2009**, *28*, 6636.
- (160) Hartwig, J. F.; Cook, K. S.; Hapke, M.; Incarvito, C. D.; Fan, Y.; Webster, C. E.; Hall, M. B. *J. Am. Chem. Soc.* **2005**, *127*, 2538.
- (161) Cho, J.-Y.; Iverson, C. N.; Smith, M. R. *J. Am. Chem. Soc.* **2000**, *122*, 12868.
- (162) Tse, M. K.; Cho, J.-Y.; Smith, M. R. *Org. Lett.* **2001**, *3*, 2831.
- (163) Murata, M.; Odajima, H.; Watanabe, S.; Masuda, Y. *Bull. Chem. Soc. Jpn.* **2006**, *79*, 1980.
- (164) Shimada, S.; Batsanov, A. S.; Howard, J. A. K.; Marder, T. B. *Angew. Chem. Int. Ed.* **2001**, *40*, 2168.
- (165) Robbins, D. W.; Boebel, T. A.; Hartwig, J. F. *J. Am. Chem. Soc.* **2010**, *132*, 4068.
- (166) Ghaffari, B.; Preshlock, S. M.; Plattner, D. L.; Staples, R. J.; Maligres, P. E.; Krska, S. W.; Maleczka, R. E.; Smith, M. R. *J. Am. Chem. Soc.* **2014**, *136*, 14345.
- (167) Van Der Ent, A.; Onderdelinden, A. L.; Schunn, R. A. *Inorganic Syntheses* **1990**, *28*, 90.
- (168) Murata, M.; Kawakita, K.; Asana, T.; Watanabe, S.; Masuda, Y. *Bull. Chem. Soc. Jpn.* **2002**, *75*, 825.
- (169) Cid, J.; Carbó, J. J.; Fernández, E. *Chem. Eur. J.* **2012**, *18*, 1512.
- (170) Zhu, C.; Yamane, M. *Org. Lett.* **2012**, *14*, 4560.
- (171) Braunschweig, H.; Guethlein, F.; Mailänder, L.; Marder, T. B. *Chem. Eur. J.* **2013**, *19*, 14831.

- (172) Dolomanov, O. V.; Bourhis, L. J.; Gildea, R. J.; Howard, J. A. K.; Puschmann, H. *J. Appl. Crystallogr.* **2009**, *42*, 339.
- (173) Zhu, Y.; Fan, L.; Chen, C.-H.; Finnell, S. R.; Foxman, B. M.; Ozerov, O. V. *Organometallics* **2007**, *26*, 6701.
- (174) Whited, M. T.; Zhu, Y.; Timpa, S. D.; Chen, C.-H.; Foxman, B. M.; Ozerov, O. V.; Grubbs, R. H. *Organometallics* **2009**, *28*, 4560.
- (175) Herbert, D. E.; Ozerov, O. V. *Organometallics* **2011**, *30*, 6641.
- (176) Gupta, M.; Hagen, C.; Kaska, W. C.; Cramer, R. E.; Jensen, C. M. *J. Am. Chem. Soc.* **1997**, *119*, 840.
- (177) Göttker-Schnetmann, I.; White, P. S.; Brookhart, M. *Organometallics* **2004**, *23*, 1766.
- (178) Davidson, J. J.; DeMott, J. C.; Douvris, C.; Bhuvanesh, N.; Chen, C.-H.; Herbert, D. E.; Lee, C.-I.; McCulloch, B. J.; Foxman, B. M.; Ozerov, O. V. *Submitted*.
- (179) Calimano, E.; Tilley, T. D. *Dalton Trans.* **2010**, *39*, 9250.
- (180) Crabtree, R. H. *Chem. Rev.* **2012**, *112*, 1536.
- (181) Hebden, T. J.; Denney, M. C.; Pons, V.; Piccoli, P. M. B.; Koetzle, T. F.; Schultz, A. J.; Kaminsky, W.; Goldberg, K. I.; Heinekey, D. M. *J. Am. Chem. Soc.* **2008**, *130*, 10812.
- (182) Phadke, N.; Findlater, M. *Organometallics* **2013**, *33*, 16.
- (183) Bruce, M. I. *Chem. Rev.* **1991**, *91*, 197.
- (184) Esteruelas, M. A.; López, A. M.; Mora, M.; Oñate, E. *Organometallics* **2012**, *31*, 2965.
- (185) Ortmann, D. A.; Weberndörfer, B.; Ilg, K.; Laubender, M.; Werner, H. *Organometallics* **2002**, *21*, 2369.
- (186) Steinert, P.; Werner, H. *Chem. Ber.* **1997**, *130*, 1591.
- (187) Fryzuk, M. D.; Huang, L.; McManus, N. T.; Paglia, P.; Rettig, S. J.; White, G. S. *Organometallics* **1992**, *11*, 2979.

- (188) Grotjahn, D. B.; Hoerter, J. M.; Hubbard, J. L. *J. Am. Chem. Soc.* **2004**, *126*, 8866.
- (189) Grüger, N.; Wadepohl, H.; Gade, L. H. *Eur. J. Inorg. Chem.* **2013**, *2013*, 5358.
- (190) Templeton, J. L. *Adv. Organomet. Chem.* **1989**, *29*, 1.
- (191) Frolov, V. V.; Mazhuga, A. G.; Beloglazkina, E. K.; Zyk, N. V.; Egorov, M. P. *Russ. Chem. Bull.* **2010**, *59*, 544.
- (192) Gilman, H.; Zuech, E. A. *J. Org. Chem.* **1961**, *26*, 3481.
- (193) Masuda, J. D.; Jantunen, K. C.; Ozerov, O. V.; Noonan, K. J. T.; Gates, D. P.; Scott, B. L.; Kiplinger, J. L. *J. Am. Chem. Soc.* **2008**, *130*, 2408.
- (194) Flynn, A. B.; Ogilvie, W. W. *Chem. Rev.* **2007**, *107*, 4698.
- (195) Itami, K.; Yoshida, J.-I. *Bull. Chem. Soc. Jpn.* **2006**, *79*, 811.
- (196) Ishiyama, T.; Yamamoto, M.; Miyaura, N. *Chem. Lett.* **1996**, *12*, 1117.
- (197) Shimizu, M.; Nakamaki, C.; Shimono, K.; Schelper, M.; Kurahashi, T.; Hiyama, T. *J. Am. Chem. Soc.* **2005**, *127*, 12506.
- (198) Nishihara, Y.; Miyasaka, M.; Okamoto, M.; Takahashi, H.; Inoue, E.; Tanemura, K.; Takagi, K. *J. Am. Chem. Soc.* **2007**, *129*, 12634.
- (199) Iwadate, N.; Suginome, M. *J. Am. Chem. Soc.* **2010**, *132*, 2548.
- (200) Hata, T.; Kitagawa, H.; Masai, H.; Kurahashi, T.; Shimizu, M.; Hiyama, T. *Angew. Chem.* **2001**, *113*, 812.
- (201) Kurahashi, T.; Hata, T.; Masai, H.; Kitagawa, H.; Shimizu, M.; Hiyama, T. *Tetrahedron* **2002**, *58*, 6381.
- (202) Ishiyama, T.; Matsuda, N.; Miyaura, N.; Suzuki, A. *J. Am. Chem. Soc.* **1993**, *115*, 11018.
- (203) Takaya, J.; Iwasawa, N. *ACS Catal.* **2012**, *2*, 1993.
- (204) Ishiyama, T.; Matsuda, N.; Murata, M.; Ozawa, F.; Suzuki, A.; Miyaura, N. *Organometallics* **1996**, *15*, 713.
- (205) Mann, G.; John, K. D.; Baker, R. T. *Org. Lett.* **2000**, *2*, 2105.

- (206) Lesley, G.; Nguyen, P.; Taylor, N. J.; Marder, T. B.; Scott, A. J.; Clegg, W.; Norman, N. C. *Organometallics* **1996**, *15*, 5137.
- (207) Thomas, R. L.; Souza, F. E. S.; Marder, T. B. *J. Chem. Soc., Dalton Trans.* **2001**, 1650.
- (208) Lillo, V.; Mata, J.; Ramírez, J.; Peris, E.; Fernandez, E. *Organometallics* **2006**, *25*, 5829.
- (209) Prokopcová, H.; Ramírez, J.; Fernández, E.; Kappe, C. O. *Tetrahedron Lett.* **2008**, *49*, 4831.
- (210) Grirrane, A.; Corma, A.; Garcia, H. *Chem. Eur. J.* **2011**, *17*, 2467.
- (211) Lillo, V.; Fructos, M. R.; Ramírez, J.; Braga, A. A. C.; Maseras, F.; Díaz-Requejo, M. M.; Pérez, P. J.; Fernández, E. *Chem. Eur. J.* **2007**, *13*, 2614.
- (212) Yoshida, H.; Kawashima, S.; Takemoto, Y.; Okada, K.; Ohshita, J.; Takaki, K. *Angew. Chem.* **2012**, *124*, 239.
- (213) Takahashi, K.; Ishiyama, T.; Miyaura, N. *J. Organomet. Chem.* **2001**, *625*, 47.
- (214) Ali, H. A.; El Aziz Al Quntar, A.; Goldberg, I.; Srebnik, M. *Organometallics* **2002**, *21*, 4533.
- (215) Cotton, F. A.; Feng, X.; Matusz, M.; Poli, R. *J. Am. Chem. Soc.* **1988**, *110*, 7077.
- (216) Rodman, G. S.; Mann, K. R. *Inorg. Chem.* **1985**, *24*, 3507.
- (217) Rodman, G. S.; Mann, K. R. *Inorg. Chem.* **1988**, *27*, 3338.
- (218) Che, C. M.; He, L. Y.; Poon, C. K.; Mak, T. C. W. *Inorg. Chem.* **1989**, *28*, 3081.
- (219) Yip, H.-K.; Lai, T.-F.; Che, C.-M. *J. Chem. Soc., Dalton Trans.* **1991**, 1639.
- (220) Xia, B.-H.; Che, C.-M.; Zhou, Z.-Y. *Chem. Eur. J.* **2003**, *9*, 3055.
- (221) Yan, X.; Batchelor, R. J.; Einstein, F. W. B.; Zhang, X.; Nagelkerke, R.; Sutton, D. *Inorg. Chem.* **1997**, *36*, 1237.
- (222) Luo, J.; Khusnutdinova, J. R.; Rath, N. P.; Mirica, L. M. *Chem. Comm.* **2012**, *48*, 1532.

- (223) Novoa, J. J.; Aullon, G.; Alemany, P.; Alvarez, S. *J. Am. Chem. Soc.* **1995**, *117*, 7169.
- (224) Aullón, G.; Alemany, P.; Alvarez, S. *Inorg. Chem.* **1996**, *35*, 5061.
- (225) Ho, H. E.; Asao, N.; Yamamoto, Y.; Jin, T. *Org. Lett.* **2014**, *16*, 4670.
- (226) Burger, P.; Bergman, R. G. *J. Am. Chem. Soc.* **1993**, *115*, 10462.
- (227) Schnabel, R. C.; Roddick, D. M. *Organometallics* **1996**, *15*, 3550.
- (228) Crabtree, R. H.; Mellea, M. F.; Mihelcic, J. M.; Quirk, J. M. *J. Am. Chem. Soc.* **1982**, *104*, 107.
- (229) MacLean, D. F.; McDonald, R.; Ferguson, M. J.; Caddell, A. J.; Turculet, L. *Chem. Comm.* **2008**, 5146.
- (230) Casalnuovo, A. L.; Calabrese, J. C.; Milstein, D. *J. Am. Chem. Soc.* **1988**, *110*, 6738.
- (231) Morgan, E.; MacLean, D. F.; McDonald, R.; Turculet, L. *J. Am. Chem. Soc.* **2009**, *131*, 14234.
- (232) McLaughlin, M. P.; Adduci, L. L.; Becker, J. J.; Gagné, M. R. *J. Am. Chem. Soc.* **2013**, *135*, 1225.
- (233) Albietz, P. J.; Cleary, B. P.; Paw, W.; Eisenberg, R. *J. Am. Chem. Soc.* **2001**, *123*, 12091.
- (234) Atesin, A. C.; Zhang, J.; Vaidya, T.; Brennessel, W. W.; Frontier, A. J.; Eisenberg, R. *Inorg. Chem.* **2010**, *49*, 4331.
- (235) Albietz, P. J.; Cleary, B. P.; Paw, W.; Eisenberg, R. *Inorg. Chem.* **2002**, *41*, 2095.
- (236) Janka, M.; He, W.; Frontier, A. J.; Eisenberg, R. *J. Am. Chem. Soc.* **2004**, *126*, 6864.
- (237) Li, X.; Chianese, A. R.; Vogel, T.; Crabtree, R. H. *Org. Lett.* **2005**, *7*, 5437.
- (238) Yang, J.; Brookhart, M. *J. Am. Chem. Soc.* **2007**, *129*, 12656.
- (239) Weng, W.; Guo, C.; Moura, C.; Yang, L.; Foxman, B. M.; Ozerov, O. V. *Organometallics* **2005**, *24*, 3487.

- (240) Zhu, Y.; Ozerov, O. V. *unpublished results*.
- (241) Barrera, J.; Orth, S. D.; Harman, W. D. *J. Am. Chem. Soc.* **1992**, *114*, 7316.
- (242) Orth, S. D.; Barrera, J.; Rowe, S. M.; Helberg, L. E.; Harman, W. D. *Inorg. Chim. Acta* **1998**, *270*, 337.
- (243) Iluc, V. M.; Fedorov, A.; Grubbs, R. H. *Organometallics* **2011**, *31*, 39.
- (244) Golden, J. T.; Andersen, R. A.; Bergman, R. G. *J. Am. Chem. Soc.* **2001**, *123*, 5837.
- (245) Chen, S.; Song, G.; Li, X. *Tetrahedron Lett.* **2008**, *49*, 6929.
- (246) Tse, S. K. S.; Xue, P.; Lin, Z.; Jia, G. *Adv. Synth. Catal.* **2010**, *352*, 1512.
- (247) Suenobu, T.; Guldi, D. M.; Ogo, S.; Fukuzumi, S. *Angew. Chem.* **2003**, *115*, 5650.
- (248) Precht, M. H. G.; Hölscher, M.; Ben-David, Y.; Theyssen, N.; Loschen, R.; Milstein, D.; Leitner, W. *Angew. Chem. Int. Ed.* **2007**, *46*, 2269.
- (249) Fan, L. *PhD dissertation* **2006**.
- (250) Hiyama, T.; Yamamoto, H. *Organofluorine Compounds: Chemistry and Applications*; Springer-Verlag: Berlin, 2000.
- (251) Kiplinger, J. L.; Richmond, T. G.; Osterberg, C. E. *Chem. Rev.* **1994**, *94*, 373.
- (252) Burdeniuc, J.; Jedicka, B.; Crabtree, R. H. *Chem. Ber.* **1997**, *130*, 145.
- (253) Shine, K. P.; Sturges, W. T. *Science* **2007**, *315*, 1804.
- (254) Scott, V. J.; Çelenligil-Çetin, R.; Ozerov, O. V. *J. Am. Chem. Soc.* **2005**, *127*, 2852.
- (255) Douvris, C.; Ozerov, O. V. *Science* **2008**, *321*, 1188.
- (256) Gusev, D. G.; Ozerov, O. V. *Chem. Eur. J.* **2011**, *17*, 634.
- (257) Williams, V. C.; Irvine, G. J.; Piers, W. E.; Li, Z.; Collins, S.; Clegg, W.; Elsegood, M. R. J.; Marder, T. B. *Organometallics* **2000**, *19*, 1619.
- (258) Bahr, S. R.; Boudjouk, P. *J. Org. Chem.* **1992**, *57*, 5545.

- (259) Straus, D. A.; Zhang, C.; Tilley, T. D. *J. Organomet. Chem.* **1989**, 369, C13.
- (260) Vadim Yu, K.; Yurii, N. K. *Russ. Chem. Rev.* **1986**, 55, 901.
- (261) Strazzolini, P.; Giumanini, A. G.; Verardo, G. *Tetrahedron* **1994**, 50, 217.
- (262) Xie, Z.; Liston, D. J.; Jelinek, T.; Mitro, V.; Bau, R.; Reed, C. A. *J. Chem. Soc., Chem. Commun.* **1993**, 384.
- (263) Xie, Z.; Bau, R.; Benesi, A.; Reed, C. A. *Organometallics* **1995**, 14, 3933.
- (264) Xie, Z.; Manning, J.; Reed, R. W.; Mathur, R.; Boyd, P. D. W.; Benesi, A.; Reed, C. A. *J. Am. Chem. Soc.* **1996**, 118, 2922.
- (265) Horn, M.; Metz, C.; Mayr, H. *Eur. J. Org. Chem.* **2011**, 2011, 6476.
- (266) Olah, G. A.; Comisarow, M. B. *J. Am. Chem. Soc.* **1967**, 89, 1027.
- (267) Filler, R.; Wang, C.-S.; McKinney, M. A.; Miller, F. N. *J. Am. Chem. Soc.* **1967**, 89, 1026.
- (268) Vougioukalakis, G. C.; Roubelakis, M. M.; Orfanopoulos, M. *J. Org. Chem.* **2010**, 75, 4124.
- (269) Wang, Z. *Pinacol Coupling Reaction*; John Wiley & Sons, Inc.: Weinheim, 2010.
- (270) Ashby, E. C.; Wiesemann, T. L. *J. Am. Chem. Soc.* **1978**, 100, 189.
- (271) Ashby, E. C.; Bowers, J. R. *J. Am. Chem. Soc.* **1981**, 103, 2242.
- (272) Walling, C. *J. Am. Chem. Soc.* **1988**, 110, 6846.
- (273) Snyder, L. R. *J. Chromatogr. A* **1974**, 92, 223.
- (274) Kulkarni, S. V.; Schure, R.; Filler, R. *J. Am. Chem. Soc.* **1973**, 95, 1859.
- (275) Horn, M.; Mayr, H. *Eur. J. Org. Chem.* **2011**, 2011, 6470.
- (276) Neumann, W. P.; Penenory, A.; Stewen, U.; Lehnig, M. *J. Am. Chem. Soc.* **1989**, 111, 5845.
- (277) Neumann, W. P.; Uzick, W.; Zarkadis, A. K. *J. Am. Chem. Soc.* **1986**, 108, 3762.
- (278) Gibbs, L. W.; Wedegaertner, D. K. *J. Org. Chem.* **1991**, 56, 7320.

(279) Reed, C. A. *Acc. Chem. Res.* **2009**, *43*, 121.

(280) Bour, J. R.; Green, J. C.; Winton, V. J.; Johnson, J. B. *J. Org. Chem.* **2013**, *78*, 1665.